The Loma Prieta, California, Earthquake of October 17, 1989—Tectonic Processes and Models

ROBERT W. SIMPSON, *Editor*

EARTHQUAKE OCCURRENCE
WILLIAM H. BAKUN and WILLIAM H. PRESCOTT, *Coordinators*

U.S. GEOLOGICAL SURVEY PROFESSIONAL PAPER 1550–F

UNITED STATES GOVERNMENT PRINTING OFFICE, WASHINGTON : 1994

DEPARTMENT OF THE INTERIOR

BRUCE BABBITT, *Secretary*

U.S. GEOLOGICAL SURVEY

Gordon P. Eaton, *Director*

Manuscript approved for publication, December 2, 1993

Text and illustrations edited by George A. Havach

Library of Congress catalog-card No. 92–32287

U.S. Geological Survey, Map Distribution
Box 25286, MS 306, Federal Center
Denver, CO 80225

CONTENTS

TECTONIC PROCESSES AND MODELS

INTRODUCTION

By Robert W. Simpson,
U.S. Geological Survey

If there is a single theme that unifies the diverse papers in this chapter, it is the attempt to understand the role of the Loma Prieta earthquake in the context of the earthquake "machine" in northern California: as the latest event in a long history of shocks in the San Francisco Bay region, as an incremental contributor to the regional deformation pattern, and as a possible harbinger of future large earthquakes.

One of the surprises generated by the earthquake was the rather large amount of uplift that occurred as a result of the reverse component of slip on the southwest-dipping fault plane. Preearthquake conventional wisdom had been that large earthquakes in the region would probably be caused by horizontal, right-lateral, strike-slip motion on vertical fault planes.

In retrospect, the high topography of the Santa Cruz Mountains and the elevated marine terraces along the coast should have provided some clues. With the observed ocean retreat and the obvious uplift of the coast near Santa Cruz that accompanied the earthquake, Mother Nature was finally caught in the act. Several investigators quickly saw the connection between the earthquake uplift and the long-term evolution of the Santa Cruz Mountains and realized that important insights were to be gained by attempting to quantify the process of crustal deformation in terms of Loma Prieta-type increments of northward transport and fault-normal shortening.

Three papers in this chapter explore how the geometry of the Loma Prieta fault plane and the oblique slip recorded during the earthquake can be used to explain the structural and topographic features of the Santa Cruz Mountains. Shaw and others present a detailed, three-dimensional kinematic model, based on repeated earthquakes on a nonplanar Loma Prieta rupture surface, that explains the location and evolution of synclines mapped in the southern Santa Cruz Mountains. Their method allows them to infer the depth and position of fault bends in the subsurface from surface geologic structures. The inferred geometry compares favorably with the locations of aftershocks and is consistent with the observed main-shock slip direction. They suggest that Loma Prieta-type events should recur every 132±26 years. Their approach shows promise for inferring information about deformation modes at depth in regions where earthquakes have not been recorded during historical time.

Valensise uses the present elevations of the first and third marine terraces near Santa Cruz and the geometry on the base of the Upper Miocene and Pliocene Purisima Formation to explore the relative contributions of strike-slip and reverse-slip earthquake offsets to the northward transport and uplift of the Santa Cruz region. From his models, he concludes that the location of Loma Prieta-type events has remained stationary relative to the North American plate over the past million years and that only a fraction of the topography in the Santa Cruz Mountains can be explained by such events. He suggests that the remaining uplift may have been generated by distributed deformation in the upper 5 km of crust caused by regional compression perpendicular to the plate boundary.

Schwartz and others point out that although deformation associated with a restraining bend can explain many of the topographic features in the bay region, Loma Prieta-type events cannot be the only source of topographic change because Loma Prieta, the highest point in the southern Santa Cruz Mountains, actually subsided in the earthquake. This observation suggests that motion on other faults, notably the nearby Sargent-Berrocal fault zone, must occur periodically to complement the uplift accompanying the Loma Prieta main shock. If these motions occur as earthquakes, then there may be a part of the seismic cycle in the bay region that we have not yet witnessed.

These attempts to relate geologic structures and topography, generated over hundreds of thousands to millions of years, to the deformations produced by a single earthquake have proved most enlightening for understanding the place of the 1989 Loma Prieta earthquake in the larger scheme of things. By using quantitative models, discrepancies have been identified in the regional deformation budget, and hypotheses have been presented to explain these discrepancies. Although the final word on the subject has probably not yet been heard, the results from these initial efforts are quite exciting.

Three additional papers in this chapter examine the interactions of the various faults in the San Francisco Bay region and the interplay of stresses on these faults, using rather different approaches and presenting results that span

different time intervals. In the short term, the Loma Prieta rupture changed the static-stress loads on other bay-region faults. Simpson and Reasenberg calculate these changes, using dislocation theory in an elastic half-space. Sections of the San Andreas fault to the north and south of the Loma Prieta rupture zone now have greater stress loads as a result of the earthquake, whereas the Hayward fault has been slightly relaxed in most models. If the earthquake pairs in 1836/38 and 1865/68 on the Hayward and San Andreas faults were caused by triggering across the bay, the most likely way for the 1989 earthquake to trigger an event on the Hayward fault during the next several years would be through extensional normal stresses applied at the south end of the Hayward fault. If pore fluids are present, the full effect of this unclamping might not be felt for several years as the fluids reequilibrate.

Looking at the record of historical earthquakes, Bodin and Bilham use two-dimensional dislocation models to investigate the overall slip budget on the San Andreas fault since 1800. They load an elastic plate at an azimuth representing the relative motion between the North American and Pacific plates, and allow faults, represented as vertical cuts in the plate, to slip frictionlessly along segments corresponding to the estimated rupture lengths of historical earthquakes. Slip from the 1989 Loma Prieta earthquake is underestimated by their model, suggesting either higher failure strain for this event or limitations of a two-dimensional approach. The concept of using geometrically realistic mechanical models that include fault interactions to account for slip and stress budgets for earthquake-prediction purposes is an important advance over simple time- or slip-predictable models of earthquake recurrence.

Taking the very long view, Furlong and Verdonck use finite-element modeling to explore how bay-region faults, including the Loma Prieta rupture surface, interact. Their preferred model uses a viscously deforming shear zone in the lower crust to connect the San Andreas fault with the Hayward and Calaveras faults in the east bay. Most of the deep plate-boundary motion occurs under these east-bay faults in this model, and motion is transferred to the San Andreas fault in the Loma Prieta region via a horizontal shear zone. Their model suggests that Loma Prieta-type events may represent decoupling of the Santa Cruz crustal block from its underlying mantle in response to stress accumulation after large, 1906-type earthquakes.

Although these modeling efforts are still limited in scope and complexity, they do suggest that useful insight can be gained with relatively simple models, and they offer the hope that someday we may know enough about the Earth's crust and mantle beneath the San Francisco Bay region to devise models able to do justice to the earthquake "machine."

THE LOMA PRIETA, CALIFORNIA, EARTHQUAKE OF OCTOBER 17, 1989:
EARTHQUAKE OCCURRENCE

TECTONIC PROCESSES AND MODELS

RELATIONS BETWEEN FOLDING AND FAULTING IN THE LOMA PRIETA EPICENTRAL ZONE: STRIKE-SLIP FAULT-BEND FOLDING

By John H. Shaw, Richard E. Bischke, and John Suppe,
Princeton University

CONTENTS

ABSTRACT

We present balanced kinematic models of strike-slip fault-bend folding that demonstrate how synclines in the 1989 Loma Prieta epicentral zone grow in transpression. Right-lateral motion along left-stepping restraining bends in the San Andreas and Zayante faults results in transpression and uplift of rocks adjacent to the fault bends. Uplift is caused by thrusting over nonplanar fault surfaces, causing folding of the hanging-wall block. We model fold growth by kink-band migration, with deformation of the overriding block localized along active axial surfaces, which are pinned to subsurface fault bends. Applied to the epicentral zone, these balanced models yield predictions of the subsurface fault geometry. The orientation of the Glenwood syncline, which emanates in map view from a restraining bend in the San Andreas fault, suggests a steepening-upward subsurface bend in the underlying fault at a depth of about 8 km. The Scotts Valley syncline, which emanates in map view from a bend in the nearby Zayante fault, suggests a similar steepening-upward bend in the underlying fault at a depth of about 15 km.

We test our predictions of the subsurface fault geometry in the Loma Prieta epicentral zone by examining hypocenters of the earthquake and its aftershocks. A contour map and series of cross sections of the fault surface, based on aftershock locations, confirm the existence of a steepening-upward subsurface bend in the San Andreas fault at 8-km depth. Furthermore, the geometry of this fault bend agrees with the fold orientation. The consistency between the fault geometry predicted by our models applied to surface data and the shape of the subsurface fault rupture outlined by aftershocks confirms the relation between fold and fault shape. These results suggest that fault-bend-folding theory is a viable explanation for the origin of folds that lie adjacent to strike-slip faults.

We further test our models by comparing their predicted slip directions with slip vectors inferred from seismology and regional stress. Our predicted slip directions are found to be consistent with both the slip vector of the main shock and shear-stress directions resolved onto the various fault segments from regional stresses. Assuming that these favorable slip directions approximate the long-term slip directions, the 12-mm/yr slip rate on the San Andreas fault southeast of the rupture zone must increase to 15.2 mm/yr onto the rupture surface. This increase in slip rate within restraining bends may explain why the 1989 Loma Prieta and, possibly, other strike-slip earthquakes originate at fault bends. This 15.2-mm/yr slip rate resolves to a 11.6-mm/yr strike-slip, 9.8-mm/yr dip-slip, and 9.2-mm/year uplift rate above the inclined fault rupture. This uplift rate, once it is corrected for isostatic compensation, falls within the range of uplift rates in the Loma Prieta epicentral zone predicted from dated marine terraces along the nearby Santa Cruz coastline. This result suggests that most slip on the adjacent San Andreas fault is transferred onto the inclined rupture surface, and if this slip is released in Loma Prieta-type events (2±0.4 m of slip), a major earthquake should recur every 132±26 yr. In addition, a study of syntectonic sediment deposited along the adjacent Zayante fault indicates large motions before deposition of the Pliocene section. More recent strike-slip motion that began during the middle Pliocene appears to continue into the present.

INTRODUCTION

The 1989 Loma Prieta earthquake occurred along a left-stepping bend of the San Andreas fault in the Santa Cruz Mountains of central California (fig. 1). In analogy with the Transverse Ranges north of the Los Angeles Basin (Crowell, 1974a, b), right-lateral motion on the San Andreas fault into a left-stepping restraining bend has resulted in transpression, uplift, and deformation of the hanging-wall rocks adjacent to the fault. In support of these conclusions, (1) earthquake focal-mechanism solutions of the Loma Prieta main shock suggest a combination of reverse and strike-slip motion on a 70°±10° SW.-dipping fault (Oppenheimer, 1990), and (2) modeling of geodetic data by Lisowski and others (1990) indicates that 1.6 m of right-lateral slip and 1.2 m of reverse-slip occurred during the earthquake.

In this paper, we examine young geologic structure in the Loma Prieta epicentral zone, which includes deformed Pliocene to Holocene syntectonic (growth) sedimentary deposits adjacent to bends in the San Andreas and nearby Zayante faults (fig. 2). Right-lateral motion along these faults into left-stepping bends in the Loma Prieta epicentral zone generates synclines within recently deposited sediment. Material entering the restraining bends is thrust upward, causing monoclinal folding of the hanging-wall block. Quaternary sedimentary deposits and the upper Miocene and Pliocene Purisima Formation have been deformed into the Glenwood syncline as material has moved past a restraining bend in the San Andreas fault (fig. 2). Another syncline that folds the Purisima Formation runs through Scotts Valley, formed as material passed through a similar restraining bend in the nearby Zayante fault.

We present balanced models of strike-slip fault-bend folding that show how these folds grow in restraining bends. Fold growth is modeled by kink-band migration, with deformation of the overriding block localized along axial surfaces pinned to subsurface fault bends. Application of these models to the folds in the Loma Prieta epicentral zone predicts the subsurface fault geometry, including the orientation of fault surfaces and depth to subsurface fault bends. To test our predictions of subsurface fault geometry, we examine hypocenters of the 1989 Loma Prieta aftershock sequence. A contour map of the fault-surface rupture, a series of cross sections, and fault models confirm the existence of a subsurface bend in the San Andreas fault system, consistent with that predicted by the location and orientation of the Glenwood syncline. The subsurface geometry of the Zayante fault is also inferred from the location and orientation of the Scotts Valley syncline and other available data.

Surface geology and aftershocks of the earthquake suggest that the Loma Prieta epicentral zone is characterized not by a single active throughgoing fault but by active segments of the San Andreas, Zayante, and Sargent(?) faults, which compose the San Andreas fault system. To test our model of the subsurface fault system, we compare the slip direction of the M_S=7.1 main shock (Oppenheimer, 1990) and slip directions inferred from our models with shear-stress directions resolved onto the various fault segments from components of the regional stress tensors of

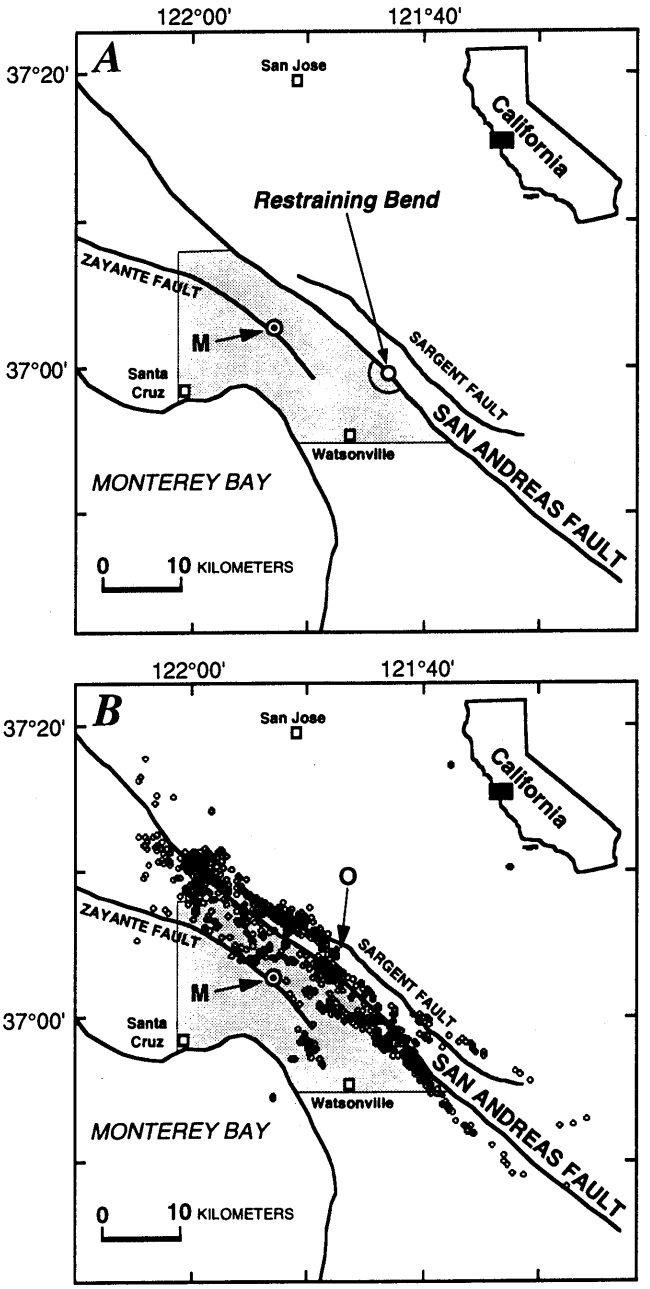

Figure 1.—Loma Prieta area, Calif., showing location of epicenter of 1989 earthquake (M). *A*, Location of a restraining bend in the San Andreas fault. *B*, Epicenters of selected aftershocks (from Dietz and Ellsworth, 1990). O, offset in seismicity between events along the San Andreas fault to southeast and shallow events east of fault to northwest. Shading marks area of figure 2.

Michael and others (1990). In addition, we use these slip directions, the subsurface fault geometry, and long-term slip rates on the San Andreas fault southeast of the Loma Prieta rupture zone to calculate Pliocene and Quaternary uplift rates above the San Andreas fault and the Loma Prieta fault segment. We compare the results with uplift rates in the Loma Prieta epicentral zone predicted by several investigators from marine-terrace elevations along the Santa Cruz coastline.

To constrain past movements on the Zayante fault, which did not rupture in the earthquake, we examine electric logs from wells located on opposite sides of the fault. We apply a new technique to examine syntectonic (growth) strata, and we demonstrate that more recent motions initiated on the Zayante fault during the late Pliocene have continued into the Quaternary and, possibly, into the present day.

FOLDING AND FAULTING IN THE EPICENTRAL ZONE

SURFACE RELATIONS BETWEEN FOLDS AND FAULTS

Both the San Andreas and Zayante faults have major left-stepping or restraining bends in the vicinity of the Loma Prieta epicentral zone. The surface trace of the San Andreas fault changes trend from 320° in the southeast to 310° in the northwest in the study area (figs. 1, 2); a minor right-stepping bend marks this transition. The Glenwood syncline emanates in map view from this left-stepping restraining bend in the right-lateral San Andreas fault. The surface trace of the axial surface of the Glenwood syncline diverges from the fault trace, reaching a maximum distance of about 4 km and maintaining this distance it parallels the

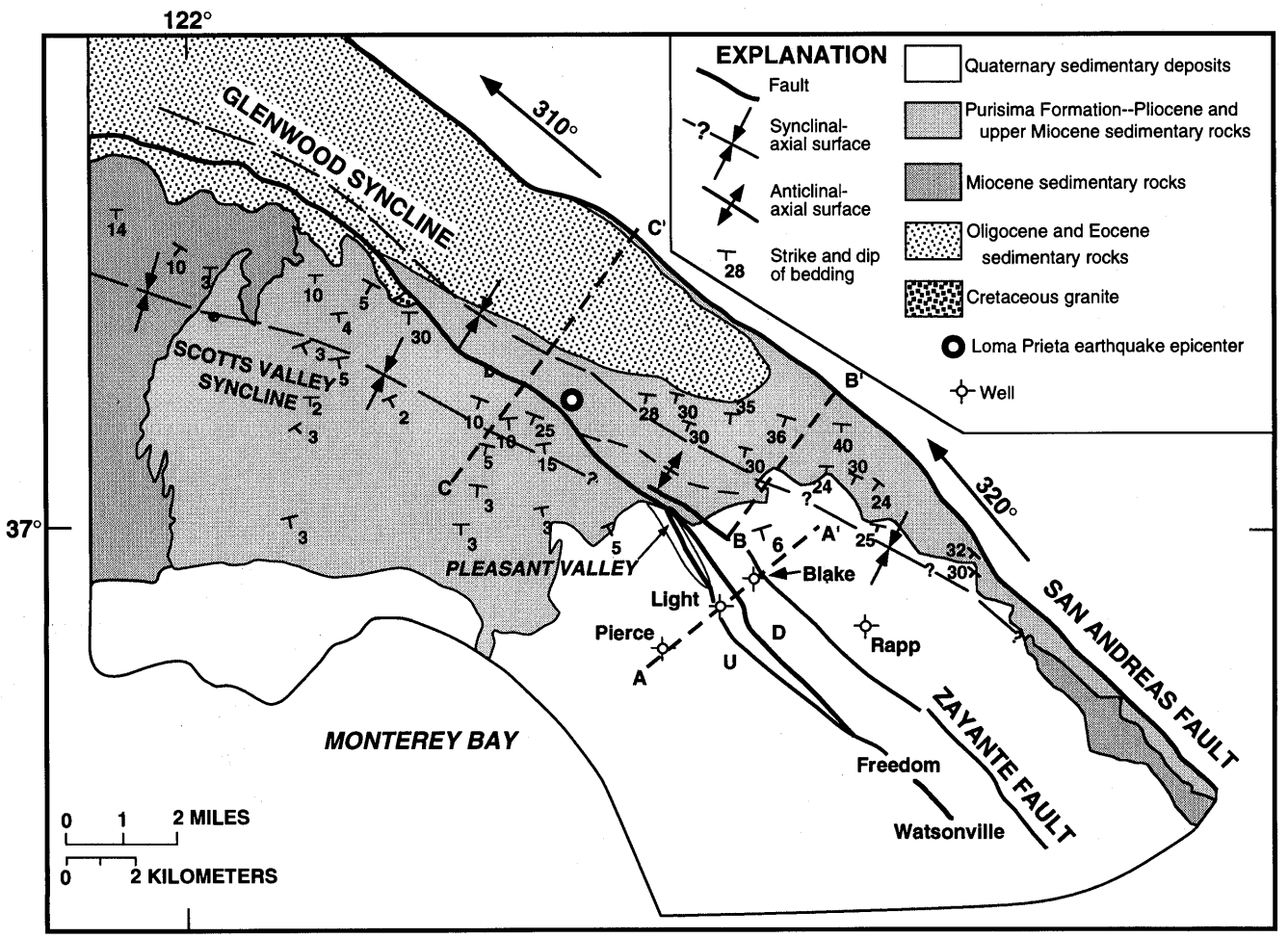

Figure 2.—Geologic map of Loma Prieta epicentral zone (modified from Brabb, 1989), showing orientations of synclinal-axial surfaces that fold Pliocene and younger strata emanating from restraining bends in the San Andreas and Zayante faults and locations of cross sections *A–A'* through *C–C'* in figures 6, 9, 10, 15, and 18. A minor right-stepping bend marks left-stepping change in trend of the San Andreas fault from 320° in southeast to 310° in northwest. Axial surfaces queried where inferred or uncertain. Fault blocks: D, downthrown; U, uplifted.

Andreas fault to the northwest for more than 17 km. The axial surface separates a gently southwest dipping panel to the south from a more steeply southwest dipping panel to the north, as shown by bedding dips at the surface (Brabb, 1989) and well-log correlation data (Muir, 1972). At the surface, the Glenwood syncline folds semiconsolidated Quaternary sedimentary deposits and parts of the upper Miocene and Pliocene Purisima Formation.

The Zayante fault also has a restraining bend in the Loma Prieta epicentral zone due west of a similar bend in the San Andreas fault (fig. 2). Southeast of this bend, the most active branch of the Zayante fault trends 320° through Pleasant Valley and the Freedom-Watsonville, Calif., areas (see subsection below entitled "Motion on the Zayante Fault"). Northwest of this bend, the surface trace of the Zayante fault trends approximately 310° for about 13.5 km, subparallel to the adjacent San Andreas fault. Clark and Rietman (1973) interpreted the Zayante fault to be a large, near-vertical fault active during the Oligocene. More recent, Pliocene and Quaternary motion on the Zayante fault offsets the upper Miocene and Pliocene Purisima Formation (Clark, 1981). In addition, recent motion is indicated by deformed Quaternary horizons and a fault scarp of probable Holocene age (Hall and others, 1974; Clark and others, 1984). We suggest that Pliocene and Quaternary motions are predominantly strike slip in the Loma Prieta epicentral zone, causing local thrusting and uplift in a restraining bend of the Zayante fault (fig. 2). Consistent with this interpretation, (1) Clark and others (1984) reported oblique-reverse, right-lateral offsets across the fault; and (2) the surface trace of the near-vertical Zayante fault south of the bend parallels and merges with the San Andreas fault along the Vergeles fault (Clark, 1981).

The Scotts Valley syncline emanates in map view from a left-stepping bend in the Zayante fault, similar to the relation between the nearby Glenwood syncline and the San Andreas fault (fig. 2). The axial-surface trace of the Scotts Valley syncline runs 2 to 4 km southwest of and subparallel to the Zayante fault for 8 km northwest of the fault bend. Farther to the northwest, the distance between the axial surface and fault trace decreases as the Zayante fault trace curves sharply to trend nearly due west (Clark, 1981). The synclinal-axial surface separates a near-horizontal southern limb from a gently south dipping limb to the north.

Eocene and Oligocene rocks adjacent to the San Andreas and Zayante faults are more strongly folded. The age and intense folding of these rocks suggest that they may have been deformed before the development of the modern San Andreas fault system during the late Miocene, associated with opening of the Gulf of California (Curray and Moore, 1984). These rocks may also have been folded while passing through other restraining bends in the modern San Andreas and Zayante faults southeast of the study area. To model deformation solely associated with the restraining fault bends in the Loma Prieta epicentral zone, we concentrate on the more recent Pliocene and Quaternary growth sediment deposited while the faults were active. These younger strata are less likely to have been intensely deformed before entering the restraining bends, an interpretation consistent with areas of near-horizontal strata south of the axial surfaces. Locally steeper dips very close to the fault traces (Brabb, 1989) are attributed to minor restraining bends or to other local fault-zone processes.

THREE-DIMENSIONAL BALANCED MODELS OF STRIKE-SLIP FOLDING

Balanced models of strike-slip deformation that illustrate how folds grow in restraining fault bends are shown in figure 3. Construction of these models has been governed by the two basic assumptions of Suppe's (1983) fault-bend-folding theory; (1) at depth, rocks are too weak to support large voids opened by movement of rigid blocks over nonplanar fault surfaces; and (2) rock volume is conserved during deformation. As focal-mechanism and ground-motion studies of the 1989 Loma Prieta earthquake have demonstrated, movement of material into a left-stepping bend in the San Andreas fault system has caused thrusting. This thrust component of motion results in folding of the hanging-wall block as it moves over bends in the underlying fault. Rich (1934) and Suppe (1983) demonstrated that rigid-block translation over nonplanar fault surfaces generates unreasonable "overlap" or subsurface voids in the underlying rock between fault surfaces (fig. 4). At depth, these voids cannot be supported, assuming reasonable rock strengths. As detailed in fault-bend-folding theory (Suppe, 1983), collapse of these voids and removal of the "overlap" may be accommodated by deformation of the overriding block localized along active axial surfaces pinned to subsurface fault bends (fig. 4). Folds develop as material shears through active axial surfaces, and grow by kink-band migration during progressive fault slip. The quantitative relations between fold shape and fault shape are those derived for fault-bend folding by Suppe (1983). In cases of oblique slip, which may arise in transpression, the limb lengths or kink-band widths of the folds, measured normal to the active and inactive axial-surface pairs, are minimum estimates of the dip slip on the underlying faults. Additional constraints on slip direction and subsurface fault geometry are required to determine the total slip vector.

The four models shown in figure 3 all illustrate folds developed within restraining bends along left-stepping, right-lateral fault systems. The progression of models, presented in order of increasing complexity, shows how specific changes in fault geometry affect fold growth and fault slip. In this and the following sections, we test aspects of these simplified models and apply them to the San

Andreas and Zayante fault systems. All the models consist of vertical, dominantly strike-slip faults connected by dipping thrust or oblique-slip faults. Thrusting causes uplift of material above the connecting fault plane between the vertical faults. Uplift is accomplished with fold growth by kink-band migration, in which active axial surfaces are pinned to subsurface bends in the underlying thrust or oblique-slip faults. In these models, axial surfaces bisect mechanical-bedding units, and bed thickness and volume are conserved. These balanced models therefore represent

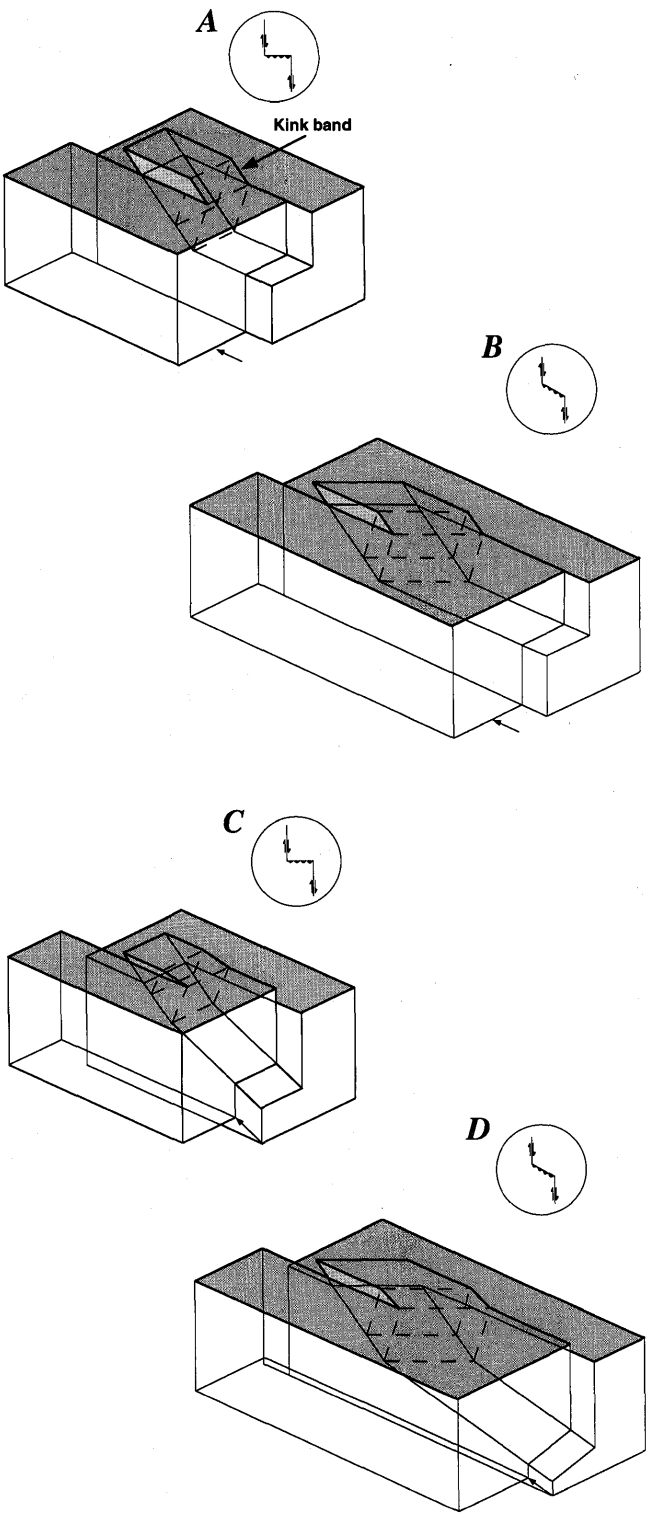

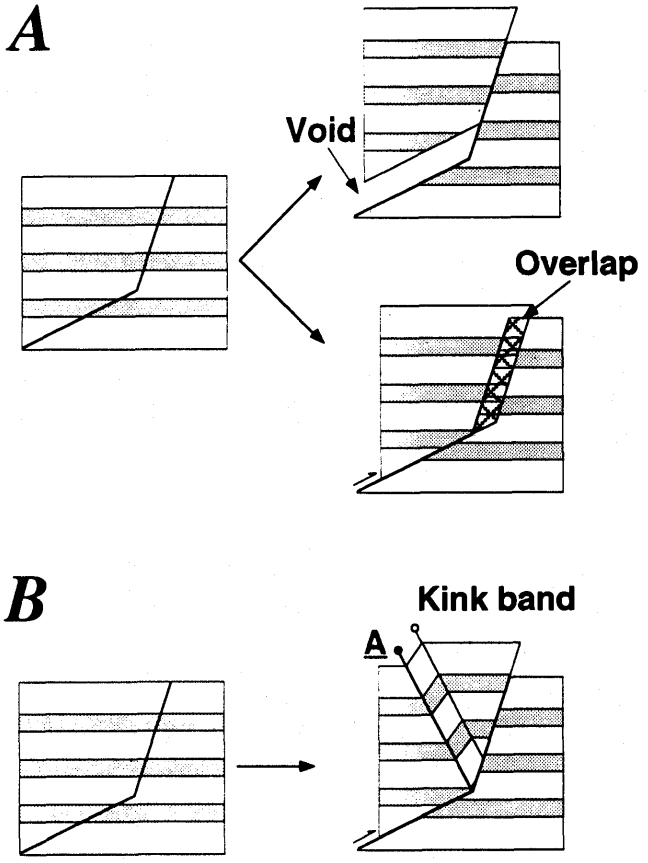

Figure 4.—Balanced fault models. *A*, Rigid-block translation over nonplanar fault surfaces results in unreasonable "overlap" (hatched pattern) or subsurface voids between fault surfaces. *B*, Folding of hanging-wall block, localized along active axial surfaces (A) pinned to fault bends, accommodates fault slip without resulting in "overlap" or voids.

Figure 3.—Balanced three-dimensional models of fold growth adjacent to restraining bends in right-lateral strike-slip fault systems, showing uplift and fold growth by kink-band migration above a thrust or oblique-slip fault that connects vertical strike-slip faults. Dark surface layer represents mechanical bedding; arrows indicate directions of relative motion. *A*, Horizontal detachment surface ramps upward and strikes normal to adjacent vertical faults. Width of kink band equals fault slip. *B*, Oblique-slip right-lateral thrust ramp strikes oblique to trend of strike-slip faults. Kink-band width represents only dip slip on underlying ramp. *C*, Dipping thrust with steepening-upward ramp strikes normal to adjacent vertical faults. Dip of thrust results in relative uplift of hanging-wall block relative to footwall, and kink-band width above ramp is less than slip on underlying fault. *D*, Dipping oblique-slip, right-lateral thrust with steepening-upward ramp strikes oblique to adjacent vertical fault. Only dip-slip component of motion on connecting faults results in uplift and kink-band growth.

geometrically and kinematically reasonable solutions to fold growth in transpression.

In model A, the connecting thrust ramps to the surface from a horizontal detachment at depth. This ramp is perpendicular to the strike of the adjoining vertical faults. The orientation of mechanical bedding is represented in all of the models in figure 3 by a dark surface layer. The horizontal-detachment fault at depth is bedding parallel and contains a slip vector parallel and equal in magnitude and direction to that on the adjoining strike-slip faults. During progressive fault slip, a dipping kink band forms above the ramp, with its inclined surface parallel to the underlying thrust ramp. Because this surface (bedding) parallels the underlying fault plane, the kink-band width, measured normal to the axial surfaces along bedding, is equal to the fault slip.

Model B differs from model A in that the strike of the connecting fault ramp is not perpendicular to the strike of the adjoining vertical faults. The inclined surface of the fold again parallels the underlying fault ramp, although the kink-band width represents only the dip-slip component of motion on the oblique-slip fault ramp. Thus, for a given amount of slip entering a restraining bend, fold-limb width and uplift decrease as the strike of the connecting ramp approaches that of the adjacent vertical faults. In places where the subsurface fault geometry is known and the slip direction can be inferred, the magnitude of fault slip can be calculated from the kink-band width by resolving the vector triangle on the fault surface.

In model C, the horizontal detachment in models A and B is replaced by an inclined connecting thrust that has a steepening-upward bend as it approaches the surface. The slip vector on the deeper segment of the thrust is again equal to the slip on the oblique-slip vertical faults. Unlike in models A and B, however, this inclined slip vector results in uplift of the hanging-wall block relative to the footwall above the deeper thrust-fault segment. Mechanical bedding (dark surface layer, fig. 3*C*) does not parallel the lower thrust-fault segment, and so fault slip must increase slightly onto the steepening-upward thrust ramp (Suppe, 1983). Moreover, the inclined surface of the fold limb dips less than the underlying thrust ramp because bedding does not parallel the deeper thrust segment. Because only the dip-slip component of motion generates the folds in these models, the relations between fold shape and fault shape are those derived for fault-bend folding by Suppe (1983). In this model where the fold limb dips less than the underlying thrust, the kink-band or fold-limb width represents a minimum estimate of dip slip on the fault. In places where the subsurface fault geometry is known, fault slip can be calculated. In places where the subsurface fault geometry is poorly constrained, however, fold-limb width provides a reasonable estimate (generally within 20 percent) of fault dip slip (Suppe and others, 1992).

Model D, which combines aspects of models B and C, is presented as a simplified representation of fold growth in the Loma Prieta epicentral zone along the San Andreas and Zayante faults. As in model C, the dipping lower segment of the thrust fault ramps upward toward the surface. The strikes of the connecting thrusts, however, are not perpendicular to the adjacent vertical faults, as in model B. The dip-slip component of motion on the lower segment of the oblique thrust results in uplift of the hanging-wall block relative to the footwall. Because bedding does not parallel the lower connecting fault segment, slip slightly increases in magnitude onto the thrust ramp. Also, the inclined surface of the kink band, which develops as material shears through the active axial surface, dips more shallowly than the underlying ramp. Thus, the kink-band width in this model represents only a minimum estimate of the dip-slip component of motion on the underlying oblique-thrust ramp. As for the previous models, in places where the subsurface fault geometry is known and the slip direction can be inferred, fault-slip magnitude can be calculated.

PREDICTING SUBSURFACE FAULT GEOMETRY

Application of the relations between folds and faults illustrated in the models (fig. 3) to natural transpressive environments allows detailed predictions of the subsurface fault geometry along strike-slip fault systems. Axial surfaces that emanate from bends in strike-slip faults can be projected to depth if their orientations are known or are assumed to bisect adjacent fold limbs. The intersections at depth of faults and active axial surfaces predict the positions of subsurface fault bends. In addition, the acute angles between (1) bedding and the axial surface (γ) and (2) bedding and the upper fault segment (β) can be used to predict the change in dip of the fault across the bend (ϕ) and the lower hanging-wall cutoff (θ), using fault-bend-folding equations (fig. 5; see Suppe, 1983).

Applying these models to the Loma Prieta epicentral zone, the location of the Glenwood synclinal-axial surface, which emanates in map view from a restraining bend in the San Andreas fault (fig. 2), predicts a steepening-upward subsurface bend in the underlying fault. The 72° E. dip of this axial surface, estimated from the dip of adjacent strata mapped by Brabb (1989), predicts an intersection of the fold hinge with the near-vertical San Andreas fault (which dips >75° from surface geology) at 7- to 12-km depth (fig. 6). This depth estimate is refined and the change in dip across the fault bend predicted in the next subsection, where the dip of the San Andreas fault is more accurately determined. The Scotts Valley synclinal-axial surface, which in map view emanates from a restraining bend in the Zayante fault (fig. 2), suggests a similar steepening-upward subsurface bend in the underlying fault. The intersection of the 83° E.-dipping axial surface with the vertical Zayante fault should occur at about 15-km depth. Alternative subsurface geometries for the Zayante fault are discussed below in the next subsection.

SUBSURFACE FAULT GEOMETRY INFERRED FROM LOMA PRIETA SEISMICITY

Because seismicity can provide important constraints on fault geometry, we examined the hypocenters of the earthquake (fig. 1), as located by Dietz and Ellsworth (1990) and provided by the U.S. Geological Survey, to test our predictions of the subsurface fault geometry in the Loma Prieta epicentral zone. The sequence that we used consists of the 1,173 best constrained aftershocks (from a total of 3,750) processed by October 1989. The hypocenters were located using two one-dimensional velocity models separated by the San Andreas fault. Horizontal standard errors <0.5 km and vertical standard errors <1.0 km were assigned to the selected hypocenters, although relative locations are thought to be more accurate (average relative epicentral error, ±0.3 km; average relative vertical error, ±0.6 km).

Fault-surface contour maps generated from subsurface data have proved to be an effective first step toward developing reasonable structural interpretations of faulted terrains (Tearpock and Bischke, 1991). To create a contoured fault-surface map of the Loma Prieta rupture from the seismicity in the epicentral zone, we divided hypocenters into horizontal sections corresponding to 2-km-depth intervals. Contour lines of the rupture surface were drawn freehand through the hypocenters for each horizontal section. Typically, this technique has proved to yield the most accurate

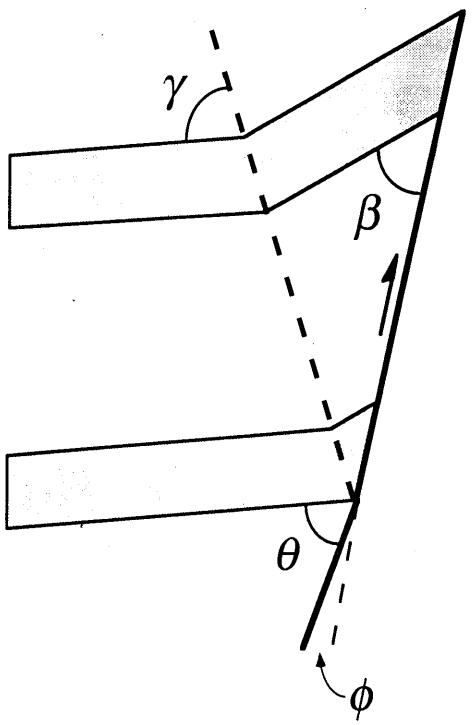

$$\phi = \tan^{-1}\left\{\frac{-\sin(\gamma-\theta)\,[\sin(2\gamma-\theta)-\sin\theta]}{\cos(\gamma-\theta)\,[\sin(2\gamma-\theta)-\sin\theta]-\sin\gamma}\right\}$$

$$\beta = \theta - \phi + (180 - 2\gamma)$$

Figure 5.—Synclinal-axial surface emanating from a steepening-upward bend in underlying fault. Fold shape is related to fault shape by fault-bend-folding equations of Suppe (1983). Arrow indicates direction of slip. Note that axial surface bisects fold limbs, conserving layer thickness.

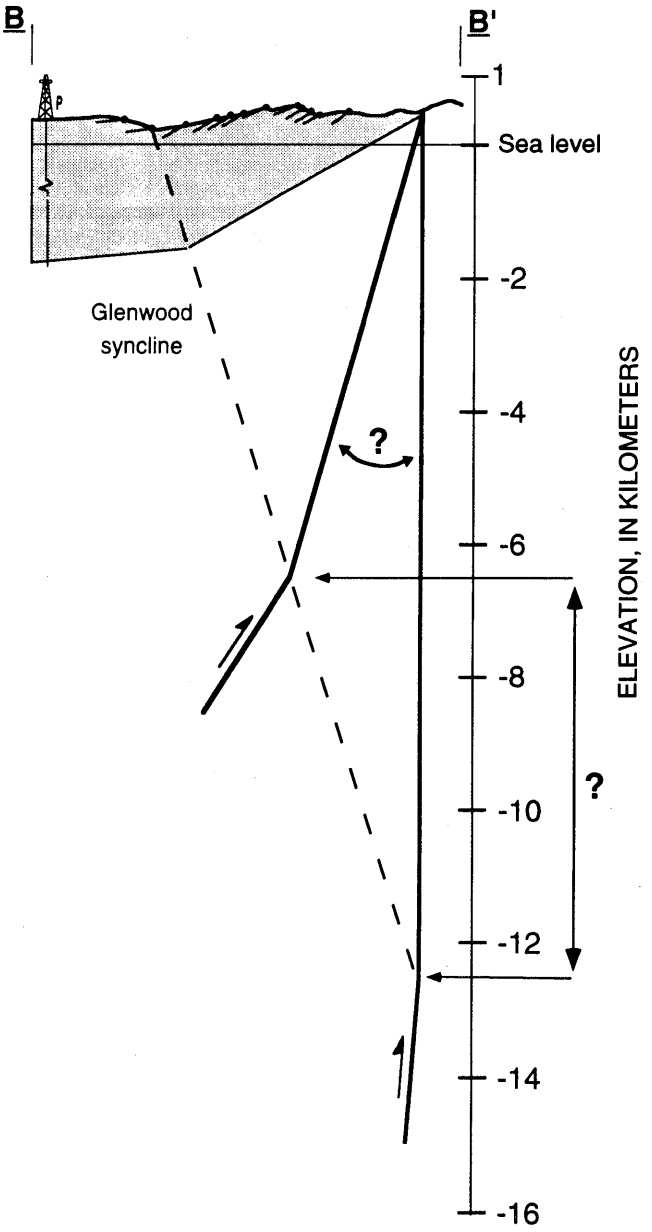

Figure 6.—Preliminary cross section *B–B'* across the Glenwood syncline and San Andreas fault (see fig. 2 for locations). Ball and bar indicates local dip of bedding. Orientation of synclinal-axial surface (dashed line), which bisects bedding, predicts a steepening-upward subsurface bend beneath the steeply dipping San Andreas fault at a depth of 7 to 12 km. True dip of upper segment of the San Andreas fault, to be determined from hypocentral locations of 1989 Loma Prieta earthquake, further constrains depth to fault bend. P, projected Blake well. Arrow indicates direction of slip.

representation of subsurface fault geometry (Tearpock and Bischke, 1991). Contour lines were assigned depths equal to the depth of the center of their corresponding horizontal sections, and were projected vertically to the surface to form a contour map of the fault (fig. 7). Vertical cross sections were then constructed through the contour map to highlight fault bends and to show changes in the subsurface fault geometry along strike.

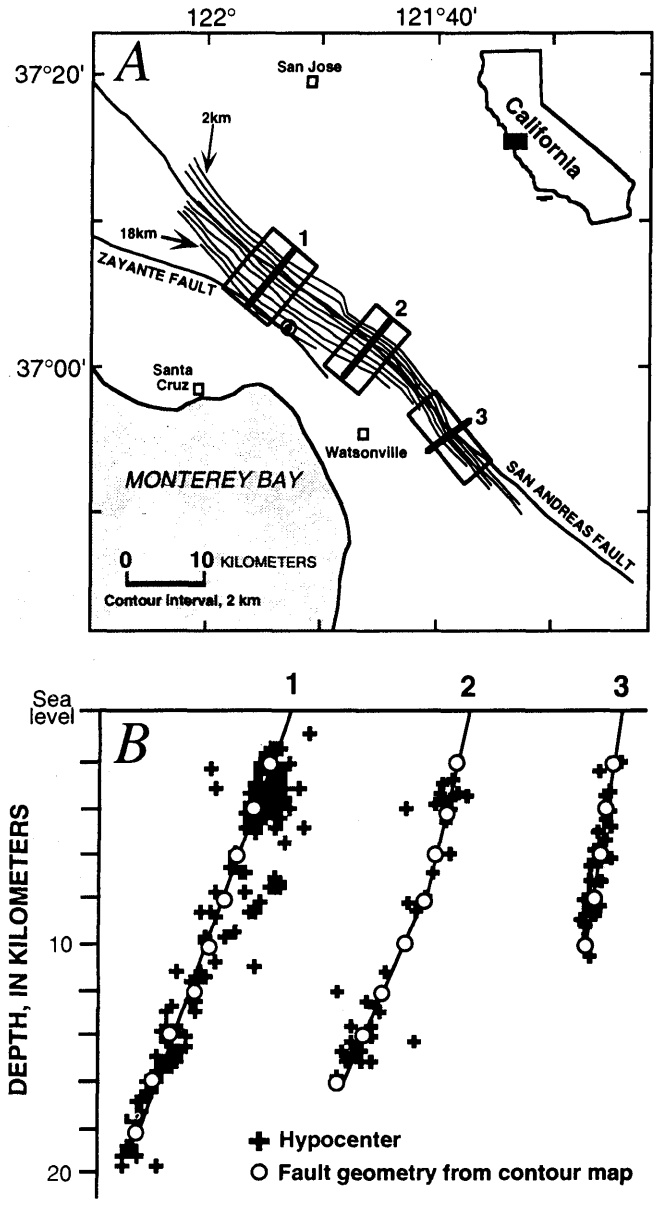

Figure 7.—Contour map (*A*) and cross sections (*B*) of Loma Prieta rupture zone, derived from hypocentral locations reported by Dietz and Ellsworth (1990). Change in trend of contours from southeast to northwest highlights restraining bend in fault system. Boxes outline areas within which hypocenters are plotted around profiles 1 through 3, showing dipping fault segments and locating a steepening-upward fault bend in central part of rupture zone (profile 2).

Changes in the relative spacing and trends of contour lines in the fault-surface map indicate that the Loma Prieta rupture occurred not on a single planar fault but on a complex system composed of multiple fault segments. The subsurface fault geometry outlined by the contour map and cross sections (fig. 7) is illustrated by the models in figure 8. The contour map and cross section 3 in figure 7 suggest that the southeastern part of the aftershock zone defines a steeply dipping plane beneath the surface trace of the San Andreas fault, consistent with the observation of Dietz and Ellsworth (1990). This segment of the San Andreas fault strikes 320° and dips 82° W. (fault segment 1, fig. 8*A*). Focal-mechanism solutions of selected aftershocks along this fault segment, which lies to the southeast of the restraining bend, show large components of right-lateral slip (Oppenheimer, 1990).

The main shock and aftershocks in the deep central and northwestern parts of the Loma Prieta rupture zone outline a different planar fault segment (2, fig. 8*A*) that strikes 310° and dips 70° SW.. The orientation of this fault segment coincides with that of the preferred nodal plane of the focal-mechanism solution of the main shock reported by Oppenheimer (1990). The change in strike between this northwestern fault segment and the fault rupture to the south forms the restraining bend that caused the thrusting in Loma Prieta seismicity.

Shallow hypocenters at the northwest edge of the aftershock zone suggest that the Loma Prieta rupture in this area projects eastward of the surface trace of the San Andreas fault (fig. 1*A*; cross sec. 1, fig. 7). The northwestward extension of the 78° W.-dipping San Andreas fault (fault segment 3, fig. 8*A*) apparently did not rupture during the earthquake. The 70° W.-dipping fault rupture is therefore addressed in the following discussion as the Loma Prieta fault segment, a component of the San Andreas fault system. Schwartz and others (1990) suggested that shallow slip may have been transferred from the Loma Prieta fault

▶ Figure 8.—Fault-bend fold models of the Loma Prieta epicentral zone. *A*, Subsurface fault geometry derived from contour map and cross sections shown in figure 7. Fault system is composed of multiple fault segments that include (1) the San Andreas fault southeast of restraining bend; (2) the west-dipping Loma Prieta fault segment (completely buried), which corresponds to main-shock preferred nodal plane of Oppenheimer (1990); and (3) a segment of the San Andreas fault northwest of restraining bend that forms an active steepening-upward bend above the underlying Loma Prieta fault segment. The Glenwood syncline emanates at depth from this fault bend. Northwest of rupture zone, above the Loma Prieta fault segment, long-term slip may be transferred to shallower dipping thrusts in the eastern Santa Cruz Mountains. *B*, Balanced three-dimensional model of hanging-wall deformation above fault geometry shown in figure 8*A*. Thrusting results in growth of the Glenwood syncline by kink-band migration, with shearing of materials through axial surface pinned to an underlying subsurface fault bend. Formation of the Scotts Valley syncline is attributed to a similar steepening-upward bend beneath the Zayante fault.

segment to the Sargent-Berrocal fault zone east of the San Andreas fault (fig. 1). Seeber and Armbruster (1990) reported that seismicity in the 20-yr period before the earthquake and faults mapped to the east of the San Andreas fault (McLaughlin and others, 1988) indicate that long-term slip on the Loma Prieta fault segment may in part be transferred onto a series of shallowly dipping thrusts beneath the eastern Santa Cruz Mountains (fig. 8*A*).

The fault rupture outlined by aftershocks breaks approximately due east of the main-shock epicenter (fig. 1*B*).

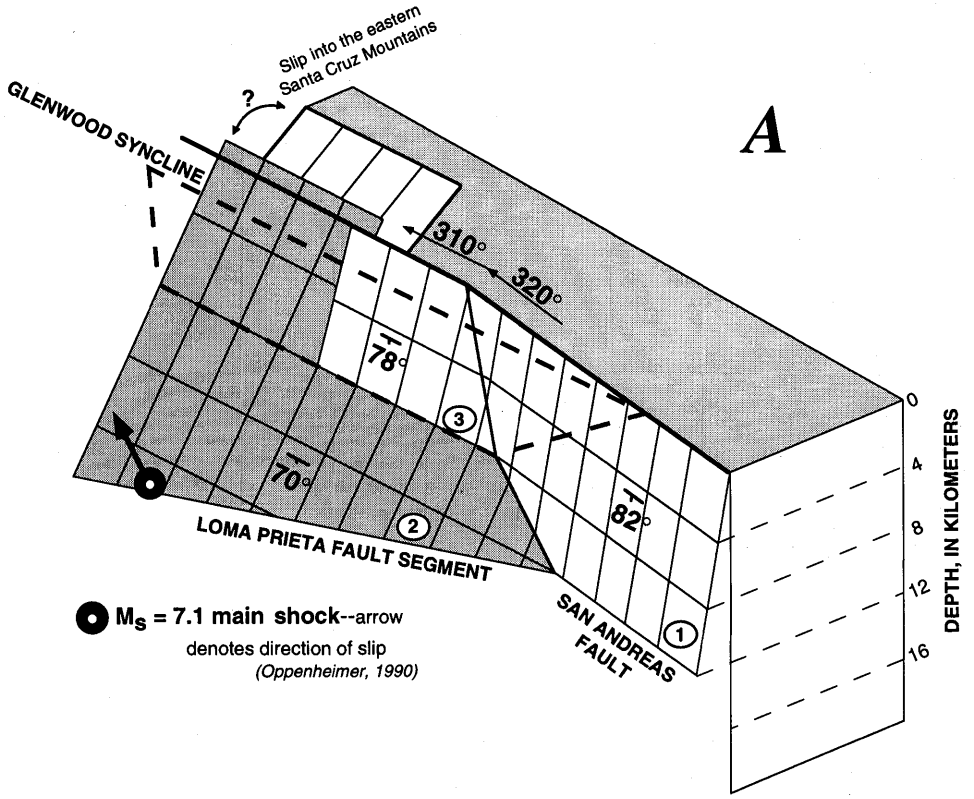

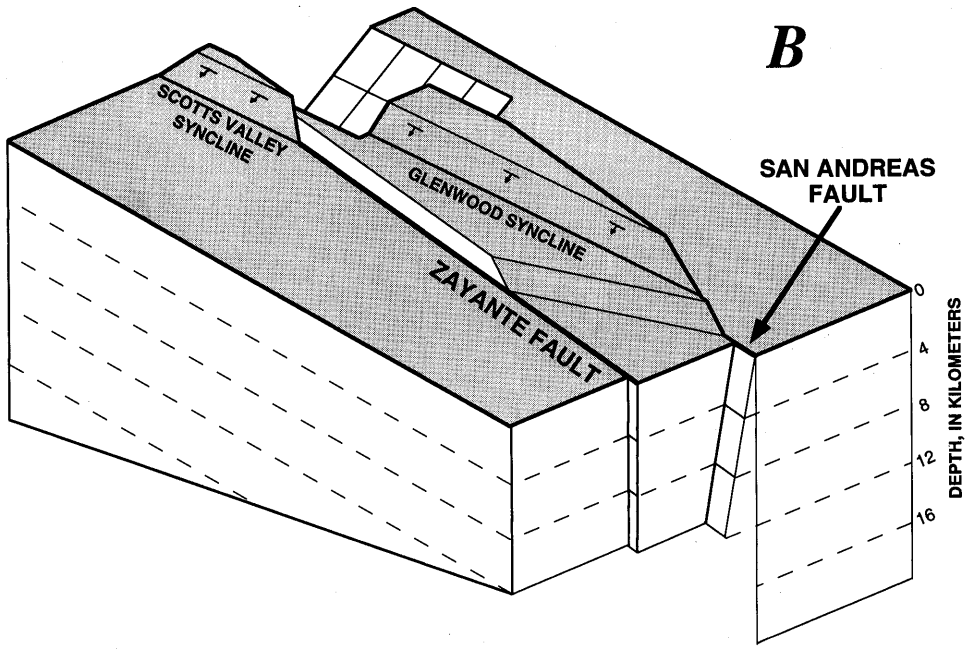

This break represents a change from shallow rupture in the northwest that occurs east of the San Andreas fault (cross sec. 3, fig. 7), to rupture in the southeast primarily beneath the surface trace of the San Andreas fault (cross secs. 1, 2, fig. 7). Southeast of this break, in the central part of the aftershock zone, the fault rupture steepens upward from the Loma Prieta fault segment (cross sec. 2, fig. 7). The seismicity defines a 78° W.-dipping fault segment (3, fig. 8) beneath the surface trace of the San Andreas fault. This segment, thought to be part of the San Andreas fault, and the underlying Loma Prieta fault segment form an active flat-to-ramp system, or steepening-upward fault bend, that slipped during the earthquake. This inferred fault geometry is similar to that suggested by Dietz and Ellsworth (1990), who also reported a concave-upward shape of the Loma Prieta rupture surface in the vicinity of the restraining bend.

As discussed in the preceding section, dip slip across this fault bend, formed by the Loma Prieta fault segment (2, fig. 8*A*) and the San Andreas fault (segment 3, fig. 8*A*), must result in deformation of the overriding block (see fig. 4). As illustrated in the models in figure 3, deformation should be localized along active axial surfaces pinned to subsurface fault bends. Similarly, movement of the hanging-wall block over the subsurface fault geometry shown in figure 8*A* results in fold growth above the fault bends (fig. 8*B*).

Applying the balanced models in figure 3 to the Loma Prieta epicentral zone, the location and orientation of the Glenwood syncline predict an underlying bend at 7- to 12-km depth in the San Andreas-Loma Prieta fault system (fig. 6). The seismicity, contour maps, and cross section 2 in figure 7 confirm the existence of a steepening-upward bend at 8-km depth. The geologic cross section in figure 9 combines the surface geology with subsurface fault data provided by the seismicity. This steepening-upward fault bend is located at the intersection of the projected Glenwood syncline and the steeply dipping San Andreas fault. Using fault-bend-folding theory (fig. 5; Suppe, 1983), the 47° cutoff angle (β) between the fault and adjacent strata, and the 77° angle between strata and the Glenwood syncline (γ), an 8° change in fault dip is predicted across the bend (ϕ). This predicted 8° bend corresponds to the 78°–70° change in fault dip across the bend inferred from the seismicity (fig. 9).

During past slip on the San Andreas-Loma Prieta fault system and growth of the Glenwood syncline, the inactive axial surface, or other end of the kink band, has probably been uplifted and eroded. In addition, the rupture of the steepening-upward fault bend only in the central part of the aftershock zone (fig. 7) suggests that the Glenwood syncline grew only in this region during the earthquake. Past ruptures that involved slip on the steeply dipping San Andreas fault northwest of the restraining bend, which did not rupture in the 1989 earthquake, as well as on the Loma Prieta fault segment, are most likely responsible for the northwestward extension of recent deformation along the syncline.

The consistent fault geometry inferred from the applied balanced models, surface geology, and the seismicity confirms the predicted relations between subsurface fault bends and folds observed at the surface. These consistent relations suggests that fault-bend folding is, indeed, a folding mechanism of transpressional environments. Furthermore, fault-bend-folding theory may be used to predict subsurface fault geometry and slip directions in other transpressive structures without the aid of seismicity.

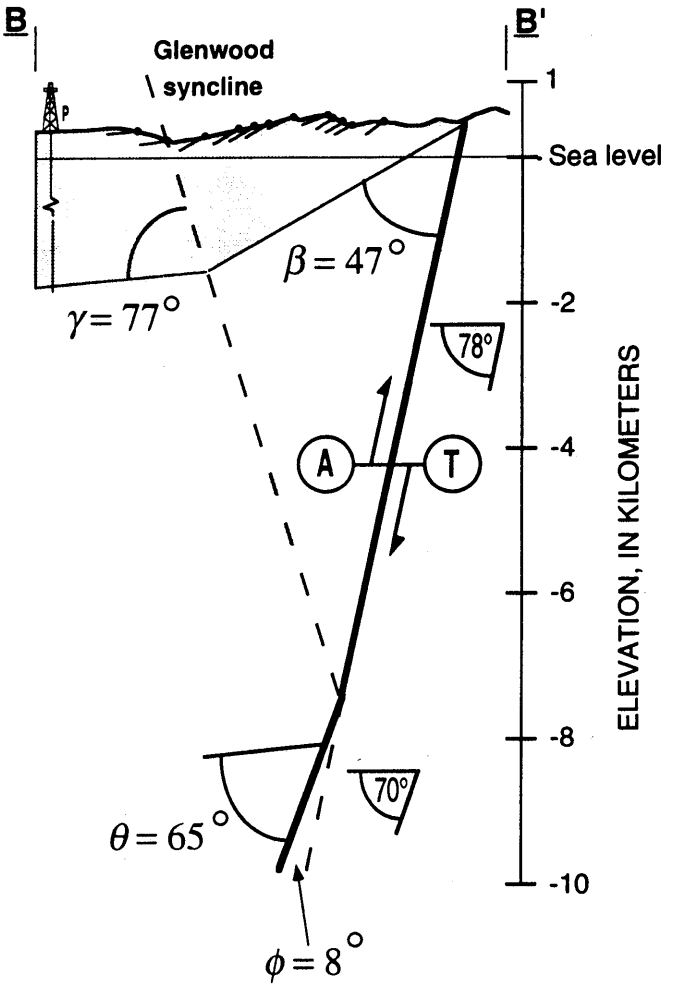

Figure 9.—Geologic cross section *B–B'* across the Glenwood syncline, the San Andreas fault, and the Loma Prieta fault segment (see fig. 2 for locations). Syncline emanates from steepening-upward bend in fault surfaces outlined by hypocentral locations (see fig. 7). Ball and bar indicates local dip of bedding. Using fault-bend-folding theory (Suppe, 1983), angle between bedding and axial surface (γ) and upper hanging-wall cutoff (β) are consistent with 8° fault-dip change (ϕ) and lower hanging-wall cutoff (θ) determined from seismicity (see figs. 5, 6). P, projected Blake well. Arrows indicate directions of dip-slip motion: A, lateral motion away; T, lateral motion toward.

The similarities in the shape and location of the Scotts Valley and Glenwood synclines in restraining bends along strike-slip faults (fig. 2) suggest that the theories and models that explain the development of the Glenwood syncline should be applicable to the Scotts Valley syncline and Zayante fault. If the Zayante fault is near-vertical within its restraining bend, as indicated by Clark and Rietman (1973), then the fault should intersect the projected east-dipping Scotts Valley syncline at a depth of approximately 15 km (fig. 10). Alternatively, if the Zayante fault dips west, similar to the Loma Prieta fault segment, the fault and fold intersection should occur at a shallower depth. The 80° cutoff angle between strata and the vertical fault, and the 83.5° interlimb angle of the syncline, suggest only a few-degree change in dip of the fault across the subsurface bend. We note that this potential fault-bend and fold intersection occurs near the main-shock hypocenter, which lies on the adjacent Loma Prieta fault segment (fig. 10). If this predicted subsurface fault geometry is correct, then this geometrically complex region with multiple fault and fold intersections may have acted to concentrate stress, localizing the initial main-shock rupture on the Loma Prieta fault segment. We suggest that further development and application of this technique of modeling subsurface faults and folds holds promise in locating future hypocenters along other strike-slip fault systems.

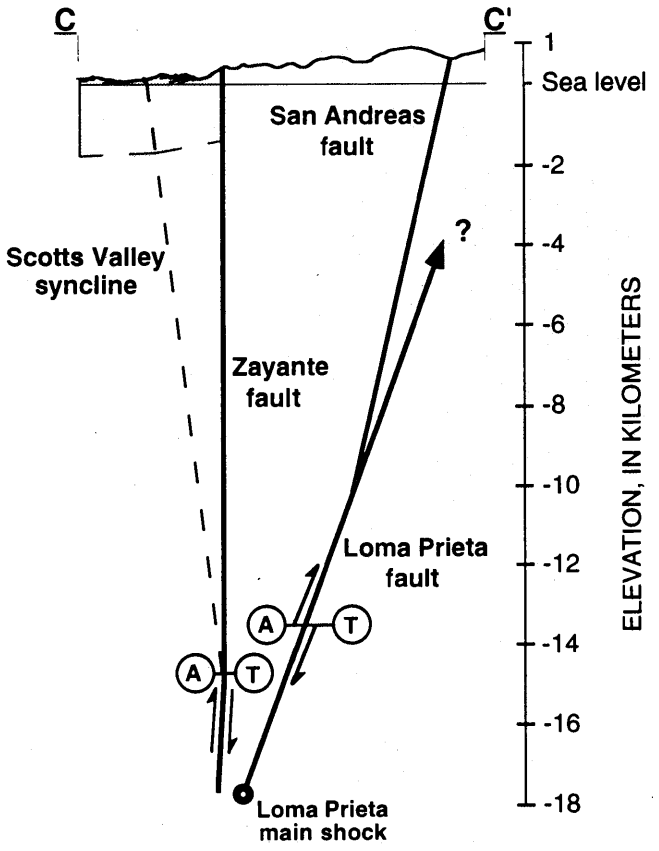

Figure 10.—Geologic cross section *C–C′* across the Scotts Valley syncline and the Zayante and San Andreas (Loma Prieta) faults (see fig. 2 for locations). Orientation of synclinal-axial surface (assumed to bisect bedding) predicts a few-degree steepening-upward bend in the underlying Zayante fault at 15-km depth. This predicted subsurface fault geometry suggests that Loma Prieta main shock initiated in a complex region of multiple fault-fold intersections. Arrows indicate directions of dip-slip motion: A, lateral motion away; T, lateral motion toward.

FAULT SLIP

The transpressive fault-bend-folding model for the Loma Prieta epicentral zone may also be compared with fault-slip data. Focal-mechanism solutions from the Loma Prieta seismicity yield important constraints on slip within this complex, multiple-fault system. The M_S=7.1 main shock was reported to have oblique-reverse, right-lateral slip directed 40° from southeast (rake) on a fault plane striking 310° and dipping 70° SW. (Oppenheimer, 1990). Focal-mechanism solutions of selected aftershocks, however, suggest that other fault segments with different orientations also slipped. The model of subsurface fault geometry and fold development discussed in the preceding section (see fig. 8) also provides insight into slip direction on the various fault segments. To conserve rock volume during long-term fault slip, both dip-slip and strike-slip components of motion must be resolved between the adjacent fault segments illustrated in figure 8*A*. Slip directions are also constrained to avoid opening large subsurface voids between fault surfaces.

In the following subsections, we combine fault-slip information provided by the regional seismicity with reasonable slip directions inferred from our balanced models to describe slip along the San Andreas fault system during the Loma Prieta rupture. To test the validity of our inferred slip directions on different fault segments, we compare these slip directions with shear-stress directions resolved onto the fault planes from regional stresses. The regional stresses were derived by Michael and others (1990) by using an inverse method from preearthquake and postearthquake seismicity. In the following subsection, assuming that these coseismic-slip directions approximate the long-term slip directions, we calculate long-term slip rates on the San Andreas fault and uplift rates above the Loma Prieta fault segment. We then compare the results with the uplift rates calculated by Anderson (1990) and Valensise and Ward (1991) from dated marine terraces on the nearby Santa Cruz coastline. Finally, we calculate uplift rates for the Zayante fault, which did not rupture in the earthquake, by analysis of syntectonic (growth) sediment. Electric logs from wells located on opposite sides of the fault record different stratal thicknesses that have resulted from uplift of one side of the fault relative to the other.

FAULT-SLIP DIRECTIONS AND REGIONAL STRESS

It has long been proposed that the direction of slip is equivalent to the direction of resolved shear stress on a fault plane (Bott, 1959). Thus, a straightforward test of the validity of the slip directions inferred from our models in the Loma Prieta epicentral zone is to compare them with the applied shear-stress directions calculated from the regional stress field. Michael and others (1990) examined events before and during the earthquake, using an inverse method (Michael, 1987a, b) to estimate the relative magnitudes and directions of the three principal stress axes. They calculated tensor components for the southern, the shallow and deep central, and the northern parts of the Loma Prieta rupture zone. We test whether our inferred slip directions (determined from fault geometry and models, not first motions) agree with the shear-stress directions resolved on the various fault segments by the regional stresses estimated by Michael and others (1990). This analysis simply confirms that the slip directions in our model (fig. 8) are reasonable within the inferred stress field. We used the Fortran program FMSI of Gephart (1990) to resolve shear-stress directions on the fault segments from regional stresses.

Our fault-bend-folding model has right lateral strike-slip motion along the San Andreas fault (fault segment 1, fig. 8*A*) in the southern part of the Loma Prieta rupture zone, which is consistent with focal-mechanism solutions of local aftershocks (Oppenheimer, 1990) and strong motions (Beroza, 1991). We find that components of the inferred regional stress tensor (σ_1 trends 000°, σ_2 is vertical, ϕ^*=0.39, R=0.61, fig. 11*A*; Michael and others, 1990)[1] resolve into a shear stress on the southern segment of the San Andreas fault (320°, 82° W.), directed essentially parallel to the inferred horizontal strike-slip vector 1. The angle between the resolved shear stress and the fault-slip direction measured in the fault plane, which is an accepted measure of error between slip and a predicted stress state, is here less than 1°. Pure right-lateral strike slip on the San Andreas fault southeast of the restraining bend at Loma Prieta, as inferred from geologic evidence, is therefore consistent with regional seismicity and the inferred stress field.

Michael and others (1990) reported a stress tensor within the 95-percent-confidence limit of their inversion, yielding a 25° discrepancy between the applied shear-stress direction and the slip direction of the main shock on the Loma Prieta fault segment (310°, 70° W.; rake, 40° from SE.; Oppenheimer, 1990). They indicated that this discrepancy is less than the average variance in the data used in the inversion and that the main-shock slip direction is therefore consistent with their predicted regional stresses. The main-shock slip direction inferred from the seismicity (Oppenheimer, 1990) is also consistent with the subsurface fault geometry that we derive by analysis of the hypocentral locations (fig. 8*A*). The slip vector very closely approximates the line of intersection between the Loma Prieta fault segment and the southeastern section of the San Andreas fault (fig. 12). In fact, slip on two simultaneously active fault planes must be in the direction of the line of intersection of the two faults to avoid subsequent deformation of the fault blocks. Slip in any other direction on the Loma Prieta fault segment would require additional deformation along the faults to close subsurface voids or to alleviate "room" problems. Similarly, we suggest a slip direction on a shallow segment of the San Andreas fault (310°, 78° W.; fault segment 3, fig. 8*A*) above the Loma Prieta fault segment, parallel to the intersection of this fault with a bounding segment of the San Andreas fault (fault segment 1, fig. 8*A*). We calculate that another stress tensor (σ_1=029°, σ_3 is vertical, ϕ^*=0.6, R=0.4) within the 95-percent-confidence limit of Michael and others (1990) applies a shear-stress direction parallel to the inferred slip direction on this shallow fault segment (fig. 11*B*).

These results suggest that the slip directions in the Loma Prieta epicentral zone calculated from our balanced models and the fault geometry defined by hypocentral locations are generally consistent with the inferred regional stresses. Slip directions on the San Andreas fault southeast and northwest of the restraining bend parallel the shear-stress directions applied by stress tensors that lie within the confidence limit of inferred regional stresses (fig. 11).

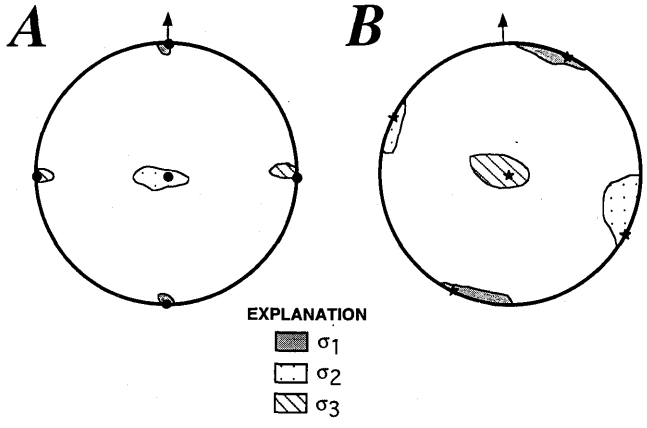

Figure 11.—Equal-area stereonets showing 95-percent-confidence limits of principal stress directions (σ_1 through σ_3) in Loma Prieta epicentral zone calculated by Michael and others (1990). Symbols (dots, stars) mark principal stress directions that yield shear-stress parallel to the slip directions we infer on various fault segments shown in figure 8*A*. Components of stress tensors were inverted by using preearthquake seismicity in south (*A*) around fault segment 1 in figure 8*A* and shallow aftershocks in center of Loma Prieta rupture (*B*) around fault segment 3 in figure 8*A*.

[1] $\phi^*=(\sigma_2-\sigma_3)/(\sigma_1-\sigma_3)$, where σ_1, σ_2, and σ_3 are the three principal stresses, from most compressional to most tensional (Angelier, 1979), and $R=1-\phi^*=(\sigma_2-\sigma_1)/(\sigma_3-\sigma_1)$ (Etchecopar and others, 1981). Note that $\phi^*\neq\phi$, the change in fault dip of the fault-bend-folding equations in figure 5.

Slip during the main shock on the Loma Prieta fault segment, although it does not agree as well with the applied shear-stress direction, is consistent with the inferred regional stresses (Michael and others, 1990). Moreover, the main-shock slip direction is consistent with the subsurface fault geometry in the Loma Prieta epicentral zone (fig. 12). The line of intersection of the San Andreas fault and the Loma Prieta fault segment may have set a geometric boundary condition controlling the direction of slip during the earthquake. These faults, acting as discontinuities, may have locally modified the regional stress field, resulting in the geometrically favorable slip direction of the main shock.

The continuous lateral extent and similar dips of the limbs of the Glenwood syncline (fig. 2) suggest that the subsurface fault geometry in the Loma Prieta epicentral zone has remained essentially uniform throughout the Quaternary. Significant changes in this fault geometry would produce irregular fold limbs and offsets in the synclinal-axial surface. Therefore, we suggest that the geometrically favorable slip directions of the Loma Prieta rupture may provide a reasonable estimate of the long-term slip direction on these fault segments. In the following section, we explore this suggestion, using these inferred slip directions and estimates of the long-term slip rate on the San Andreas fault to calculate slip and uplift rates in the Loma Prieta epicentral zone.

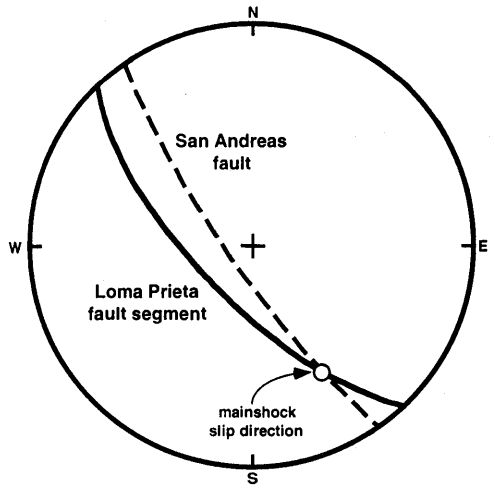

Figure 12.—Equal-area stereonet showing orientation of the Loma Prieta fault segment (solid curve) and a segment of the San Andreas fault (dashed curve) southeast of restraining bend (fault segments 2 and 1, respectively, fig. 8A). Line of intersection of fault planes closely corresponds to orientation of main-shock slip direction calculated from first-motion studies by Oppenheimer (1990).

RECURRENCE INTERVALS, LONG-TERM SLIP, AND UPLIFT RATES

The long-term motion inferred by geologic and seismic (Hall, 1984) and geodetic (Prescott and others, 1981) data is consistent with the predominantly right lateral strike-slip motion derived from focal-mechanism solutions of aftershocks located on the San Andreas fault in the southeastern part of the Loma Prieta rupture zone (Oppenheimer, 1990). Geologic and geodetic estimates of the long-term slip rate on the San Andreas fault in this area are reported at 12 mm/yr (Hall, 1984) and 12.2 mm/yr (Prescott and others, 1981). Slip on the Loma Prieta fault segment inferred from first-motion studies, however, is oblique-reverse, right-lateral motion (Oppenheimer, 1990). Geodetic data suggest that 1.6±0.3 m of strike slip and 1.2±0.3 m of reverse slip (total slip, 2±0.4 m) took place during the earthquake (Lisowski and others, 1990), resulting in a ratio of strike slip to dip slip of 1.3. Similarly, Marshall and others (1991) reported a best-fit model to vertical deformation with 2.1±0.1 m of total slip. As discussed in the preceding subsection, the slip direction of the Loma Prieta main shock parallels the intersection of the San Andreas fault with the Loma Prieta fault segment (fig. 12). Therefore, as modeled in figure 3, rigid-block translation over these faults would produce parallel slip on the Loma Prieta fault segment (vector **C**, fig. 13) and on the adjacent segment of the San Andreas fault (vector **B**). If long-term slip on this small segment of the San Andreas fault were not equivalent to slip on the Loma Prieta fault segment, then a large amount of unrecognized hanging-wall deformation would have to occur to conserve volume during deformation and to collapse large subsurface voids. Similarly, the long-term-slip vector on the small segment of the San Andreas fault (vector **B**) must contain a strike-slip component equivalent to the long-term slip rate on the San Andreas fault farther to the southeast of the restraining bend (vector **A**, fig. 13). Using the 12-mm/yr rate (vector A) and simply solving the slip-vector triangle yields a 15.2-mm/yr long-term slip rate on the small segment of the San Andreas fault (vector **B**) and the adjacent Loma Prieta fault segment (vector **C**). This change in the long-term-slip vectors from predominantly strike slip in the southeast to oblique-reverse, right-lateral slip in the northwest is consistent with the slip directions of the earthquake inferred from strong motions (Beroza, 1991; Steidl and others, 1991) and vertical deformation (Marshall and others, 1991). The 15.2-mm/yr long-term slip rate on the Loma Prieta fault segment (310°, 70° W.) resolves to a dip-slip rate of 9.8 mm/yr and a strike-slip rate of 11.6 mm/yr that correspond to the estimated 1.3 slip ratio of the Loma Prieta main shock (Lisowski and others, 1990). In addition, this increase in slip rate on the Loma Prieta fault segment in the restraining bend may explain why the Loma Prieta and, possibly, other strike-slip earthquakes initiate at fault bends.

Resolution of the slip-vector triangle that includes the 9.8-mm/yr dip-slip rate on the 70° SW.-dipping Loma Prieta fault segment yields an uplift rate above the fault of 9.2 mm/yr (fig. 13). However, using dated, uplifted marine terraces along the Santa Cruz coastline, several investigators calculated much smaller average uplift rates of 0.77 mm/yr (Valensise and Ward, 1991) and 0.8 mm/yr (Anderson, 1990) adjacent to the fault in the Loma Prieta epicentral zone. They suggested that repeated Loma Prieta-type events, which encompass all the slip on the adjacent San Andreas fault, would produce higher uplift rates than they calculated. They also suggested that ruptures similar to the 1989 earthquake alternate with events on the fault that consist of greater amounts of strike slip relative to reverse motion. They contended that this alternation would allow all of the long-term slip on the San Andreas fault to be transferred to the Loma Prieta fault segment, yet produce lower uplift rates consistent with their results. Alternatively, we suggest that slip in the 1989 earthquake parallel to the line of intersection of the two fault segments that form the restraining bend (fig. 12) was not fortuitous. Slip in any other direction on the Loma Prieta fault segment would necessitate additional deformation, as yet unrecognized, to conserve volume and close subsurface voids caused by slip over this fault-segment intersection. Furthermore, as Crowell (1974a, b) recognized, strike-slip motion in this restraining bend necessitates uplift or lateral motion of material away from the fault bend to conserve rock volume. That is, pure strike-slip motion on the Loma Prieta fault segment cannot cause uplift. Lateral motion of material away from the restraining bend would require additional reverse or thrust faulting in the western block in the vicinity of the fault bend, which has not been observed (fig. 2). Strike-slip motion on a near-vertical San Andreas fault that bends and passes below the Loma Prieta fault segment does not avoid these conservation-of-volume restrictions. Therefore, we suggest that when motion occurs on the San Andreas-Loma Prieta fault system, slip likely occurs parallel to the line of intersection between the two fault segments.

Several effects may explain the discrepancy between the uplift rates calculated by Anderson (1990) and Valensise and Ward (1991) and the higher uplift rates that we calculated by assuming repeated Loma Prieta-type events. Foremost, the geometrically constrained values that we calculated are uncorrected for isostatic compensation. Presumably, repeated thrusting in Loma Prieta-type events would produce crustal thickening that would lead in turn

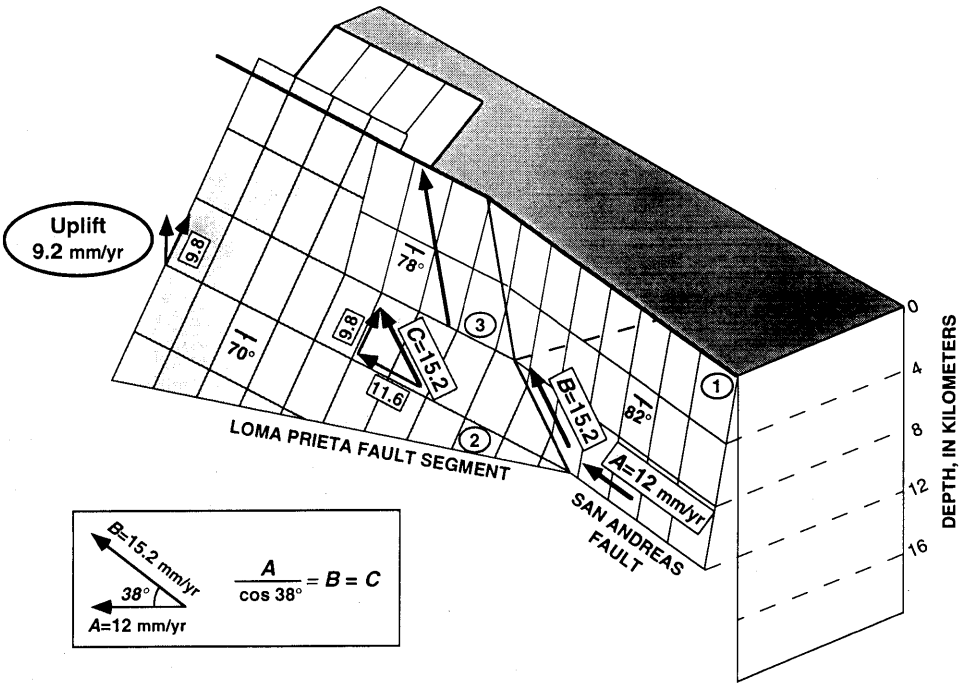

Figure 13.—Subsurface fault model of Loma Prieta epicentral zone (see fig. 8A), with long-term-slip vectors calculated by using inferred slip directions and 12 mm/yr (vector **A**) estimate of long-term slip rate on the San Andreas fault southeast of rupture zone (Hall, 1984). Slip rates on the Loma Prieta fault segment (vector **C**) and the adjacent San Andreas fault (vector **B**) are equal (both 15.2 mm/yr) and in direction of 1989 main shock. 15.2 mm/yr rate was calculated by assuming that slip on small segment of the San Andreas fault (vector **B**) must account for 12 mm/yr of right-lateral strike slip southeast of rupture zone (vector **A**). 15.2 mm/yr rate on the Loma Prieta fault segment (vector **C**) resolves to a 9.8-mm/yr dip-slip and 11.6-mm/yr strike-slip component and a 9.2-mm/yr uplift rate above fault (uncorrected for isostatic compensation).

to downward vertical displacements of the lithosphere to achieve stable density distributions within the crust and upper mantle (Bott, 1971; Suppe, 1985). Therefore, uplift rates measured at the surface would be only a fraction of those summed from slip in repeated Loma Prieta-type events. Using the equations of pointwise isostasy,

$$\Delta E = \Delta h_c + \Delta h_m + \Delta h_a$$

and

$$\Delta(\rho_c h_c) + \Delta(\rho r_m h_m) + \Delta(\rho_a h_a) = 0,$$

where ΔE is the total change in elevation, h_c is the thickness of the crust, h_m is the thickness of the mantle lithosphere, h_a is the thickness of the mantle asthenosphere, ρ_c is the density of the crust, ρ_m is the density of the mantle lithosphere, and ρ_a is the density of the mantle asthenosphere. Using the reasonable average densities of Bott (1971) and Suppe (1985), and assuming no change in the thickness of mantle lithosphere,

$$(3{,}000\ \text{kg/m}^3)\Delta h_c + (3{,}300\ \text{kg/m}^3)\Delta h_a = 0$$

and

$$\Delta h_c + \Delta h_a = \Delta E.$$

Therefore, for each 9.2 mm/yr of uplift and thickening of the crust, only 0.8 mm/yr of total elevation change occurs above the fault after isostatic compensation:

$$(3{,}000\ \text{kg/m}^3)(9.2\times10^{-3}\text{m}) + (3{,}300\ \text{kg/m}^3)\Delta h_a = 0$$

and

$$9.2\times10^{-3}\ \text{m} + \Delta h_a = \Delta E.$$

Solving for Δh_a and ΔE,

$$\Delta h_a = -8.4\times10^{-3}\ \text{m} = -8.4\ \text{mm}$$

and

$$\Delta E \approx 0.8\times10^{-3}\ \text{m} = 0.8\ \text{mm}.$$

This corrected uplift rate (0.8 mm/yr) falls within the range of uplift rates (0.77–0.8 mm/yr) reported by Valensise and Ward (1991) and Anderson (1990), which also account for elasticity and isostatic compensation of the crust. Although we cannot exclude the possibility of other types of slip events in the Loma Prieta epicentral zone, we suggest that the uplift rates calculated in these other studies are generally consistent with the rates we derive by assuming that all long-term slip on the San Andreas fault is released in repeated Loma Prieta-type events. It is therefore plausible that the 1989 earthquake was a typical rupture along this part of the San Andreas fault system and that long-term slip rates on the San Andreas fault can be used to estimate earthquake-recurrence intervals.

To consume slip on the San Andreas fault at a rate of 12 mm/yr, oblique slip must occur on the Loma Prieta fault segment at an average rate of 15.2 mm/yr (fig. 13). Assuming that this slip rate is correct, if all of this slip occurs during earthquakes similar to the 1989 Loma Prieta main shock, which released 2±0.4 m of slip (Lisowski and others, 1990), then an earthquake should recur every 132±26 yr. The 1865 Santa Cruz Mountains earthquake may therefore be a viable candidate for the previous break on this fault segment (Toppozada and others, 1981). In accordance, McNutt and Toppozada (1990) reported that the 1865 earthquake had an estimated magnitude (M=6.6) and epicentral location similar to those of the 1989 earthquake.

MOTION ON THE ZAYANTE FAULT

We have presented evidence that the Glenwood syncline developed by slip over a subsurface fault bend between the San Andreas fault and the Loma Prieta fault segment. Similarly, we suggest that the deformed Purisima Formation along the Scotts Valley syncline indicates that motion has occurred along a restraining bend in the Zayante fault in the Loma Prieta epicentral zone since the early Pliocene. Deformed Pliocene and Quaternary horizons (Hall and others, 1974; Clark and others, 1984) and several surface fault breaks through Quaternary sedimentary deposits to the south of this bend (fig. 2) suggest recent activity on the Zayante fault. To constrain fault-motion history and to identify active fault segments without the aid of recorded seismicity, we apply the technique of Bischke and Suppe (1990) and Bischke (in press) to analyze growth sediment coevally deposited with fault motion. Thickness changes in growth sedimentary sequences measured in electric logs from wells that straddle the fault record rates of uplift across splays of the Zayante fault. Only the differential dip-slip component of motion between any two wells is recorded. A brief description of the method follows.

The vertical-displacement method ($\Delta D/d$) identifies expanded or syntectonic sedimentary sections that record the local tectonic history. An assumption of this method is that the sedimentation rate is greater than or nearly equal to the uplift rate (Bischke, in press). For example, the method may consider two wells located on opposite sides of a fault (fig. 14). If sedimentary sequences can be correlated between these two wells, then the vertical distance that the sequences have been displaced relative to one another (ΔD) can be determined. A convenient graphical method of determining growth section in the two wells is to plot the relative vertical displacement between the sequence boundaries (ΔD) versus

the depth to the same horizons in the structurally higher well (*d*). In a plot of strata deposited before fault motion, data points that correspond to correlated horizons of pregrowth strata lie along a near-horizontal line (fig. 14*A*). However, in a similar plot of strata deposited coevally with fault motion, growth horizons lie along sloping lines or curves (fig. 14*B*). The steep slope of the lines results from thickness changes in strata on opposite sides of the fault brought on by the accumulation of thicker sediment on the downthrown side of the fault. Using this plotting convention, large positive slopes on these diagrams represent expanded growth sections, whereas large negative slopes represent reduced or condensed sections. This technique, applied to strata on opposite sides of a fault, therefore provides an easy method of distinguishing between growth and pregrowth strata that identify periods of fault motion and quiescence.

In wells located across splays of the Zayante fault (fig. 2) we are able to correlate 17 stratal sequences within the Pliocene and Pleistocene section (fig. 15). Motion along splays of the Zayante fault between Pierce, Light, and Blake wells (fig. 2) are recorded in growth-sedimentary sections. Lacking significant onlap, the well section (fig. 15) indicates no substantial bathymetry/topography across these fault splays during deposition of the Pliocene and Pleistocene sediment. Therefore, the sedimentation rate exceeded the rate of tectonic uplift during this period. A vertical-displacement/depth ($\Delta D/d$) diagram generated from Pierce and Light well-log data shows that growth (in the form of an expanded section) was initiated during the late Pliocene, between the deposition of horizons 5 and 6 (fig. 16). The sloping, linear growth above horizon 5 shows that section expansion has continued into the Quaternary. This expansion rate, continuing into the Holocene, also appears to account for the present terrace relief across the fault (fig. 16), suggesting that the Pleasant Valley splay of the Zayante fault may still remain active.

A $\Delta D/d$ plot of horizons recorded in Light and Blake wells (fig. 17) shows a slightly different growth history across the central splay of the Zayante fault (fig. 2). The negative slope of the growth phase between horizons 1 to 9 indicates a condensed section that is contemporaneous with the expanded section between Pierce and Light wells (fig. 16). This west-to-east transition from an expanded section across the western splay of the Zayante fault to the condensed section across the central splay suggests that a delta may have prograded away from the western, uplifted block of the Pleasant Valley fault (fig. 18). The condensed section above horizon 9, and the slightly expanded section between horizons 9 and 17 between Light and Blake wells (fig. 17), suggest that motion on the central splay of the Zayante fault was initiated before that on the western splay. The 670-m expanded section below 950-m in Blake well (figs. 15, 17) records early (pre-Pliocene) motion on the central splay of the Zayante fault. Motion on this ancestral Zayante fault created the basin between the Zayante and San Andreas faults (fig. 15; Clark and Rietman, 1973).

The surface breaks and expanded and condensed sections across these two splays of the Zayante fault, which merge both to the north and south (fig. 2), suggest that these splays have moved during the Quaternary. Although there is no confirmed historical seismicity on the Zayante fault, the available evidence is consistent with its activity. Therefore, the Zayante fault may pose an earthquake hazard to the adjacent populated area. If this fault is active, our estimated average uplift rate of the west side relative to the east side of the fault splays has been small (≈0.07 mm/yr) since the beginning of the Pleistocene (≈1.8 Ma). This 0.07-mm/yr uplift rate falls within the range of preferred uplift rates (0.06–0.1 mm/yr) along the Zayante fault reported by Clark and others (1984). However, the location of the Scotts Valley syncline in the restraining bend and the orientation of this near-vertical fault (fig. 2) with respect to the regional stress field (Michael and others, 1990) and the San Andreas fault suggest that most recent fault motion is strike slip. Further analysis of geologic data, or future seismicity, is required to constrain more precisely the slip rate and earthquake hazard posed by the Zayante fault.

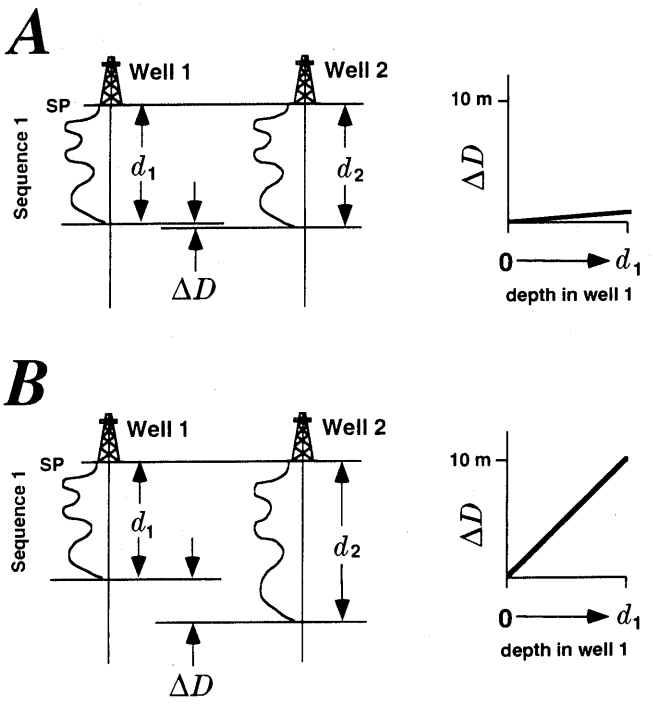

Figure 14.—Schematic diagrams of stable (*A*) and unstable (*B*) tectonic environments where stratigraphic sequences can be correlated between wells, with plots of vertical displacement ΔD of correlated pregrowth (*A*) and growth (*B*) horizons versus depth d to horizons in structurally higher well. In figure 14*A*, shallow slope of $\Delta D/d$ curve establishes a pregrowth section; in figure 14*B*, steep slope of $\Delta D/d$ curve indicates growth sedimentation, whereby section expansion is attributed to differential tectonic motion between wells, with thicker strata accumulating on downthrown fault block.

SUMMARY AND CONCLUSIONS

Right-lateral motion along left-stepping restraining bends in the San Andreas and Zayante faults has resulted in thrusting and uplift of the hanging-wall rocks. Thrusting over nonplanar fault surfaces within these restraining bends has folded the hanging-wall strata into synclines. Fold growth is illustrated in geometrically and kinematically reasonable balanced models constructed by using fault-bend-folding theory (Suppe, 1983). Application of these models to the Loma Prieta epicentral zone yields predictions of the dip and location of subsurface bends in the fault segments. We have confirmed these predictions for the San Andreas fault and the Loma Prieta fault segment by using the hypocenters of aftershocks to determine subsurface fault geometry. The consistent subsurface fault geometry inferred by these two independent methods suggests that fault-bend folding is a viable theory for the origin of the folds that lie adjacent to strike-slip faults.

The seismicity, the surface geology, and the subsurface models indicate that the Loma Prieta epicentral zone consists of several active fault segments that compose the San Andreas fault system. Slip on the various fault segments, inferred from seismicity, geodesy, and the subsurface fault geometry, is found to be consistent with regional stresses, assuming that the slip directions on the faults parallel the applied shear-stress directions. Furthermore, the subsurface fault geometry of the Loma Prieta epicentral zone suggests

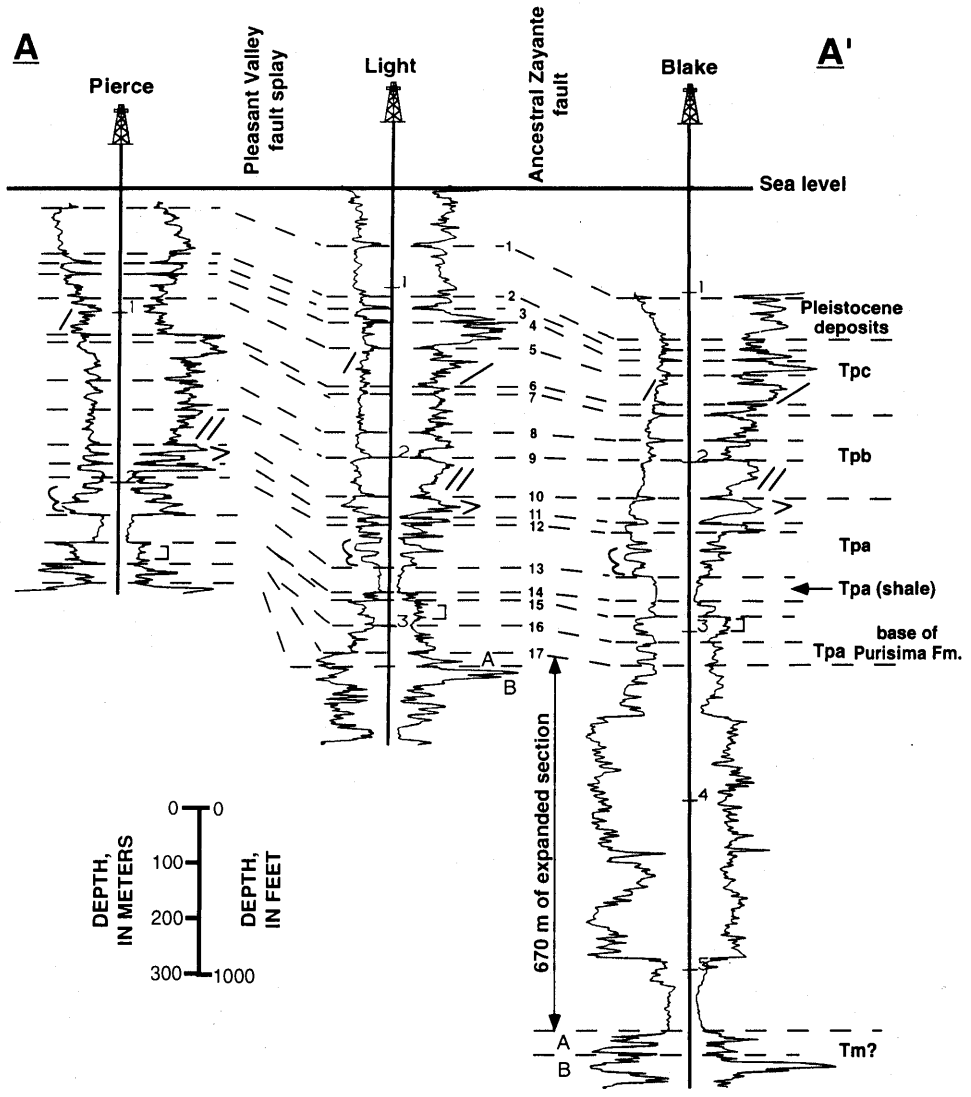

Figure 15.—Correlation section *A–A'* of electric-resistivity and spontaneous-potential logs from wells located on opposite sides of strands of the Zayante fault (see fig. 2 for locations). A total of 17 Pliocene and Pleistocene stratigraphic sequences are correlated between wells, with expanded or growth section defining periods of fault motion. Units: 1 through 17, Pliocene and Pleistocene stratigraphic sequences; A and B, horizons in Miocene section; Tpa through Tpc, Purisima Formation (upper Miocene and Pliocene), units a through c; Tm?, Monterey(?) Formation (middle Miocene).

that long-term slip must increase in this restraining bend. The 12-mm/yr long-term slip rate on the San Andreas fault southeast of the Loma Prieta rupture zone must increase to a 15.2-mm/yr slip rate on the Loma Prieta fault segment.

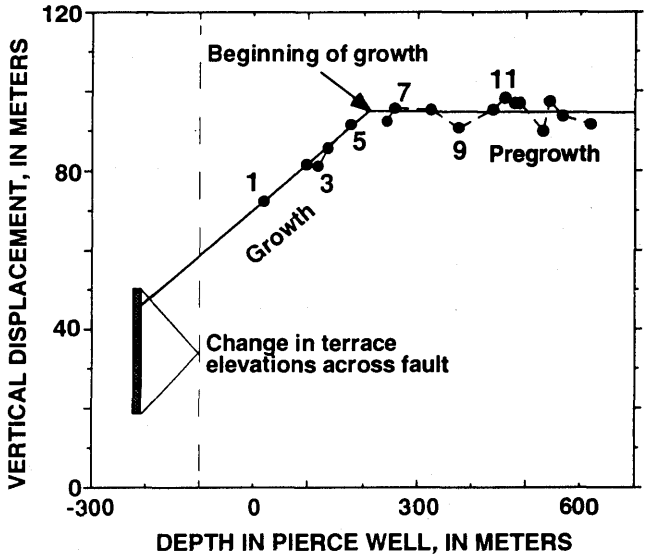

Figure 16.—Vertical displacement of correlated stratigraphic horizons between Pierce and Light wells versus depth to horizons in Pierce well (see fig. 15 for locations). Horizontal least-squares best-fit curve through data marks an early period of pregrowth, below 200-m depth, followed by expanded section (growth) above 200-m depth. Pliocene and Quaternary expanded section is attributed to coeval motion on splay of the Zayante fault between wells. Fault motion continuing to present may account for change in terrace elevations across fault.

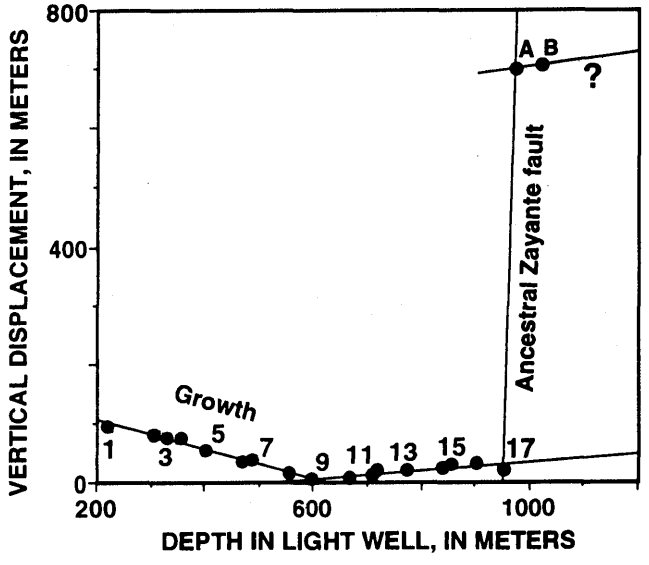

Figure 17.—Vertical displacement of correlated stratigraphic horizons between Blake and Light wells versus depth to horizons in Light well (see fig. 15 for locations). Inclined least-squares best-fit curves through data mark early (below 960-m depth) and more recent (above 600-m depth) periods of growth. Early Miocene growth is attributed to motion on the ancestral Zayante fault.

This increase in slip rate in the restraining bend may explain why the 1989 Loma Prieta and, possibly, other strike-slip earthquakes initiate at fault bends. In addition, long-term uplift rates calculated by using our observed fault geometry and reported long-term slip rates on the San Andreas fault in the region agree with the rates calculated by Anderson (1990) and Valensise and Ward (1990) from marine-terrace elevations along the Santa Cruz coastline, once they are corrected for isostatic compensation. Moreover, this result suggests that the 1989 earthquake may have been a typical rupture for this section of the San Andreas fault system. Furthermore, if slip on the San Andreas fault is released in repeated Loma Prieta-type events, then an earthquake should recur every 132±26 yr. Expanded sedimentary sections deposited across splays of the Zayante fault suggest that this fault is also presently active. Therefore, faults in the Santa Cruz Mountains continue to pose a significant earthquake hazard to the adjacent populated area.

ACKNOWLEDGMENTS

This research was supported by National Earthquake Hazards Reduction Program (NEHRP) grant 14–08–0001–G1827 from Princeton University and by Texaco, Inc. We thank Chris Connors, Paul Genovese, Stephen Hook, Craig Nicholson, David Pollard, and Leonardo Seeber for helpful discussions and comments. Thanks go also to Daniel Tearpock for reviewing well-log correlations, and to John Gephart for providing his program FMSI, which we used to resolve shear-stress directions on the fault segments from regional stresses. In addition, we are grateful for beneficial reviews of the manuscript by Joseph Clark, Oona Scotti, Robert Simpson, and George Havach.

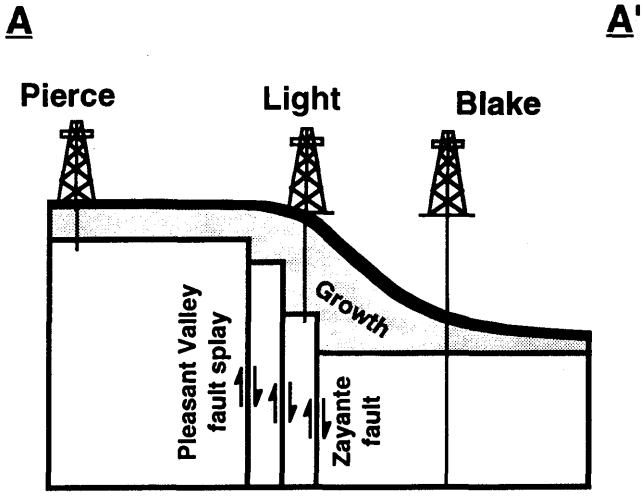

Figure 18.—Schematic diagram showing thicker accumulation of deltaic sediment on downthrown side of the Zayante fault system along line A–A′ (see fig. 2 for locations). Arrows indicate directions of dip-slip motion.

REFERENCES CITED

Anderson, R.S., 1990, Evolution of the northern Santa Cruz Mountains by advection of crust past a San Andreas fault bend: Science, v. 249, no. 4967, p. 397–401.

Angelier, Jacques, 1979, Determination of the mean principal directions of stresses for a given fault population: Tectonophysics, v. 56, no. 3–4, T17–T26.

Beroza, G.C., 1991, Near-source modeling of the Loma Prieta earthquake: Evidence for heterogeneous slip and implications for earthquake hazard: Seismological Society of America Bulletin, v. 81, no. 5, p. 1603–1621.

Bischke R.E., in press, Interpreting sedimentary growth structures from well-log and seismic data, with examples: American Association of Petroleum Geologists Bulletin.

Bischke, R.E., and Suppe, John, 1990, Calculating uplift rates on the Zayantes fault utilizing well log correlations [abs.]: Eos (American Geophysical Union Transactions), v. 71, no. 17, p. 555.

Bott, M.H.P., 1959, The mechanics of oblique slip faulting: Geological Magazine, v. 96, no. 2, p. 109–117.

———1971, The interior of the earth: London, Edward Arnold, 315 p.

Brabb, E.E., 1989, Geologic map of Santa Cruz County, California: U.S. Geological Survey Miscellaneous Investigations Series Map I–1905, scale 1:62,500.

Clark, J.C., 1981, Stratigraphy, paleontology, and geology of the central Santa Cruz Mountains, California Coast Ranges: U.S. Geological Survey Professional Paper 1168, 51 p.

Clark, J.C., and Rietman, J.D., 1973, Oligocene stratigraphy, tectonics, and paleogeography southwest of the San Andreas fault, Santa Cruz Mountains and Gabilan Range, California Coast Ranges: U.S. Geological Survey Professional Paper 783, 18 p.

Clark, M.M., Harms, K.K., Lienkaemper, J.J., Harwood, D.S., Lajoie, K.R., Matti, J.C., Perkins, J.A., Rymer, M.J., Sarna-Wojcicki, A.M., Sharp, R.V., Sims, J.D., Tinsley, J.C., III, and Ziony, J.I., 1984, Preliminary slip-rate table and map of late-Quaternary faults of California: U.S. Geological Survey Open-File Report 84–106, 12 p.

Crowell, J.C., 1974a, Origin of late Cenozoic basins in southern California, *in* Dickinson, W.R., ed., Tectonics and sedimentation: Society of Economic Paleontologists and Mineralogists Special Publication 22, p. 190–204.

———1974b, Sedimentation along the San Andreas Fault, *in* Dott, R.H., Jr., and Shaver, R.H., eds., Modern and ancient geosynclinal sedimentation: Society of Economic Paleontologists and Mineralogists Special Publication 19, p. 292–303.

Curray, J.R., and Moore, D.G., 1984, Geologic history of the mouth of the Gulf of California, *in* Crouch, J.K., and Bachman, S.B., eds., Tectonics and sedimentation along the California margin: Society of Economic Paleontologists and Mineralogists, Pacific Section Field Trip Guidebook, v. 38, p. 17–35.

Dietz, L.D., and Ellsworth, W.L., 1990, The October 17, 1989, Loma Prieta, California, earthquake and its aftershocks; geometry of the sequence from high-resolution locations: Geophysical Research Letters, v. 17, no. 9, p. 1417–1420.

Etchecopar, Arnaud, Vasseur, Guy, and Daignieres, Marc, 1981, An inverse problem in microtectonics for the determination of stress tensors from fault striation analysis: Journal of Structural Geology, v. 3, no. 1, p. 51–65.

Gephart, J.W., 1990, FMSI; FORTRAN program for inverting fault/slickenside and earthquake focal mechanism data to obtain the regional stress tensor: Computers and Geosciences, v. 16, no. 7, p. 953–989.

Hall, N.T., 1984, Holocene history of the San Andreas fault between Crystal Springs Reservoir and San Andreas Dam, San Mateo County, California: Seismological Society of America Bulletin, v. 79, no. 1, p. 281–299.

Hall, N.T., Sarna-Wojcicki, A.M., and Dupré, W.R., 1974, Faults and their potential hazards in Santa Cruz County, California: U.S. Geological Survey Miscellaneous Field Studies Map MF–626, scale 1:62,500, 3 sheets.

Lisowski, Michael, Prescott, W.H., Savage, J.C., and Johnston, M.J.S., 1990, Geodetic estimate of coseismic slip during the 1989 Loma Prieta, California, earthquake: Geophysical Research Letters, v. 17, no. 9, p. 1437–1440.

Marshall, G.A., Stein, R.S., and Thatcher, Wayne, 1991, Faulting geometry and slip from co-seismic elevation changes; the 18 October 1989, Loma Prieta, California, earthquake: Seismological Society of America Bulletin, v. 81, no. 5, p. 1660–1693.

McLaughlin, R.J., Clark, J.C., and Brabb, E.E., 1988, Geologic map and structure sections of the Loma Prieta 7.5′ quadrangle, Santa Clara and Santa Cruz counties, California: U.S. Geological Survey Open-File Report 88–752, 32 p., scale 1:24,000, 2 sheets.

McNutt, S.R., and Toppozada, T.R., 1990, Seismological aspects of the 17 October 1989 earthquake: Sacramento, California Division of Mines and Geology, 27 p.

Michael, A.J., 1987a, Use of focal mechanisms to determine stress; a control study: Journal of Geophysical Research, v. 92, no. B1, p. 357–368.

———1987b, Stress rotation during the Coalinga aftershock sequence: Journal of Geophysical Research, v. 92, no. B8, p. 7963–7979.

Michael, A.J., Ellsworth, W.L., and Oppenheimer, D.H., 1990, Coseismic stress changes induced by the Loma Prieta, California earthquake: Geophysical Research Letters, v. 17, no. 9, p. 1441–1444.

Muir, K.S., 1972, Geology and ground water of the Pajaro Valley area, Santa Cruz and Monterey Counties, California: U.S. Geological Survey Open-File Report, 33 p.

Oppenheimer, D.H., 1990, Aftershock slip behavior of the 1989 Loma Prieta earthquake: Geophysical Research Letters, v. 17, no. 8, p. 1199–1202.

Prescott, W.H., Lisowski, Michael, and Savage, J.C, 1981, Geodetic measurement of crustal deformation on the San Andreas, Hayward, and Calaveras faults near San Francisco, California: Journal of Geophysical Research, v. 86, no. B11, p. 10853–10869.

Rich, J.L., 1934, Mechanics of low-angle overthrust faulting as illustrated by Cumberland thrust block, Virginia, Kentucky, and Tennessee: American Association of Petroleum Geologists Bulletin, v. 18, no. 12, p. 1584–1596.

Schwartz, S.Y., Orange, D.L., and Anderson, R.S., 1990, Complex fault interactions in a restraining bend on the San Andreas fault, southern Santa Cruz Mountains, California: Geophysical Research Letters, v. 17, no. 8, p. 1207–1210.

Seeber, Leonardo, and Armbruster, J.G., 1990, Fault kinematics in the 1989 Loma Prieta rupture area during 20 years before that event: Geophysical Research Letters, v. 17, no. 9, p. 1425–1428.

Steidl, J.H., Archuleta, R.J., and Hartzell, S.H., 1991, Rupture history of the 1989 Loma Prieta, California, earthquake: Seismological Society of America Bulletin, v. 81, no. 5, p. 1573–1602.

Suppe, John, 1983, Geometry and kinematics of fault-bend folding: American Journal of Science, v. 283, no. 7, p. 684–721.

———1985, Principals of structural geology: Englewood Cliffs, N.J., Prentice-Hall, 537 p.

Suppe, John, Chou, G.T., and Hook, S.C., 1992, Rates of folding and faulting determined from growth strata, *in* McKlay, K.R., ed., Thrust tectonics: London, Unwin Hyaman, p. 105–121.

Tearpock, D., and Bischke, R.E., 1991, Applied subsurface geological mapping: Englewood Cliffs, N.J., Prentice-Hall, 648 p.

Toppozada, T.R., Real, C.R., and Parke, D.L., 1981, Preparation of isoseismal maps and summaries of reported effects for pre-1900 California earthquakes: California Division of Mines and Geology Open-File Report 81–11 SAC, 182 p.

Valensise, Gianluca, and Ward, S.N., 1991, Long-term uplift of the Santa Cruz coastline in response to repeated earthquakes along the San Andreas fault: Seismological Society of America Bulletin, v. 81, no. 5, p. 1694–1704.

This page intentionally left blank

TECTONIC PROCESSES AND MODELS

GEOLOGIC ASSESSMENT OF THE RELATIVE CONTRIBUTION OF STRIKE-SLIP FAULTING, REVERSE-SLIP FAULTING, AND BULK SQUEEZING IN THE CREATION OF THE CENTRAL SANTA CRUZ MOUNTAINS, CALIFORNIA

By Gianluca Valensise,
Istituto Nazionale di Geofisica, Rome

CONTENTS

ABSTRACT

To deduce the tectonic history of the central Santa Cruz Mountains in relation to the activity of the San Andreas fault, I have investigated the state of deformation of three geologic datums: the first (125 ka) and third (320 ka) Santa Cruz Terraces, and the base of the Upper Miocene and Pliocene Purisima Formation. Terrace data were taken from published work, whereas the Purisima Formation was investigated by reconstructing its structural contours on the basis of the elevations of its contact with underlying formations. The shape and elevation of these three datums were compared to explore the relative importance of two major tectonic processes: uplift of the Santa Cruz region by repeated Loma Prieta-type events, and progressive northwestward advection of the Pacific plate. The main conclusions of this study are that (1) the source of Loma Prieta-type events is stationary relative to the North American plate and in motion relative to the Pacific plate over time scales of ≈1 m.y.; (2) the central Santa Cruz Mountains have been uplifted at an average rate of <0.5 mm/yr after repeated oblique-reverse slip at a rate of ≈3 mm/yr on the Loma Prieta fault and northwestward motion of the Pacific plate at a geologic rate of 5 to 20 mm/yr; (3) only a fraction of the topography in the Santa Cruz Mountains is explainable by motion along the Loma Prieta fault; and (4) geologic evidence shows that much of the observed topography is generated by a process which dissipates plate-boundary-normal compression in the upper 5 km of the crust.

INTRODUCTION

Only a few hours after the earthquake, many scientists realized that more than one misconception existed regarding the Santa Cruz Mountains section of the San Andreas fault. The large and unexpected reverse-slip component of the earthquake's fault motion made clear that more complex processes are active along that section of the fault than only relative right-lateral motion of the Pacific and North American plates. Before 1989, however, the only evidence that could be used to foresee an anomalous behavior of this stretch of the plate boundary was a hypothesized slip deficit after the 1906 San Francisco earthquake (Thatcher, 1975) and the existence of several bends and other complexities in the local fault trend (Pampeyan, 1979) in some cases associated with anomalously high topography (Scholz, 1985). Among these complexities, the ≈40-km-long double restraining bend formed by the San Andreas fault in the southern Santa Cruz Mountains was universally thought to have played an important role in the tectonic evolution of the region.

Nonetheless, there was abundant geologic evidence of recent compression and uplift requiring a source of tectonic

strain other than pure lateral shear along the San Andreas fault. For example, Vanderhurst and others (1982) and Aydin and Page (1984) documented the extreme state of deformation of lower Pleistocene coastal and fluvial deposits along the foothills of the southern Santa Cruz Mountains east of the San Andreas fault; Clark and Rietman (1973), Greene and Clark (1979), Clark (1981), Crouch and others (1984) recognized the progressive transition from a marine to a subaerial environment of the ≈3-Ma-old top of the Tertiary sequence in the Santa Cruz Basin; and Harbert and Cox (1989) and Harbert (1991) correlated the onset of compression across the plate boundary and uplift of the Santa Cruz Mountains with a sharp change in Pacific-plate motion 4–3 Ma. Along the coast, more youthful records of sustained uplift were described as early as the 1890's by the first investigators of California geology, and later by Röde (1930), Alexander (1953), and Bradley and Griggs (1976). As many as five distinct wave-cut platforms composing one of the most spectacular flights of marine terraces in California were accurately described and mapped, but no one was able to identify the source of their uplift or to explain why their elevation differed so drastically from place to place.

LARGE-SCALE TECTONIC DEFORMATION ASSOCIATED WITH THE EARTHQUAKE

As soon as preliminary instrumental data on the earthquake became available, various investigators of its geologic impact focused on the coastal uplift that should have resulted from the large reverse-slip component shown by the focal mechanism. Compelling evidence of sudden uplift of the coastline in association with the earthquake came from several individuals who witnessed an impressive ocean retreat at different locations between Santa Cruz and Aptos (fig. 1). Early, rather old fashioned attempts to assess the extent of coseismic uplift were based on readings from two tidal gages located in downtown Santa Cruz and on the height of barnacles on the piers of the Capitola wharf. However, the only fact that could be ascertained was that the coseismic uplift was smaller than the uncertainty associated with nontidal fluctuations in ocean level (≈0.3 m) and with the height distribution of the barnacles with respect to the mean higher high water (≈0.5 m).

From a wider standpoint, McNally and others (1989) argued that the similarity between the region's landforms and the predicted pattern of coseismic uplift reflected a close relation between the seismic source and the recent evolution of the Santa Cruz Mountains. Their hypothesis was frustrated, however, by the observation that even though the general trend of uplift mimicked fairly well the gentle seaward slope of the southern Santa Cruz Mountains west of the San Andreas fault, subsidence was predicted for Loma Prieta, the highest point in the study area (1,155 m; LP, fig. 1). Other investigators used various types of evidence to hypothesize that the 1989 earthquake was not a characteristic San Andreas event (Kanamori and Satake, 1990) or that Loma Prieta-type events may be repetitive but do not represent the only active tectonic process in the Santa Cruz Mountains (Dietz and Ellsworth, 1990).

Subsequent investigators focused on the lowest emergent Santa Cruz terrace (figs. 1–3). Anderson (1990) and Valensise and Ward (1990) noticed that the pattern of elevation of the terrace's inner edge is reminiscent of the pattern of coseismic uplift predicted for the 1989 earthquake. Also, the elevation of a specific site on any of the best recognizable terraces appeared to be inversely proportional to the site's distance from the San Andreas fault—that is, from the source of tectonic strain. On the basis of a comparison between all the available terrace elevations and the predicted coseismic-uplift pattern, Anderson proposed a recurrence interval of ≈700 yr for a Loma Prieta-type event. Valensise and Ward (1991) performed a formal inversion to infer the full parameters of a fault that would raise the lowest terrace to its present elevation by repeated discrete slip events. The geometric parameters of their Geological Fault Model (GFM, fig. 4) turn out to be similar to those estimated for the earthquake, although the ratio of strike slip to reverse slip and the fault length were found to be significantly larger than those observed coseismically. Valensise and Ward (1991) also calculated a recurrence interval of ≈600 yr for a Loma Prieta-type event. Paradoxically, Anderson's and Valensise and Ward's solutions shared a similar estimate of recurrence interval, even though their proposed terrace ages and uplift rates differed completely.

A second major object of scientific dispute was identification of the source of uplift of the marine terraces between Santa Cruz and Point Año Nuevo (fig. 1), a stretch of the coast where 1989 uplift was mild (Marshall and others, 1991) but terrace elevations are comparable with those observed farther east. To account for the observed discrepancy, Anderson (1990) invoked the activity of a section of the San Andreas fault north of the 1989 rupture zone, whereas Anderson and Menking (1991) proposed a model based on oblique-reverse slip on the San Gregorio fault. In contrast, Valensise and Ward (1991) maintained that the existence of terraces west of Santa Cruz is consistent with repeated motion on the Loma Prieta fault alone, provided that the ratio of right-lateral to reverse slip is much larger than that observed in 1989, as predicted by the GFM. To reconcile the short-term (coseismic) and long-term (GFM) estimates of the fault rake, they hypothesized that what is shown in the geologic record is a combination of motion on the Loma Prieta fault as seen in 1989 and on the San Andreas fault proper. This hypothesis is further supported by the observation that the pattern of elevation of the first terrace between

Santa Cruz and Pajaro Valley requires a strong asymmetry in the distribution of uplift, regardless of the existence and elevation of terraces west of Santa Cruz. As first pointed out by K.R. Lajoie (unpub. data, 1991), connecting inner-edge positions with the same elevation (α–α′, β–β′, γ–γ′, fig. 4) results in a series of widely divergent lines. This

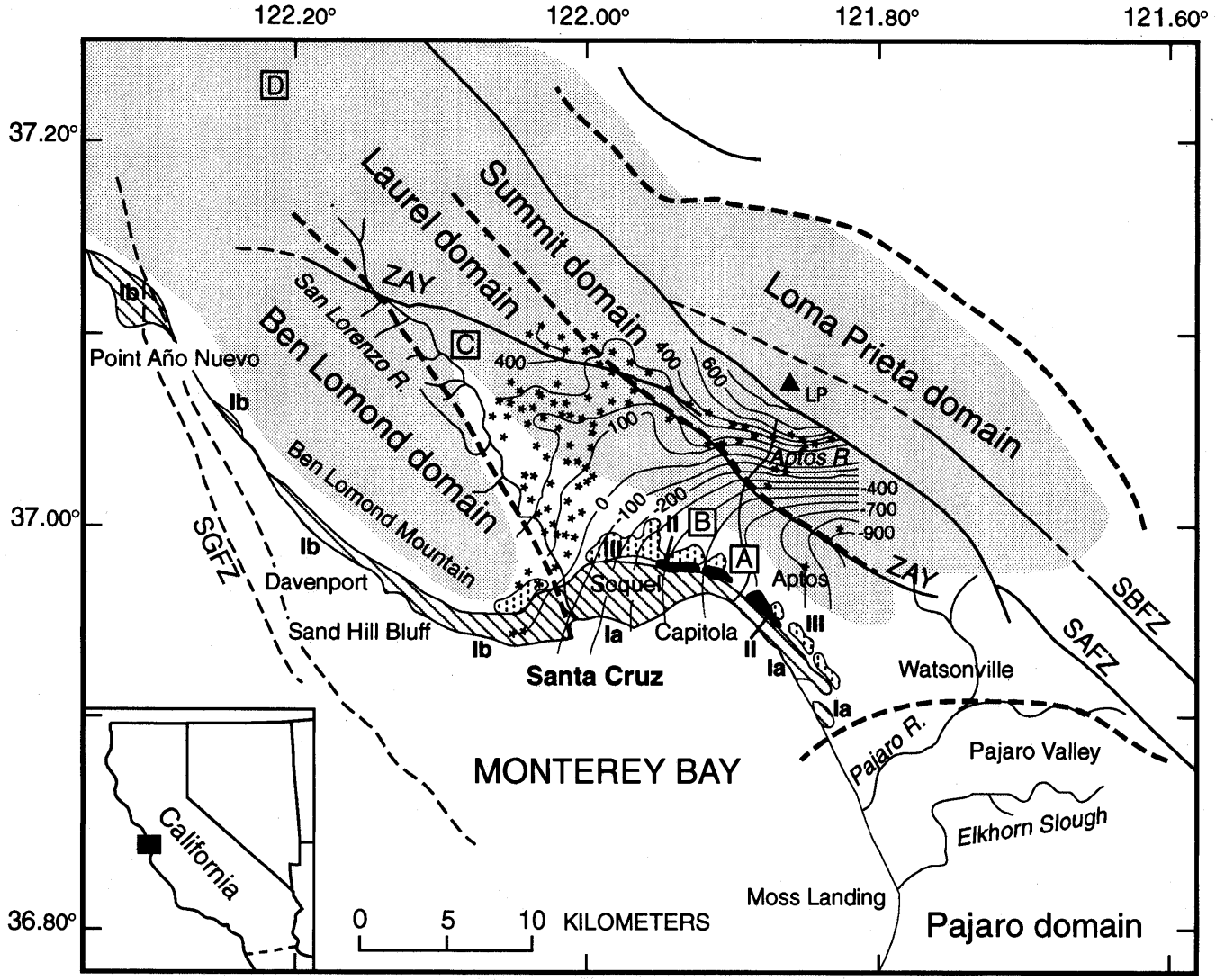

Figure 1.—Central Santa Cruz Mountains, Calif., showing location of major faults, marine terraces, and topographic domains associated with tectonic processes of varying nature and age. LP, Loma Prieta, highest point (elev, 1,155 m) in study area; SAFZ, San Andreas fault zone; SBFZ, Sargent-Berrocal fault zone (dashed where inferred); SGFZ, San Gregorio fault zone (dashed where inferred); ZAY, Zayante fault. Ia and Ib (diagonally ruled areas), western and eastern limbs, respectively, of First Terrace (Röde, 1930; Alexander, 1953), which Bradley and Griggs (1976) recognized as formed by three distinct platforms, highest of which coincides with platform of First Terrace as originally designated (two lower platforms not shown for simplicity); II (black areas) and III (stippled areas), Second and Third Terraces, respectively, as originally defined by Alexander between Santa Cruz and the Pajaro Valley (see fig. 2). Higher terraces recognized west of Santa Cruz do not correspond to those defined by Alexander and are not considered further here. A and B, culminations of First and Third Terraces, respectively; C, northwesternmost and highest outcrops of the Purisima Formation in the central Santa Cruz Mountains; D, southernmost outcrop of the Purisima Formation in the northern Santa Cruz Mountains. Stars, outcrops of base of the Purisima Formation (see fig. 7); contour interval, 100 m. Light shading indicates areas where elevation is above 300 m. On the basis of distribution of relief and gross geologic features, study area is divided into five topographic domains, extending original scheme by Aydin and Page (1984): (1) Laurel domain (elev, 0–450 m, avg 250 m), a hilly terrain that includes drainage basins of main streams originating in the central Santa Cruz Mountains southwest of the Zayante fault and that directly overlies source region of 1989 earthquake; (2) Ben Lomond domain (elev, 0–750 m, avg 500 m), comprising a prominent coastal range corresponding to a structural high of Salinian basement (see fig. 5); (3) Summit domain (elev, 400–900 m, avg 600 m), a 5-km-wide band between the San Andreas and Zayante faults that forms a northwest-trending ridge overlooking the Pacific Ocean; (4) Loma Prieta domain (elev, 600–1,155 m, avg 800 m), a 5- to 10-km-wide band comprising a series of slivers of the Franciscan Complex (see fig. 5) offset by a swarm of regional faults; and (5) Pajaro domain (elev, 0–100 m), which includes late Pleistocene and Holocene alluvial plain of the Pajaro River in foothills of the Santa Cruz Mountains but, unlike other coastal domains, has no marine terraces.

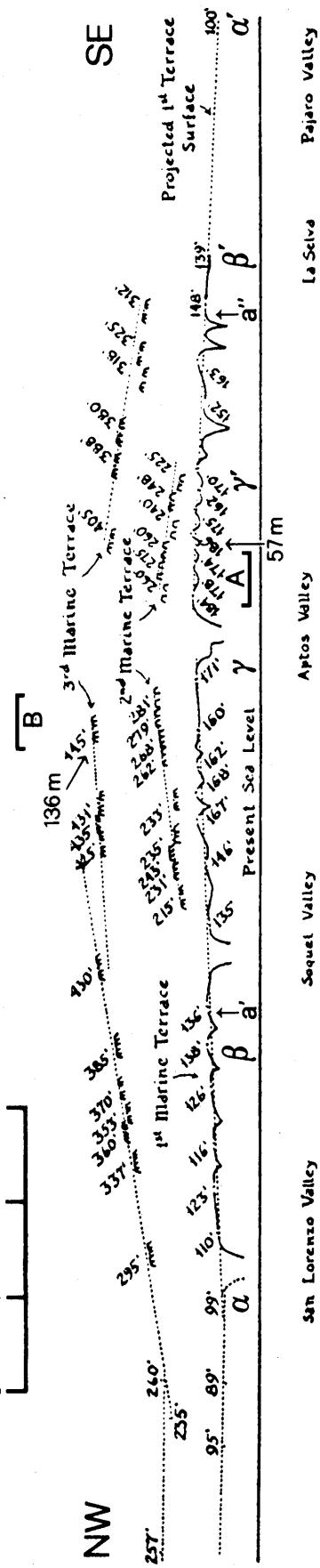

Figure 2.—Longitudinal profiles of inner edges of marine terraces between Santa Cruz and the Pajaro Valley (from Alexander, 1953). Third Terrace is interpreted as resulting from coalescence of two distinct platforms around the Soquel Valley. a′ and a″, sites where First and Second Terraces merge into a single surface (that is, Second Terrace can be identified only between sites a′ and a″). α–α′, β–β′, and γ–γ′, sites at same elevation on First Terrace (see figs. 4, 11); 57 m and 136 m, highest inner-edge positions of First and Third Terraces, respectively. As noted by several investigators after 1989 earthquake, elevation of lowest emergent terrace is inversely proportional to distance from the Loma Prieta fault, suggesting local control by repeated slip along 1989 rupture plane. However, culmination of Third Terrace (B) is shifted northwestward relative to culmination of First Terrace (A) and, possibly, Second Terrace, suggesting that source of tectonic uplift is not stationary over time. First, Second, and Third Terraces were dated at 125, 212, and 320 ka, respectively, by Valensise and Ward (1991) (see table 1), implying a late Pleistocene coastal-uplift rate of ≤0.35 mm/yr.

model-independent approach yields an average spacing of the uplift contours that is twice as large near Santa Cruz as near the Pajaro Valley, in good agreement with the GFM's predictions but in marked contrast with the nearly symmetrical pattern of 1989 vertical coseismic displacement (Marshall and others, 1991, fig. 4).

Anderson's (1990) and Valensise and Ward's (1990, 1991) results furnished convincing evidence for the generation of recent landforms by repeated earthquakes in the Santa Cruz region. The interpretations discussed above, however, are too different to be of much use—for example, to assess whether significant seismic potential remains in the area. In addition, none of them can satisfactorily explain the distribution of relief in the Santa Cruz Mountains and, in particular, the presence of high topography east of the San Andreas fault. Schwartz and others (1990) attributed the topography in this area to slip on one of the well-identified southwest-dipping faults of the Sargent-Berrocal system or on a northeast-dipping, blind, undetected reverse fault (figs. 1, 5). The main trace of the Sargent fault, however, lies to the southwest of Loma Prieta (McLaughlin and others, 1988), which would subside rather than be uplifted by the reverse component of slip. Although the existence of this undetected fault is suggested by limited seismologic observations (Olson, 1990), there is no evidence that it might significantly contribute to the generation of the Santa Cruz Mountains. The Monte Vista fault and the other frontal faults bounding the north flank of the southern Santa Cruz Mountains (Pampeyan, 1979) would be the best candidates to explain the uplift of Loma Prieta, but it is uncertain whether these faults are active, what the rate of their activity could be, and whether the orientation of the slip vector would imply a significant component of vertical motion. Davis and Namson (1991) invoked the growth of two late Cenozoic anticlinoria to explain the present configuration of the central and southern Santa Cruz Mountains in relation to the San Andreas fault and the 1989 earthquake; the first anticlinorium is centered about halfway between the San Andreas fault and the coastline, whereas the axis of the second anticlinorium runs parallel and to the east of the Sargent-Berrocal fault system (fig. 1). Both of these structures are interpreted as fault-bend or fault-propagation folds. Although Davis and Namson's model easily accounts for uplift of the western anticlinorium as a result of repeated Loma Prieta-type events, uplift of the eastern anticlinorium would require the action of a shallowly dipping, northeast-verging thrust fault extending from 12- to 17-km depth and overlying a southwest-dipping subduction zone. However, owing to the presence of a regional detachment at 16- to 17-km depth, no direct link is envisioned between the occurrence of the earthquake and the structure of the upper crust. If such a condition proved correct, this highly suggestive model would indeed impose major changes in the way we investigate seismogenic faults on the basis of surface geologic data, starting with the approach described in this paper.

To address these different models and issues and to verify whether repeated Loma Prieta-type events may be responsible not only for uplift of the lowest Santa Cruz terrace but also for the creation of the entire central Santa Cruz Mountains, I decided to investigate and compare the tectonic deformation recorded at different levels of the local geologic history. Because we are dealing with a partially or occasionally blind faulting seismogenic source, that of the 1989 earthquake, as well as processes of continuous deformation associated with motion of the Pacific plate relative to a stable frame of reference, we cannot rely on such traditional approaches as evaluating fault displacements or identifying reliable piercing points. Instead, we locate and describe geologic features that may have been areally deformed after the onset of compression across the central California basins. For this purpose, we select extended and reliable geologic datums spanning the 3 to 4 m.y. since the major plate-reorientation event that conceivably marks the inception of uplift in the Santa Cruz Mountains, and treat them as instantaneous pictures of cumulative deformation to infer the principal traits of the local tectonic history.

GEOLOGIC DATUMS IN THE CENTRAL SANTA CRUZ MOUNTAINS

Suitable geologic datums belong to two main categories: The first category includes wave-cut platforms, whereas the second category includes sedimentary deposits composing major members of a regional marine sequence. Because wave-cut platforms approximate paleo-sea levels within a few meters, these datums represent the most faithful record of subsequent tectonic uplift. A commonly overlooked property of emergent coastal-erosional features is that they may also supply a reliable record of horizontal strain, especially when the sense of tectonic transport does not align with the coastline. Assuming that the carving of wave-cut platforms proceeds at about the same rate in comparable rock types, residual or anomalous offsets between strandlines of different age could be interpreted as a response to progressive advection of the land through the source of uplift. In contrast, datums of the second category carry large uncertainties related to the geometric characteristics of the depositional environment (for example, when deposition occurs on a sloping sea floor), to the depth of deposition, and to difficulties in identifying and dating the contact with underlying deposits (for example, when the bottom of the investigated unit is time transgressive). These combined uncertainties may result in a global inaccuracy of approximately a few hundred meters in the determination of the total uplift.

The accuracy in dating each datum depends directly on its genetic characteristics. Wave-cut platforms can be indirectly dated on the basis of the age of the erosional events by which they were generated, which, in turn, reflect independently established global fluctuations of sea level, or by direct radiometric dating of fossils found in the terrace deposits. Dating by the first approach can be extremely

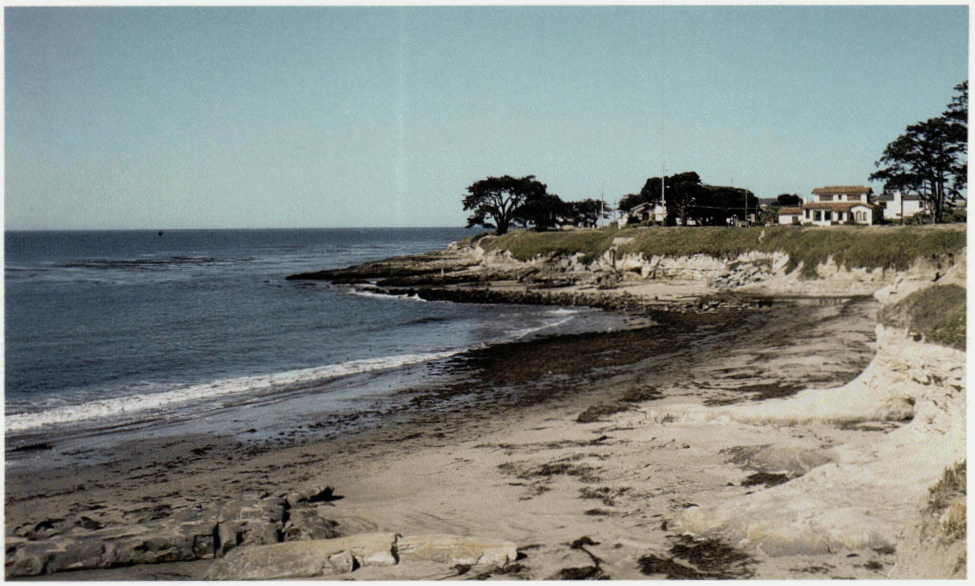

Figure 3.—Outer edge of First Terrace along West Cliff Drive, Santa Cruz (see fig. 5 for location and orientation). Upper part of wave-cut platform is carved in the upper Miocene and Pliocene Purisima Formation, which, in turn, overlies unconformably the upper Miocene Santa Cruz Mudstone. East and southeast of this site, First Terrace is consistently carved in the Purisima Formation (see fig. 7), whereas to the west it is carved in the Santa Cruz Mudstone. Purisima beds dip ≈3° SSE., whereas terrace slopes ≈30° more westerly, consistent with prediction from Geological Fault Model (see fig. 4). In itself, this discrepancy indicates that orientation of strain field has rotated since onset of uplift at this site.

precise, but because major episodes of sea-level fluctuation occur every 100 ka or so, correlation with the wrong highstand may result in a dating inaccuracy comparable to the age itself. An incorrect correlation may have an even larger effect, considering the fact that each highstand is associated with a different formation elevation (difference in elevation between sea level at the time of the incision and modern sea level), which implies that the cumulative uplift between the original and present height of a specific platform also varies with the age assignment. Therefore, tectonic rates calculated in a region subject to moderate uplift (<0.5 mm/yr) may change by as much as 100 percent in response to an age uncertainty of 20 percent. Dating by the second approach is more straightforward in principle but is subject to the availability of suitable fossil species and to analytical limitations. Because the last major highstand has left well-preserved platforms and associated deposits all over the world, reliable dating of at least one terrace is generally possible everywhere, more so in central California. Higher platforms, which are normally depleted of datable fossils, owing to their age and to greater erosion, can then be dated by extrapolating backward the rate of uplift calculated for the younger terrace.

The ages of generic marine units are obtained directly from the deposits, following standard stratigraphic criteria. Direct radiometric dating of specific minerals or magnetostratigraphic correlation is sometimes possible when dealing with clastic sedimentary deposits. Unlike datums of the first category, datums of this category should be considered for their ability to illustrate processes of continuous deformation at time scales of ≈1 m.y. rather than for assessing instantaneous tectonic rates.

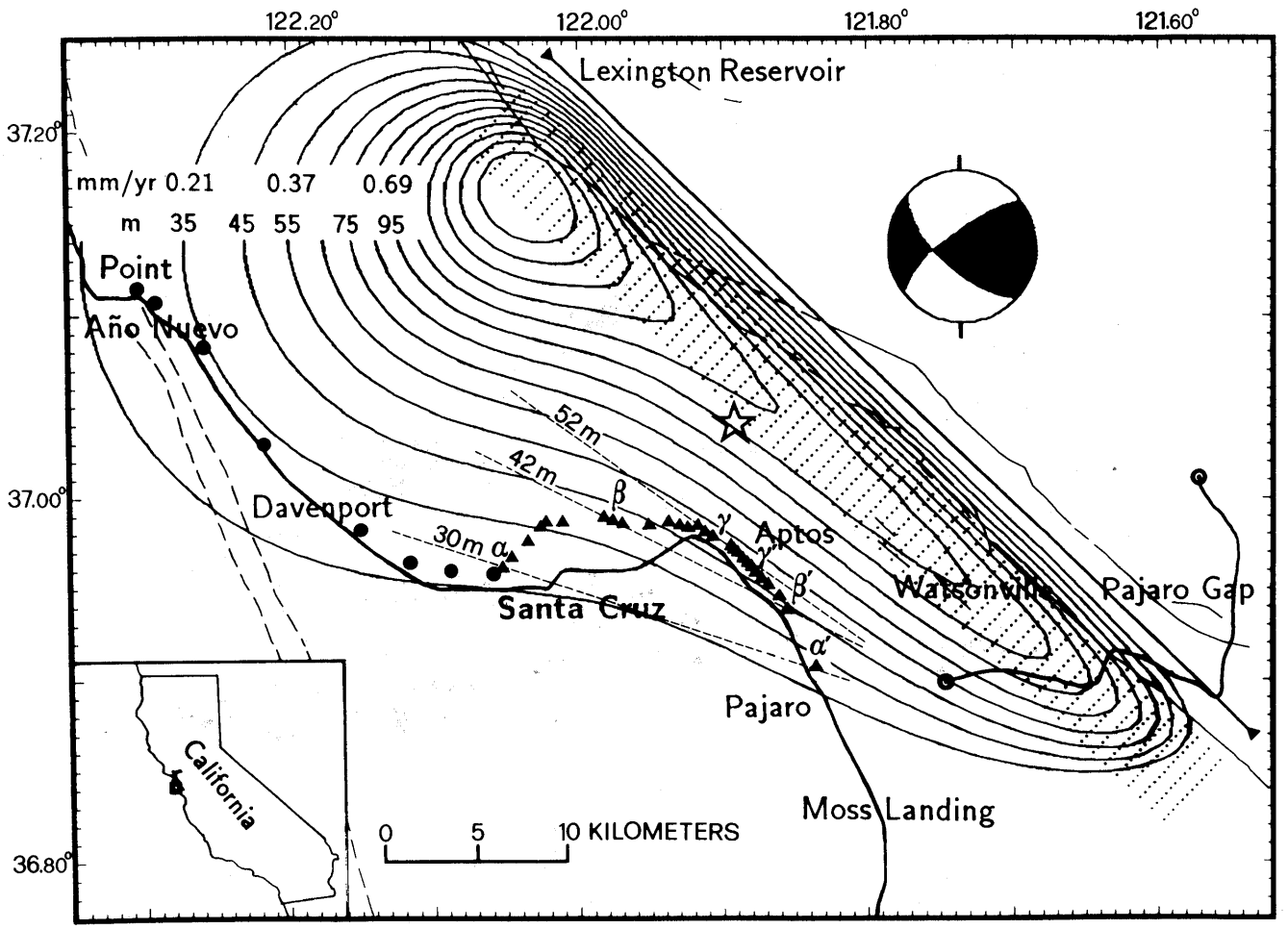

Figure 4.—Central Santa Cruz Mountains, Calif., showing predicted elevations (contour interval, 10 m) and uplift rates (contour interval, 0.08 mm/yr) from Geological Fault Model (GFM) of Valensise and Ward (1991). GFM strikes 134° and dips 65° SW. Fault length, width, and minimum depth are 60, 13, and 5 km, respectively; rake is 162°, corresponding to ratio of right-lateral to reverse slip of 3:1. Triangles, 28 inner-edge positions along Alexander's (1953) First Terrace (see fig. 2); dots, inner-edge positions along Bradley and Griggs' (1976) Highway 1 platform; straight solid line ending in triangles, surface trace of GFM, which matches fairly well trend and extent of 1989 aftershock zone (Dietz and Ellsworth, 1990); dotted area, surface projection of GFM; irregular solid line ending in circles, path of leveling line in figure 13; star, Loma Prieta main shock (McNally and others, 1989). Dashed lines connect sites marked by α–α′, β–β′, and γ–γ′ in figure 2; divergent trends of these lines suggest that long-term pattern of uplift is not symmetrical along strike of fault, as detailed by contours of GFM. Irregular long-dashed lines, San Gregorio fault zone.

The following sections discuss in detail two datums of the first category, the first and third Santa Cruz terraces (figs. 1, 3; table 1), and one datum of the second category, the upper Miocene and Pliocene Purisima Formation (figs. 5, 6). Even though in recent literature the two terraces have been renamed, for simplicity I prefer to use the nomenclature of Alexander (1953) (fig. 2). Common features of these three datums are: (1) the exceptional extent and continuity throughout the investigated region; (2) their conspicuous characteristics, which make them easy to identify; and (3) the availability of nearly a century of descriptions, field maps, and studies on specific aspects. Finally, the ratio among the ages of the three datums (≈0.1:≈0.3:≈3.0), which is comparable to the ratio among the uncertainties discussed above, should ensure a correct quantitative appraisal of the contribution of the identified agents of long-term tectonic strain to the final geologic structure.

FIRST TERRACE

The first Santa Cruz terrace was described as "First Terrace" by Röde (1930) and Alexander (1953), respectively for the coastline west (Ib, fig. 1) and east (Ia, fig. 1) of Santa Cruz. The stretch of this terrace between Santa Cruz

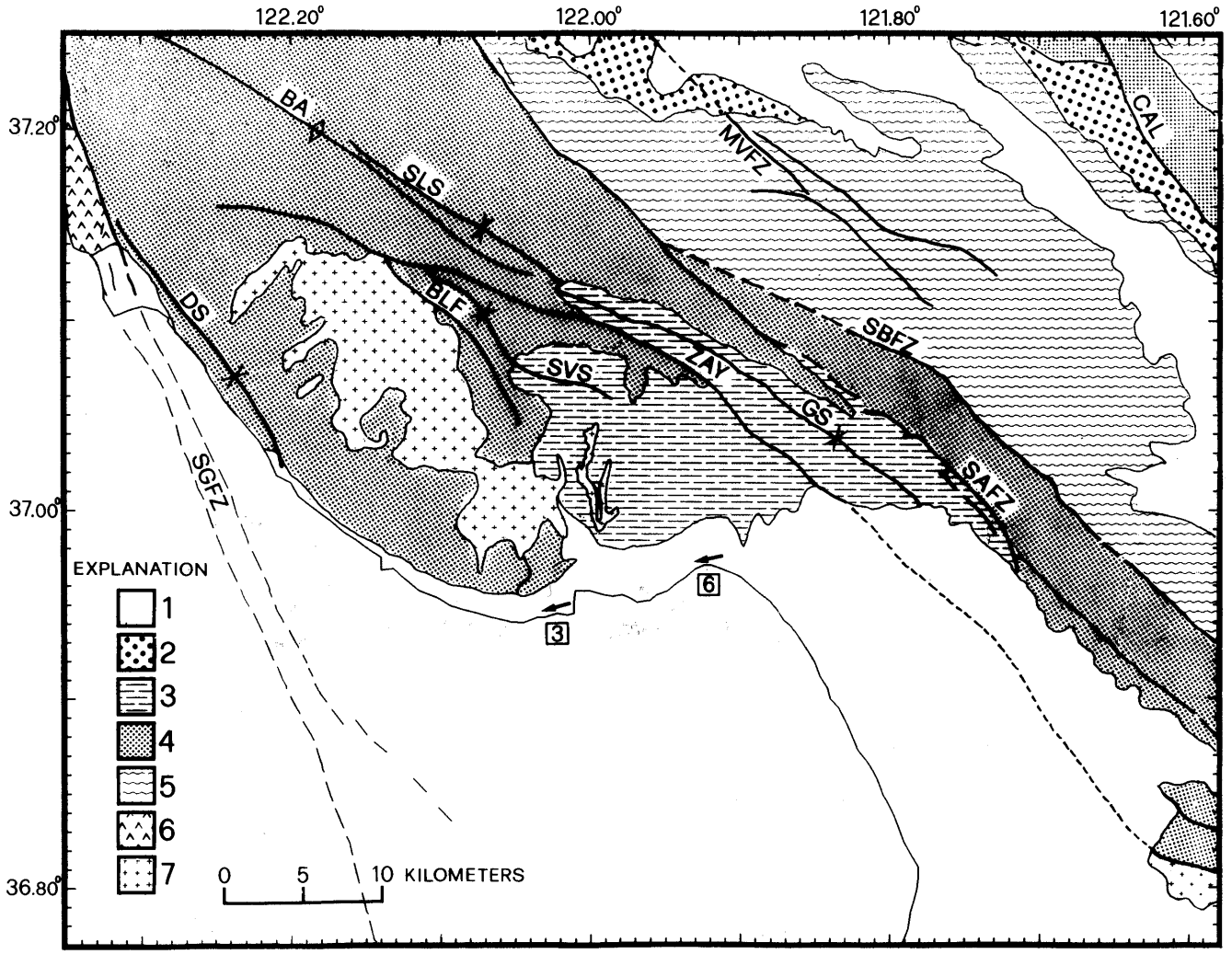

Figure 5.—Simplified geologic map of the central Santa Cruz Mountains, Calif., based on published data of Clark (1981), Aydin and Page (1984), and Brabb (1989). Numbered squares denote locations, and arrows orientations, of photographs in figures 3 and 6. Units: 1, alluvial and coastal deposits (Holocene and Pleistocene)—includes the Aromas Sand; 2, nonmarine sedimentary rocks (late Miocene to Pleistocene)—primarily the Santa Clara Formation; 3, Purisima Formation (late Miocene and Pliocene); 4, marine sedimentary rocks (Tertiary)—excludes the Purisima Formation; 5, sandstone (Upper Cretaceous); 6, plutonic and metamorphic rocks (Cretaceous)—consists of granitic plutonic and metamorphic rocks of the Salinian block; 7, Franciscan Complex (Cretaceous and Jurassic). BA, Butano anticline; BLF, Ben Lomond fault; CAL, Calaveras fault; DS, Davenport syncline; GS, Glenwood syncline; MVFZ, Monte Vista fault zone; SAFZ, San Andreas fault zone; SBFZ, Sargent-Berrocal fault zone; SGFZ, San Gregorio fault zone (dashed where inferred); SLS, San Lorenzo syncline; SVS, Scotts Valley syncline; ZAY, Zayante fault (dashed where inferred).

Table 1.—*Nomenclature and ages of Santa Cruz marine terraces*

[All ages (in parentheses) in thousands of years. A given terrace may or may not correlate with adjacent terraces described by other investigators. The nomenclature of Valensise and Ward is the same as that introduced by Alexander (1953)]

Bradley and Griggs (1976)	Hanks and others (1984)	Anderson (1990)	Valensise and Ward (1991)	Lajoie (1991)
Santa Cruz[1]	---	Santa Cruz (81–105).	---	---
Davenport[1,2] (85–105).	Davenport[1] (83).	---	---	Davenport (102).
Highway 1[1,2] (125).	Highway 1[1] (105).	---	Highway 1, First (125).	Highway 1 (124).
Greyhound[1,2] (160)	---	---	---	---
Cement[1] (260).	Cement[1] (124).	Cement (120).	Second[3] (212).	Cement[1] (320).
Western[1] (450).	Western[1] (230).	Western (212).	Third[3] (320).	Western (430).
Wilder[1] (700).	Wilder[1] (370).	Wilder[1] (330).	---	Wilder (800).

[1]Investigated only between Santa Cruz and Point Año Nuevo.
[2]Originally identified as a separate platform within the terrace.
[3]Investigated only between Santa Cruz and the Pajaro Valley.

and Point Año Nuevo (Ib, fig. 1) was later reanalyzed in great detail by Bradley and Griggs (1976), who divided it into three distinct platforms that together form what they named "Santa Cruz Terrace" (table 1). The inner edge of the highest and best developed of these three platforms, which they named "Highway 1 platform," coincides with that of First Terrace of the previous investigators.

The incision of First Terrace was correlated (table 1) with the Sangamon (125–85 ka) global sea-level highstand by Alexander (1953), with the 125-ka highstand (corresponding to stage 5e of the oxygen-isotope time scale) by Bradley and Griggs (1976), with the 105- to 103-ka highstand (oxygen-isotope stage 5c) by Hanks and others (1984) and Lajoie (1986), with either the 81-ka (oxygen-isotope stage 5a) or the 105-ka (oxygen-isotope stage 5c) highstand by Anderson (1990), and again with the 125-ka highstand by Valensise and Ward (1991). As discussed above, the assignment to the 125-ka or a subsequent highstand implies significantly different estimates for the formation elevation and, thus, of the cumulative tectonic uplift undergone by a specific platform. For example, Anderson's (1990) assignment to the 81- or 105-ka highstand (formation elevation, –19 and –9 m, respectively) implies an uplift rate in the range 0.3–0.9 mm/yr. In contrast, accepting the 125-ka assignment of Valensise and Ward (1991) and the formation elevation of 8.9±3 m obtained by inversion as a free parameter of their GFM (fig. 4) implies a significantly slower uplift rate in the range

Figure 6.—Purisima Formation in seacliff at New Brighton State Beach, about 5 km west-northwest of Aptos (see fig. 5 for location and orientation). Seacliff is much higher than in downtown Santa Cruz (fig. 3), consistent with large difference in uplift rate predicted for these two sites by Geological Fault Model (GFM; see fig. 4). As discussed in figure 3, east-southeastward dip of Tertiary bedrock is inconsistent with local terrace slope, which is perpendicular to northwestward trend of shoreline, and with orientation of gradient of uplift predicted by GFM. At this site, however, discrepancy is >90°, suggesting that major reorientation of strain field has occurred since onset of compression in this area.

0.13–0.35 mm/yr, corresponding to a tilt rate in the range 0.7°–2.5°/m.y. These results would change by ±10 percent or less if we replaced the GFM's 8.9-m formation elevation with the widely accepted 6- to 10-m estimate from studies of coastal geology.

Direct dating of the Santa Cruz terraces has been attempted by many investigators, but owing to the absence of suitable fossils, the results are dispersed within the fairly wide range 68–130 ka. However, on the basis of a reevaluation of the field data, a new scheme of correlation with the global sea-level history, and the observation that none of the dated fossils was collected on the highest platform, K.R. Lajoie (unpub. data, 1991) changed his own age assignment from 105–103 ka (Hanks and others, 1984; Lajoie, 1986) to 125 ka for Highway 1 platform of First Terrace.

THIRD TERRACE

As anticipated above, this section describes Third Terrace as originally defined by Alexander (1953). This higher terrace is far less continuous and generally narrower than First Terrace, reflecting a combination of erosional degradation and different formation conditions. It was initially described as "Second Terrace" by Röde (1930) but then renamed "Third Terrace" by Alexander (1953), who updated the local nomenclature after recognizing another, more subdued terrace (which he named "Second Terrace") emerging from the inner edge of the First Terrace and extending for a few kilometers around the mouth of the Aptos River (figs. 1, 2).

Third Terrace (table 1) appears to continue west of the San Lorenzo River (fig. 1) with Western Terrace of Bradley and Griggs (1976). On the basis of the results from First Terrace, Valensise and Ward (1991) assigned the incision of the part of this surface lying east of Santa Cruz to the 320-ka (oxygen-isotope stage 9) highstand, whereas west of Santa Cruz it was dated at 450 ka by Bradley and Griggs (1976). In fact, the carving of Western Terrace during the 320 ka highstand is incompatible with the 0.13- to 0.21-mm/yr uplift rate calculated for the part of the 125-ka terrace west of Santa Cruz. Thus, Third Terrace may reflect the reoccupation of a platform carved during the Western Terrace highstand, a hypothesis seemingly suggested also by Alexander (1953) (fig. 2), or the 320-ka terrace west of Santa Cruz may have been removed by subsequent highstands.

Though not used in our analysis, Alexander's (1953) Second Terrace deserves special attention because it provides strong evidence to constrain the age assignments proposed by Valensise and Ward (1991) for First and Third Terraces. Alexander noticed that Second Terrace does not parallel First Terrace but is, instead, cut by it, and that it is found only where the uplift rate is highest. Simple analytical arguments (Lajoie, 1986) indicate that these two conditions are evidence that Second Terrace was cut at a substantially lower elevation than First Terrace. Assuming that First and Second Terraces merge into a single wave-cut platform at an elevation of 40 to 45 m (sites a′, a″, fig. 2), and assuming that First Terrace is 125 ka old, we conclude that a minimum uplift rate of 0.26 to 0.29 mm/yr is required to compensate for this difference in formation elevation. Therefore, any estimate for the age of Second Terrace will translate directly into a formation elevation, which, in any case, will be lower than that of First Terrace. Assuming that Second Terrace formed during the 212-ka highstand (oxygen-isotope stage 7; Valensise and Ward, 1991), the formation elevation would be ≈–15 m. Because global sea level is generally believed to have been lower during the 212-ka highstand (oxygen-isotope stage 7) than during the 125- and 320-ka highstands (oxygen-isotope stages 5e and 9, respectively), this conclusion indirectly supports the age assignments proposed by Valensise and Ward (1991) for Second and Third Terraces, although these results also imply that Second Terrace is not a suitable datum for the purposes of our investigation.

PURISIMA FORMATION

The Purisima Formation is the youngest and, probably, most extensively exposed marine unit of the Tertiary sequence in the central Santa Cruz Mountains west of the San Andreas fault (Greene, 1977; Greene and Clark, 1979; Clark, 1981; Stanley, 1985, 1990). The unit consists of thick, yellowish-gray, tuffaceous and diatomaceous siltstone beds, with thick andesitic sandstone interbeds. Abundant glassy debris, presumably from the Sierra Nevada and Cascades volcanoes, differentiates the Purisima from older marine formations. Its age is constrained by various sets of paleontologic, radiometric, and paleomagnetic observations to the range late Miocene to late Pliocene (Stuart and others, 1982).

Overall, the Purisima Formation records a rapid late Miocene transgression followed by slow regression and basin filling during the Pliocene. The coincidence between the onset of compression and uplift across the Coast Ranges (4–3 Ma; Harbert and Cox, 1989; Harbert, 1991), the end of volcanism, and the end of marine sedimentation during the late Pliocene (Crouch and others, 1984; Clark and others, 1991) suggests that the Purisima Formation bears a complete record of all the tectonic processes leading to the post-Pliocene creation of the Santa Cruz Mountains. To extract this information, we must select a structural surface for which both the present configuration and a reasonable hypothesis on the original shape and elevation are available. The contact between the Purisima Formation and the underlying middle to late Tertiary units is generally unconformable and marked by a characteristic glauconitic sandstone, which makes it one of the most reliable

landmarks in central California stratigraphy. I reconstructed the structural contours of the base of the Purisima Formation by interpolating elevations of its contact with the underlying formations (fig. 7; tables 2, 3), using published geologic maps (McLaughlin and others, 1988; Brabb, 1989), geologic maps in preparation (R.J. McLaughlin, written commun., 1990), and well data (Clark and Rietman, 1973; E.E. Brabb, written commun., 1990).

A precise age for this datum is difficult to assess because the basal part of the Purisima Formation is time transgressive from northwest to southeast (Greene and Clark, 1979). For our purposes, however, all we need to know is the timing of the latest major regression in the study area, which we will infer on the basis of plate-tectonic arguments, assuming that deformation has since proceeded rather uniformly until the present.

With respect to the original shape of this datum, the simplest and most convenient assumption is that it was a flat, horizontal surface. Alternatively, we should prove that the present-day departure from planarity and horizontality is large in comparison with that inferred for the depositional environment of the Purisima Formation. Not much

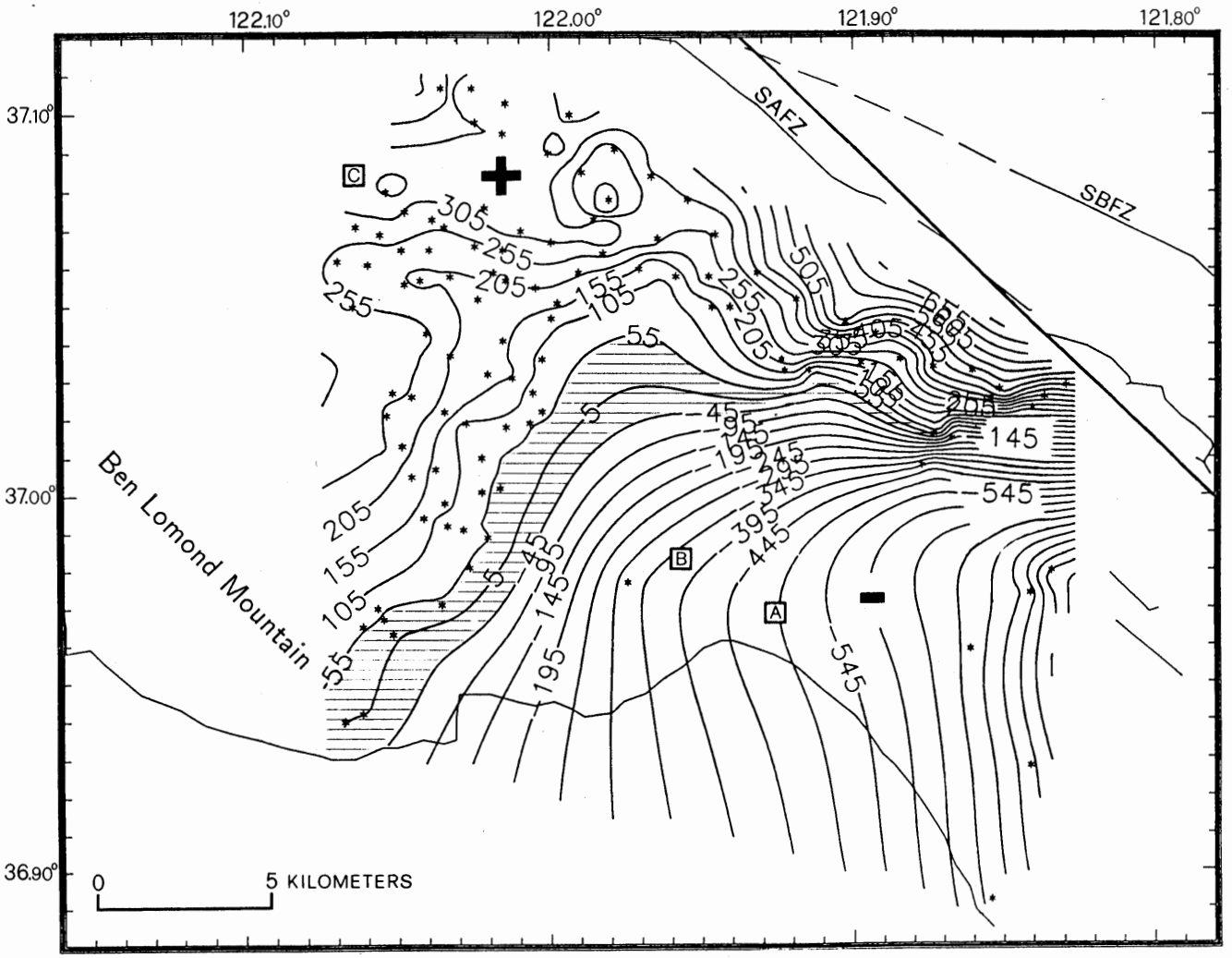

Figure 7.—Structural map of base of the Purisima Formation in the central Santa Cruz Mountains, Calif., constructed by using elevations of contact between the Purisima and underlying formations from published and unpublished geologic maps and well data (see fig. 5; tables 2, 3). Elevations in meters above or below sea level; contour interval, 50 m. Stars, data points; straight solid line, surface trace of Geological Fault Model (fig. 4); large plus and minus signs, location of highest and lowest parts of datum, respectively; lined area, part of datum currently within 50 m of present sea level. A and B, culminations of First and Third Terraces, respectively (Alexander, 1953); C, northwesternmost and highest outcrops of the Purisima Formation in the central Santa Cruz Mountains. The Purisima is gently warped west-northwestward against Ben Lomond Mountain and tightly warped northeastward against the San Andreas fault. In both directions, edge of contoured area marks places where extrapolated base of the Purisima is higher than present topography—in other words, where all of the Purisima has been removed by erosion and older rocks are exposed. To east, the Purisima is buried beneath as much as 600 m of Pleistocene sedimentary deposits of the Aromas Sand and other coastal units marking end of marine cycle. Away from the mountains, Purisima datum can be approximated by a surface dipping about 3° ESE. SAFZ, San Andreas fault zone; SBFZ, Sargent-Berrocal fault zone (dashed where inferred).

Table 2.—*Elevations of the base of the Purisima Formation from outcrop data*

[a.s.l., above sea level; SC, Santa Cruz]

No.	Latitude N.	Longitude W.	Elevation (m a.s.l.)	Location
1	36.950	122.047	6	West Cliff Drive I, SC
2	36.952	122.041	6	West Cliff Drive II, SC
3	36.973	122.031	12	City Hall, SC
4	36.977	122.034	40	High Street E., SC
5	36.980	122.036	76	Harvey West, SC
6	36.975	122.041	61	Laurel and Escalona Streets, SC
7	36.981	122.015	43	Water and Branciforte Streets, SC
8	36.991	122.006	47	DeLaveaga Golf Course S., SC
9	36.999	122.000	54	DeLaveaga Golf Course N., SC
10	37.001	122.008	61	Branciforte Creek E., SC
11	37.002	122.013	73	Branciforte Creek W., SC
12	37.004	122.021	134	Highway 17, Pasatiempo Drive
13	37.015	122.025	170	Highway 17, Sims Road
14	37.023	122.028	231	Highway 17, Brook Knoll School
15	37.031	122.033	244	Graham Hill Road
16	37.037	122.031	268	Camp Evers S.
17	37.036	122.025	244	Highway 17 and Mount Hermon Road
18	37.008	122.014	122	Carbonera Creek S.
19	37.017	122.017	146	Glen Canyon Road
20	37.032	122.014	183	Carbonera Creek N.
21	37.029	122.007	97	Redwood Drive
22	37.020	122.002	67	N. Delaveaga I
23	37.011	122.002	61	N. Delaveaga II
24	37.047	122.012	195	Highway 17, San Augustin
25	37.053	122.020	268	Scotts Valley
26	37.062	122.003	189	Highway 17 and Scotts Valley Drive
27	37.068	122.012	207	Bean Creek Road
28	37.076	122.004	244	Glenwood Drive
29	37.086	122.001	335	Redwood Glen Camp
30	37.081	122.014	256	Mackenzie Creek and Bean Creek
31	37.067	122.022	207	Nelson Road
32	37.066	122.027	198	Mission Springs
33	37.060	122.044	259	Bean Creek Fault
34	37.071	122.039	219	Scotts Valley syncline I
35	37.072	122.049	244	Scotts Valley syncline II
36	37.081	122.043	280	Zayante Creek
37	37.079	122.035	280	Lockhart Gulch I
38	37.090	122.033	366	Zayante
39	37.075	122.028	244	Lockhart Gulch II
40	37.085	122.027	293	Lockhart Gulch III
41	37.083	122.018	293	Mackenzie Creek I
42	37.075	122.019	219	Mackenzie Creek II
43	37.080	121.989	329	Bethany Park
44	37.077	121.979	305	Highway 17 and Vinehill Road
45	37.075	121.995	256	Bethany Bible College
46	37.069	121.998	219	Highway 17 and Carbonera Creek W.
47	37.067	121.994	213	Highway 17 and Carbonera Creek E.
48	37.065	121.984	207	Vinehill Road
49	37.057	121.979	125	Vinehill Road and Jarvis Road
50	37.046	121.982	91	Branciforte Drive N.
51	37.051	121.995	162	Granite Creek N.
52	37.042	122.000	168	Granite Creek S.
53	37.041	121.992	152	Granite Creek E.
54	37.029	121.986	61	Branciforte Drive and Crystal Creek
55	37.032	121.982	76	Crystal Creek
56	37.037	121.985	85	Happy Valley School N.
57	37.028	121.994	98	Happy Valley School S.
58	37.012	121.996	55	Happy Valley Conference Ground
59	37.061	121.977	171	Blackburn Gulch S.
60	37.070	121.950	128	Soquel Creek
61	37.069	121.970	204	Jarvis Road
62	37.074	121.962	280	Blackburn Gulch N
63	37.083	121.965	320	Glenwood Basin
64	37.068	121.938	134	Hester Creek
65	37.060	121.926	146	Olive Spring Quarry
66	37.043	121.902	183	Bridge Creek
67	37.078	121.944	274	Old San Jose Road
68	37.105	121.995	305	Mountain Charlie Road S.
69	37.113	121.994	305	Mountain Charlie Road N.
70	37.100	121.980	366	St. Mary's Girl Camp
71	37.110	121.973	366	Laurel Tunnel
72	37.095	121.969	244	Glenwood Basin N.
73	37.101	121.958	244	Soquel Creek W. Branch
74	37.088	121.960	158	Glenwood Basin S.
75	37.094	121.946	305	Hester Creek Church
76	37.068	121.927	244	Sugarloaf Mountain
77	37.088	121.934	305	Amaya Creek
78	37.079	121.925	259	Soquel Creek and Amaya Creek
79	37.060	121.920	183	Olive Springs
80	37.046	121.903	232	Bridge Creek
81	37.069	121.911	366	Hinckley Creek N
82	37.062	121.898	366	Hinckley Creek S.
83	37.056	121.882	549	China Ridge
84	37.117	122.005	366	San Lorenzo syncline
85	37.108	122.004	305	Mountain Charlie Gulch
86	37.117	122.015	219	Camp Wasibo
87	37.053	121.872	366	Aptos Creek W.
88	37.046	121.864	244	Aptos Creek E.
89	37.044	121.853	427	Buzzard Lagoon Road W.
90	37.043	121.840	488	Buzzard Lagoon Road E.
91	37.038	121.831	488	Eureka Gulch
92	37.033	121.820	183	Eureka Canyon W.
93	37.036	121.816	305	Eureka Canyon E.
94	37.039	121.809	427	Eureka School

is known, however, about the paleobathymetry and paleoecology of this formation. A compilation by Stanley (1985) suggests a depositional depth of ≤500 m below present-day sea level. Clark (1981) reported fossils indicative of inner neritic depths (≤50 m) collected a few kilometers north of Santa Cruz (fig. 1), and suggested that the Purisima Formation was deposited in a continental-shelf environment. All investigators agree that the formation was deposited in a tectonically active basin, possibly owing to the vicinity of such major faults as the San Andreas and San Gregorio, and that localized uplift occurred within the basin well before the end of marine sedimentation, as evidenced by internal disconformities and by rapid vertical and lateral variations. Sedimentologic arguments

Table 3.—*Elevations of the base of the Purisima Formation from well data*

[a.s.l., above sea level]

No.	Latitude N.	Longitude W.	Elevation (m a.s.l.)	Well/year
1	37.043	121.894	88	Loma Prieta 1 (1949)
2	37.045	121.877	195	Loma Prieta 2 (1949)
3	37.025	121.847	-158	Bean Hill Hihn 1 (1946)
4	37.026	121.853	29	Union Oil Hihn 1 (1951)
5	37.018	121.857	-391	Union Oil Hihn 2 (1952)
6	36.990	121.814	-953	Blake 1 (1954)
7	36.984	121.821	-830	Light 1 (1951)
8	36.969	121.841	-717	Pierce 1 (1950)
9	36.902	121.834	-715	Blake 1 (1953)
10	36.938	121.821	-835	Carpenter 1 (1953)
11	36.987	121.954	<-320	Soquel County (1977)

also suggest that the sea floor on which the Purisima Formation was being deposited was not everywhere regular; for example, its contact with the underlying formations is generally conformable throughout the central Santa Cruz Mountains but unconformable in the vicinity of Ben Lomond Mountain (figs. 1, 5). In combination with other lines of evidence, this observation suggests that Ben Lomond Mountain was already delineated topographically by the middle Miocene, well before initial deposition of the Purisima Formation.

To test more quantitatively whether the Purisima Formation was deformed during or after deposition, I compared (fig. 8; table 4) actual attitudes of the Purisima Formation from geologic maps or directly collected in the field with local gradients of the base of the formation inferred from the structural map (fig. 7). Correspondence between the attitudes observed at the surface and those inferred for the base of the formation can be taken as evidence that the formation was originally deposited in flat, subhorizontal layers and subsequently deformed as a whole. If this were true throughout the study area, then the present dip of the Purisima Formation could be taken as representative of postsedimentary tectonic processes, rather than as reflecting irregularities of the sea floor or peculiar depositional conditions (for example, clinostratification associated with the evolution of a delta). An upper limit on the departure from purely horizontal deposition is set by the observation that the Purisima Formation dips <3° over the entire southernmost part of the study area, both from outcrop data and from the structural map (fig. 7).

MODES OF TECTONIC DEFORMATION IN THE CENTRAL SANTA CRUZ MOUNTAINS

As pointed out earlier, the generation of coastal landforms by repeated Loma Prieta-type events is established by more than 2 years of investigations since 1989, although important ambiguities and discrepancies in major aspects of this process are still unresolved. To address these aspects, I selected three geologic datums, each of which supplies an instantaneous picture of cumulative tectonic deformation at different periods of the geologic history. The following section describes how the interplay between the information contained in each picture can be used to investigate processes undetected by studies on the deformation of First Terrace, and to extend backward the record of tectonic events in the central Santa Cruz Mountains.

LATERAL MIGRATION OF THE SHORELINES

Observations from rising coastlines around the world indicate that shorelines migrate over time in the same direction as the gradient of local uplift and that they tend to parallel each other if the source of uplift remains fixed (for example, Woodring and others, 1946; Chappell, 1974; Muhs, 1983; Keraudren and Sorel, 1987). Minor lateral fluctuations in the rate at which a coastline migrates away from the source of uplift can generally be accounted for by the varying interaction among the parameters controlling coastal evolution. However, if such fluctuations persist through two or more subsequent complete climatic and sea-level cycles, some form of tectonic control becomes more plausible. For example, we could invoke the action of a second, more localized tectonic force contrasting the positive movement or simply shifting the land away from the source of uplift. The first and third Santa Cruz terraces parallel each other southeast of Aptos and northwest of Sand Hill Bluff (halfway between Santa Cruz and Davenport, fig. 1), where they are perpendicular to the local gradient of uplift, whereas between these two sites they diverge, describing a sigmoidal gap (fig. 9). This gap is centered on the region where the characteristic curvature of the Santa Cruz coastline is tightest and where both shorelines align nearly parallel to the gradient of uplift predicted by the GFM (fig. 4). Comparison of the 125-ka strandline with the modern shoreline shows a similar, though more pronounced pattern. If the tendency of a coastline subjected to pure uplift is to move forward (that is, away from the source of uplift), then the formation of these gaps—that is, the migration of the shoreline in a direction nearly perpendicular to the local gradient of uplift—requires that the pattern of vertical strain be modified over time, either by simple shifting of the source of uplift

relative to the land or by the action of an additional source of vertical strain which disrupts the pattern of uplift caused by the main source.

We test these hypotheses with a graphical restoration procedure to calculate the amount of motion required to fit shorelines of different ages one on top of the other (fig. 10). Our approach considers only tectonic deformation and disregards possible lithologic inhomogeneities and other conditions leading to differential erodibility, which simply serve as additional sources of uncertainty. The limited breadth fluctuations of First and Third Terraces away from Santa Cruz (fig. 9), and the observation that both of these terraces are carved into rocks of the Purisima Formation all along the above-described gap (figs. 3, 6), suggest that the contribution of such effects is modest in comparison with the main tectonic effect.

The first step in the restoration (figs. 10*A*, 10*B*) indicates that the shoreline has migrated away from the source of uplift by about 1.5 km in the interval between the age of First and Third Terraces (300–200 ka). This result has no direct tectonic meaning but simply indicates that the shoreline has advanced by ≈1,500 m for every 50 to 70 m of uplift (assuming 0.24 mm/yr as an average uplift rate for the Santa Cruz coastline; see fig. 4) and thus that the average gradient of the offshore part of a typical Santa Cruz platform ranges from 30 to 50 m/km, in agreement with the 7- to 40-m/km gradients measured on modern platforms in the same area by Bradley and Griggs (1976). These simple calculations and their match with field observations indicate that the breadth of a marine terrace is strongly controlled by the seafloor slope, which, in turn, is controlled by the geometry of the uplift pattern and by the rate of offshore sedimentation.

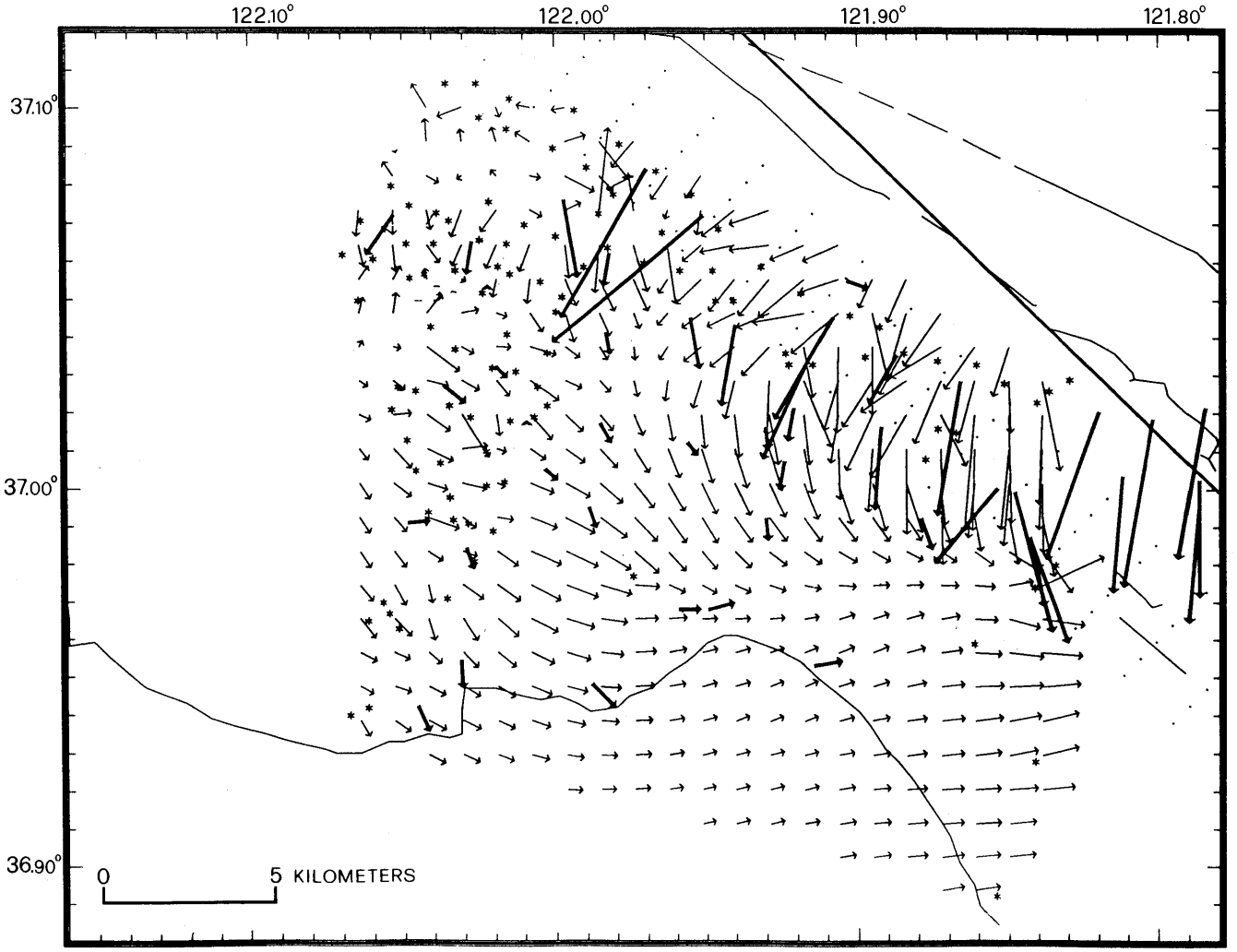

Figure 8.—Sketch map of southern Santa Cruz Mountains, Calif., comparing observed attitudes of the Purisima Formation (heavy arrows) from published geologic maps and field data (table 4), with local gradients of the formation inferred from structural map (fig. 7). Length of arrow is proportional to dip angle. Good agreement supports hypothesis that the Purisima was deposited on a fairly flat, subhorizontal surface and thus that its present setting is largely an effect of true tectonic deformation. Dips of 0°–4° ESE. on Purisima strata just seaward of Soquel-Aptos area (fig. 1; Greene and Clark, 1979) are also consistent with expected attitudes.

Table 4.—*Attitudes of outcrops of the Purisima Formation*

No.	Latitude N.	Longitude W.	Dip angle	Dip direction
1	36.952°	122.025°	155°	4°
2	36.964°	122.011°	177°	4°
3	37.075°	122.007°	190°	5°
4	37.001°	122.028°	85°	3°
5	37.064°	122.002°	0°	0°
6	37.037°	122.016°	130°	4°
7	37.082°	122.033°	215°	8°
8	37.015°	121.983°	130°	2°
9	37.022°	121.936°	140°	2°
10	37.002°	121.910°	175°	3°
11	37.017°	121.904°	190°	4°
12	37.031°	121.901°	190°	5°
13	37.026°	121.910°	175°	3°
14	37.065°	121.883°	110°	3°
15	37.053°	121.920°	190°	16°
16	37.055°	121.935°	170°	9°
17	37.005°	121.969°	160°	3°
18	37.027°	121.965°	150°	3°
19	37.051°	121.963°	170°	3°
20	37.028°	121.989°	0°	0°
21	37.042°	121.999°	135°	2°
22	37.072°	121.962°	190°	5°
23	37.086°	121.977°	170°	15°
24	37.094°	121.950°	210°	40°
25	37.082°	121.931°	230°	48°
26	37.055°	121.888°	210°	25°
27	37.044°	121.896°	205°	23°
28	37.002°	121.859°	160°	5°
29	37.026°	121.872°	185°	16°
30	37.038°	121.846°	190°	30°
31	37.045°	121.867°	210°	10°
32	37.010°	121.834°	220°	20°
33	37.009°	121.828°	165°	33°
34	37.031°	121.765°	190°	35°
35	37.030°	121.800°	200°	36°
36	37.013°	121.792°	185°	25°
37	37.028°	121.782°	190°	40°
38	37.012°	121.767°	180°	25°
39	37.005°	121.767°	185°	25°
40	36.963°	121.894°	80°	4°
41	36.978°	121.929°	75°	4°
42	36.978°	121.939°	90°	3°
43	36.958°	121.968°	135°	5°
44	36.994°	122.009°	160°	3°
45	36.991°	121.821°	170°	8°
46	36.997°	121.823°	160°	24°

I also considered fitting the modern shoreline to the shoreline of First Terrace. This would have required a slightly larger offset for a considerably shorter time interval than in the previous fit. The evolution of the modern shoreline, however, is far from complete (in fact, it is actively receding at a rate of a few centimeters per year), and so the comparison with the fully mature shoreline of First Terrace would be distorted.

Unlike the previous step, what is left after removal of the contribution of simple forward migration appears to have an interesting tectonic meaning. Restoration of the coastline-perpendicular component has turned the sigmoidal gap into two separate rectangular gaps (shaded area, fig. 10). Fitting the two shorelines (figs. 10*B*, 10*C*) now requires 1.5 to 2.0 km of apparent northwestward (parallel to the San Andreas fault) motion of the land, a process reminiscent of the generation of pullapart basins that could reflect progressive northwestward advection of the Pacific plate through the source region of the 1989 earthquake at a rate of 5 to 10 mm/yr. Quite surprisingly, this result implies that the local source of uplift is stationary with respect to the North American plate over time scales of a fraction of a million years, a hypothesis that should be verifiable on the basis of the setting of our oldest datum.

LATERAL MIGRATION OF THE PATTERN OF LONGITUDINAL WARPING

The hypothesis that the local source of uplift is stationary with respect to the North American plate can also be tested by using the trend of vertical warping of our datums, rather than their shape in map view. A simple observation is that the site where Third Terrace is highest is situated to the northwest relative to the culmination of both First and Second Terraces (figs. 2, 9). As pointed out earlier, the broad upwarping of an individual terrace reflects its varying distance from the Loma Prieta fault. The highest point on Third Terrace (site marked with "136 m" in figs. 2, 11), however, is not observed at the inner-edge position that falls closest to the fault but is shifted ≈3 km to the northwest of this site. The highest point on First Terrace ("57 m", figs. 2, 11) is one of the closest to the fault, but it is also the southeasternmost of a series of four positions whose heights fall within 4 m of the peak elevation. (Owing to the quality of available inner-edge observations, Second Terrace is omitted from this analysis.)

A possible explanation for the existence of such "bumps" along the inner-edge trends may be found in a notable characteristic of the 1989 earthquake. To account for discrepancies among its main source parameters, Wallace and others (1991) hypothesized that a significant amount of "slow slip" could have been released from the hypocentral region of the fault, where little aftershock activity was observed but no moment release was detected by conventional seismometric analyses. Marshall and others' (1991) fit of coseismic elevation changes (see line 2

in fig. 7 of Marshall and others, 1991) also shows some unmodeled uplift along the leveling line that runs closest to the earthquake epicenter. Both of these observations may reflect a concentration of moment release near the hypocenter, which would translate into excess uplift in the area between the epicenter and the shoreline. If this uplift were a permanent characteristic of the Loma Prieta source region, the "bumps" in the elevation trend of First and Third Terraces might simply record a cumulative effect of the passage of the Pacific plate through the epicenter of the 1989 earthquake. Again, different terraces would record different positions of the source of uplift relative to the land, thus allowing the rate of northwestward shifting to be evaluated on the basis of the time interval between subsequent highstands. However, quantifying this process is made difficult by the following observations (fig. 11): (1) There is a 3-km-wide data gap around the apex of Third Terrace; (2) the culminations occur along ≈2-km-long sections of the terraces rather than at well-identified sites; and (3) identification of the culminations is subject to an additional uncertainty related to the fact that the strandlines do not perfectly parallel each other but instead indent more or less deeply the pattern of long-term uplift, implying that part of the difference in elevation between adjacent inner-edge positions on the same terrace simply reflects varying distance from the fault. Figure 11 shows that for First Terrace we can expect elevations to fluctuate by ±4 m in response to variations of ±1 km in the distance between the inner edge and the fault. Because the average difference in elevation between adjacent positions on First Terrace is ≤3 m, this effect must be carefully considered.

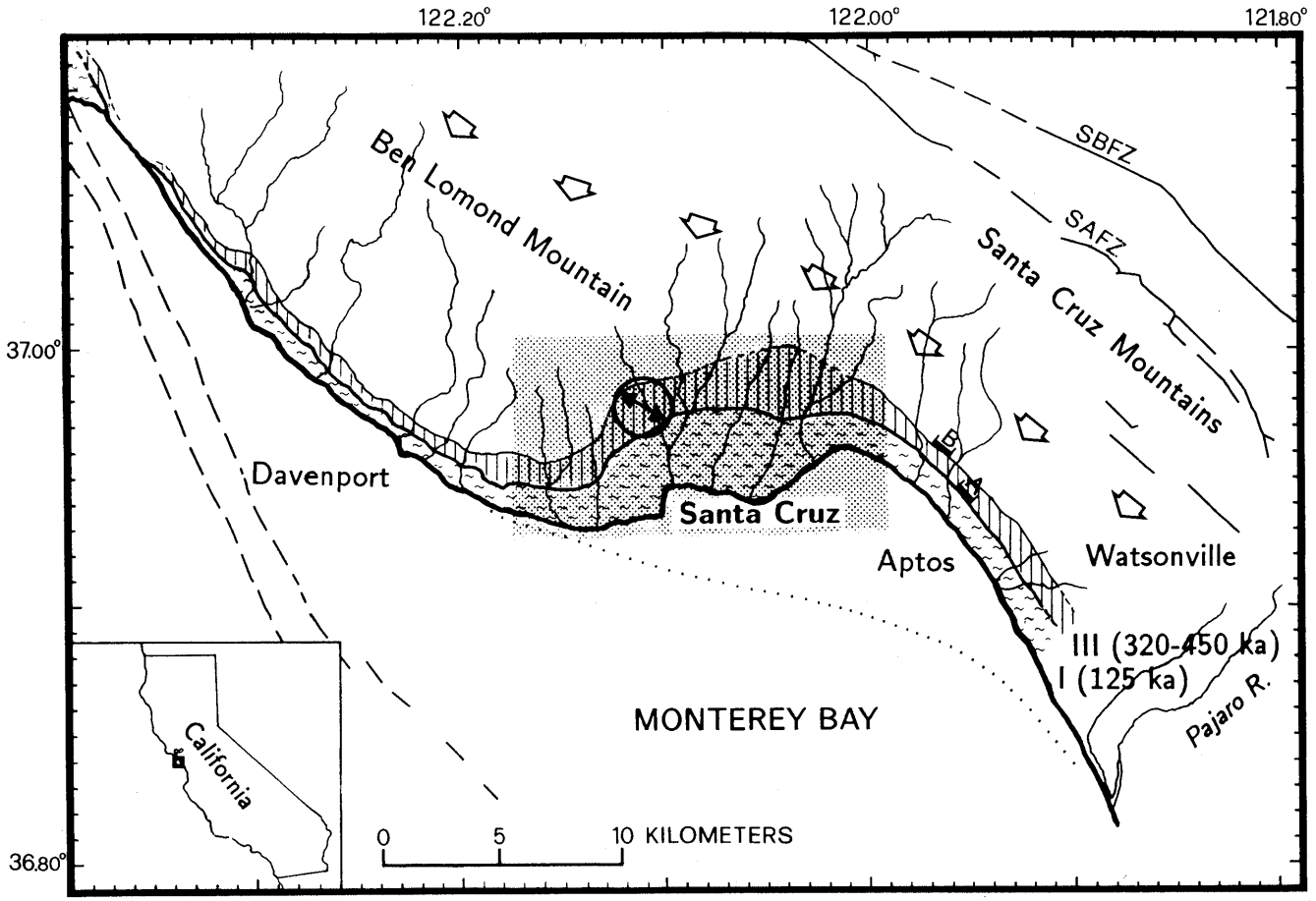

Figure 9.—Santa Cruz, Calif., area, showing reconstructed inner edges of two best expressed late Pleistocene marine terraces, First (125 ka) and Third (320–450 ka) Terraces, based on data of Alexander (1953) and Bradley and Griggs (1976). A and B, culminations of First and Third Terraces, respectively (see figs. 1, 2, 7). Arrows denote local direction of gradient of uplift along 0.5-mm/yr contour, as predicted by Geological Fault Model (fig. 4). Shaded area (detailed in fig. 10) includes region where both modern shoreline and paleoshorelines may reflect migration of land relative to source of uplift. Double-headed arrows indicate how land may have migrated northwestward by 1.5 to 2.0 km during 200- to 300-ka interval between incision of Third and First Terraces (corresponding to migration rate of 5–10 mm/yr). Distance of ≈3.0 km between culminations of First and Third Terraces also suggests that land has moved relative to source of uplift that has created elevated coastal features in Santa Cruz area. Dotted line (approximately corresponding to 90-ft depth contour) marks expected position of shoreline during a hypothetical future highstand 100 ka from present. SAFZ, San Andreas fault zone; SBFZ, Sargent-Berrocal fault zone (dashed where inferred).

Our preferred pick for the culmination of First and Third Terraces (sites A and B, respectively, fig. 11) implies a total shift of about 3±1 km. Because this part of Third Terrace was assigned to the 320-ka highstand, we can calculate a shift rate of 10 to 20 mm/yr. Although the associated uncertainty is very large, this estimate is consistent with the rate independently obtained from the map shape of the inner edges. What I believe to be extremely important, however, is that if the process of progressive uplift and advection has continued for time scales of ≥1 m.y., we should see large accumulation of topography at a considerable distance northwest of Santa Cruz, a hypothesis that

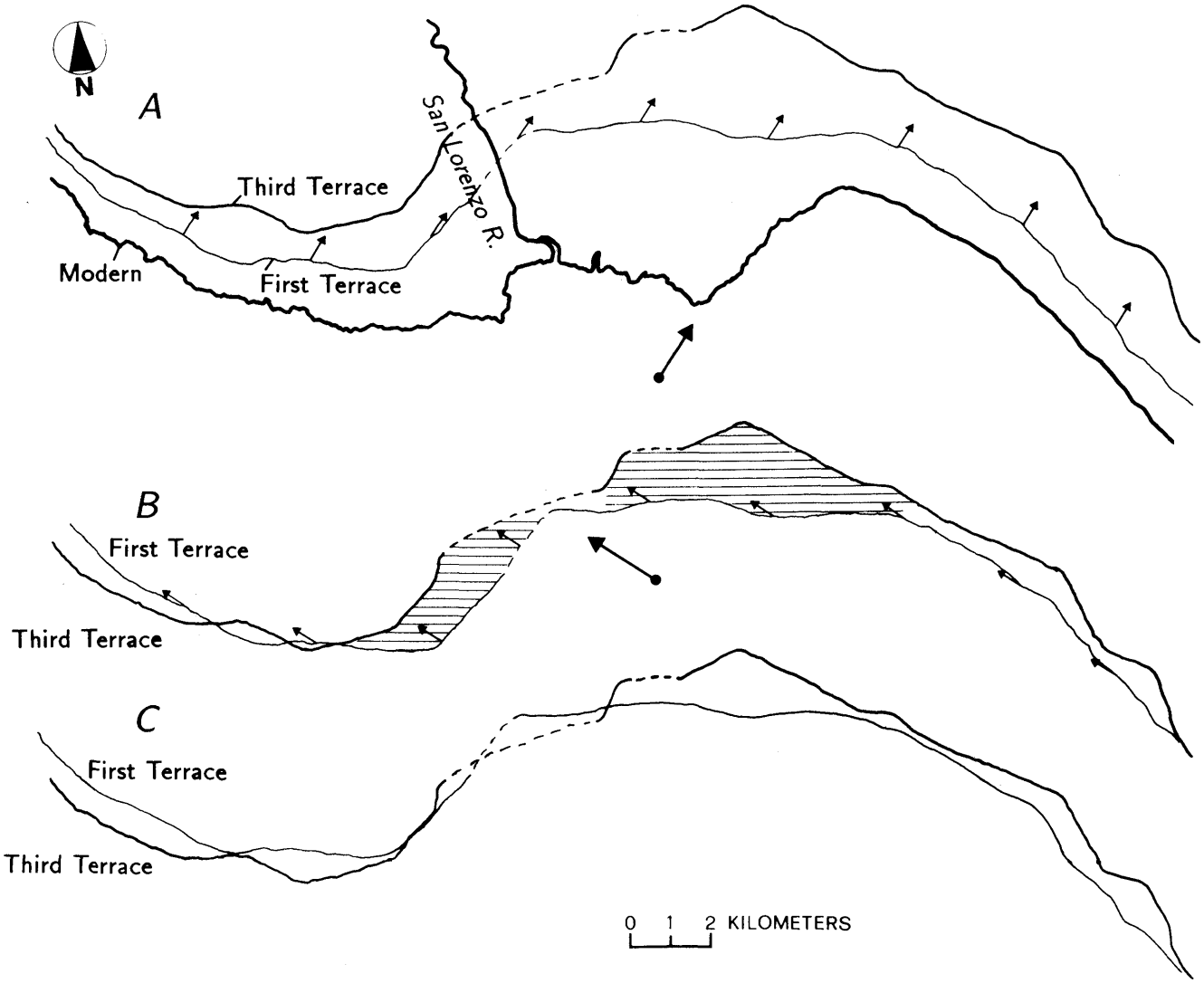

Figure 10.—Coastal area near Santa Cruz, Calif. (see fig. 9 for location), showing migration of shoreline and subsequent modifications of landscape in response to tectonic forces and processes during interval enclosed by ages of First and Third Terraces (Alexander, 1953). *A*, Present setting, showing location of modern, First Terrace, and Third Terrace shorelines. Small arrows on First Terrace shoreline point in direction opposite to that of forward migration of shoreline after pure uplift, as predicted by Geological Fault Model (fig. 4); length of lower large arrow indicates amount of motion (~1.5 km) necessary to match visually shorelines of First and Third Terraces. Rate of forward migration is controlled by uplift rate and a combination of elements controlling original slope of sea floor. *B*, Paleoshorelines of First and Third Terraces after backmigration of younger shoreline parallel to gradient of uplift. Small arrows on First Terrace shoreline point in a direction opposite to that of its apparent lateral migration; length of upper large arrow indicates amount of motion (≈1.5 km) necessary to match visually shorelines of First and Third Terrace. For simplicity, younger shoreline is moved rigidly, in contrast to field evidence that uplift rate and, thus, rate of forward migration double between east and west ends of figure, possibly partly explaining gaps and overlaps observed at both ends. Two main gaps (lined areas) remain in central part of figure between sharp bends where orientation of shoreline changes from northwestward to southwestward, suggesting that shoreline may also have migrated laterally. *C*, Paleoshorelines of First and Third Terraces after backmigration illustrated in figure 10*B* and lateral migration parallel to orientation of Pacific-North American plate boundary. Visual match of two shorelines requires 1.5 to 2.0 km of motion in direction indicated by arrows in figure 10*B*. Because shorelines are farther from source of tectonic strain than in figure 10*B*, match should not be affected by assumption of rigid-body translation.

we can test on the basis of the state of deformation of our oldest datum.

It would have been interesting to test the other end of our record of tectonic uplift, that is, verify whether the peak of 1989 coseismic uplift is centered to the southeast of the culmination of First Terrace (site A, fig. 1), as expected. However, the leveling line that extends from Santa Cruz to Pajaro Gap through the Pajaro Valley (see Marshall and others, 1991, fig. 1) does not parallel the fault or the pattern of coseismic uplift and cuts the inner edge of First Terrace at an angle of ≈30°. The peak uplift (≈0.13 m) is observed at the bench mark located closest to the fault, which lies within 1 km of the culmination of First Terrace.

PROGRESSIVE UPLIFT OF THE CENTRAL SANTA CRUZ MOUNTAINS

The structural maps in figure 7 and 8 provide convincing evidence that the Purisima Formation has been highly deformed since its deposition. In general, the formation has been warped quite gently toward the northwest and against Ben Lomond Mountain, and tightly warped and locally folded in the narrow corridor between the San Andreas and Zayante faults, and has subsided several hundred meters beneath the Pajaro Valley and the inner part of Monterey Bay. Assuming a depositional depth in the range 50–500 m and assuming that the deformation process started ≥3 Ma, as suggested by studies of plate motion (Harbert and Cox, 1989) and regional geology (Clark and others, 1991), we can calculate individual maximum rates of long-term uplift and tilt for two of the topographic domains defined in figure 1. Assuming an earlier date for the inception of uplift (or assuming that the datum had been deformed by previous tectonic phases when uplift started 3 Ma) would proportionally reduce all the estimates. In the Laurel domain, the Purisima Formation has been tilted southeastward at a maximum rate of 1°/m.y.: The upper part of the domain records uplift at a maximum rate of 0.15 to 0.30 mm/yr, whereas its coastal part records subsidence at a rate of 0.10 to 0.25 mm/yr. This motion is pivoted along a northeast-trending line running through Santa Cruz, where the base of the Purisima Formation is exposed near sea level. In contrast, south-southwestward tilting at much more severe rates is observed in the Summit domain. Tilting at an average 5°/m.y. is observed close

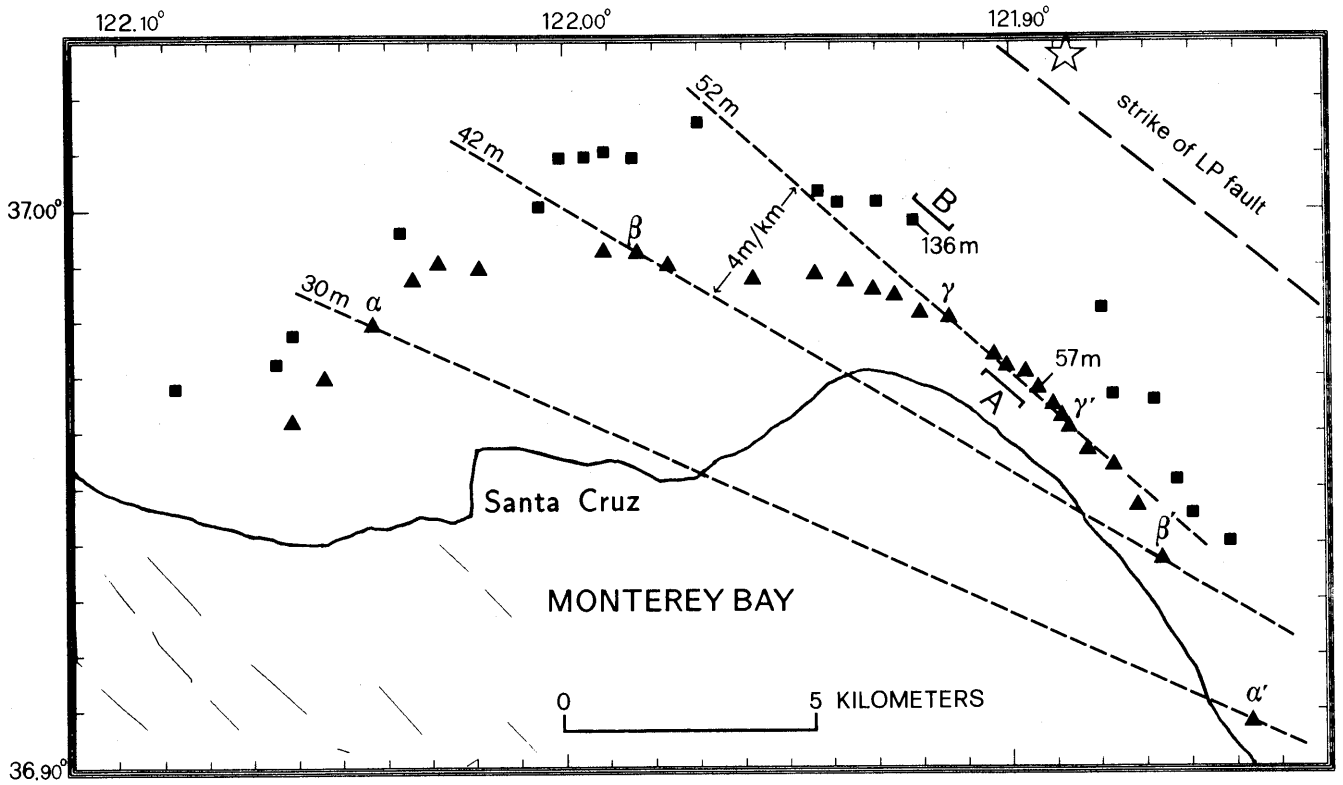

Figure 11.—Santa Cruz, Calif., area, showing locations of 28 positions of First Terrace (triangles) and 20 positions of Third Terrace (squares) as mapped by Alexander (1953). 57 m and 136 m, highest inner-edge positions of First and Third Terraces, respectively (see fig. 2 for elevations of other positions). A and B, preferred positions of culminations of First and Third Terraces, respectively (same as in figs. 1, 2, 7, 9). Dashed lines connect sites marked by α–α′, β–β′, and γ–γ′ in figure 2, indicating that for a comparable distance from the Loma Prieta (LP) fault, long-term uplift is higher near Santa Cruz than near the Pajaro Valley (see fig. 1). Star, epicenter of 1989 earthquake.

to the Zayante fault, whereas closer to the San Andreas fault the Purisima Formation has been folded in a series of tight synclines and anticlines. Throughout this domain, the Purisima Formation records uplift at a maximum rate of 0.2 to 0.4 mm/yr. Note that the peak Summit domain rates are, in fact, minimums for this domain, considering that the Purisima has been completely removed from much of the Santa Cruz Mountains northwest of the study area.

Although the uplift and tilting recorded by the Purisima Formation are generally comparable in magnitude to those recorded by late Pleistocene marine terraces, the distribution of uplift and the pattern of tilting displayed by the older datum differ substantially from those inferred for the younger features. For example, the culmination of First Terrace (site A, figs. 1, 7, 11), where uplift proceeds at 0.35 mm/yr, sits above a section of the Purisima Formation that records net subsidence of a few hundred meters, and the site where the growth of First Terrace has been slowest locates where long-term deformation has been modest. Even considering that the actual elevation of the Purisima Formation is not well constrained in the area where late Pleistocene uplift is largest, these observations testify to drastic changes not only in the intensity but also in the polarity of the displacement field. Indeed, these changes may simply indicate that the tectonic agent responsible for the deformation of the Purisima Formation differs from that causing such oblique-reverse slip earthquakes as the 1989 main shock and, thus, modern uplift along the coast (figs. 3, 6). Whether the regional strain field can be assumed constant for time scales of 1 m.y. is a fascinating issue of enormous potential for earthquake-prediction studies (Gordon and Stein, 1992), but extrapolation of modern deformation rates to the 3- to 4-m.y. history of the Purisima Formation seems against common sense.

Nonetheless, two issues raised in the previous paragraphs—the northwestward shift of the land relative to the source of uplift and possibly progressive accumulation of much of the topography to the northwest of Santa Cruz—suggest that the Purisima Formation furnishes an extended version of what we have seen recorded by the marine terraces. The base of the formation culminates at ≈400 m about 15 km north-northwest of Santa Cruz and about 19 km northwest of site A in figure 1, along the same trend of northwestward shift delineated by a comparison of the pattern of elevation of late Pleistocene marine terraces. To the northwest (site C, figs. 1, 7), the extrapolated base of the Purisima Formation is higher than the topography, and older rocks are exposed for a length of about 18 km. The formation appears again at elevations <350 m near Portola Park in the La Honda quadrangle (site D, fig. 1; Brabb and Pampeyan, 1983), at the northwest end of the central Santa Cruz Mountains, suggesting that its true culmination along an axis parallel to the plate boundary occurs somewhere between there and site C, 28±9 km away from the culmination of First Terrace (site A, fig. 1). Similarly to our comparison of terrace elevations, we interpret this distance as evidence for progressive northwestward advection of the Pacific plate through the source region of the 1989 earthquake at an average rate of 5.4 to 10.6 mm/yr.

TOPOGRAPHIC DOMAINS IN THE CENTRAL SANTA CRUZ MOUNTAINS: EVIDENCE FOR MULTIPLE TECTONIC PROCESSES

After the earthquake, many seismologists wondered whether it had been a characteristic earthquake and, if so, what its recurrence interval would be. For most investigators, the large reverse-slip component in the earthquake mechanism was a convincing argument in favor of a relatively infrequent occurrence, in contrast to most pre-1989 opinions envisioning a ≈100-yr recurrence interval for large earthquakes rupturing this section of the San Andreas fault. Even accounting for significant interseismic relaxation of the lower crust and for fast erosional degradation, the repetition of 50-cm-high jolts with a frequency of about a century would have produced a 3,000- to 4,000-m-high ridge, comparable to the Swiss Alps and much higher than the Santa Cruz Mountains. Therefore, when Anderson (1990) and Valensise and Ward (1990) provided geologic evidence that a Loma Prieta-type event may occur as rarely as every 600 to 700 yr, most of the seismological community agreed that this estimate was reasonable. The results reported here, however, indicate that even such an infrequent rate would produce significantly more topography than observed. For instance, the GFM (fig. 4) predicts 0.7 to 0.9 mm/yr of uplift and 5°–7°/m.y. of tilting in the upper part of the Laurel domain (fig. 1), which would ultimately produce at least 400 m/m.y. of topography. Field evidence (fig. 7), however, shows that, on average, the deformation recorded by the Purisima Formation within this domain cannot be more than 0.15 to 0.30 mm/yr of uplift and 1°/m.y. of tilting. In addition, the Purisima Formation is tilted south-southeastward, almost perpendicular to the southwestward direction predicted by the GFM for modern tilt. Anderson's (1990) rates of coastal uplift and tilting are 2 to 3 times higher than those predicted by the GFM and thus would at least double this 1:3 discrepancy.

In the previous sections, I have discussed different lines of evidence suggesting that what we see in the Santa Cruz Mountains is a process not only of creation but also of progressive passive transport of the topography parallel to the San Andreas fault. We can envision the geologic structure that should result from such a process as an arch elongated parallel to the plate boundary and culminating at a distance from the source of uplift proportional to the time elapsed since the onset of compression. Anderson (1990) developed this concept on the basis of purely topographic arguments, concluding that the present configuration of the

Santa Cruz Mountains can, in fact, be reproduced simply by repeating a Loma Prieta-type event at the same time that the land is moved northwestward at the rate normally assumed for strike slip on this section of the San Andreas fault. However, many important features of the Santa Cruz Mountains are not explained by Anderson's model, and so I present here an alternative analytical forward model by combining the effects of repeated Loma Prieta-type faulting (expressed by the GFM, fig. 4) and progressive northwestward advection of the crust along the plate boundary (fig. 12).

Our computer algorithm can be summarized as follows: (1) The source of the 1989 earthquake is initially shifted northwestward by a distance corresponding to the San Andreas slip rate multiplied by the time of slipping (for example, 12 mm/yr×3 m.y.=36 km); (2) the source of the 1989 earthquake is shifted back southeastward in steps corresponding to the right-lateral slip accumulated during 1,000 yr (for example, 12 mm/yr×1 ka=12 m); (3) the Loma Prieta fault is assumed to have slipped by an amount corresponding to the oblique-reverse slip accumulated during 1,000 yr (for example, 3 mm/yr×1 ka=3 m), and the expected vertical displacement field is calculated; and (4) steps 2 and 3 are iterated as many times as needed to bring the source of the 1989 earthquake back to its present position (for example, 3 m.y./1 ka=3,000 cycles). This algorithm allows the center of uplift to migrate relative to the land from its hypothesized position beneath the central Santa Cruz Mountains at the time of inception of uplift, to its present position beneath the San Lorenzo Valley-Santa Cruz area (fig. 1). To reduce the uncertainty associated with the evaluation of rates of erosional degradation, we refer all our predictions to an arbitrary horizontal datum and all our interpretations to a real datum, represented here by the Purisima Formation. To account at least in part for the reduction of topography by relaxation of the lower crust and mantle, we set the rigidity of the half-space equal to zero (Ward, 1986).

The main conclusions of our modeling are as follows: (1) the model (fig. 12*A*) appears to reproduce the elevation and, to some extent, the shape of the datum in the Laurel domain (fig. 1); (2) the model also seems to reproduce quite well the overall topography of the Santa Cruz Mountains, at least in the Laurel domain and along its northwestward extension; and (3) the site where the model predicts the peak long-term uplift of the datum falls about halfway between its northernmost outcrop in the central Santa Cruz Mountains and its southernmost outcrop in the northern Santa Cruz Mountains (sites C, D, figs. 1, 12).

Therefore, in parallel with what we inferred from the younger datums, our first conclusion is that the present morphology of the Purisima datum records the overprint of at least two simultaneously active tectonic processes. Our second conclusion concerns the rate of lateral advection of the Pacific crust around the Santa Cruz Mountains bend of the San Andreas fault. We find this rate to be compatible both with short-term estimates of 12.2±3.9 mm/yr from conventional geodesy (Prescott and others, 1981) and 10 mm/yr from very long baseline interferometric observations (Ward, 1990); with long-term geologic estimates of ≈14 mm/yr from displacement of early Pleistocene sedimentary deposits (Cummings, 1968), ≈14 mm/yr from displacement of late Pliocene sedimentary deposits (Addicott, 1969), and ≥12 mm/yr from paleoseismology (Hall, 1984); and with the multidisciplinary estimate of 19 mm/yr proposed by the Working Group on California Earthquake Probabilities (1990). Our third conclusion concerns a further constraint on the slip rate of the Loma Prieta fault. A comparison between figures 12*A* and 12*B* demonstrates that increasing by fourfold the 3-mm/yr average oblique-reverse slip rate of Valensise and Ward (1991) for the Loma Prieta fault, which implies reducing the expected recurrence interval of a Loma Prieta-type event to ≈150 yr, will produce uplift of the Purisima Formation up to 1,000 m in the Laurel domain (fig. 1), in strong contrast to field evidence (fig. 7). Including figure 12*C* in the comparison indicates that even changing the rate of lateral advection by 50 percent does not alter substantially the predicted elevation of the Purisima Formation in the Laurel domain, where control is best. A final conclusion concerns the model fit in the Pajaro domain (fig. 1), where Pleistocene subsidence is well documented (Dupré, 1990) and the Purisima Formation is found at its lowest elevation in the study area (down to −800 m, fig. 7). Both our model and the GFM predict long-term subsidence in this domain, but even considering the uncertainty in the original elevation of the Purisima Formation, the expected displacement is substantially smaller than observed.

Indeed, the depth of the Purisima Formation beneath the Pajaro Valley represents a major morphologic feature that is only part accounted for by our model. Another obvious misfit is represented by Ben Lomond Mountain (figs. 1, 7), an island of crystalline rocks embedded in the Tertiary sequence of the Santa Cruz Mountains. Both our model and the GFM show that Ben Lomond Mountain has undergone only a fraction of the long-term uplift sustained by the adjacent Laurel domain (fig. 1), which, in contrast, exhibits an average elevation about half that of the Coast Ranges. However, the observation that Ben Lomond Mountain is an inherited topographic feature—that is, a structural high of Salinian basement uplifted at least 15 Ma along the now-inactive Ben Lomond fault (fig. 7; Stanley and McCaffrey, 1983)—convincingly explains this discrepancy. The example of Ben Lomond Mountain underscores the role played by large inherited structural features in determining the topographic setting of an active region. The GFM predicts that ≈1 m.y. will be necessary to compensate for the 250-m average elevation contrast between the Ben Lomond and Laurel domains. At the same time, however, the contrast will be rejuvenated by the differential erodibility between the Salinian basement

of Ben Lomond Mountain and the Tertiary sequence underlying the Laurel domain, and so complete compensation may never take place before the next major reorientation of the strain field.

A second major and potentially more worrisome example of a topographic or geologic feature unaccounted for by both our and Anderson's (1990) models is the elevation of the Purisima datum in the Summit domain (fig. 1). The

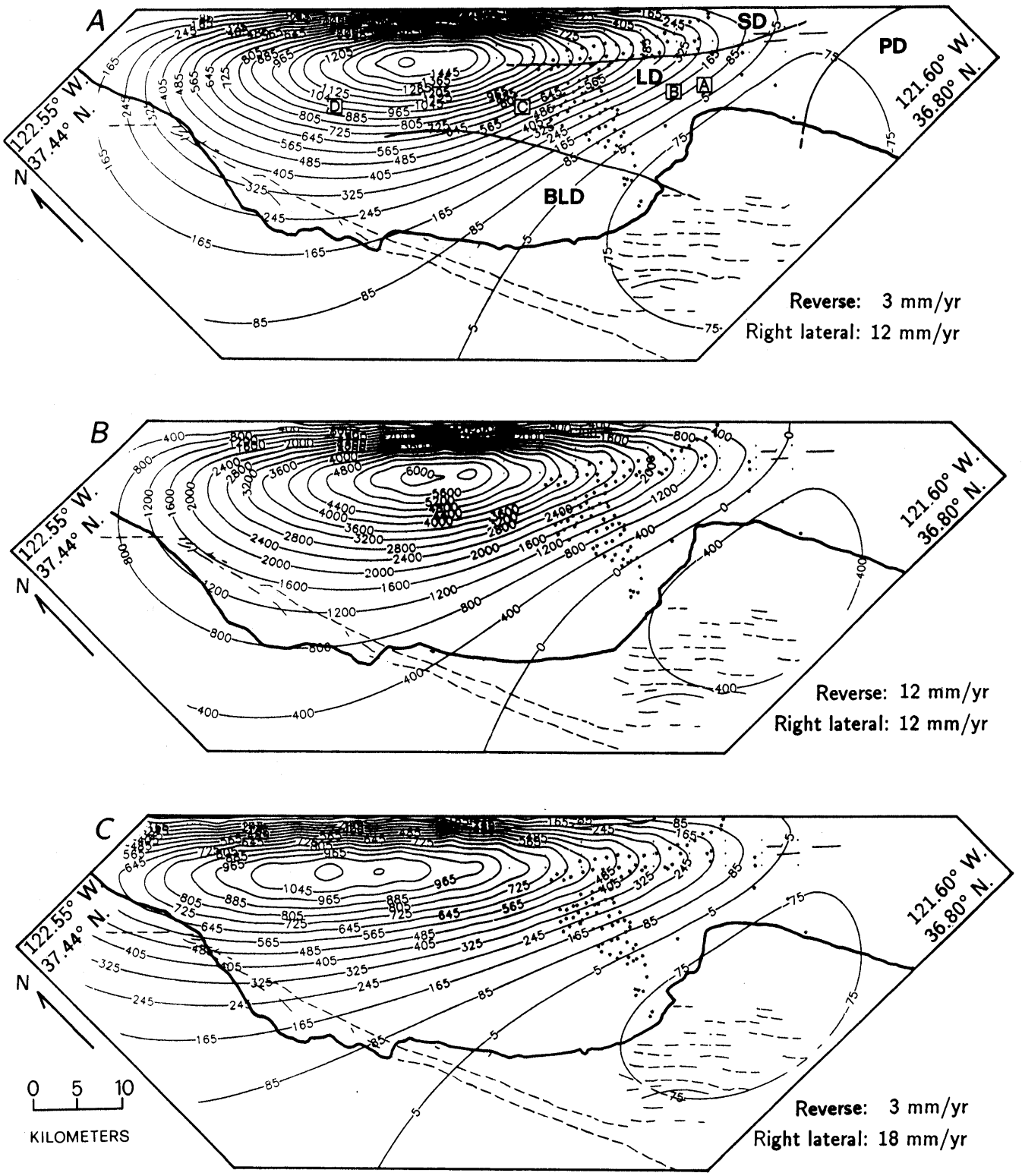

GFM predicts no to moderate uplift within this domain, consistent with leveling observations after the 1989 earthquake (Marshall and others, 1991). An even more difficult task is to explain the state of extreme deformation of the Purisima Formation in the corridor between the San Andreas and Zayante faults (McLaughlin, 1990), a feature unexplained by either the modest coseismic shortening observed in 1989 (Snay and others, 1991) or by a reevaluation of the 1906 earthquake slip vector (Segall and Lisowski, 1990).

Having considered all the known sources of tectonic strain, we must conclude that the generation of high topography in the Summit domain is driven by a separate and unknown process. The absence of surface faulting after the 1989 earthquake, the unusual upper depth of fault slip (≈5 km), and the comparability of this depth to the width of the Summit domain suggest that deformation of a 5- by 5-km parallelepiped of crust elongated parallel to the Pacific side of the San Andreas fault cannot be simply described by slip on regional faults. Instead, evidence from repeated pre-1989 leveling surveys showing a possible rate of uplift of 1 to 2 mm/yr (fig. 13) in the absence of significant coseismic release suggests that this domain undergoes continuous and, probably, aseismic deformation. This deformation could represent a form of bulk squeezing of the shallow crust as a result of the plate-boundary-perpendicular compression predicted by Harbert and Cox (1989), the same process that is ultimately responsible for Loma Prieta-type events at greater depths. This process could be invoked to account for at least part of the topography of the adjacent Loma Prieta domain, where it would represent a shallow-seated alternative to Davis and Namson's (1991) deep-thrusting model to explain the uplift of the Santa Cruz Mountains east of the San Andreas fault. Extreme deformation in the vicinity of the San Andreas fault could also be invoked to explain the discrepancy between the observed and predicted directions of tilting of the Purisima Formation in the Laurel domain. Diffuse compressional deformation of the shallow crust in the Summit and Loma Prieta domains is suggested by an analysis of the local pre-1989 seismicity (Seeber and Armbruster, 1990) that shows several small earthquakes with *P* axes almost perpendicular to the San Andreas fault.

◀ Figure 12.—Models of topography generation due to combination of oblique-reverse motion along Loma Prieta fault plane (simulated by repeated dislocation in a totally relaxed half-space) and right-lateral motion across Pacific-North American plate boundary (simulated by simple aseismic northwestward advection of the Pacific plate) for different combinations of oblique-slip and strike-slip rates, assuming that the Loma Prieta fault is stationary with respect to the North American plate. Process iterates by small, discrete slip increments for an equivalent duration of 3 m.y., estimated age of present compressional tectonism. Contour intervals (80, 400, and 80 m, respectively, in figs. 12*A*, 12*B*, and 12*C*) represent cumulative deformation of an arbitrary horizontal datum originally at sea level. Stars, outcrops of base of the Purisima Formation (see fig. 7); irregular thin lines, faults, dashed where inferred. Predictions can be directly compared with structural map in figure 7 (after correction for depth of deposition of the Purisima Formation), whereas a comparison with actual topography requires assumption about rate of erosional denudation of range. BLD, Ben Lomond domain; LD, Laurel domain; PD, Pajaro domain; SD, Summit domain. Solutions in figures 12*B* and 12*C* are largely unrealistic (topography is too high in fig. 12*B*; too much topography is predicted in the northern Santa Cruz Mountains in fig. 12*C*), whereas figure 12*A* produces a reasonable approximation to observed and extrapolated morphology of the Purisima Formation. Note that site where figure 12*A* predicts culmination of datum is about halfway between northwesternmost outcrop of the Purisima Formation in the central Santa Cruz Mountains (C) and southernmost outcrop of the Purisima in the northern Santa Cruz Mountains (D). In all three models, however, no topography is predicted in area corresponding to the Summit domain (and the Loma Prieta domain, not shown), indicating that complete modeling of topography generation in the central Santa Cruz Mountains requires at least one more agent of long-term tectonic strain (see fig. 13). A and B, culminations of First and Third Terraces, respectively.

OPEN QUESTIONS AND CONCLUSIONS

Analysis of three well-identified geologic datums has allowed the identification of different but coexisting processes of tectonic deformation and the quantification of their average rates. This section summarizes the main findings concerning each of these processes, emphasizing what I believe is reasonably ascertained and what instead requires further investigation.

The first process we analyzed is responsible for the creation of the Santa Cruz terraces. Although broad agreement exists about the causal relations between slip on the Loma Prieta fault and coastal uplift in the area between Santa Cruz and the Pajaro Valley, uncertainty still remains concerning two aspects of this relation: (1) the presence of elevated coastal features to the west of Santa Cruz and (2) the rates at which deformation proceeds throughout the study area. The first aspect was addressed by Anderson and Menking (1991), who proposed that uplift of the coastal region west of Santa Cruz could be driven by a component of reverse motion on the San Gregorio fault (figs. 4, 5), and by Valensise and Ward (1991), who invoked slip on the San Andreas fault proper to explain the existence and pattern of elevation of First Terrace between Santa Cruz and Point Año Nuevo. Not much is known, however, about the slip rate and sense of motion of the San Gregorio fault, and the only available estimates diverge quite drastically (1 mm/yr: Hamilton and others, 1979; 6/11 mm/yr: Weber and Cotton, 1981). However, various lines of geologic evidence contradict Anderson and Menking's (1991) hypothesis. (1) The local orientation of the San Gregorio fault is ≈10° more northerly than the local direction of plate motion (N. 34°±2° W.; Ward, 1990), suggesting that a dip-slip component of motion on the right-lateral San Gregorio fault would more likely be normal than reverse. (2) The largest uplift from motion on the San Gregorio fault should be recorded closest to the

fault itself, in contrast with field observations showing a local culmination of Bradley and Griggs' (1976) Highway 1 platform ≈5 km southeast of the site where the fault cuts the terrace's inner edge (fig. 4). This pattern would be consistent with burial of the San Gregorio fault at ≈3-km depth, in contrast with the observation that it clearly is not a blind fault. (3) Coastal uplift by reverse motion on the San Gregorio fault would produce terraces dipping inland, in contrast with field evidence (particularly for the older terraces) that the Santa Cruz terraces display a progressive seaward tilting (see Bradley and Griggs, 1976, fig. 14). In any case, the mechanism envisioned by Valensise and Ward (1991) is not substantiated by the results of the present study, and so the dissimilarity between the pattern of 1989 coseismic elevation changes and the pattern of elevation of the Santa Cruz terraces is still an open question.

Reducing the scatter in the timing of terrace formation (table 1) and, thus, the uncertainties in the rate of coastal uplift is also a difficult task. Addressing this second aspect requires the availability of reliable direct ages on fossils collected from at least one of the best expressed terraces, a condition that may never be fulfilled in the Santa Cruz region. Nevertheless, the lowest uplift rates among all those published (Bradley and Griggs, 1976; K.R. Lajoie, unpub. data, 1991; Valensise and Ward, 1991) are substantially higher than the rates of deformation recorded by the Purisima Formation and likely represent upper limits for the average rate of vertical strain in the study area, at least during the late Pleistocene.

Comparison of the map shape and the elevation of strandlines of different ages fully supports the fascinating hypothesis that the elevated coastal features in the Santa Cruz region also bear a strong imprint of the relative horizontal motion between the North American and Pacific plates. The rates of right-lateral motion that we calculated are comparable to both short- and long-term estimates of the rate of right-lateral slip on the Santa Cruz Mountains section of the San Andreas fault. This hypothesis leads to the prediction that most of the topography created by Loma Prieta-type reverse faulting should be found a few tens of kilometers northwest of the present position of the fault. Although this prediction is, indeed, supported by observations, obtaining precise estimates of the rate of lateral advection is made difficult by the erosion of key parts of the Purisima datum and by the interference of other, more efficient modes of topography generation, such as the bulk squeezing described previously.

An intriguing problem revealed by the model of topography generation shown in figure 12 is the excess subsidence detected in the Pajaro Valley. None of the tectonic processes considered in the present study can be invoked to explain why the Purisima datum has dropped in this area at a rate of 0.10 to 0.25 mm/yr since its deposition (fig. 7). Indirect evidence for continuing subsidence is supplied by a comparison of the present bathymetry of northern Monterey Bay and the coastal topography between Santa Cruz and Aptos (fig. 1). Extrapolating the present uplift rate forward to a hypothetical highstand

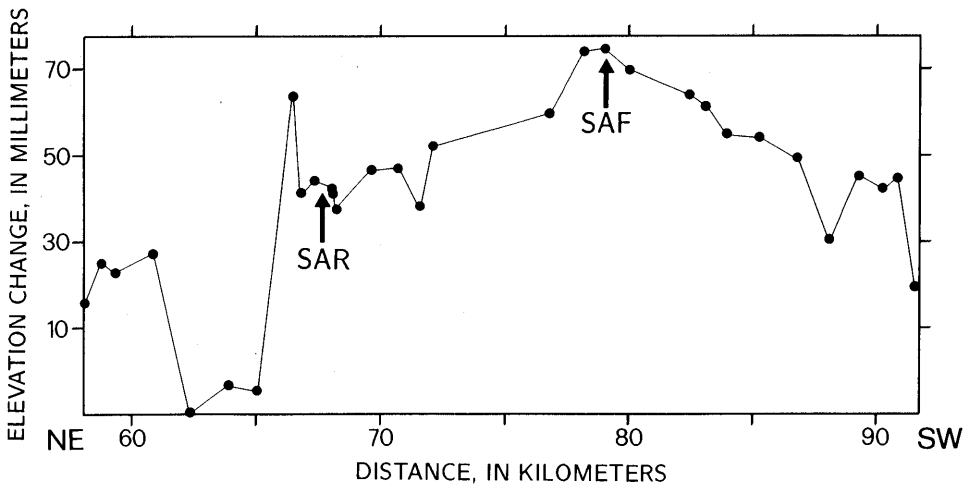

Figure 13.—Elevation changes along leveling line across south end of the Loma Prieta rupture zone (see fig. 4 for locations), using data of Marshall and others (1991). SAF and SAR, crossings of the San Andreas and Sargent faults, respectively. Note that measured elevation changes are relative to an arbitrary, not absolute, datum. Anomalous signal observed in distance range 62–65 km was interpreted by Marshall and others (1991, fig. A2) as nontectonic subsidence associated with ground-water withdrawal. Profile suggests uplift of the southern Santa Cruz Mountains relative to adjacent plains at a rate of 1 to 2 mm/yr during interval 1972–89. Observed pattern suggests same bulk-squeezing deformational style recorded by the Purisima Formation in vicinity of the San Andreas fault (see Summit domain, fig. 1). Even though area is affected by persistent microseismicity, no earthquake of $M>4$ has occurred since 1972 (Olson, 1990), suggesting that observed strain is result of diffuse deformation rather than of slip on regional faults.

100 ka from now shows that the shoreline should then appear nearly rectilinear (dotted line, fig. 9), in contrast to the curved shape of First, Second, and Third Terraces and of the modern shoreline. The action of an unknown tectonic force causing subsidence centered near Aptos would locally counteract the uplift, with the final effect of giving the new shoreline the same shape as that of its fossil counterparts. This unknown force producing subsidence at a rate of <0.25 mm/yr appears as the mirror image of the previously discussed, yet unexplained, force that causes coastal uplift at <0.20 mm/yr between Santa Cruz and Point Año Nuevo (figs. 1, 4). Interestingly, the bipolar arrangement of these two forces has a reverse correspondence on the opposite side of the San Andreas fault, where uplift of the Loma Prieta domain (fig. 1) is balanced by documented late Pleistocene subsidence of southern San Francisco Bay at 0.2 to 0.4 mm/yr (Atwater and others, 1977). At this time, we can only speculate that this quadrupole of forces producing deformation of opposite sign at comparable rates owes its existence to the geometric and dynamic complexities associated with the Santa Cruz Mountains bend in the San Andreas fault.

Possibly the most important conclusion of this study concerns the process responsible for the generation of high topography in the vicinity of the San Andreas fault, which also represents the highest relief in the entire Santa Cruz Mountains. In addition to the geodetic evidence discussed above (fig. 13), geologic evidence is now available in the form of a series of terraces on the Pajaro River that have been uplifted several hundred meters as they cross the San Andreas fault around Pajaro Gap (fig. 1). Hall and others (1991) reconstructed these terraces, showing that the strongest upwarping has a wavelength of 5 to 10 km and that late Pleistocene uplift has locally proceeded at ≥0.2 to 0.3 mm/yr. To account for the absence of substantial vertical displacement across the main faults in the study area, Hall and others (1991) hypothesized that the Pajaro River terraces, along with most of the southern Santa Cruz Mountains, have been uplifted by the activity of a southwest-dipping, low-angle, buried thrust fault rooted in the San Andreas fault near 8-km depth. Hall and others' model compares directly with other previously discussed hypotheses for explaining the presence of high topography east of the San Andreas fault, such as (1) activity of the Sargent-Berrocal fault system (Schwartz and others, 1990), (2) activity of a shallowly northeast dipping thrust fault extending from 12- to 17-km depth (Davis and Namson, 1991), and (3) the bulk-squeezing deformational style proposed in this paper. The third hypothesis, however, is the only one that may also account for uplift in the Summit domain (fig. 1), an area where mild subsidence is expected on the basis of the other models. Paradoxically, although the bulk-squeezing deformational mode should sooner or later bring to light all the main faults in the study area, none of them would necessarily be active seismic sources; instead, each of them would be required to relieve some of the stress accumulated in the top few kilometers of the crust, a task that would be made easier by large nearby earthquakes, as seen in 1906 and 1989. The accumulation of sympathetic slip would make these faults appear active in the geologic record, but the individual long-term slip rates would be negligible in comparison with the rate of other plate-boundary-related processes. Once the activity of these faults has been established, deciding whether they act as independent sources of seismicity or as passive participants in broader scale plate-boundary events becomes the key question for seismic-hazard assessment in the densely populated San Francisco Bay region. We believe that this question could be fruitfully addressed by extending the concepts and methodology of the present study to the region east of the San Andreas fault.

ACKNOWLEDGMENTS

This research was performed while I was a Visiting Scientist at the U.S. Geological Survey in Menlo Park, Calif. I am indebted to Earl Brabb, Jo Clark, Bob McLaughlin, and Ross Stein of the U.S. Geological Survey and to Bob Anderson and Steve Ward of the University of California, Santa Cruz, for providing valuable data and suggestions about central aspects of this work. In particular, I thank Earl Brabb for supplying the original well data, and Bob McLaughlin for making available a preprint of his geologic map of the Laurel quadrangle. I am especially grateful to Ross Stein for his help in obtaining financial and logistic support for this research and for his encouragement, and to Enzo Boschi for the continuing opportunity to extend my research to different parts of the world. Critical reviews by Bob Anderson, Bob Simpson, and Ross Stein substantially improved the manuscript.

REFERENCES CITED

Addicott, W.O., 1969, Late Pliocene mollusks from San Francisco Peninsula, California, and their paleogeographic significance: California Academy of Sciences Proceedings, ser. 4, v. 37, no. 3, p. 57–93.

Alexander, C.S., 1953, The marine and stream terraces of the Capitola-Watsonville area [Calif.]: Berkeley, University of California Publications in Geography, v. 10, no. 1, p. 1–44.

Anderson, R.S., 1990, Evolution of the northern Santa Cruz Mountains by advection of crust past a San Andreas fault bend: Science, v. 249, no. 4967, p. 397–401.

Anderson, R.S., and Menking, K.M., 1991, The Santa Cruz marine terraces, constraints on the Loma Prieta and other seismic events: poster shown at Workshop on the Seismotectonic Significance of the Loma Prieta Earthquake, Pacific Grove, Calif., 1991.

Atwater, B.F., Hedel, C.W., and Helley, E.J., 1977, Late Quaternary depositional history, Holocene sea-level changes, and vertical crustal movement, southern San Francisco Bay, California: U.S. Geological Survey Professional Paper 1014, 15 p.

Aydin, Atilla, and Page, B.M., 1984, Diverse Pliocene-Quaternary tectonics in a transform environment, San Francisco Bay region, California: Geological Society of America Bulletin, v. 95, no. 11, p. 1303–1317.

Brabb, E.E., 1989, Geologic map of Santa Cruz County, California: U.S. Geological Survey Miscellaneous Investigations Series Map I–1905, scale 1:62,500.

Brabb, E.E., and Pampeyan, E.H., 1983, Geologic map of San Mateo County, California: U.S. Geological Survey Miscellaneous Investigations Series Map I–1257–A, scale 1:62,500.

Bradley, W.C., and Griggs, G.B., 1976, Form, genesis, and deformation of central California wave-cut platforms: Geological Society of America Bulletin, v. 87, no. 3, p. 433–449.

Chappell, John, 1974, Geology of coral terraces, Huon Peninsula, New Guinea; a study of Quaternary tectonic movements and sea-level changes: Geological Society of America Bulletin, v. 85, no. 4, p. 553–570.

Clark, D.H., Hall, N.T., Hamilton, D.H., and Heck, R.G., 1991, Structural analysis of late Neogene deformation in the central offshore Santa Maria Basin, California: Journal of Geophysical Research, v. 96, no. B4, p. 6435–6457.

Clark, J.C., 1981, Stratigraphy, paleontology, and geology of the central Santa Cruz Mountains, California Coast Ranges: U.S. Geological Survey Professional Paper 1168, 51 p.

Clark, J.C., and Rietman, J.D., 1973, Oligocene stratigraphy, tectonics, and paleogeography southwest of the San Andreas fault, Santa Cruz Mountains and Gabilan Range, California Coast Ranges: U.S. Geological Survey Professional Paper 783, 18 p.

Crouch, J.K., Bachman, S.B., and Shay, J.T., 1984, Post-Miocene compressional tectonics along the central California margin, in Crouch, J.K., and Bachman, S.B., eds., Tectonics and sedimentation along the California margin: Society of Economic Paleontologists and Mineralogists, Pacific Section Field Trip Guidebook, v. 38, p. 37–54.

Cummings, J.C., 1968, The Santa Clara Formation and possible post-Pliocene slip on the San Andreas fault in central California, *in* Dickenson, W.R., and Grantz, Arthur, eds., Proceedings of conference on geologic problems of the San Andreas fault system: Stanford, Calif., Stanford University Publications in the Geological Sciences, v. 11, p. 191–207.

Davis, Thomas, and Namson, Jay, 1991, Loma Prieta earthquake and late Cenozoic structure of the southern Santa Cruz Mountains; possibilities and uncertainties of crustal structure: technical report to U.S. Geological Survey under contract 14–08–0001–G1830, 21 p.

Dietz, L.D., and Ellsworth, W.L., 1990, The October 17, 1989, Loma Prieta, California, earthquake and its aftershocks; geometry of the sequence from high-resolution locations: Geophysical Research Letters, v. 17, no. 9, p. 1417–1420.

Dupré, W.R., 1990, Quaternary geology of the Monterey Bay region, California, *in* Garrison, R.E., Greene, H.G., Hicks, K.R., Weber, G.E., and Wright, T.L., eds., Geology and tectonics of the central California Coast region, San Francisco to Monterey: American Association of Petroleum Geologists Field Trip Guidebook, p. 185–191.

Gordon, R.G., and Stein, Seth, 1992, Global tectonics and space geodesy: Science, v. 256, no. 5055, p. 333–342.

Greene, H.G., 1977, Geology of the Monterey Bay region: U.S. Geological Survey Open-File Report 77–718, 340 p.

Greene, H.G., and Clark, J.C., 1979, Neogene paleogeography of the Monterey Bay area, California, *in* Armentrout, J.M., Cole, M.R., and TerBest, Harry, Jr., eds., Cenozoic paleogeography of the western United States; Pacific Coast Paleogeography Symposium: Los Angeles, Society of Economic Paleontologists and Mineralogists, Pacific Section, p. 277–298.

Hall, N.T., 1984, Holocene history of the San Andreas fault between Crystal Springs reservoir and San Andreas dam, San Mateo County, California: Seismological Society of America Bulletin, v. 74, no. 1, p. 281–299.

Hall, N.T., Lettis, W.R., de Wit, M.W., and Angell, M., 1991, Late Quaternary uplift along the Pajaro River, southern Santa Cruz Mountains, California: technical report to U.S. Geological Survey under contract 14–08–0001–G1828, 45 p.

Hamilton, D.H., Fisher, D.L., and Jahns, R.H., 1979, Evidence of Quaternary right slip and other deformation along the San Gregorio fault, California; another view [abs.]: Geological Society of America Abstracts with Programs, v. 11, no. 7, p. 437–438.

Hanks, T.C., Bucknam, R.C., Lajoie, K.R., and Wallace, R.E., 1984, Modification of wave-cut and faulting-controlled landforms: Journal of Geophysical Research, v. 89, no. B7, p. 5771–5790.

Harbert, William, 1991, Late Neogene relative motions of the Pacific and North America plates: Tectonics, v. 10, no. 1, p. 1–15.

Harbert, William, and Cox, Allan, 1989, Late Neogene motion of the Pacific Plate: Journal of Geophysical Research, v. 94, no. B3, p. 3052–3064.

Kanamori, Hiroo, and Satake, Kenji, 1990, Broadband study of the 1989 Loma Prieta earthquake: Geophysical Research Letters, v. 17, no. 8, p. 1179–1182.

Keraudren, Bertrand, and Sorel, Denis, 1987, The terraces of Corinth (Greece)—a detailed record of eustatic sea-level variations during the last 500,000 years: Marine Geology, v. 77, no. 1–2, p. 99–107.

Lajoie, K.R., 1986, Coastal tectonics, in Active tectonics: Washington D.C., National Academic Press, p. 95–124.

Marshall, G.A., Stein, R.S., and Thatcher, Wayne, 1991, Faulting geometry and slip from co-seismic elevation changes; the 18 October, 1989, Loma Prieta, California, earthquake: Seismological Society of America Bulletin, v. 81, no. 5, p. 1660–1693.

McLaughlin, R.J., 1990, Sargent fault zone at Loma Prieta, stop 4 *of* Schwartz, D.P, and Ponti, D.J., eds., Field guide to neotectonics of the San Andreas fault system, Santa Cruz Mountains, in light of the 1989 Loma Prieta earthquake: U.S. Geological Survey Open-File Report 90–274, p. 19–22.

McLaughlin, R.J., Clark, J.C., and Brabb, E.E., 1988, Geologic map and structure sections of the Loma Prieta 7½′ quadrangle, Santa Clara and Santa Cruz Counties, California: U.S. Geological Survey Open-File Map 88–752, scale 1:24,000.

McNally, K.C., Lay, Thorne, Protti-Quesada, Marino, Valensise, Gianluca, Orange, D.L., and Anderson, R.S., 1989, Santa Cruz Mountains (Loma Prieta) earthquake: Eos (American Geophysical Union Transactions), v. 70, no. 45, p. 1463–1467.

Muhs, D.R., 1983, Quaternary sea-level events on northern San Clemente Island, California: Quaternary Research, v. 20, no. 3, p. 322–341.

Olson, J.A., 1990, Seismicity in the twenty years preceding the Loma Prieta, California earthquake: Geophysical Research Letters, v. 17, no. 9, p. 1429–1432.

Pampeyan, E.H., 1979, Preliminary map showing recency of faulting in coastal north-central California: U.S. Geological Survey Miscellaneous Field Studies Map MF–1070, scale 1:250,000.

Prescott, W.H., Lisowski, Michael, and Savage, J.C., 1981, Geodetic measurement of crustal deformation on the San Andreas, Hayward and Calaveras faults near San Francisco, California: Journal of Geophysical Research, v. 86, no. B11, p. 10853–10869.

Röde, Karl, 1930, Geomorphogenie des Ben Lomond (Kalifornien), eine Studie über Terrassenbildung durch marine Abrasion [Geomorphogeny of Ben Lomond (California), a study of terrace formation through marine abrasion]: Zeitschrift für Geomorphologie, v. 5, no. 1–2, p. 16–78.

Scholz, C.H., 1985, The Black Mountain asperity; seismic hazard of the southern San Francisco peninsula, California: Geophysical Research Letters, v. 12, no. 10, p. 717–719.

Schwartz, S.Y., Orange, D.L., and Anderson, R.S., 1990, Complex fault interactions in a restraining bend on the San Andreas fault, southern Santa Cruz Mountains, California: Geophysical Research Letters, v. 17, no. 8, p. 1207–1210.

Seeber, Leonardo, and Armbruster, J.G., 1990, Fault kinematics in the 1989 Loma Prieta rupture area during 20 years before that event: Geophysical Research Letters, v. 17, no. 9, p. 1425–1428.

Segall, Paul, and Lisowski, Michael, 1990, Surface displacements in the 1906 San Francisco and 1989 Loma Prieta earthquakes: Science, v. 250, no. 4985, p. 1241–1244.

Snay, R.A., Neugebauer, H.C., and Prescott, W.H., 1991, Horizontal deformation associated with the Loma Prieta earthquake: Seismological Society of America Bulletin, v. 81, no. 5, p. 1647–1659.

Stanley, R.G., 1985, Middle Tertiary sedimentation and tectonics of the La Honda basin, central California: U.S. Geological Survey Open-File Report 85–596, 263 p.

———1990, Evolution of the Tertiary La Honda basin, central California, *in* Garrison, R.E., Greene, H.G., Hicks, K.R., Weber, G.E., and Wright, T.L., eds., Geology and tectonics of the central California Coast region, San Francisco to Monterey: American Association of Petroleum Geologists Field Trip Guidebook, p. 1–29.

Stanley, R.G., and McCaffrey, Robert 1983, Extent and offset history of the Ben Lomond fault, Santa Cruz County, California, *in* Andersen, D.W., and Rymer, M.J., eds., Tectonics and sedimentation along faults of the San Andreas system: Los Angeles, Society of Economic Paleontologists and Mineralogists, Pacific Section, p. 79–90.

Stuart, R.M., Madrid, V.M., and Verosub, K.L., 1982, Late Neogene tectonics and sedimentation, Santa Cruz Mountains, California [abs.]: Geological Society of America Abstracts with Programs, v. 14, no. 4, p. 237–238.

Thatcher, Wayne, 1975, Strain accumulation on the northern San Andreas fault zone since 1906: Journal of Geophysical Research, v. 80, no. 35, p. 4873–4880.

Valensise, Gianluca, and Ward, S.N., 1990, Recurrence interval of Loma Prieta-type earthquakes based on long-term uplift patterns along the Santa Cruz coastline [abs.]: Seismological Research Letters, v. 61, no. 1, p. 23.

———1991, Long-term uplift of the Santa Cruz coastline in response to repeated earthquakes along the San Andreas fault: Seismological Society of America Bulletin, v. 81, no. 5, p. 1694–1704.

Vanderhurst, W.L., Cumming, J.C., and Andersen, D.W., 1982, The Santa Clara Formation as a record of late Cenozoic uplift of the Santa Cruz Mountains, Santa Clara County, California, *in* Ingersoll, R.V., and Woodburne, M.O., eds., Cenozoic nonmarine deposits of California and Arizona: Los Angeles, Society of Economic Paleontologists and Mineralogists, Pacific Section, p. 23–33.

Wallace, T.C., Velasco, Aaron, Zhang, Jiajun, and Lay, Thorne, 1991, A broadband seismological investigation of the 1989 Loma Prieta, California, earthquake; evidence for deep slow slip?: Seismological Society of America Bulletin, v. 81, no. 5, p. 1622–1646.

Ward, S.N., 1986, A note on the surface volume change of shallow earthquakes: Royal astronomical Society Geophysical Journal, v. 85, no. 2, p. 461–466.

———1990, Pacific-North America plate motions: new results from very long baseline interferometry: Journal of Geophysical Research, v. 95, no. B13, p. 21965–21981.

Weber, G.E., and Cotton, W.R., 1981, Geologic investigation of recurrence intervals and recency of faulting along the San Gregorio fault zone, San Mateo County, California: U.S. Geological Survey Open-File Report 81–263, 99 p.

Woodring, W.P., Bramlette, M.N., and Kew, W.S.W., 1946, Geology and paleontology of the Palos Verdes Hills, California: U.S. Geological Survey Professional Paper 207, 145 p.

Working Group on California Earthquake Probabilities, 1990, Probabilities of large earthquakes in the San Francisco Bay region, California: U.S. Geological Survey Circular 1053, 51 p.

This page intentionally left blank

THE LOMA PRIETA, CALIFORNIA, EARTHQUAKE OF OCTOBER 17, 1989:
EARTHQUAKE OCCURRENCE

TECTONIC PROCESSES AND MODELS

COMPLEX FAULT INTERACTIONS IN A RESTRAINING BEND ON THE SAN ANDREAS FAULT, SOUTHERN SANTA CRUZ MOUNTAINS, CALIFORNIA

By Susan Y. Schwartz, Daniel L. Orange, and Robert S. Anderson,
University of California, Santa Cruz

CONTENTS

ABSTRACT

The unusual oblique-thrust mechanism of the earthquake focused attention on the complex tectonic setting of the Santa Cruz Mountains section of the San Andreas fault. Near the main-shock epicenter, the San Andreas fault curves to the left, defining a restraining bend. The large thrust component of the main-shock focal mechanism is consistent with the horizontal compression expected across restraining bends. However, repeated Loma Prieta-type events cannot exclusively produce the observed topography of the southern Santa Cruz Mountains, the highest point of which subsided during the earthquake. In this paper, we integrate seismic, geomorphic, and tectonic data to investigate the possibility that motions on faults adjacent to the San Andreas fault play an important role in producing the observed topography. The three-dimensional geometry of active faults in this region is imaged using the Loma Prieta foreshock and aftershock sequences. The most conspicuous features of the fault geometries at depth are: (1) the presence of two distinct zones of seismicity corresponding to the San Andreas and Sargent-Berrocal fault zones; (2) the concave-upward shape of the Loma Prieta rupture surface; (3) the reduction in dip of the deepest parts of the rupture plane as the main-shock hypocenter is approached; (4) the apparent transfer of shallow slip in some areas from faults in the San Andreas fault zone to those in the Sargent-Berrocal fault zone; and (5) the presence of a deep, northeasterly dipping plane associated with the Sargent-Berrocal fault zone. We find that a model of fault interactions that involves displacement on faults in both the San Andreas and Sargent-Berrocal fault zones is consistent with Loma Prieta coseismic displacements, foreshock and aftershock seismicity, and observed topography.

INTRODUCTION

Several major transcurrent fault systems compose the diffuse transform boundary between the Pacific and North American plates. Although the faults that form this boundary (fig. 1) crudely parallel the direction of relative plate motion, minor changes in fault strike are evident that introduce geometric complexities which result in local tension or compression. Sibson (1986) termed these bends in strike-slip faults "releasing" or "restraining" bends, respectively. Although the predominance of right-lateral strike-slip motion in this region has been recognized since the great 1906 San Francisco earthquake, only recently has the prevalence of compressional features been appreciated (Aydin and Page, 1984).

In the vicinity of the 1989 Loma Prieta earthquake, the San Andreas fault curves to the left, describing a restraining bend here called the Santa Cruz bend. The horizontal compression expected across this restraining bend is consistent with the large thrust component of the Loma Prieta main shock and with the abundant observed compressional features in the southern Santa Cruz Mountains, such as folds and reverse faults (Aydin and Page, 1984). The highest topography lies on the east side of the San Andreas fault, a region that subsided during the earthquake (Lisowski and others, 1990). In this paper, we investigate the complex fault interactions that occur within the Santa Cruz bend. We are particularly interested in the development of high topography on the North American plate, which coincides with the middle of the restraining bend (fig. 1). If Loma Prieta-type events are characteristic of this region on any time scale, the vertical-displacement field associated with these events requires that fault motions resulting in diverse uplift patterns

must also occur in this region to produce the topographic relief. We evaluate the Sargent-Berrocal fault zone as a possible candidate to produce the observed topography. Here, we include the Berrocal, Sierra Azul, and Sargent faults (inset, fig. 1) in our definition of the Sargent-Berrocal fault zone. We find that a model which involves displacement on faults in both the San Andreas and Sargent-Berrocal fault zones can satisfy the available data.

TECTONIC SETTING

The complexity of the fault system composing the Pacific-North American plate boundary in this region of central California is illustrated in figure 1. Although the San Andreas and Hayward faults have both produced large earthquakes in 1838 and 1906 (San Andreas fault) and 1836 and 1868 (Hayward fault), several other near-parallel faults in the area have shown observable late Quaternary activity. Of these faults, the Sargent-Berrocal fault zone has been the most seismically active in recent years. Aside from abundant microseismicity along the southern section of the Sargent-Berrocal fault zone before the 1989 Loma Prieta earthquake and along the northern section during the aftershock sequence (U.S. Geological Survey locations of seismicity between 1969 and 1989; Bakun and McLaren, 1984), an M=5.0 earthquake followed by more than 100 aftershocks occurred on the Sargent-Berrocal fault zone (inset, fig. 1) in November 1964 (McEvilly, 1966). In addition, Olson (1990) interpreted the two largest events before the Loma Prieta main shock as rupturing the Sargent fault (inset, fig. 1). Owing to the abundant seismic activity along the Sargent-Berrocal fault zone both before and immediately after the Loma Prieta main shock, we believe that careful examination is warranted to establish the possible role of this fault zone in elevating the southern Santa Cruz Mountains.

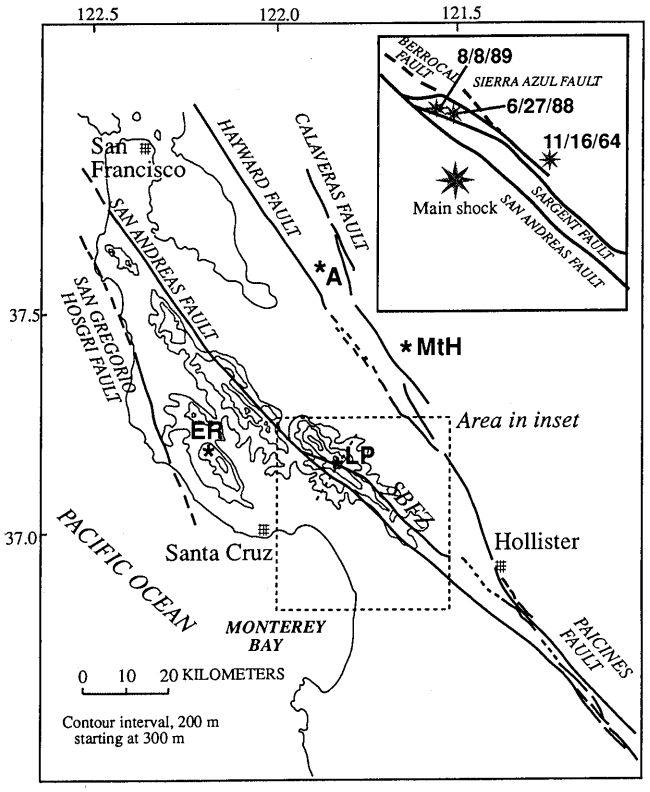

Figure 1.—Topographic and tectonic map of the San Francisco Bay region, central California, showing locations of major faults (dashed where inferred) and Global Positioning System stations (stars). Inset shows locations of faults composing Santa Cruz bend of the San Andreas fault, main shock of 1989 earthquake (large star), and recent M>5 earthquakes (small stars). A, Allison; ER, Eagle Rock; LP, Loma Prieta; MtH, Mount Hamilton; SBFZ, Sargent-Berrocal fault zone.

Field geologic studies indicate a range of surface dips from 20° SW. to vertical for the faults within the Sargent-Berrocal fault zone (McLaughlin, 1974; McLaughlin and others, 1971, 1988), although good surface outcrops of the fault are rare. McLaughlin (1974) interpreted the Sargent fault as a thrust fault over much of its length. Hay and others (1980), however, presented geologic evidence indicating that the faults of the Sargent-Berrocal fault zone have components of both strike-slip and thrust motion. They inferred a predominance of strike-slip motion on fault strands oriented parallel to the San Andreas fault and large thrust motion on strands oriented oblique to the San Andreas fault. A 5-year geodetic survey across the southern section of the Sargent-Berrocal fault zone near Hollister, Calif. (fig. 1; Prescott and Burford, 1976), indicated a present right-lateral-slip rate of 3 mm/yr. The next step toward understanding the interactions between the San Andreas fault and the Sargent-Berrocal fault zone is to obtain an accurate image of the these faults at depth.

LOMA PRIETA AFTERSHOCK SEISMICITY AND FAULTING GEOMETRY

The aftershock sequence of the 1989 Loma Prieta earthquake provides the best information on the three-dimensional geometry of the active faults in the region. A series of cross sections through the aftershock seismicity perpendicular to the strike of the San Andreas fault is shown in figure 2. The earthquakes shown were relocated by the U.S. Geological Survey, using the same velocity model as that used to locate the main shock (Dietz and Ellsworth, 1990). The topography and surface traces of the San Andreas and Sargent faults are superimposed on each cross section. The domainal analysis presented in figure 2 clearly indicates two distinct zones of seismicity in cross sections B–B' and D–D' that may correspond to separate activity on the San Andreas and Sargent-Berrocal fault zones. In contrast, cross section C–C' shows only one

zone of seismicity, indicating a significant change in the Loma Prieta rupture geometry along its strike.

The most conspicuous feature revealed by the aftershock seismicity is the striking change in fault-plane geometry as the San Andreas fault enters the Santa Cruz bend. In the bend region, the deepest parts of the fault reduce in dip to approximately 65°, whereas the shallower parts of the fault remain near-vertical, resulting in a concave-upward shape to the Loma Prieta rupture surface. Other interesting features of the seismicity are (1) the overall reduction in the depth of earthquakes to the south; (2) the apparent transfer of shallow slip from the San Andreas fault to the Sargent-Berrocal fault zone in cross section *C–C′*; and (3) the location of the main-shock hypocenter along the most shallowly dipping and deepest part of the rupture plane. The location of the hypocenter in the most contorted part of the fault plane is consistent with the notion that asperities may represent geometric complexities in fault planes.

FAULT GEOMETRY AND TOPOGRAPHY OF THE SANTA CRUZ MOUNTAINS

Anderson (1990) suggested that the northern Santa Cruz Mountains owe their elevation to repeated Loma Prieta-type events and northwestward advection of the resulting topography. As he pointed out, however, a similar argument cannot be made for the southern Santa Cruz Mountains, which lie on the opposite side of the San Andreas fault from the northern part of the range (fig. 1). Measurements of coseismic vertical displacements after the earthquake indicate that Loma Prieta (LP, fig. 1) subsided 14, 15, and 20 cm, respectively, relative to stations at Allison (A), Mount Hamilton (MtH), and Eagle Rock (ER) (Lisowski and others, 1990). Allison and Mount Hamilton, which are located more than 30 km from Loma Prieta, should have undergone very little coseismic elevation change during the earthquake. Therefore, the 14 to 15 cm of subsidence of Loma Prieta relative to these stations should approximate an absolute elevation change for this peak. Because the highest point in the southern Santa Cruz Mountains subsided during the earthquake, how might this topography have developed?

The images of the faulting geometry presented in figure 2 suggest a possible answer to this question. Cross sections *B–B′* through *D–D′* clearly show that the Sargent-Berrocal fault system was active during the aftershock sequence. Apparently, when the San Andreas and Sargent-Berrocal fault zones are close to one another, shallow slip may be accommodated on either or both fault zones. In cross section *C–C′*, all of the shallow slip occurred on the Sargent-Berrocal fault zone and almost no shallow slip on the San Andreas fault. The complex geometry of these two fault zones beneath Loma Prieta (cross sec. *D–D′*) accommodated shallow displacement during the earthquake, primarily on the more nearly vertical San Andreas fault west of the peak, resulting in subsidence of Loma Prieta. If more shallow displacement had occurred on the Sargent-Berrocal fault zone, as in cross section *C–C′*, it would have produced uplift rather than subsidence.

Evidence for yet-another fault oriented favorably to result in uplift northeast of the San Andreas fault comes from fault-plane solutions of several large deep earthquakes with epicenters located east of the fault. Olson (1990) determined northwesterly striking and 65° northeasterly dipping fault planes with reverse motion for six earthquakes before the 1989 Loma Prieta earthquake. These earthquakes, which are located in the Sargent-Berrocal fault zone near its intersection with the San Andreas fault, include the two largest events (M=5.2, 5.0) to have occurred here since 1969 (inset, fig. 1). In addition, similar fault-plane solutions have been obtained for moderate deep earthquakes on the southern section of the Sargent-Berrocal fault zone (Olson, 1990), including an M=5.0 event in November 1964 (McEvilly, 1966). The occurrence of large deep earthquakes with northeasterly dipping planes at several places along the Sargent-Berrocal fault zone suggests that these events occurred on a deep near-continuous plane that extends along this fault zone. If substantial displacement occurs on this fault plane, it would result in uplift east of the San Andreas fault, thereby contributing to the present high elevations observed there.

Thus far, we have discussed evidence for seismic activity on four fault planes in the Santa Cruz bend of the San Andreas fault, as shown schematically in figure 3*C*. Although seismic activity on these planes may be greatest at different positions along-strike of the San Andreas and Sargent-Berrocal fault zones, we present an along strike synthesis to best illustrate their possible interactions. Our hypothetical fault structure consists of plane 1, a deep (10–18 km), 65° SW.- dipping plane (activated in the main shock); plane 2, a shallow (5–10 km), vertical plane beneath the surface trace of the San Andreas fault (also activated in the main shock); plane 3, a shallow (5–10 km), ~65° SW.-dipping plane that is part of the Sargent-Berrocal fault zone (cross sec. *C–C′*, fig. 2); and plane 4, a deep, 65° NE.-dipping plane also associated with the Sargent-Berrocal fault zone (the plane generating the largest events preceding the main shock). Vertical surface displacements predicted for 1.3 m of reverse slip on each of these four fault planes were calculated by using a two-dimensional elastic-dislocation model (fig. 3*B*). Reverse motion on planes 1 and 2 would characterize the 1989 Loma Prieta earthquake, predicted displacements for which can be estimated by summing curves 1 and 2 in figure 3*B*. The observation of ~14 cm of subsidence at Loma Prieta that accompanied this earthquake (star, fig. 3*B*) agrees well with the 15 cm of subsidence predicted by this model. Motion on planes 1 and 3 or on plane 4 would result in vertical surface displacements consistent with the observed topography. Figure 3*B* shows that repeated events on rupture planes 1 and 2 cannot produce the high elevation of Loma Prieta and its surrounding mountain peaks (fig. 3*A*). Rupture on planes 1

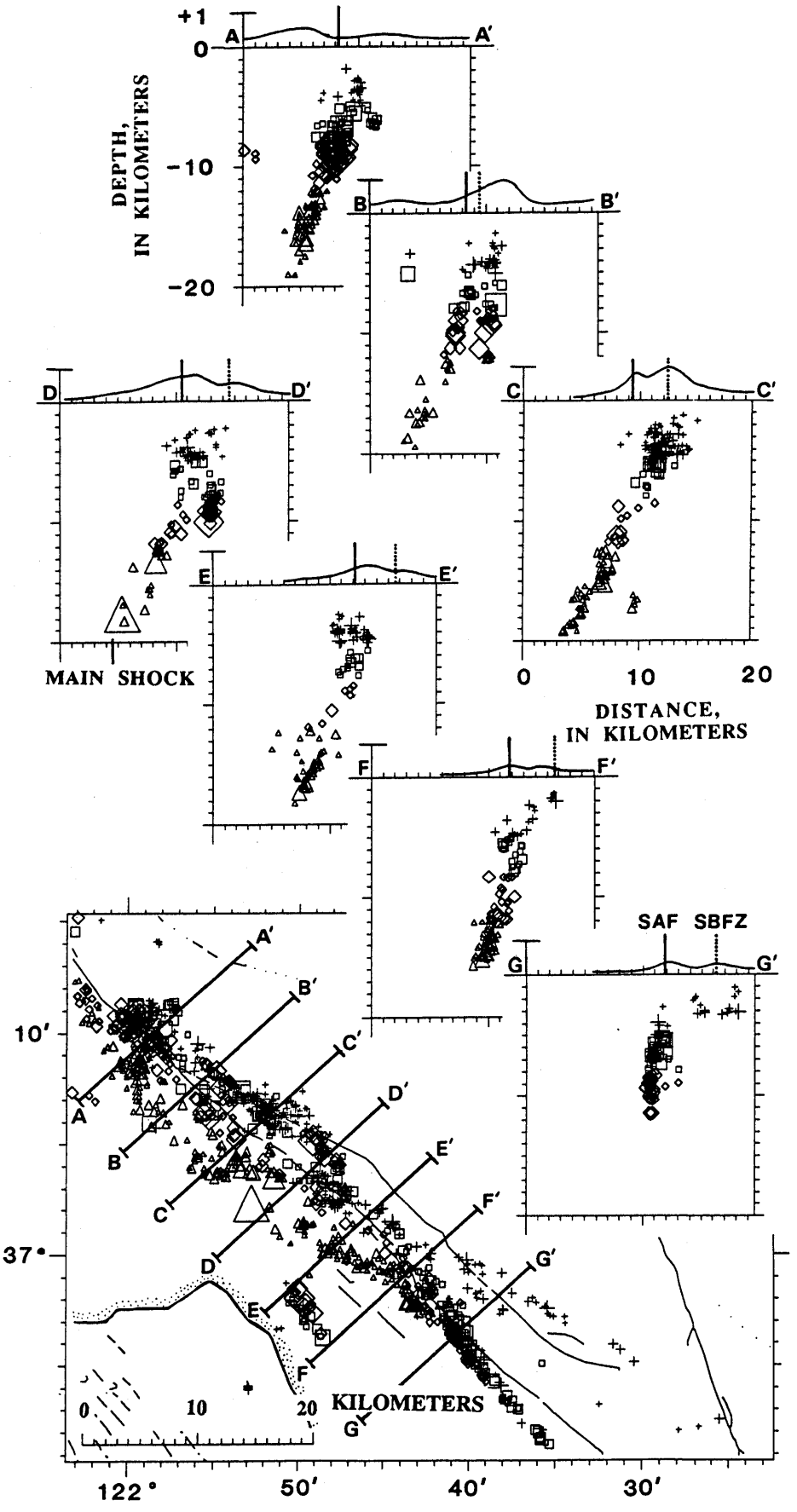
+1
0
-10
-20
DEPTH, IN KILOMETERS
A
A'
B
B'
C
C'
D
D'
E
E'
F
F'
G
G'
MAIN SHOCK
0
10
20
DISTANCE, IN KILOMETERS
SAF
SBFZ
10'
37°
0
10
20
KILOMETERS
122°
50'
40'
30'

and 3 or on plane 4, however, would produce surface displacements that act to elevate this area of presently high topography. Thus, some combination of events that rupture planes 1 and 2 with those that rupture planes 1 and 3 and (or) plane 4 is consistent with the available data.

DISCUSSION AND CONCLUSION

Although the four-plane-fault model presented here is consistent with the available data, it undoubtedly oversimplifies what must be a more complex system of faults in the region. For example, there is some evidence that the vertical San Andreas fault imaged at shallow depths by the aftershock seismicity extends to greater depths. Seismicity during the 10-yr period before the earthquake includes some deep events located directly below the surface trace of the San Andreas fault (Olson, 1990). Olson interpreted the difference in the apparent dip of the San Andreas fault at depth, imaged by seismicity before and after the earthquake, as representing two different fault planes: the vertical San Andreas fault and the southwest-dipping fault that ruptured in the Loma Prieta main shock. Geodetic data, however, require that parts of both these fault planes ruptured in the main shock. There is little evidence for a deep vertical extension of the San Andreas fault in the Loma Prieta aftershock data (with the possible exception of four deep events in cross section *C–C'*, fig. 2). Slip on a deep vertical extension of the San Andreas fault with primarily strike slip motion would produce less vertical displacement than slip on the fault planes with predominantly oblique motion.

Repeated failure of the Loma Prieta rupture plane exclusively is inconsistent with the high topography observed in the southern Santa Cruz Mountains. The transfer of shallow slip from the vertical San Andreas fault to a southwest-dipping fault of the Sargent-Berrocal fault zone provides evidence for seismic activity on a fault plane favorably oriented to uplift the southern Santa Cruz Mountains. Evidence for activity on another fault plane properly oriented to uplift these mountains comes from fault-plane solutions of the largest earthquakes to occur in the Loma Prieta aftershock zone since at least 1969 (Olson, 1990). The fault model shown in figure 3*C* is consistent with Loma Prieta coseismic displacements, both foreshock and aftershock seismicity, and can explain the high topography of the southern Santa Cruz Mountains.

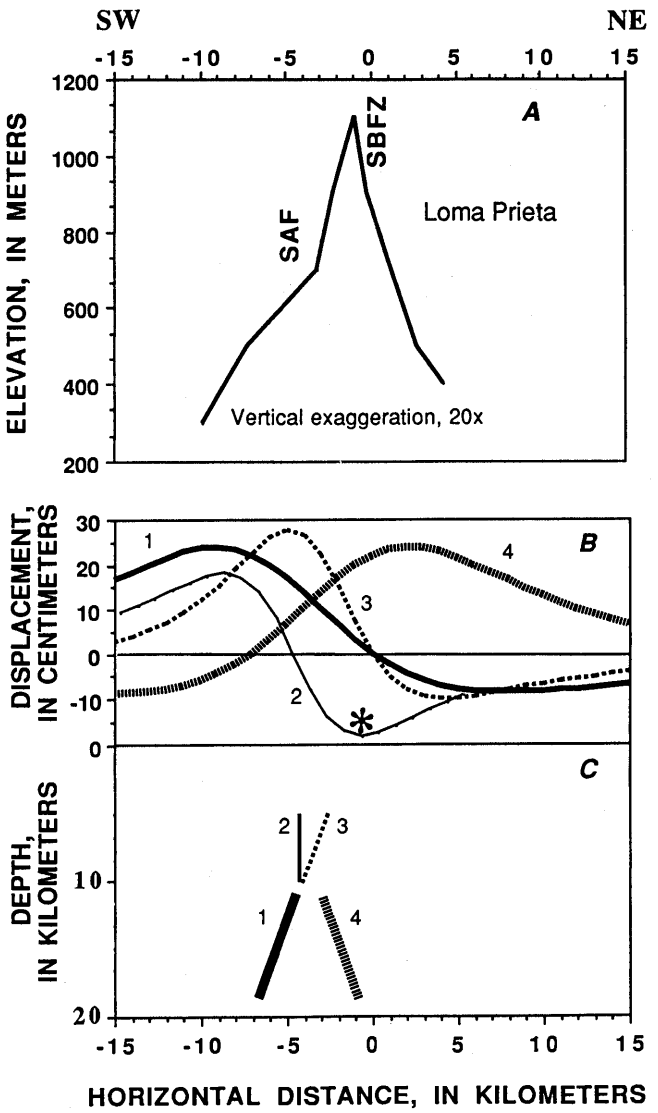

Figure 3.—Hypothetical fault structure near Santa Cruz bend of the San Andreas fault in the southern Santa Cruz Mountains, Calif. (see fig. 1 for location). *A*, Maximum elevation. *B*, Vertical displacement from 1.3 m of vertical slip on each of four buried fault planes shown in figure 3*C*. Star, measured subsidence from Global Positioning System. *C*, Hypothetical fault planes 1 through 4. SAF, San Andreas fault; SBFZ, Sargent-Berrocal fault zone.

◀ Figure 2.—Plan (bottom map) and cross-sectional (A–A' through G–G') views of main shock and aftershock sequence of 1989 earthquake (from Dietz and Ellsworth, 1990), showing topography (vertical exaggeration, 3×) and vertical projection of mapped traces of the Sargent and San Andreas faults above each cross section. Sizes of symbols are proportional to magnitude. SAF, San Andreas fault; SBFZ, Sargent-Berrocal fault zone. Irregular thin lines in plan view, faults, dashed where inferred, queried where uncertain.

REFERENCES CITED

Anderson, R.S., Evolution of the northern Santa Cruz Mountains by advection of crust past a San Andreas fault bend: Science, v. 249, no. 4967, p. 397–401.

Aydin, Atilla, and Page, B.M., 1984, Diverse Pliocene-Quaternary tectonics in a transform environment, San Francisco Bay region, California: Geological Society of America Bulletin, v. 95, no. 11, p. 1303–1317.

Bakun, W.H., and McLaren, Marcia, 1984, Microearthquakes and the nature of the creeping-to-locked transition of the San Andreas fault zone near San Juan Bautista, California: Seismological Society of America Bulletin, v. 74, no. 1, p. 235–254.

Dietz, L.D., and Ellsworth, W.L., 1990, The October 17, 1989, Loma Prieta, California, earthquake and its aftershocks; geometry of the

sequence from high-resolution locations: Geophysical Research Letters, v. 17, no. 9, p. 1417–1420.

Hay, E.A., Cotton, W.R., and Hall, N.T., 1980, Shear couple tectonics and the Sargent-Berrocal fault System in northern California, *in* Streitz, Robert, and Sherburne, R.W., eds., Studies of the San Andreas fault zone in northern California: California Division of Mines and Geology Special Report 140, p. 41–51.

Lisowski, Michael, Prescott, W.H., Savage, J.C., and Svarc, J.L., 1990, A possible geodetic anomaly observed prior to the Loma Prieta, California, earthquake: Geophysical Research Letters, v. 17, no. 8, p. 1211–1214.

McEvilly, T.V., 1966, The earthquake sequence of November 1964 near Corralitos, California: Seismological Society of America Bulletin, v. 56, no. 3, p. 755–773.

McLaughlin, R.J., 1974, The Sargent-Berrocal fault zone and its relation to the San Andreas fault system in the southern San Francisco Bay region and Santa Clara Valley, California: U.S. Geological Survey Journal of Research, v. 2, no. 5, p. 593–598.

McLaughlin, R.J., Clark, J.C., and Brabb, E.E. 1988, Geologic map and structure sections of the Loma Prieta 7½′ quadrangle, Santa Clara and Santa Cruz Counties, California, U.S. Geological Survey Open-File Map 88–752, scale 1:24,000, 2 sheets.

McLaughlin, R.J., Simoni, T.R., Osbun, E.D., and Bauer, P.G., 1971, Preliminary geologic map of the Loma Prieta-Mount Madonna area, Santa Clara and Santa Cruz Counties, California, U.S. Geological Survey Open File Map, scale 1:24,000.

Olson, J.A., Seismicity in the twenty years preceding the 1989 Loma Prieta, California earthquake: Geophysical Research Letters, v. 17, no. 9, p. 1429–1432.

Prescott, W.H. and Burford, R.P., 1976, Slip on the Sargent fault: Seismological Society of America Bulletin, v. 66, no. 3, p. 1013–1016.

Sibson, R.H., 1986, Rupture interaction with fault jogs, *in* Shamita, Das, Boatwright, John, and Scholz, C.H., eds., Earthquake source mechanics: American Geophysical Union Geophysical Monograph 37, p. 157–167.

TECTONIC PROCESSES AND MODELS

EARTHQUAKE-INDUCED STATIC-STRESS CHANGES ON CENTRAL CALIFORNIA FAULTS

By Robert W. Simpson and Paul A. Reasenberg,
U.S. Geological Survey

CONTENTS

ABSTRACT

We have calculated the static-stress changes caused by the earthquake on central California faults, using three-dimensional elastic-dislocation models in an elastic half-space. We compare the results for three different models of the Loma Prieta rupture and explore the effects of non-vertical dips on several faults, as well as the long-term redistribution of stresses that might accompany deep aseismic slip on vertical and horizontal structures. Calculated changes in the Coulomb failure function (CFF) after the earthquake correlate with observed changes in microseismicity rates and surface-creep rates, suggesting that the CFF can be used to describe the proximity of these faults to failure. The correlation favors a low apparent coefficient of friction $\mu' \approx 0.2$. Such a low value could be explained by the combination of a normal laboratory value for the coefficient of friction ($\mu \approx 0.75$) moderated by pore-fluid effects, with a Skempton's coefficient $B \approx 0.7$. Our models suggest that the earthquake-induced stress changes are unlikely to trigger an earthquake on the Hayward fault unless a high value of apparent friction applies, so that the unclamping of the south end of the Hayward fault can bring it closer to failure. Over time, reequilibration of pore fluids in this area might increase the apparent coefficient of friction from its presently low inferred values, and we suggest that the microseismicity rates and surface-creep rates at the south end of the Hayward fault need to be monitored as possible precursors to a triggered event. Stress-evolution models of central California faults after the 1906 San Francisco earthquake are consistent with the seismic quiescence in the bay region after 1906 and suggest that the 1989 earthquake effects described in this paper would be dwarfed by those accompanying a recurrence of the 1906 event.

INTRODUCTION

Should we expect the earthquake (M=7.1), with an average slip of 2 m over a 40-km-long rupture surface, to affect the probability of earthquakes on other faults in the San Francisco Bay region? As a possible example of such an effect, the 1906 San Francisco earthquake (M=7.7) was followed by a 73-yr period of unusual quiescence during which only one earthquake of M>6 occurred on bay-region faults (Ellsworth and others, 1981; Sykes and Jaumé, 1990).

About 17 days after the Loma Prieta main shock, an M=3.4 earthquake occurred on the Hayward fault about 85 km from the Loma Prieta epicenter (fig. 1). Although this earthquake was not large, it did cause some concern because on at least two occasions in the 1800's, large earthquakes on one side

of San Francisco Bay were followed within 3 yr by second large earthquakes on the opposite side of the bay (Louderback, 1947; Ellsworth, 1990; Sykes and Jaumé, 1990; Jaumé and Sykes, 1992). Because earthquakes on the San Andreas and Hayward faults were involved in both of these pairings, this M=3.4 earthquake might have been the precursor to a larger shock, and the question arose as to how the Loma Prieta rupture might have affected stress levels on other bay-region faults.

Long-term stress changes caused by fault offset are called static-stress changes, to distinguish them from the short-period dynamic-stress changes that accompany the passage of seismic waves. In this paper, static-stress changes on central California faults are calculated by using three different slip distributions that have been proposed for the Loma Prieta rupture.

We also present simple models that attempt to assess, at least qualitatively, the importance of pore fluids, fault geometry, and nonlinear time-dependent relaxation on the distribution of stresses. Additional models are designed to help visualize the evolution of the regional stress field after the earthquake, as plate-tectonic-loading stresses accumulate on bay-region faults. We also present a similar evolutionary model for the years after the 1906 earthquake. The magnitude of the 1906 effects puts the 1989 earthquake into sobering perspective.

REGIONAL STRESS CHANGES CAUSED BY THE EARTHQUAKE

CALCULATED CHANGES IN STATIC STRESS

Although the Earth is far from being a perfectly homogeneous, elastic half-space, several lines of evidence suggest that static-stress changes calculated by using this assumption are a fair approximation to the true stress changes in the Earth. For example, the magnitudes of strain steps observed on sensitive strainmeters at the times of distant earthquakes agree well with magnitudes calculated from dislocation theory (for example, Johnston and others, 1987, 1990; Shimada and others, 1987). Some success has also been reported in attempts to correlate aftershock patterns, aftershock focal mechanisms, and creep perturbations with static-stress changes calculated for moderate earthquakes (for example, Das and Scholz, 1981, 1983; Stein and Lisowski, 1983; Mavko and others, 1985; Kato and others, 1987; Li and others, 1987; Oppenheimer and others, 1988; Hudnut and others, 1989).

Slip on a surface within an elastic medium produces stress changes throughout the medium that can be calculated mathematically from dislocation theory (for example, Steketee, 1958; Chinnery, 1963; Press, 1965). For most of the models presented in this paper, stress changes were calculated at the centers of 13-km-tall by approximately 10-km-long vertical rectangular patches arrayed under the traces of major bay-region faults (figs. 1, 2). The 13-km height was selected because the midpoint coincides with the mean depth of seismicity in the bay region, which is estimated at 6 to 7 km. Three dipping fault patches (198–200, fig. 2) have also been included in the model to simulate nonvertical planes on which seismicity is occurring in two areas of special interest.

We used two computer programs to perform the calculations. Our initial calculations were based on equations derived by Glen Converse for the elastic fields generated by uniform slip on rectangular dislocation surfaces in a half-space. Scott Dunbar originally coded these equations as the program DIS3D, which Erickson (1986) subsequently improved and documented. Our later calculations used the

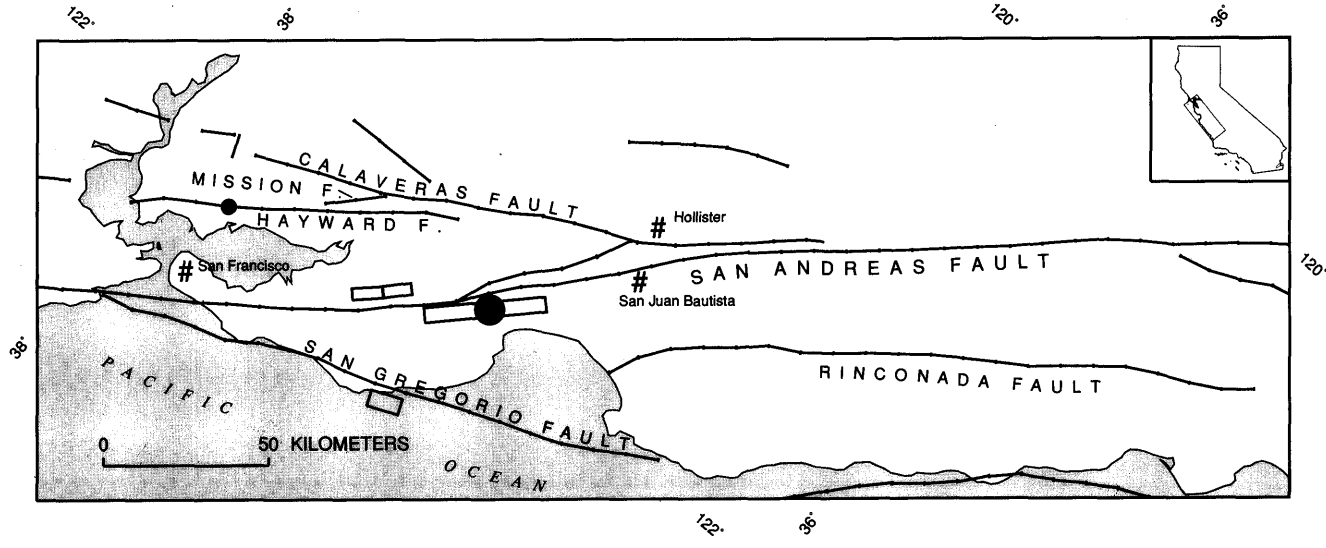

Figure 1.—Study area in central California, showing locations of selected faults. Large dot, epicenter of October 17, 1989, earthquake; small dot, epicenter of November 4, 1989, earthquake (M=3.4) on the Hayward fault. Tickmarks along faults indicate ends of vertical rectangular patches used in models to simulate faults; small rectangles are surface projections of dipping patches used in models (see fig. 2).

subroutines of Okada (1992). In all the models, a Poisson's ratio of 0.25 and a shear modulus of 3×10^5 bars were used.

To calculate the stress changes, we must define a Loma Prieta slip surface and specify a slip distribution on it. For comparative purposes, we used three slip distributions inferred from different data sets (table 1). Although several others have been proposed, these three slip distributions serve to illustrate the range of static-stress changes resulting from reasonable solutions for the slip distribution and the geometry of the slip plane.

In general, the results at large distances (min 80 km) from the Loma Prieta slip surface depend mostly on the total moment of the assumed slip distribution rather than on its finer details. The results at intermediate distances (approx 40–80 km) should be qualitatively similar, with some differences reflecting the details of the slip distribution used. Finally, the results at near distances (less than approx 40 km) may differ significantly.

The first and simplest slip distribution we used is based on a single uniform-slip dislocation inferred from geodetic line-length changes by Lisowski and others (1990). The second, more complex slip distribution is the two-dislocation model of Marshall and others (1991), based on leveling data, which uses different rakes for the slip directions on the two parts of the slip surface. The strike of their model differs by 8° from that of the first model (table 1).

The third and most complex slip distribution is that proposed by Beroza (1991) from strong-ground-motion records. He divided the fault surface into 280 separate elements with varying amounts of strike slip and dip slip. Paul Spudich (oral commun., 1991) emphasized that inversions based on strong-ground-motion records do not yield unique solutions. However, the common features predicted by all three slip distributions, at least in the intermediate and far field, suggest that nonuniqueness is not seriously biasing the stress calculations.

The results from these three slip distributions are illustrated in figure 3 and plotted for selected bay-region faults in figure 4. Stresses are calculated at the centers of the rectangular fault patches. The decay in horizontal shear stress with distance for the slip distribution of Lisowski and others (1990) is plotted in figure 5. Static-stress changes in the study area range from less than 0.001 bar to a few tens of bars. In contrast, Earth tides on the Hayward fault during the year after the earthquake produced a maximum calculated range of approximately 0.01 bar in horizontal shear and 0.05 bar in normal stress; mean daily variations were about a fourth of this maximum range, or about 0.002 and 0.01 bar, respectively.

All three slip distributions predict an increase in right-lateral shear stress on the San Andreas fault to the northwest and southeast of the Loma Prieta rupture zone. This is the result that we would intuitively expect: Failure of one fault patch increases the stress on adjacent coplanar fault patches that must now support more of the load. The magnitudes of the stress increases on the San Andreas fault adjacent to the Loma Prieta rupture zone show large differences for the three distributions, reflecting the differences in both orientation and slip distribution among the three slip surfaces. These intermodel differences suggest that given the present uncertainties in the models, static-stress changes close to the rupture zone cannot be reliably calculated. In the following discussion, we confine our interpretations mostly to static-stress changes at intermediate to far distances from the rupture zone.

Most of the Hayward fault and the northern and central sections of the Calaveras fault, which are subparallel to the Loma Prieta rupture zone, undergo a decrease in right-lateral horizontal shear stress (that is, an increase in left-lateral shear) in all three slip distributions. Although this result may be somewhat less obvious, it makes intuitive sense also: A failure on one of two parallel faults will tend to relax the shear stress on adjacent parts of the other fault if they are close enough together. (The actual geometry for relaxation to occur is illustrated in fig. 2 of Rybicki and others, 1985.)

For the southern section of the Calaveras fault and the San Gregorio fault, which form larger angles with the

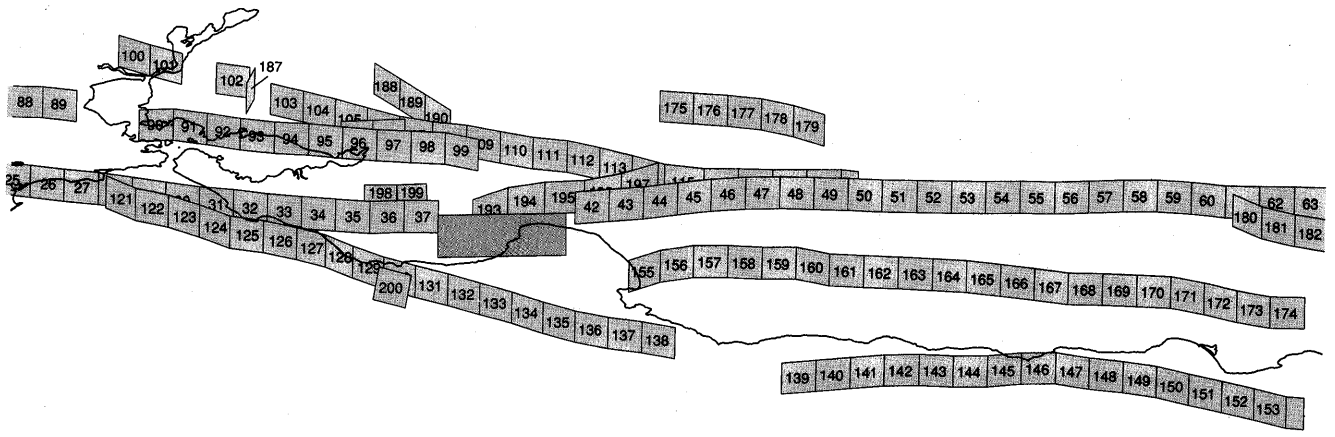

Figure 2.—Oblique view of fault patches used in models. Most fault patches are vertical, except for large rectangle that is Loma Prieta rupture surface of Lisowski and others (1990) and three small fault patches included for illustrative purposes. Coastline is shown for reference.

Table 1.–*Parameters for three Loma Prieta slip distributions*

[Some parameters are inferred from information in references. Height is vertical or updip width of rectangular surface]

Slip distribution	Number of patches	Patch length by height (km)	Overall length by height (km)	Depth to top (km)	Depth to bottom (km)	Strike	Dip	Center (lat N.)	Center (long W.)	Right-lateral strike slip (m)	Reverse slip (m)	Moment (10^{18} N-m)
Lisowski and others (1990, model 3).	1	37 by 13.3	37 by 13.3	5.0	17.5	136°	70° SW.	37.060°	121.906°	1.66	1.19	30
Marshall and others (1991, two-rake).	2	18.5 by 9	37 by 9	4.5	12.4	128°	62° SW.	37.046°	121.864°	[1].92/2.01	[1]1.89/0.61	21
Beroza (1991)----------	280	1 by 2	40 by 14	5.8	18.9	130°	70° SW.	37.055°	121.858°	([2])	([2])	24

[1]First number refers to northwest rectangle, and second number to southeast rectangle.
[2]Slip varies over patches of the slip surface.

Loma Prieta rupture surface, the horizontal shear is both right lateral and left lateral, depending on orientation and distance. Differences exist among the slip distributions between the boundaries separating domains of right- and left-lateral shear on these two fault segments.

Some of the most dramatic stress changes occur in the normal component of traction. Under the sign convention used here, positive changes in the normal component represent unclamping (less compression) on the fault patches, whereas negative changes suggest clamping (increased compression). The reverse component of motion on the dipping Loma Prieta slip surface will tend to produce unclamping to either side of this surface. The most pronounced unclamping occurs on the southern section of the Hayward fault (fig. 4*C*), on adjacent sections of the Calaveras fault (fig. 4*D*), and on the section of the San Gregorio fault opposite the Loma Prieta rupture zone (fig. 4*E*). If a Coulomb failure criterion is operating on these faults, then changes in normal stress acting on the fault patches, as well as changes in shear stress, could affect their proximity to failure.

CALCULATED CHANGES IN COULOMB FAILURE FUNCTION

To quantify the possibility of failure on nearby faults caused by static-stress changes after the earthquake, we use the Coulomb failure function (CFF), defined by

$$\mathrm{CFF} \equiv |\vec{\tau}_P| + \mu(\sigma_P + p) - S, \qquad (1)$$

where $\vec{\tau}_P$ is the shear traction on a plane P, σ_P is the normal traction (positive for tension) on plane P, p is the pore-fluid pressure, S is the cohesion, and μ is the coefficient of friction. This function is based on the Coulomb failure criterion, which applies to failure in unfractured rock, and on the mathematically identical Amonton's law for sliding on preexisting planes of weakness (for example, Jaeger and Cook, 1979; Scholz, 1990).

If the CFF applies to seismogenic faults in the Earth, then failure would be expected to occur when CFF ≥ 0. If a negative CFF increased (that is, became less negative) on a fault plane, then that plane would be expected to be closer to failure than before, with possibly greater consequent microseismicity, whereas fault planes for which a negative CFF decreased would be farther from failure, with possibly lower microseismicity. In the terminology of Armbruster and Seeber (1991), earthquakes might be encouraged or discouraged on a fault as a result of static-stress changes.

If we assume that μ and S are constant over time, then the change in CFF is given by

$$\Delta\mathrm{CFF} = \Delta|\vec{\tau}_P| + \mu(\Delta\sigma_P + \Delta p). \qquad (2a)$$

Because the magnitude of the vector $\vec{\tau}_P$ appears in this equation, ΔCFF as defined above is not readily calculated without knowledge of the absolute value of the preexisting stress field, or some simplifying assumptions. For vertical fault patches, we assume that $\Delta|\vec{\tau}_P| \approx \Delta\tau_{\mathrm{hrl}}$, where $\Delta\tau_{\mathrm{hrl}}$ is the change in horizontal right-lateral shear, so that

$$\Delta\mathrm{CFF} \approx \Delta\tau_{\mathrm{hrl}} + \mu(\Delta\sigma_P + \Delta p). \qquad (2b)$$

▶ Figure 3.—Oblique views of patches on central California faults, showing static-stress changes calculated by using slip distributions of (*A*) Lisowski and others (1990), (*B*) Marshall and others (1991), and (*C*) Beroza (1991). Top diagram, change in horizontal shear stress, where red indicates an increase and blue a decrease in right-lateral traction; middle diagram, change in updip shear stress, where red indicates an increase and blue a decrease in west-side-up traction; bottom diagram, change in normal stress, where red indicates an increase in tension (unclamping) and blue an increase in compression (clamping). Yellow patches represent Loma Prieta rupture.

A

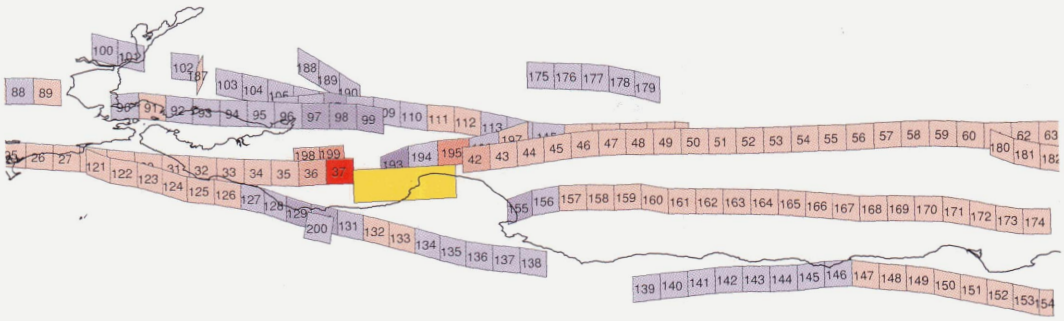

HORIZONTAL SHEAR STRESS, IN BARS - Lisowski

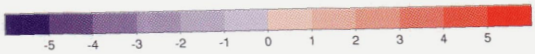

UPDIP SHEAR STRESS, IN BARS - Lisowski

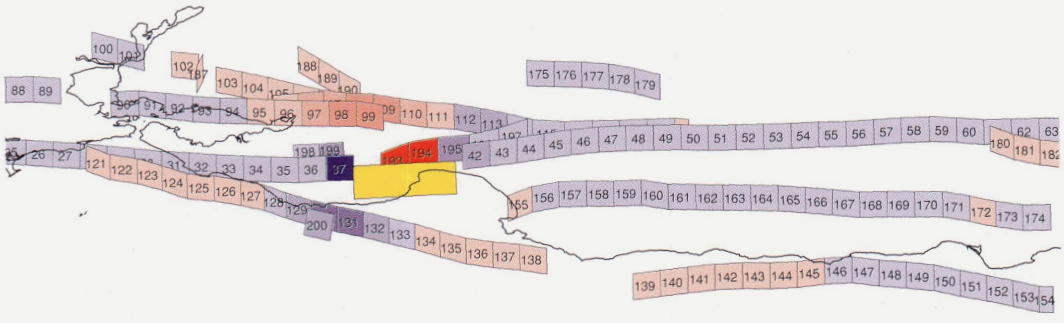

NORMAL STRESS, IN BARS - Lisowski

B

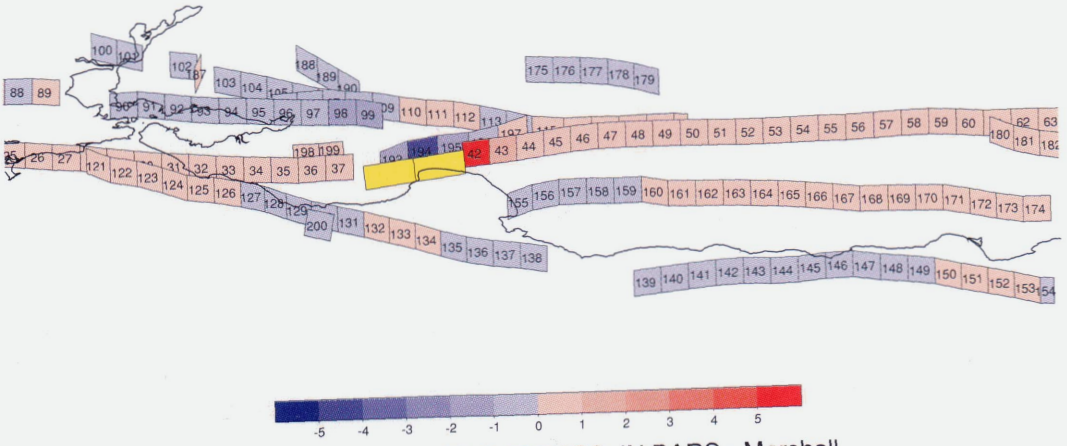

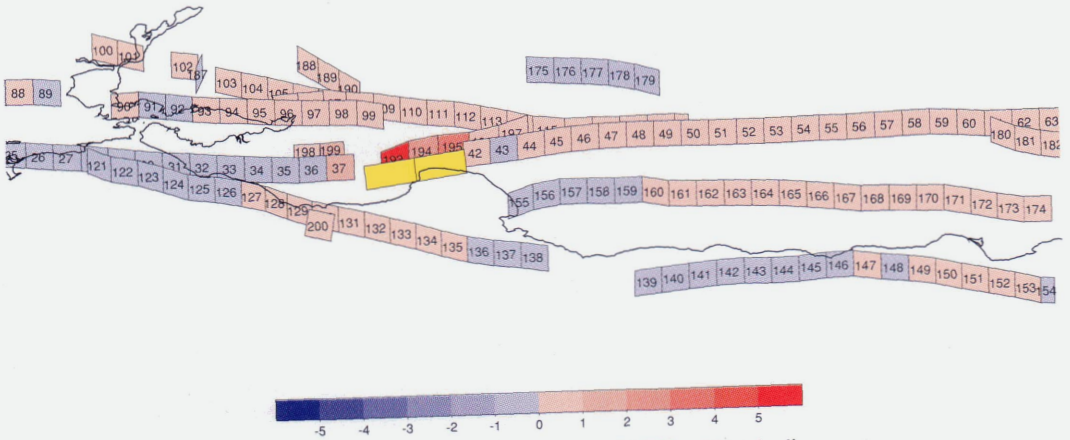

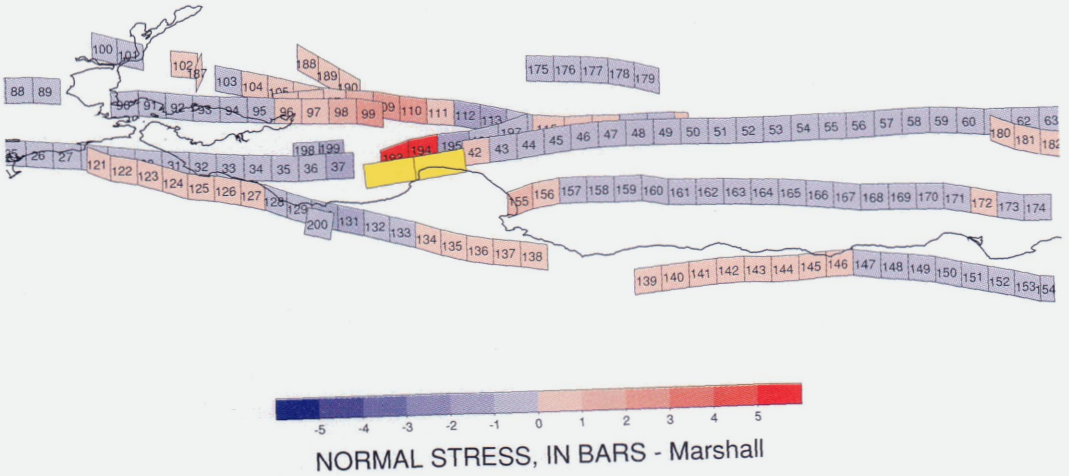

Figure 3.—Continued.

C

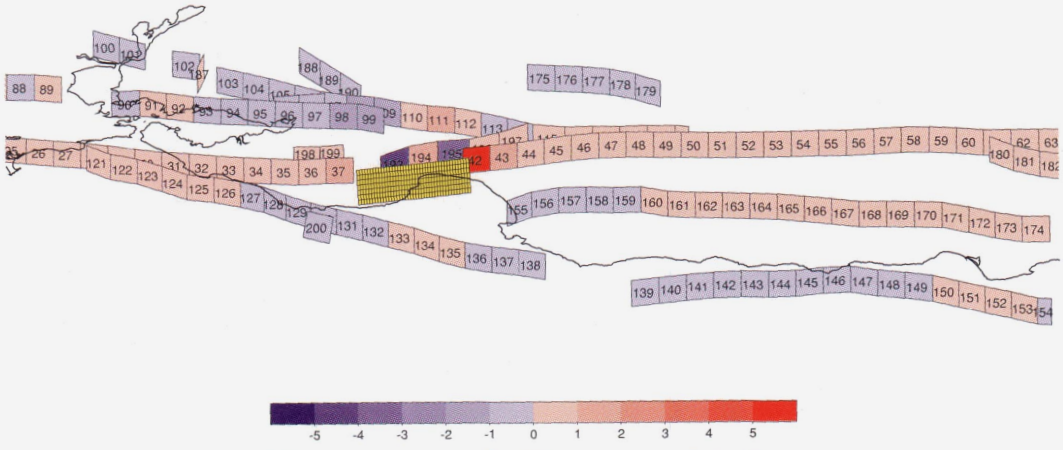

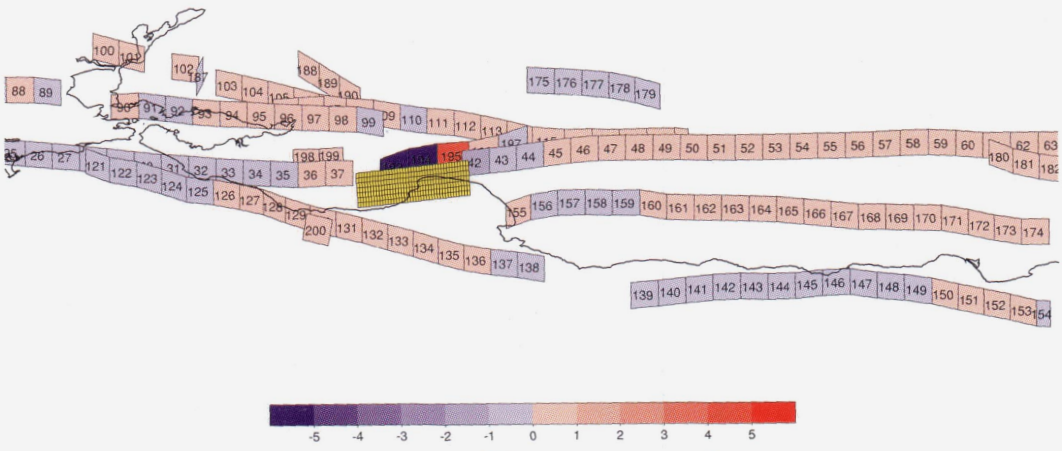

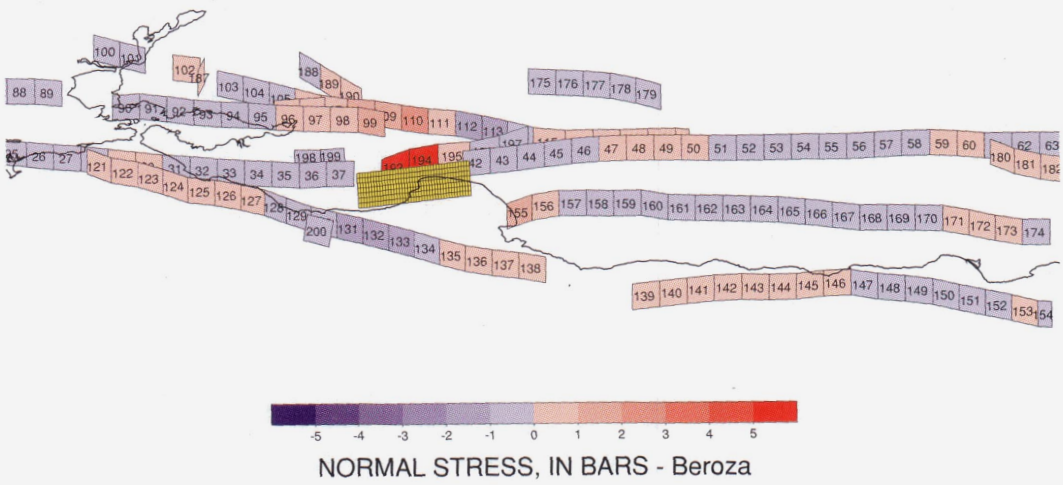

Figure 3.—Continued.

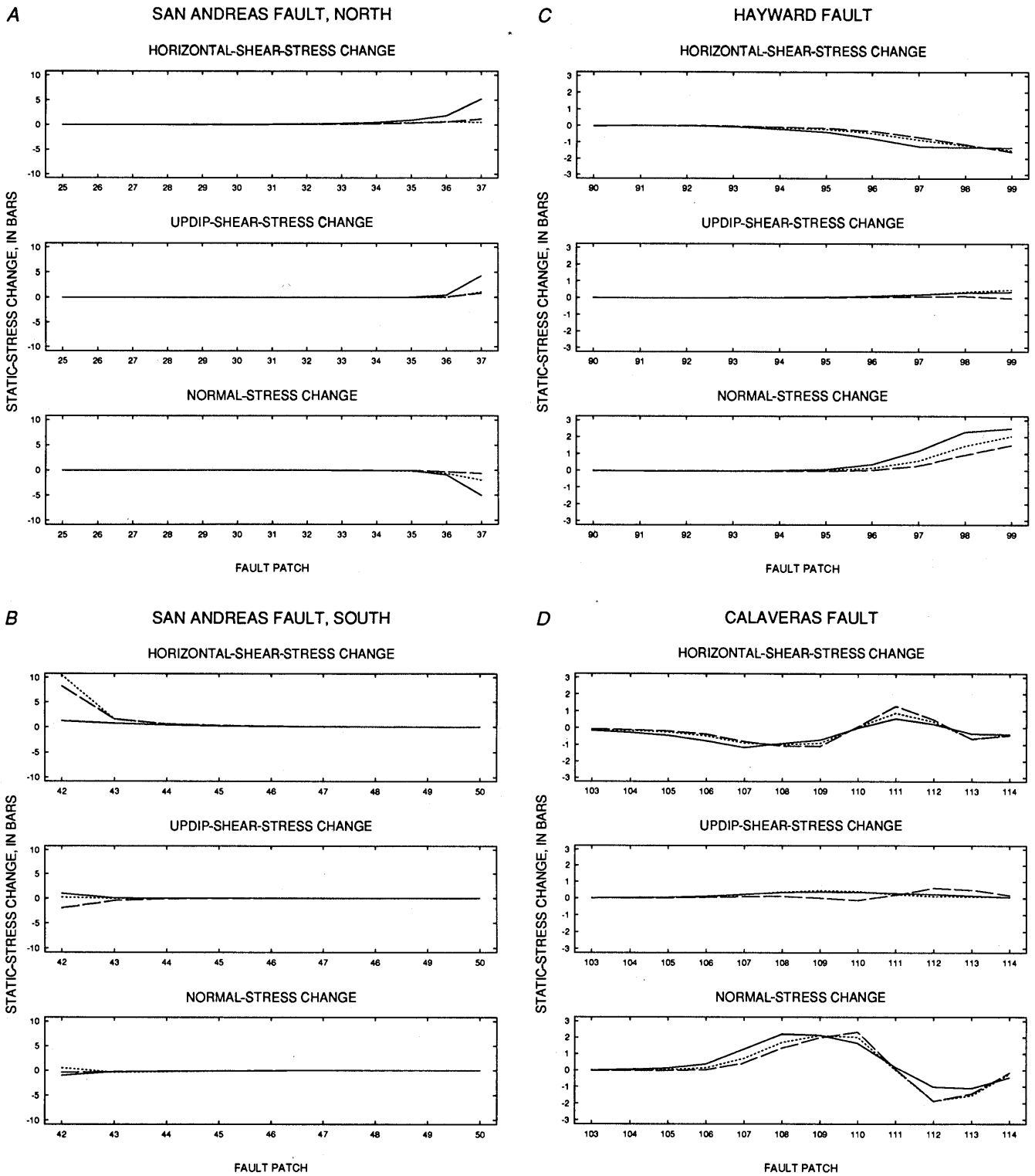

Figure 4.—Static-stress changes on patches of the San Andreas fault (*A*) north and (*B*) south of Loma Prieta rupture zone, (*C*) the Hayward fault, (*D*) the Calaveras fault, and (*E*) the San Gregorio fault. Solid line, slip distribution of Lisowski and others (1990); short dashes, slip distribution of Marshall and others (1991); long dashes, slip distribution of Beroza (1991). Distance between fault patches is approximately 10 km. Top plot, change in horizontal shear stress, where positive values indicate an increase in right-lateral traction; middle plot, change in updip shear stress, where positive values indicate an increase in west-side-up traction; bottom plot, change in normal stress, where positive values indicate an increase in tension (unclamping).

This assumption is similar to that made by Armbruster and Seeber (1991), who assumed in their analysis that induced earthquakes will always have the same slip directions as earlier earthquakes at a given site. Because most of our vertical fault patches represent faults expected to slip in predominantly right lateral earthquakes, the assumption is probably a good one. The alternative is to use information about the preearthquake state of stress acting on the fault patches to define the direction and magnitude of $\vec{\tau}$ before the static-stress changes are added, but with this approach, uncertainties introduced by the possible dependence of fault strength on the direction of slip cloud the issue.

Three nonvertical fault patches were treated differently. For dipping patches 198 and 199 (fig. 2), which were intended to represent schematically some of the reverse-slip earthquakes on the San Francisco peninsula adjacent to the San Andreas fault (Olson and Lindh, 1985; Olson, 1986), the updip shear traction was used instead of the horizontal shear traction to calculate $\Delta|\vec{\tau}_p|$ in equation 2, equivalent to assuming a rake of 90°. Slipon dipping patch 200 was assigned an oblique (reverse plus right lateral) rake of 150°, determined from nearby focal mechanisms, to calculate ΔCFF.

Pore fluids seem to play an important role in the distribution of stress and in the failure process. Raleigh and others (1976) were able to control the occurrence of small earthquakes near Rangely, Colo., by changing fluid pressures in oil wells. Numerous reports describe seismicity induced by reservoir filling (for example, Roeloffs, 1988), with both load changes and pore-pressure changes probably contributing. The distribution of aftershocks over time after a main shock has been attributed to the reequilibration of pore fluids after the main shock (for example, Nur and Booker, 1972; Li and others, 1987). Hudnut and others (1989) explained the M_S=6.6 earthquake that occurred on the Superstition Hills fault 11 hours after an M_S=6.2 earthquake on the Elmore Ranch crossfault by appealing to static-stress changes and subsequent fluid flow. Segall (1989) modeled the generation of earthquakes in regions where pore pressures are decreasing because of fluid extraction.

Although our dislocation models do not allow an incisive analysis of the role of pore fluids, we can obtain some impression of their potential importance. For example, in the undrained state immediately after the static-stress changes have been imposed, the change in pore pressure Δp in a homogeneous isotropic medium would be expected to be $-B\Delta\sigma_{kk}/3$, where B is Skempton's coefficient, which ranges from 0 to 1, and $\Delta\sigma_{kk}$ is the summation of the diagonal elements of the stress-change tensor (for example, Rice and Cleary, 1976; Roeloffs, 1988; Scholz, 1990). Thus, equation 1 becomes

$$\Delta CFF = \Delta|\vec{\tau}_p| + \mu(\Delta\sigma_P - B\Delta\sigma_{kk}/3), \quad (3a)$$

or, simplifying for horizontal slip on vertical patches,

$$\Delta CFF \approx \Delta\tau_{hrl} + \mu(\Delta\sigma_P - B\Delta\sigma_{kk}/3). \quad (3b)$$

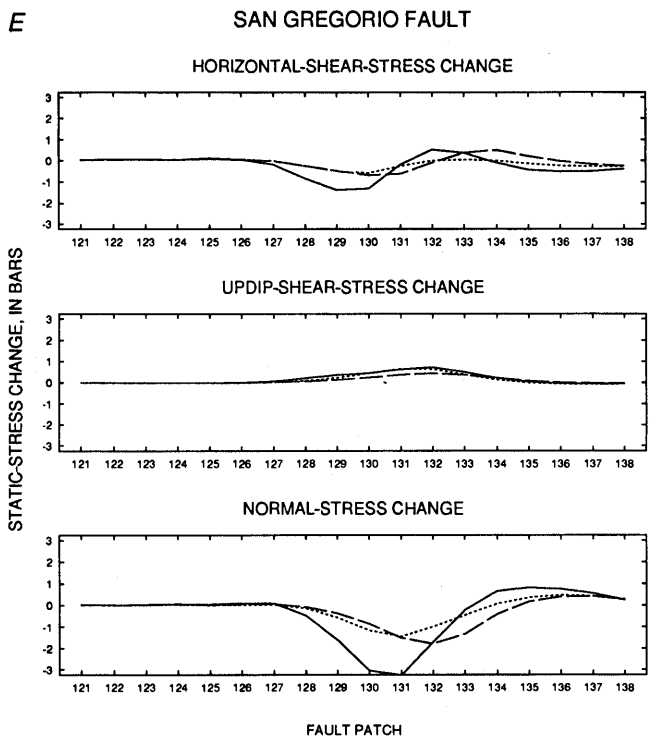

Figure 4.—Continued.

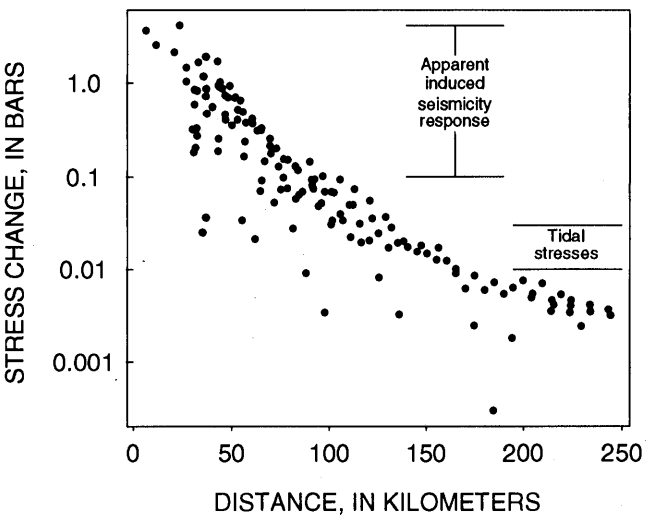

Figure 5.—Change in horizontal shear stress as a function of distance from Loma Prieta epicenter for slip distribution of Lisowski and others (1990).

We call this the homogeneous model. In this model, pore-pressure changes generally tend to counter normal-stress changes, resulting in a lower apparent coefficient of friction if pore-fluid effects are ignored, as discussed below.

If the fault-zone materials are more ductile than the surrounding materials, then Rice (1992) has demonstrated that $\sigma_{xx}=\sigma_{yy}=\sigma_{zz}$ in the fault zone, and so $\Delta\sigma_{kk}/3=\Delta\sigma_P$ and

$$\Delta\mathrm{CFF} = \Delta|\vec{\tau}_p| + \mu'\Delta\sigma_P, \tag{4a}$$

or, again simplifying,

$$\Delta\mathrm{CFF} \approx \Delta\tau_{\mathrm{hrl}} + \mu'\Delta\sigma_P, \tag{4b}$$

where $\mu'=\mu(1-B)$ is called the apparent coefficient of friction. We call this the Rice model. In this model, after the main shock but before pore fluids have had enough time to reequilibrate, the coefficient of friction would appear to be diminished by a factor depending on Skempton's coefficient over normal laboratory values, which range from 0.6 to 0.9 (Byerlee, 1990; Zoback and Healy, 1984).

If pore fluids are unimportant because $\Delta p=0$ or $B=0$, then

$$\Delta\mathrm{CFF} = \Delta\tau_{\mathrm{hrl}} + \mu\Delta\sigma_P, \tag{5}$$

which would also be the result for finite permeabilities at $t=\infty$ after pore fluids have reequilibrated so that $\Delta p=0$. We call this the dry or drained model. Note, however, that Byerlee (1990) and Rice (1992) have suggested mechanisms which might inhibit such reequilibration in a fault zone.

The results from these three pore-fluid models are illustrated in figure 6 for the three slip distributions, assuming that $\mu=0.75$ and $B=1$. This B value gives the maximum undrained-pore-fluid effect. B values ranging from 0.23 to 0.99 have been reported for various rock types (Rice and Cleary, 1976; Roeloffs, 1988). Reasenberg and Simpson (1992) reported that the best correlation of changes in microseismicity rate with calculated static-stress changes after the earthquake is obtained for low apparent coefficients of friction ($\mu'\approx0.2$). In the Rice model, for a coefficient of friction μ close to laboratory values of 0.75, this result implies a Skempton's coefficient $B\approx0.73$. As before, the results for the three slip distributions are qualitatively similar beyond about 40-km distance from the rupture surface. Substantial differences exist for fault patches closer than 40 km, but such near-field results are unreliable in any event.

A graphical comparison of the three pore-fluid models for selected bay-region faults, using the slip distribution of Lisowski and others (1990), is shown in figure 7, assuming that $\mu=0.75$ and $B=1$. Comparison of the results suggests that pore-fluid effects can substantially shift patterns of encouraged and discouraged fault patches. For example, the south end of the Hayward fault is closer to failure in the dry/drained model than in either of the models for which pore-pressure changes are important. This section of the Hayward fault exhibited lower microseismicity rates (Reasenberg and Simpson, 1992) after the earthquake than before, a behavior consistent with pore fluids playing a role in the failure criterion. If, over time, the reequilibration of fluids leads to a result for ΔCFF closer to that in the dry/drained model, then microseismicity rates may increase on this section of the fault as it moves closer to failure.

At several fault patches in the bay region, ΔCFF in the undrained state (homogeneous or Rice model) differs significantly from its value in the drained state. Fault patches 97 through 99 on the Hayward fault (fig. 2) are more prone to failure in the drained state, whereas fault patches 128 through 132 on the San Gregorio fault are less prone to failure. Changes in microseismicity rate on these fault patches over time may serve as an inplace test of the progress from undrained to drained states. The most definitive tests might be made in the near field, where the changes are largest but where our calculated results also depend most on the assumed slip distribution.

Although these models oversimplify the pore-fluid effects, some generalizations are possible about the changes in CFF over time. Undrained models are strongly controlled by changes in shear stress, whereas dry/drained models are also controlled by changes in normal stress. In general, the dry/drained model yields ΔCFF values that are either the largest (most positive) or the smallest (most negative) of the three models (fig. 6); the Rice model tends to yield results that are least extreme. Thus, if the drained/dry solution represents a $t=\infty$ end state, the largest changes in CFF over time after the earthquake will tend to occur if the appropriate starting model is the Rice model. Intermodel differences showing the direction of potential changes over time are plotted in figure 7.

The role of pore fluids in the earthquake cycle has recently been highlighted by the realization that the regional compressive-stress field in much of California is oriented perpendicular to the San Andreas fault system (Mount and Suppe, 1987; Zoback and others, 1987). This realization would seem to require that the San Andreas fault have a

▶ Figure 6.—Oblique views of patches on central California faults, showing changes in Coulomb failure function for three pore-fluid models, calculated by using distributions of (*A*) Lisowski and others (1990), (*B*) Marshall and others (1991), and (*C*) Beroza (1991). Top diagram, homogeneous model; middle diagram, Rice model; bottom diagram, dry/drained model (see text for explanation). Coefficient of friction $\mu=0.75$; Skempton's coefficient B=1. Red indicates changes that bring fault patches closer to failure, and blue changes that move fault patches farther from failure. Yellow patches represent the Loma Prieta rupture.

A

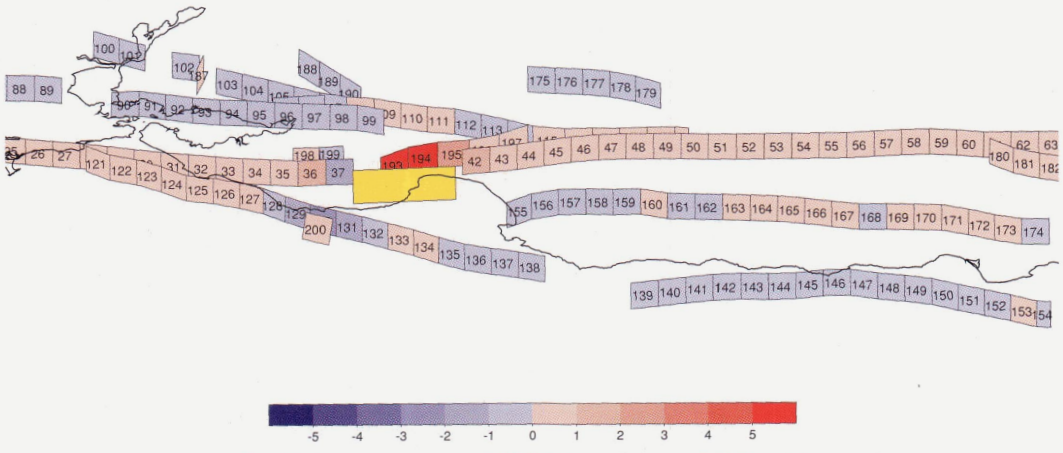

DELTA CFF, IN BARS / HOMOGENEOUS MODEL - Lisowski

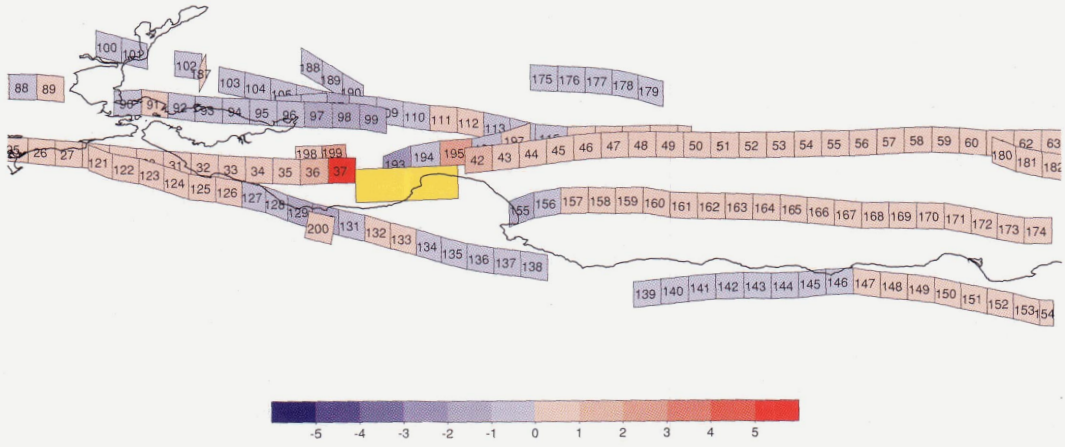

DELTA CFF, IN BARS / RICE MODEL - Lisowski

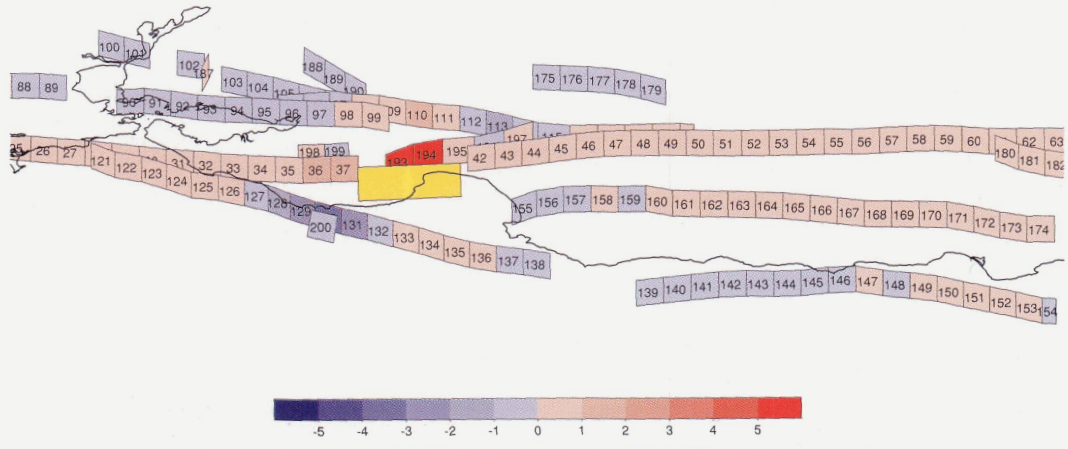

DELTA CFF, IN BARS / DRY-DRAINED MODEL - Lisowski

B

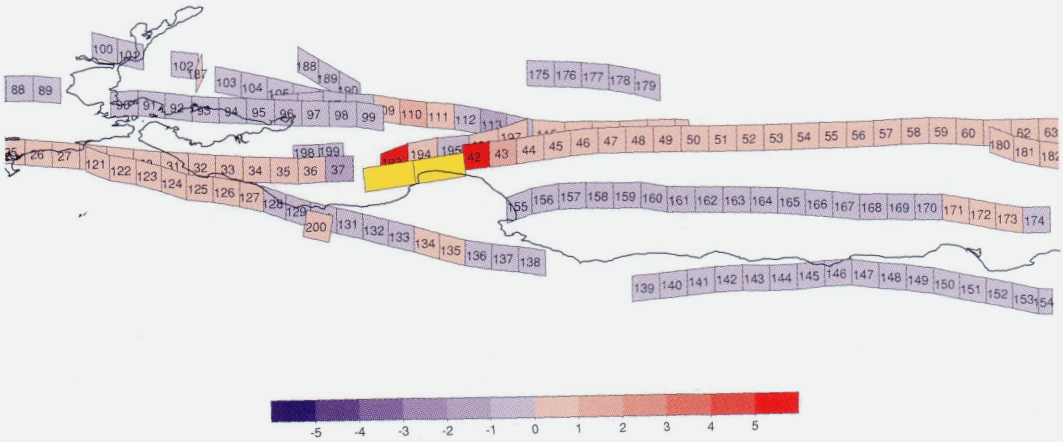

DELTA CFF, IN BARS / HOMOGENEOUS MODEL - Marshall

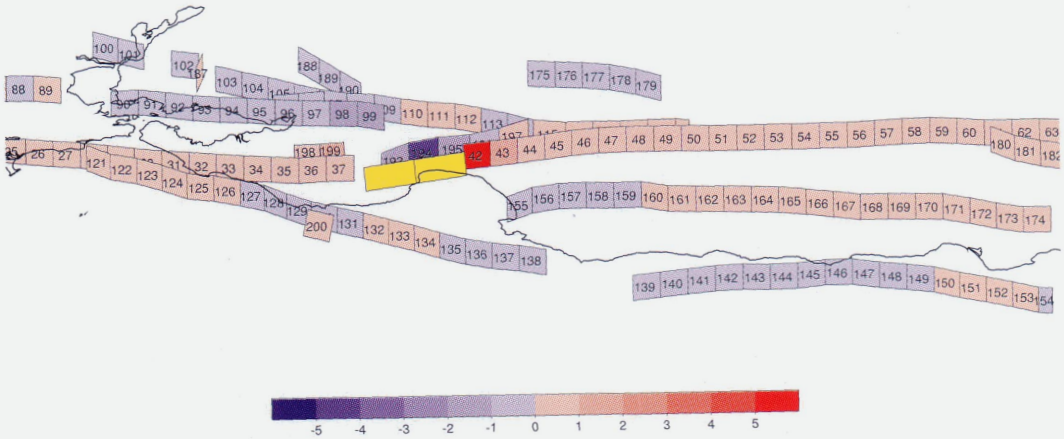

DELTA CFF, IN BARS / RICE MODEL - Marshall

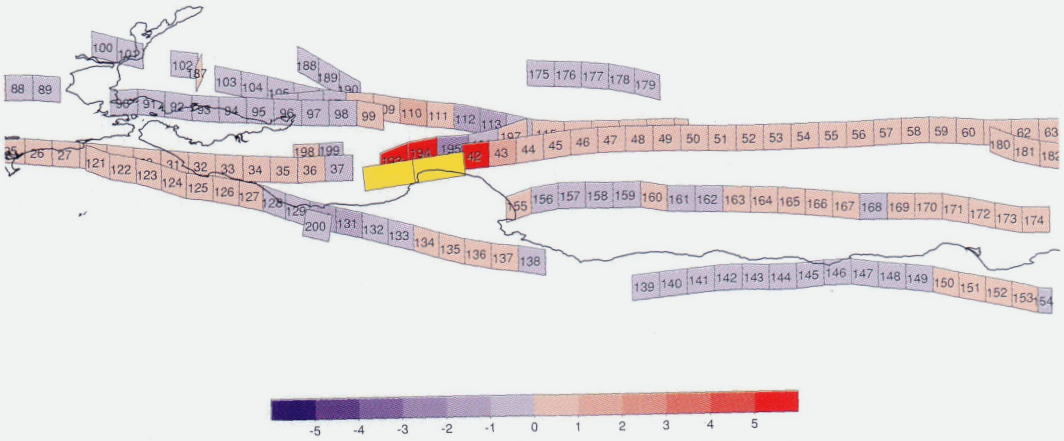

DELTA CFF, IN BARS / DRY-DRAINED MODEL - Marshall

Figure 6.—Continued.

C

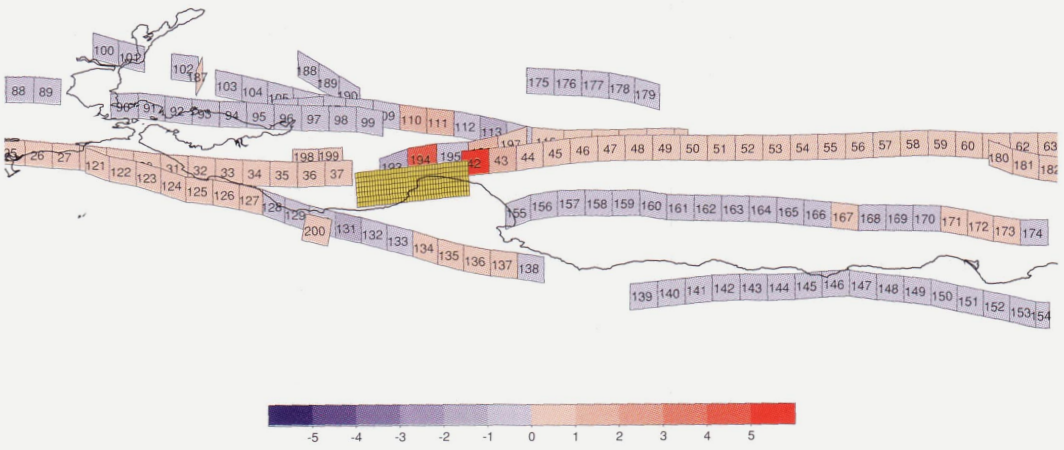

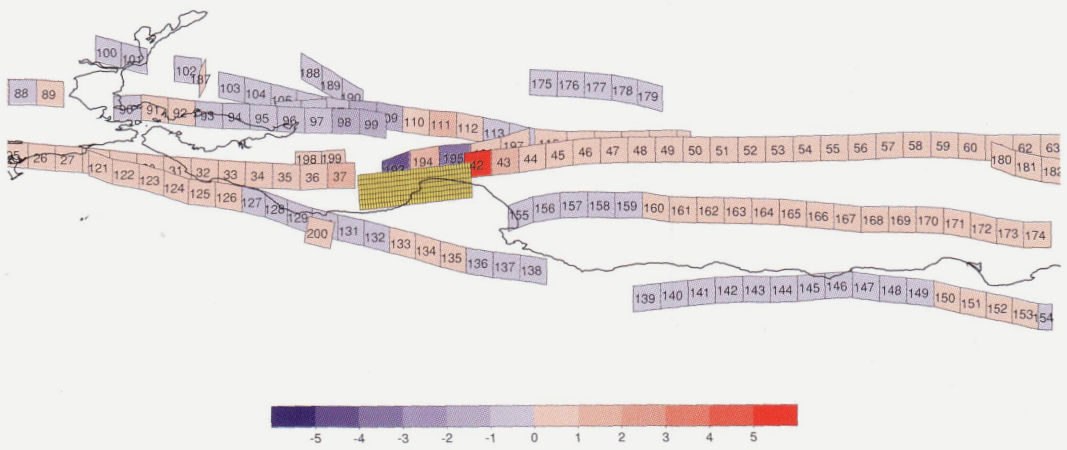

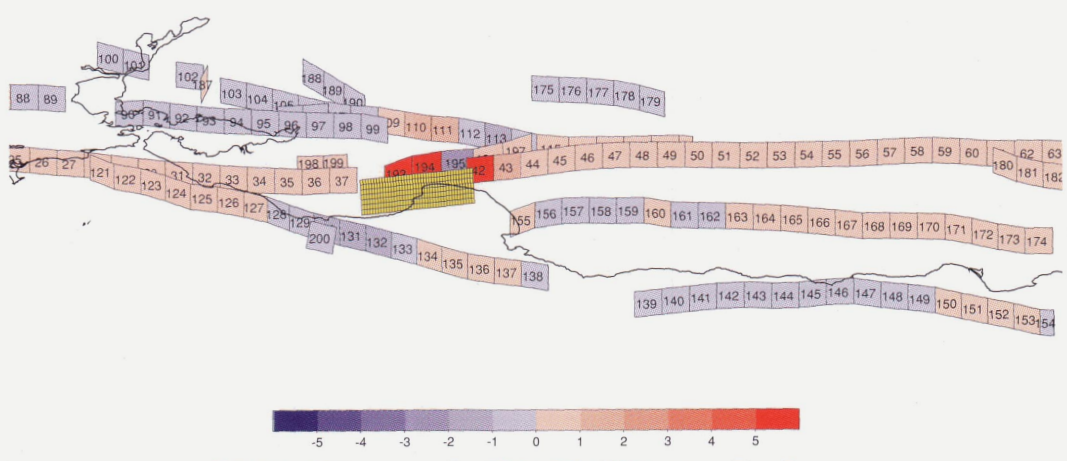

Figure 6.—Continued.

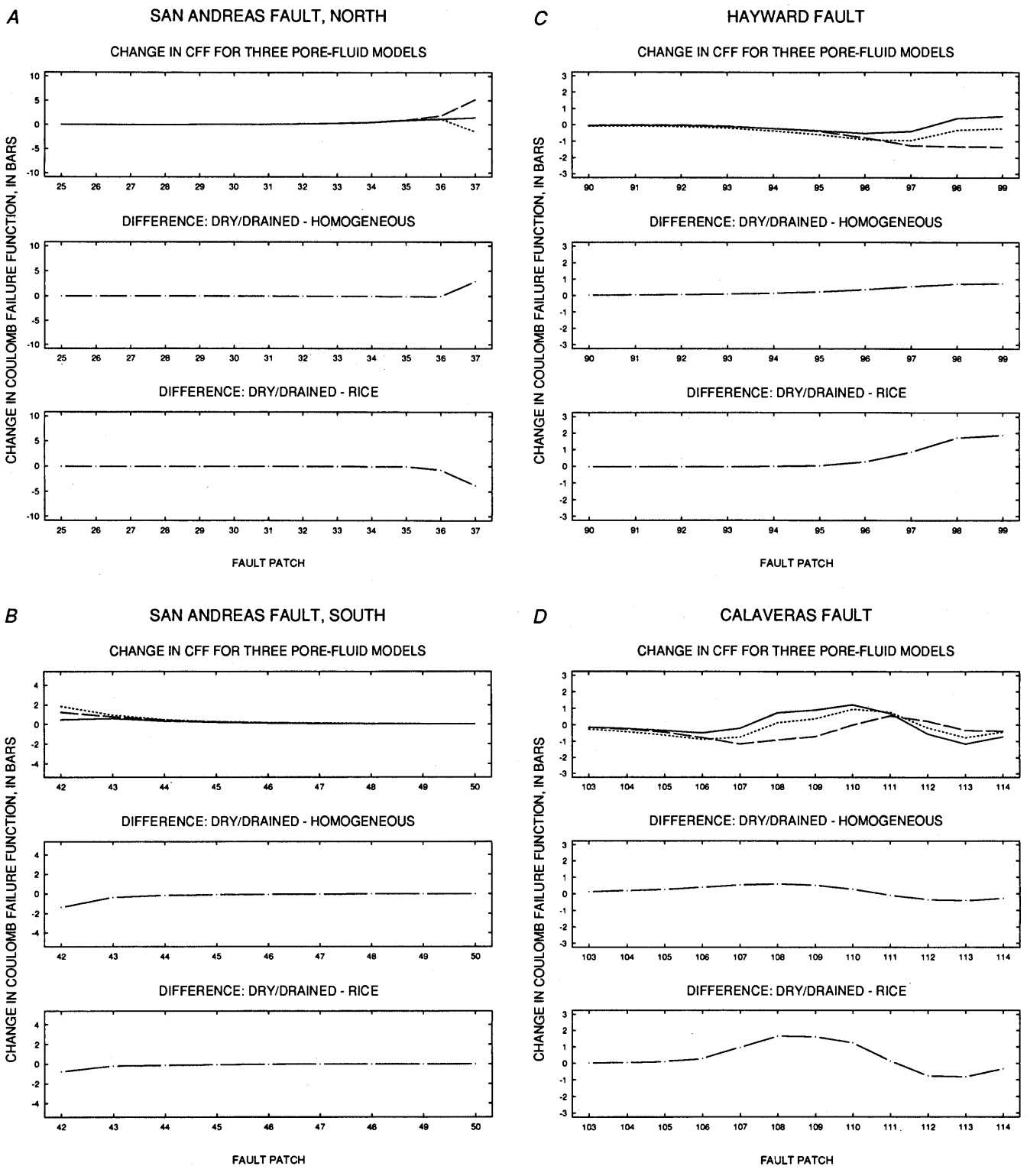

Figure 7.—Changes in Coulomb failure function (top plot) on patches of the San Andreas fault (*A*) north and (*B*) south of Loma Prieta rupture zone, (*C*) the Hayward fault, (*D*) the Calaveras fault, and (*E*) the San Gregorio fault. Positive values for patches closer to failure. Short dashes, homogeneous model; long dashes, Rice model; solid line, dry/drained pore-fluid model. Middle plot, difference between dry/drained and homogeneous models; bottom plot, difference between dry/drained and Rice models. Positive values in middle and bottom plots may indicate changes over time that move fault patches closer to failure. All models calculated by using slip distributions of Lisowski and others (1990).

low strength at seismogenic depths, so that if the Coulomb failure criterion is applicable at these depths, either a low coefficient of friction or a high pore-fluid pressure must obtain. Low shear stresses on the fault would also seem to be required by the absence of a heat-flow anomaly (Brune and others, 1969; Lachenbruch and Sass, 1980), although laboratory coefficients of friction for a wide variety of rock types are uniformly high (0.6–0.9). Maintaining high pore pressures in fault zones poses conceptual problems because the high pressures would be expected to hydrofracture the rock in simple models (Lachenbruch and McGarr, 1990), thereby releasing the pressure. Recent work by Byerlee (1990), Blanpied and others (1992), Rice (1992), and Sleep and Blanpied (1992) has offered some new ideas for maintaining high fluid pressures in fault zones that circumvent the old problems. Changes in microseismicity rate may yield some inplace tests of the role of pore fluids.

OBSERVED CHANGES IN MICROSEISMICITY RATES AND FAULT-CREEP RATES

The calculated changes in stress and CFF presented in the preceding sections are theoretical results based on simple models. Two data sets offer independent confirmation of these results: microseismicity rates and fault-creep rates.

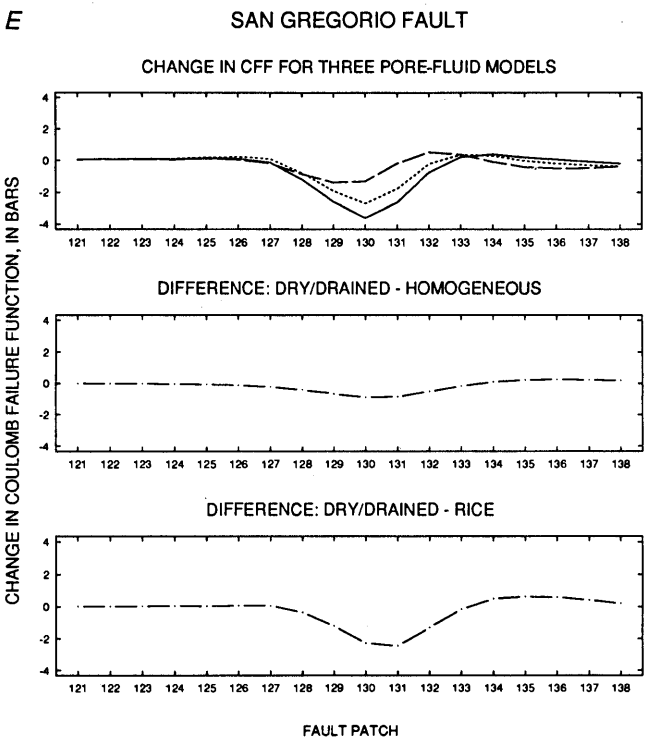

Figure 7.—Continued.

MICROSEISMICITY RATES

About 3 months after the earthquake, the microseismicity rate on the Hayward fault was observed to have diminished in comparison with that for the 3-month period before the earthquake. This change was consistent with the results of models that assumed low apparent coefficients of friction, in which the Hayward fault was relaxed by the addition of left-lateral horizontal static stress.

A detailed study of microseismicity rates on central California faults (Reasenberg and Simpson, 1992 and in press) subsequently revealed a correlation between calculated stress changes and microseismicity rates at the 95-percent-confidence level. Although the correlation works well for some faults, such as the Hayward fault and the parts of the San Andreas fault to the north and south of the Loma Prieta rupture zone, we note that other faults, especially the San Gregorio fault, do not fit the models well. The best correlation was observed for models with low apparent coefficients of friction μ', on fault patches within 100 km of the Loma Prieta epicenter. At epicentral distances greater than 80 to 100 km, the response of seismicity to stress changes is statistically undetectable at the 95-percent-confidence level. At these distances, the maximum absolute value of ΔCFF is approximately 0.1 bar or less (fig. 5).

Although it seems extraordinary that such small stress changes could influence the occurrence of earthquakes, the levels of change are comparable to those calculated at seismogenic depths under water-filled reservoirs, for which the initial filling process and subsequent seasonal cycling of water levels are known to generate earthquakes (for example, Roeloffs, 1988).

Stresses generated by Earth tides on the Hayward fault during the year after the earthquake were calculated to have a maximum range of 0.01 bar for horizontal shear stress and 0.05 bar for normal stress. (Mean daily variations were approximately 20 to 30 percent of these maximums.) Several investigators have looked for correlations of tectonic earthquakes with the tidal-stressing cycle, with only mixed success (for example, Heaton, 1975, 1982; Hartzell and Heaton, 1989, 1990; Rydelek and others, 1992). In particular, a study of central California earthquakes by McNutt and Heaton (1981) failed to uncover a statistically significant correlation. M.J.S. Johnston (oral commun., 1990), however, reported that microseismicity on the San Andreas fault does show a correlation with peak tidal stresses. If he is correct, there is little doubt that static-stress changes of the size calculated in this paper

could alter microseismicity rates out to distances of 100 to 150 km from the Loma Prieta epicenter.

We tried to infer both μ and B values in equation 3b from the microseismicity data, but the results were not statistically an improvement over simply inferring a μ' value from equation 4b. Thus, the microseismicity data do not seem to contain information that would differentiate the homogeneous model from the other two models at a statistically significant level. The low inferred apparent coefficient of friction μ' does argue for the presence of pore fluids and a non-zero value for Skempton's coefficient, because in the absence of pore-fluid effects, μ values of 0.6 to 0.9 are favored by laboratory experiments on rock friction.

FAULT-CREEP RATES

A second data set that shows some correlation with the static-stress changes caused by the earthquake consists of slip rates measured over fault traces in the San Francisco Bay region by creepmeters and alignment arrays. Behr and others (1990) reported increased rates of right-lateral slip on several creepmeters spanning the San Andreas fault south of the Loma Prieta rupture zone in the days after the main shock, Galehouse (1990) reported triggered right-lateral slip at two alignment-array sites in Hollister, Calif. (fig. 1), and McClellan and Hay (1990) reported right-lateral offsets at two sites on the Calaveras fault that occurred within hours or days of the earthquake. These right-lateral-slip observations are consistent with the stress changes predicted by the models, although faults can sometimes release an accumulated backlog of strain if they are triggered by shaking (for example, Allen and others, 1972; King and others, 1977; Fuis, 1979; Sieh, 1982; Simpson and others, 1988; Williams, 1988; Sharp, 1989).

Because of triggered slip, creepmeters or alignment arrays on right-lateral fault traces that show slowed or even reversed (that is, left lateral) motion offer potentially more reliable indicators of stress changes. The Hayward fault, which was relaxed in the low-apparent-coefficient-of-friction models described above, would seem like a good candidate for retarded slip motions. Galehouse (1992 and in press) reported lower rates at four of five alignment arrays on the Hayward fault during the 2-yr period after the earthquake. A new site at Camellia Drive in Fremont, Calif. (near fault patch 96, fig. 2), established by Galehouse after the earthquake shows a small amount of left-lateral slip, even though it is located at a site that has slipped at high right-lateral rates in the past, judging from curb offsets.

Harsh and Burford (1982) reported a possible slowing of the creep rate at an alignment array on Prune Avenue (now South Grimmer Boulevard) in Fremont about 0.7 km southwest of Galehouse's site at Camellia Drive (Lienkaemper and others, 1991) after the 1980 Livermore, Calif. (M=5.8), earthquake. A dislocation model constructed to calculate the static-stress changes from this earthquake yielded left-lateral shear stresses of less than 0.02 bar at the Prune Avenue array, as well as tensional normal stresses of about 0.06 bar. The left-lateral shear stress might have helped to slow creep, whereas the tensional normal stress might be expected to accelerate it if frictional forces are important. It would be remarkable if such small stresses were to have an effect on the creep rate at this site. The site lies on an unusual 5- to 7-km-long stretch of the fault that has displayed the highest historical creep rates (8–9 mm/yr), which Lienkaemper and others (1991) took to be an indication of slip rates at depth on the Hayward fault.

In summary, it appears that a good correlation exists between our calculated stress changes and observed microseismicity rates for low assumed apparent coefficients of friction and that a possible correlation exists with retarded surface slip rates observed at alignment arrays on the Hayward fault.

NEGLECTED VARIABLES THAT COULD BE IMPORTANT

Several important variables have been ignored in the models presented above, including elastic heterogeneities, the possibility of nonvertical dips on some major faults, and the interactions of deep faults with other structures not included in the models. In this section, we estimate the possible magnitude and importance of these effects.

ELASTIC HETEROGENEITY

Eberhart-Phillips and Stuart (1992) demonstrated that slip models for the earthquake based on geodetic information could be mislocated by as much as 2 km because of changes in elastic moduli on the two sides of the rupture. Such changes could also bias the stress calculations presented here, especially in the near field. Although we have made no attempt to correct for this effect, we suspect that middle- and far-field results will not be much changed by shifting any of the distributions used by several kilometers in any direction.

EFFECT OF DIPPING FAULTS

The magnitudes of the stress changes induced on various fault planes in the San Francisco Bay region depend on the orientations as well as the distances of these planes relative to the Loma Prieta rupture surface. For example, a small dipping fault plane near the San Gregorio fault (fault patch 200, fig. 2) can be seen in figure 6 to have a propensity for

failure opposite to that of the adjacent vertical patches aligned under the San Gregorio fault trace. The DCFF value for this fault patch was calculated by assuming oblique (reverse plus right lateral) slip on the fault plane, with a rake of 150°. The presence of dipping faults undergoing oblique slip in this region is suggested by about 40 reasonably well controlled local focal mechanisms that we examined, which also suggested the rake value used. Whether these events occurred on a dipping San Gregorio fault or on adjacent dipping faults is unclear. Jachens and Griscom (in press) report that aeromagnetic data suggest a 50°–60° NE. dip for the onland section of the San Gregorio fault and its offshore extension to the south.

Dipping fault patches 198 and 199 (fig. 2) adjacent to the San Andreas fault to the north of the Loma Prieta rupture zone were also added to the model in a region of known reverse-faulting mechanisms (Olson and Lindh, 1985) to test the importance of geometric factors. These two fault patches come closer to failure as a result of Loma Prieta stress changes, as do the adjacent vertical fault patches (36, 37) under the San Andreas fault trace.

Could the Hayward fault, though moved farther from failure in our low-apparent-coefficient-of-friction models based on vertical fault patches, be stressed closer to failure if it dipped east or west? Several investigators have pointed to compressional structures around the San Francisco Bay region (for example, Aydin and Page, 1984; Wentworth and Zoback, 1989), and Jones and others (1991) suggested that the Hayward fault itself may dip or have an associated dipping companion fault. The unexpected reverse component of slip on the Loma Prieta rupture surface does raise the possibility that other intermediate to large earthquakes which have occurred in the bay region may have had oblique (that is, both strike slip and reverse slip) motions to them. This conclusion would be consistent with the presence of fault-normal compression in California along the San Andreas fault, as noted by Mount and Suppe (1987), Zoback and others (1987), and Wentworth and Zoback (1989).

To test the effect of a dipping Hayward fault, we tried two variations of the dislocation model based on the slip distribution of Lisowski and others (1990). In the first variation, the Hayward fault was assigned a dip of 45° E., and in the second variation, a dip of 45° W.; the results are plotted in figure 8. Although the stresses on dipping fault patches differ from those on a vertical fault, no real change occurs in the relaxation picture because the dipping model faults still show an increase in left-lateral horizontal stress, which is presumably relaxing, and the unclamping effect is translated into downdip tensional stress, which also would be expected to move the Hayward fault farther from failure in a regional fault-normal compressive-stress field.

This result for the Hayward fault does not necessarily apply to other faults with other locations and geometries relative to the Loma Prieta rupture zone. For example, the result for the San Gregorio fault described above suggests that in some places dip can be important in determining the change in the proximity to failure. Griscom and Jachens (1990), Jachens and others (1990), and Jachens and Griscom (in press) suggested that several of the principle faults in the San Francisco Bay region, including the San Andreas fault, have nonvertical dips, on the basis of the geometry of gravity and aeromagnetic anomalies. More work needs to be done to refine our models of the active tectonic elements in the bay region.

EFFECT OF OTHER STRUCTURES

In most of our models, the Hayward fault seems to be relaxed rather than stressed by the Loma Prieta static-stress changes. Could a Loma Prieta-type event trigger an earthquake on the Hayward fault in other ways?

For example, a Loma Prieta-type event might trigger seismic or aseismic slip on an intermediate structure that would, in turn, trigger an earthquake on the Hayward fault. Andrews and others (1993) suggested that the Mission fault (fig. 1) could play a critical triggering role for earthquakes on the Hayward fault. Using the slip distribution of Lisowski and others (1990), we tried three models for a Mission

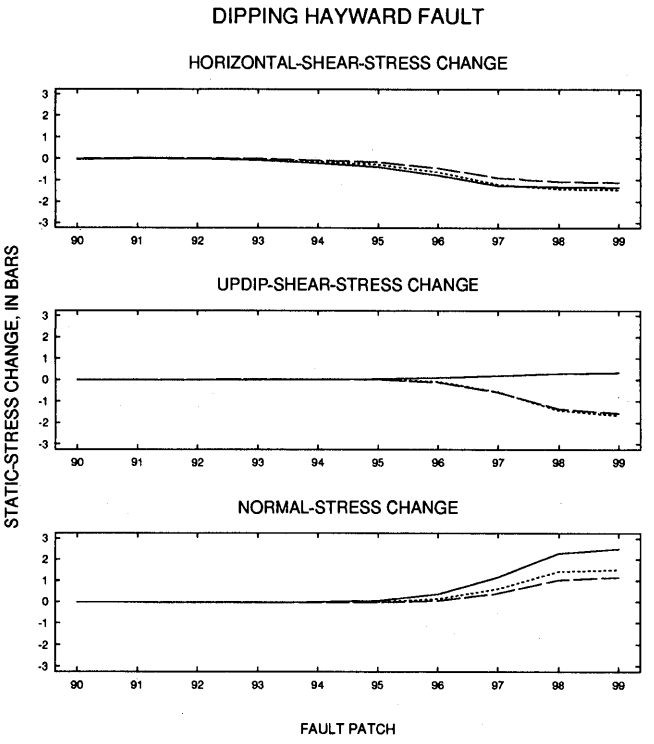

Figure 8.—Static-stress changes on patches of the Hayward fault, calculated by using slip distribution of Lisowski and others (1990). Long dashes, 45° E.-dipping fault; solid line, vertical fault; short dashes, 45° W.-dipping fault. Top plot, change in horizontal shear stress; middle plot, change in updip shear stress; bottom plot, change in normal stress.

fault dipping vertically, 45° NE., and 45° SW., assuming that the preexisting load on the fault is a combination of right-lateral horizontal shear and reverse updip shear. For all three dips used in our models, the Mission fault received a left-lateral horizontal shear-stress increment and, for the dipping models, a normal-faulting downdip shear increment as a result of the Loma Prieta rupture. Both shear components are therefore likely to relax the assumed state of shear stress on the Mission fault. Normal-stress changes for all three dips are tensional, tending to unclamp the fault, but the magnitudes of tension are mostly smaller than the shear components. Only with a vertical dip and a high coefficient of friction (0.8) does the Mission fault move closer to failure as a result of the earthquake. Thus, the Mission fault does not seem to be an effective intermediary for transferring Loma Prieta stress changes to the Hayward fault.

Other candidates for intermediary triggering structures lie under San Francisco Bay between the Loma Prieta rupture zone and the Hayward fault. Gravity and magnetic data suggest the presence of several structures at depth under the bay (Griscom and Jachens, 1990). It is not yet known whether these structures are still active and, if so, whether aseismic or seismic slip on any of them might bring the Hayward fault closer to failure.

SIMULATING TIME-DEPENDENT EFFECTS WITH DISLOCATION MODELS

Regional adjustments that occur after large earthquakes may include aseismic slip on other nearby structures and on deeper parts of the fault that ruptured in the main shock; these adjustments may occur over periods of days to years. Without a model of the pertinent rheologies, time-dependent histories of the subsequent stress changes cannot be calculated. Directions and final states, however, can be estimated by solving the boundary-value problem for which the aseismically slipping structures are required to attain a zero shear-stress state. This state is presumed to approximate the final state (after infinite time has passed) of the time-dependent solution. A better approach is to actually construct a model of the lithosphere that incorporates appropriate rheologies and to calculate the resulting evolution over time. Linker and Rice (1991 and in press) used this approach in a finite-element model.

SLIP AT DEPTH IN RESPONSE TO THE EARTHQUAKE

We consider two types of redistribution of stresses: (1) that which would result from deep afterslip, triggered by Loma Prieta static-stress changes, on vertical planes beneath the locked seismogenic layer; and (2) that which would result from slip on a horizontal-detachment surface under San Francisco Bay. Both types show that afterslip can change the magnitude and even the sign of Loma Prieta static stresses acting on other nearby faults.

AFTERSLIP ON VERTICAL PLANES

To evaluate the effect of the Loma Prieta stress impulse on the vertical, aseismically slipping parts of bay-region faults, we added a second layer of 13-km-tall vertical patches extending from 13- to 26-km depth (yellow, fig. 9*A*) that were free to slip in response to the static-stress changes. The top layer of fault patches was held locked, as in the previous models. The purpose of this exercise was to see how stresses acting on the top layer would be changed by slip at depth.

The results are shown in figure 10, using the slip distribution of Lisowski and others (1990). The stresses acting on the top layer (0- to 13-km depth) in the model do change in response to the deep vertical-slip adjustments, but not by much. No substantial increase in the danger of failure on any bay-region faults occurs as a result of such afterslip on vertical s of the faults.

AFTERSLIP ON HORIZONTAL DETACHMENT SURFACES

Horizontal detachment surfaces might offer a more effective way to convey stresses efficiently over large distances. Although there is presently no direct evidence for such surfaces in the San Francisco Bay region, their presence has been hypothesized (see Furlong and Verdonck, this chapter), and so it is of interest to explore the utility of such a horizon in redistributing stresses. Both Furlong and Verdonck (this chapter) and Linker and Rice (in press) present models that use detachment surfaces to redistribute stresses. Our model is shown in figure 9*B*. The horizontal floor of 10- by 10-km rectangular dislocations at a depth of 13 km was free to slip so as to eliminate shear stresses.

The results are shown in figure 10. As expected, the stress changes on the seismogenic layer are more striking than for vertical aseismic slip surfaces. In particular, normal-stress changes on the Calaveras and San Gregorio faults have changed by a factor of 2 or more in some places opposite the Loma Prieta model rupture. Shear stresses on the San Gregorio fault have also changed somewhat, and the boundaries between regions of increased relaxation and failure have shifted by about 10 km on these faults.

Overall, however, even slip on this simulated horizontal detachment surface does not change our results significant-

ly for faults at middle and far distances (min 40 km) from the Loma Prieta rupture. In particular, results for the Hayward fault hardly change at all. A different geometry for the detachment surface, possibly with bounding edges closer to the locations of major faults, might yield greater effects.

PLATE-TECTONIC LOADING AFTER THE 1989 EARTHQUAKE

The static-stress changes on other central California faults resulting from the Loma Prieta rupture are imposed coseismically and essentially instantaneously (within seconds or

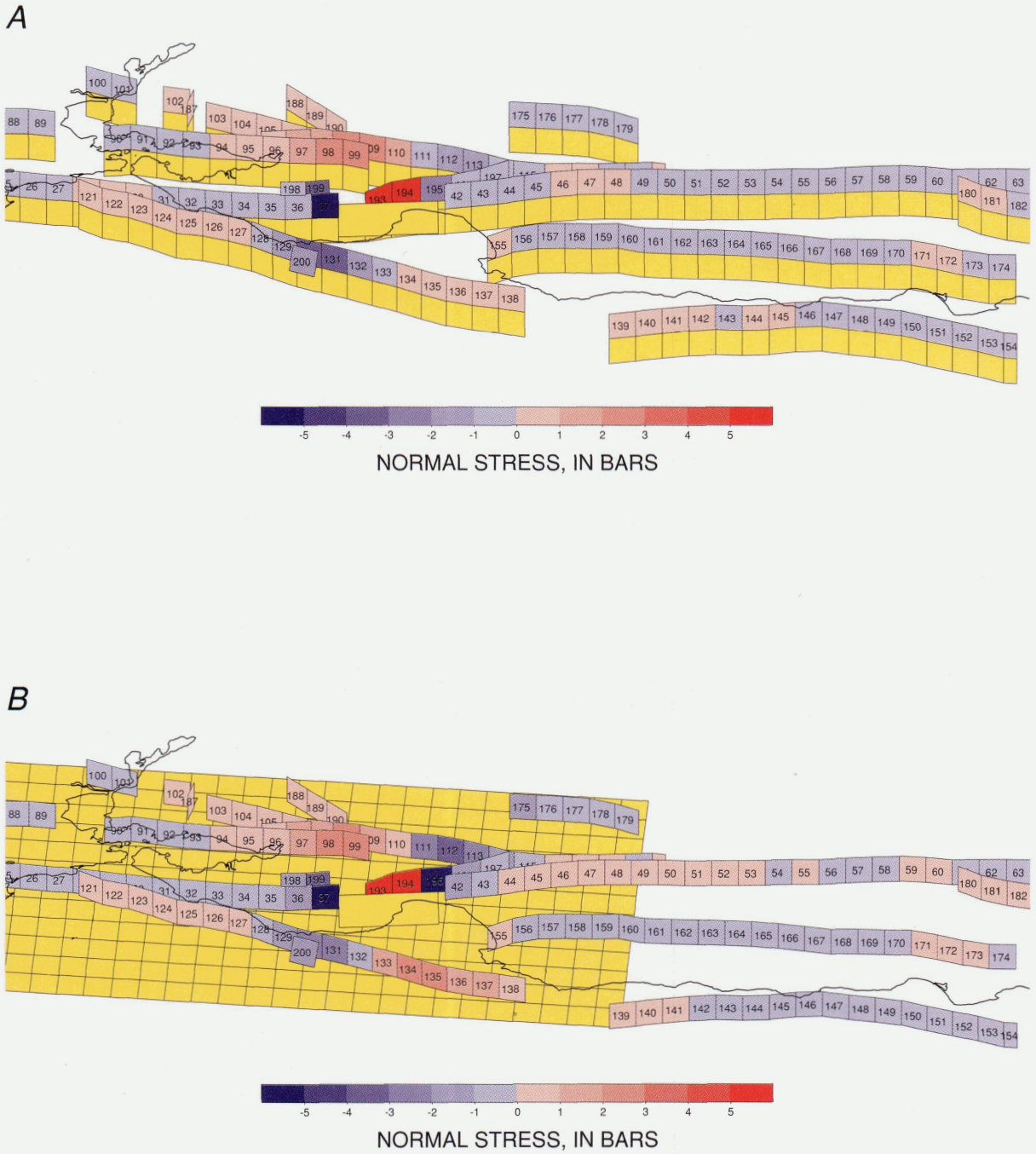

Figure 9.—Oblique views of patches on central California faults showing static-stress changes calculated by using slip distribution of Lisowski and others (1990). *A*, Oblique view of model, with freely slipping vertical layer (yellow patches) from 13- to 26-km depth under top layer of locked fault patches. *B*, Oblique view of model, with freely slipping horizontal detachment surface (yellow patches) at 13-km depth. Loma Prieta rupture, though shown in yellow, is not free to slip in either model.

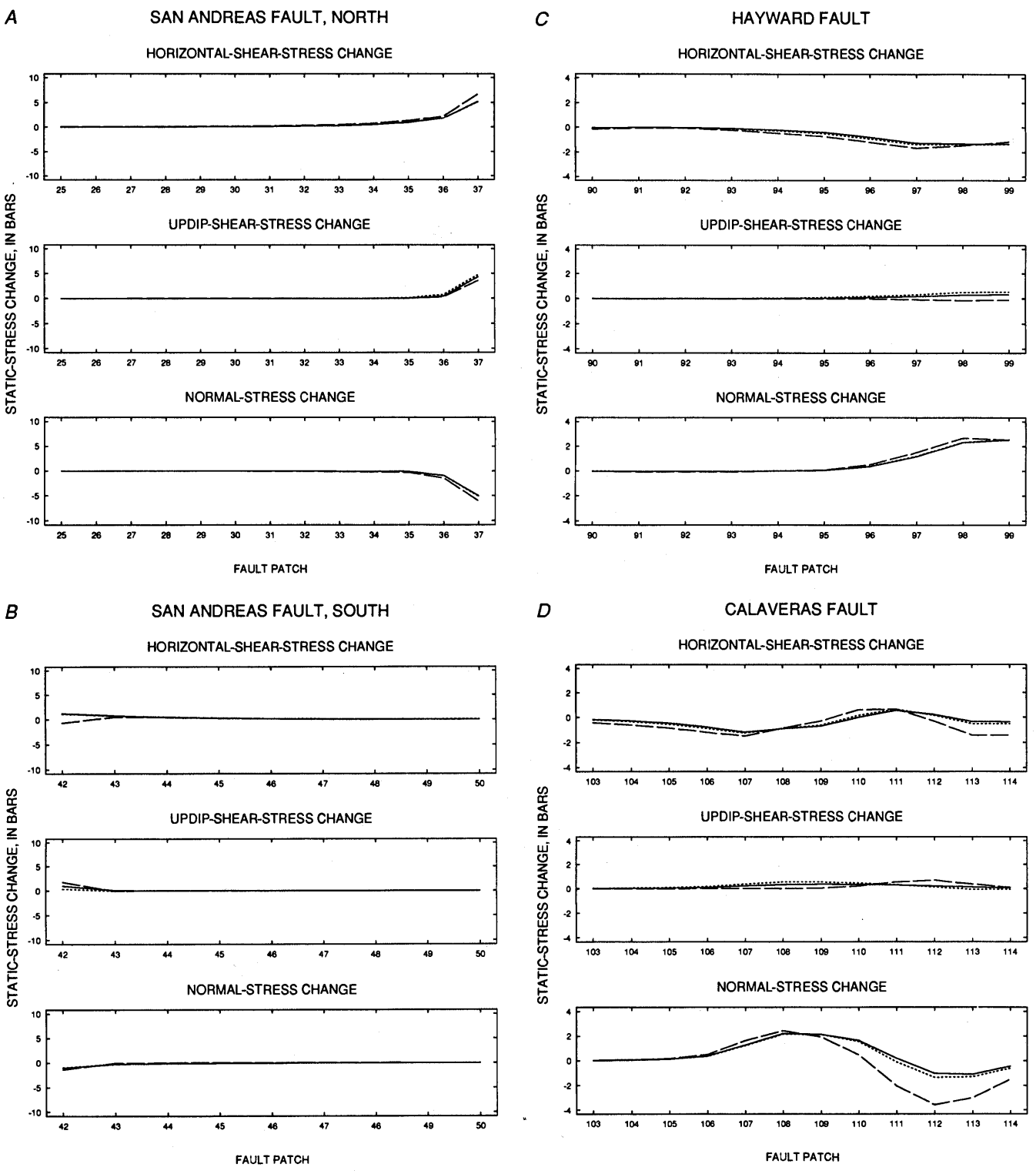

Figure 10.—Static-stress changes on patches of the San Andreas fault (*A*) north and (*B*) south of Loma Prieta rupture zone, (*C*) the Hayward fault, (*D*) the Calaveras fault, and (*E*) the San Gregorio fault, calculated by using slip distribution of Lisowski and others (1990). Solid line, changes with no afterslip; short dashes, changes with afterslip on vertical layer from 13- to 26-km depth under top layer of locked fault patches; long dashes, changes with afterslip on a horizontal detachment surface at 13-km depth. Top plot, change in horizontal shear stress, where positive values indicate an increase in right-lateral traction; middle plot, change in updip shear stress, where positive values indicate an increase in west-side-up traction; bottom plot, change in normal stress, where positive values indicate an increase in tension (unclamping).

Table 2.—*Long-term deep slip rates on selected central California faults*

[Do., ditto]

Fault	Patches (fig. 2)	Assumed slip rate (mm/yr)	References
San Andreas:			
North–coastal section	1–27	24	Prentice (1989), Niemi and Hall (1992).
Peninsular and southern sections	28–49	19	Working Group on California Earthquake Probabilities (1990), Lienkaemper and others (1991).
Central creeping section	50–71	35	Working Group on California Earthquake Probabilities (1990).
Rodgers Creek	83–89	5	Budding and others (1991).
Hayward	90–99	9	Lienkaemper and others (1991).
Calaveras:			
Northern section	103–106	6	Do.
Southern section	107–120	15	Working Group on California Earthquake Probabilities (1990).
San Gregorio	121–138	4	Clark and others (1984).

minutes). Additional changes may be added by continuing afterslip around the rupture zone (within days to months) that may for some earthquakes have a moment equal to that of the initial rupture (for example, Smith and Wyss, 1968). Over the longer term, the static-stress changes are modified by viscous relaxation and the ongoing increment of plate-loading forces. Relaxation phenomena are discussed in the preceding section.

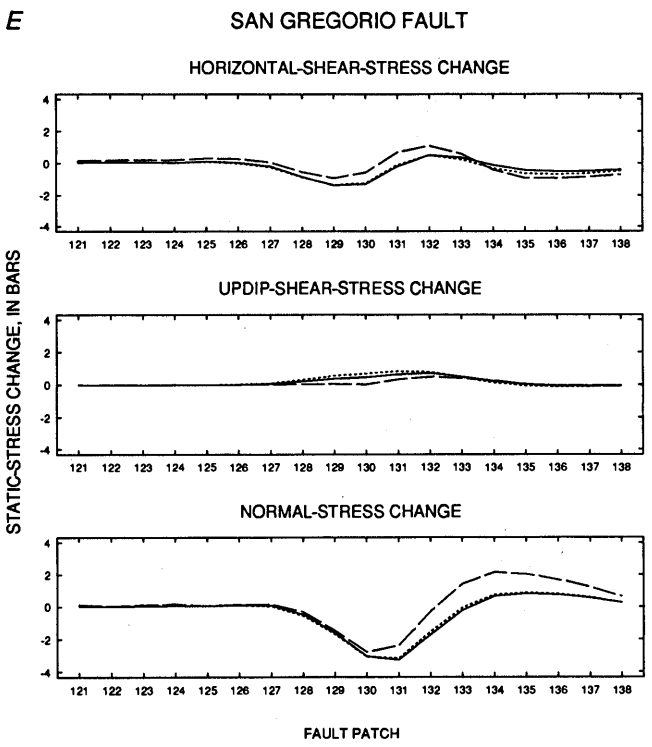

Figure 10.—Continued.

The plate-tectonic loading can be approximated by using dislocations, as described below. This approach allows an estimate of how the earthquake-induced static-stress changes on a given fault segment compare with the yearly plate-loading stress increments. For fault patches that were brought closer to failure by the Loma Prieta rupture, the ratio of these two quantities gives an estimate of by how may years failure on the patch has been advanced—assuming that the earthquake did not change the failure threshold. J.H. Dieterich (oral commun., 1992) pointed out that the dynamic effects of shaking accompanying the passage of the seismic waves might disrupt the healing process on a fault and induce it to fail earlier.

For fault patches that have been relaxed by the addition of an increment of left-lateral shear stress, estimates of the plate-loading rate allow us to calculate how long it will take the fault patch to return to its state of loading before the earthquake. During the recovery period, we would not anticipate large earthquakes on the fault patch because it had already been at higher stress levels before the earthquake relaxed it, again assuming that the earthquake did not alter the failure threshold and that failure is a fairly deterministic, rather than chaotic, process.

We assume that only the seismogenic upper layer is moving in stick-slip fashion and that the deeper layers are moving at steadier rates approximating observed long-term slip rates (table 2). These long-term slip rates are assigned to dislocations extending from 13- to 100-km depth under the major faults, which are assumed to be vertical. The results are unlikely to be sensitive to the depth to the bottom of the second slipping layer. The assignment of long-term slip

rates to the various faults, however, also introduces some long-term inconsistencies. For example, faults that change in strike will accumulate normal stresses in the model that in the real world are presumably relieved by deformation adjacent to the fault (for example, thrusting and mountain building or basin formation). Alternative models of deformation at depth in the San Francisco Bay region are becoming available that could be utilized in these estimates (see Bodin and Bilham, this chapter; Furlong and Verdonck, this chapter). Furlong and Verdonck's models, in particular, are based on the presence of horizontal detachment surfaces connecting bay-region faults under San Francisco Bay, with most of the deep slip between plates occurring at depth under the Hayward fault.

The results of our attempt to calculate long-term plate-loading rates are plotted in figure 11, where stress-change rates are shown for the slip distribution of Lisowski and others (1990). In figure 12, long-term plate-loading rates and Loma Prieta static-stress changes have been converted into equivalent years of delay or advance in failure. On fault patch 37 (fig. 2), for example, north of the Loma Prieta rupture zone, the horizontal shear-stress increment of 5.2 bars (fig. 4*A*) is nearly equal to 30 yr of loading (top plot, fig. 12*A*), with an assumed long-term slip rate of 19 mm/yr (table 2) on this section of the San Andreas fault. On fault patch 99, on the southern section of the Hayward fault, the initial earthquake-induced relaxation in the hori-

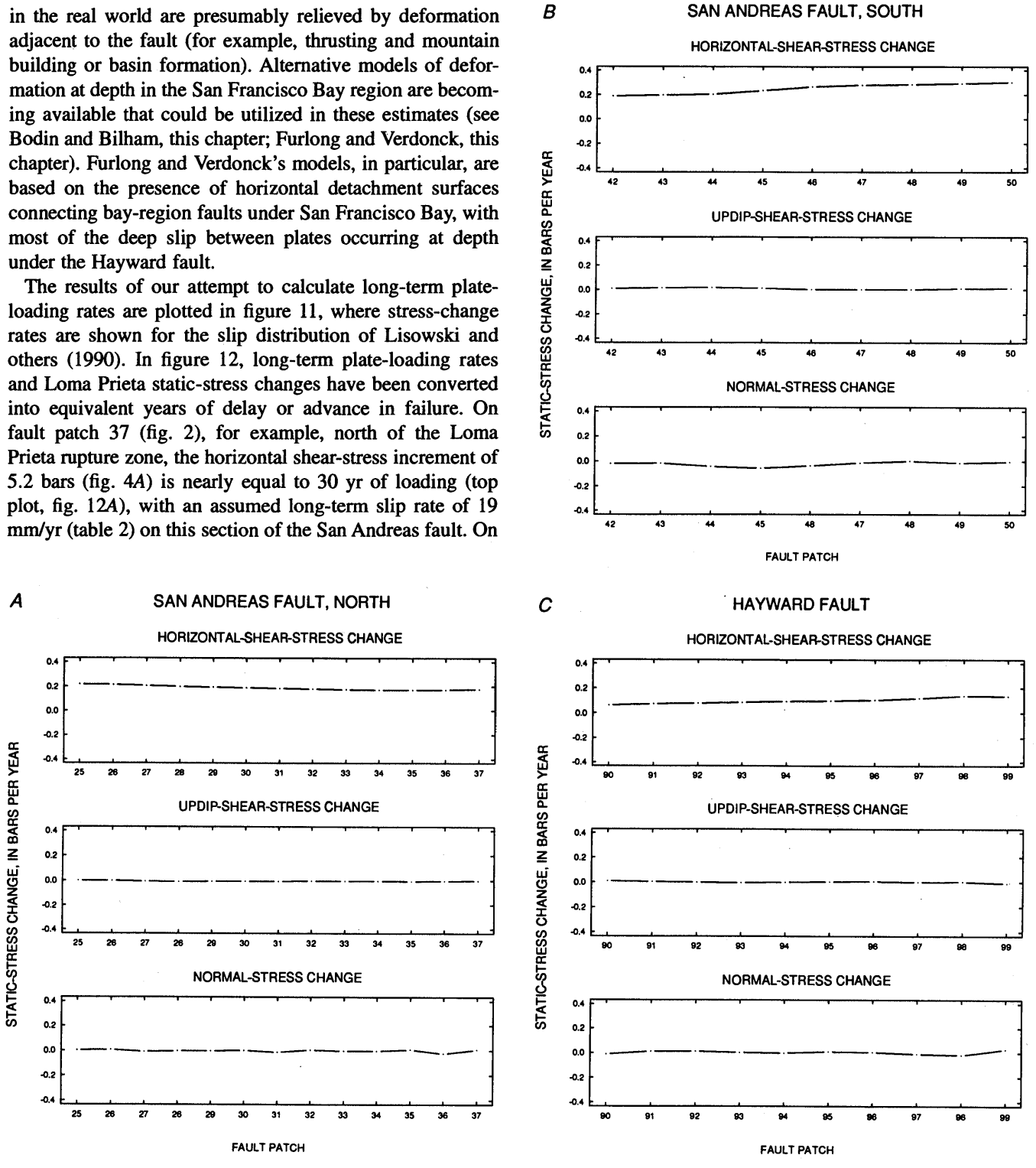

Figure 11.—Annual plate-tectonic-loading rates on patches of the San Andreas fault (*A*) north and (*B*) south of Loma Prieta rupture zone, (*C*) the Hayward fault, (*D*) the Calaveras fault, and (*E*) the San Gregorio fault, calculated by using model described in text and deep slip rates listed in table 2. Top plot, change in horizontal shear stress, where positive values indicate an increase in right-lateral traction; middle plot, change in updip shear stress, where positive values indicate an increase in west-side-up traction; bottom plot, change in normal stress, where positive values indicate an increase in tension (unclamping).

zontal shear stress of 1.34 bars (fig. 4*C*) for the slip distribution of Lisowski and others (1990) is overcome in about 10 yr (top plot, fig. 12*C*) by the long-term plate-loading rate of 0.14 bar/yr (fig. 11*C*) calculated for an assumed long-term slip rate of 9 mm/yr at depth on the Hayward fault.

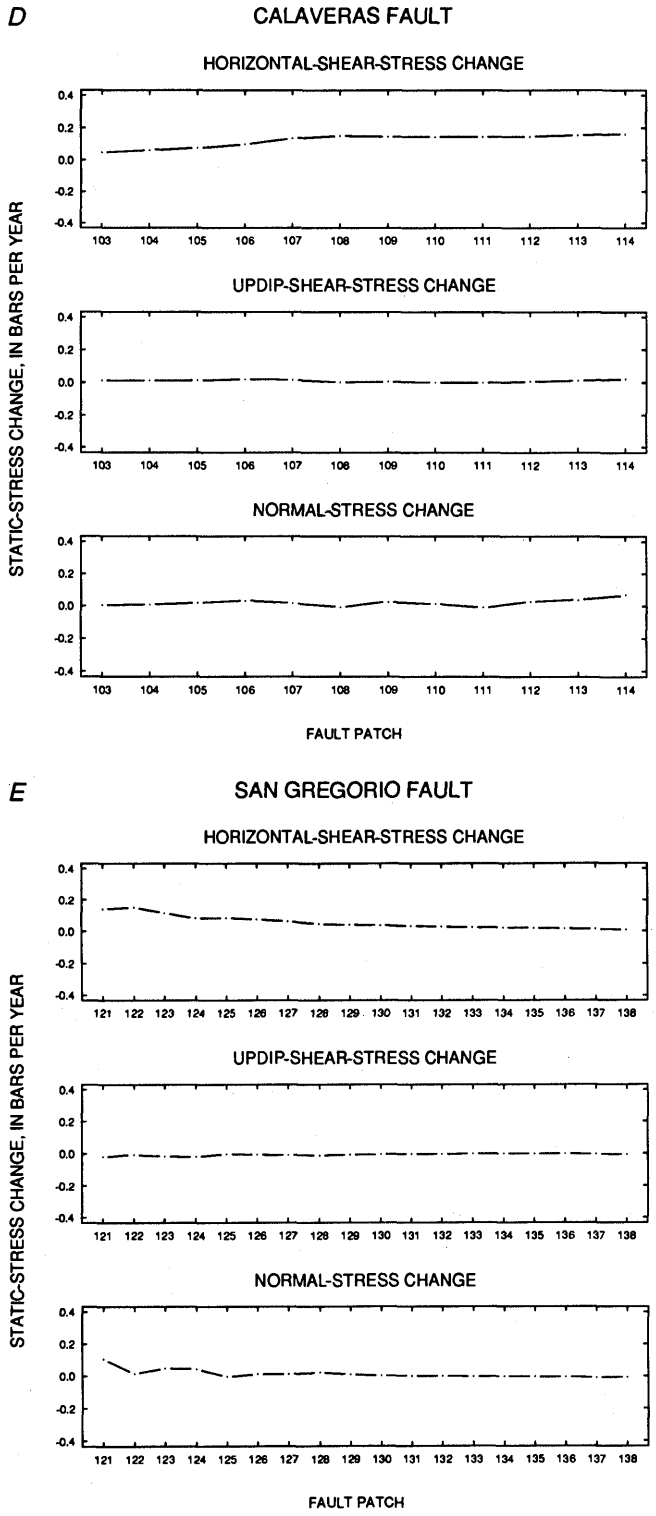

Figure 11.—Continued

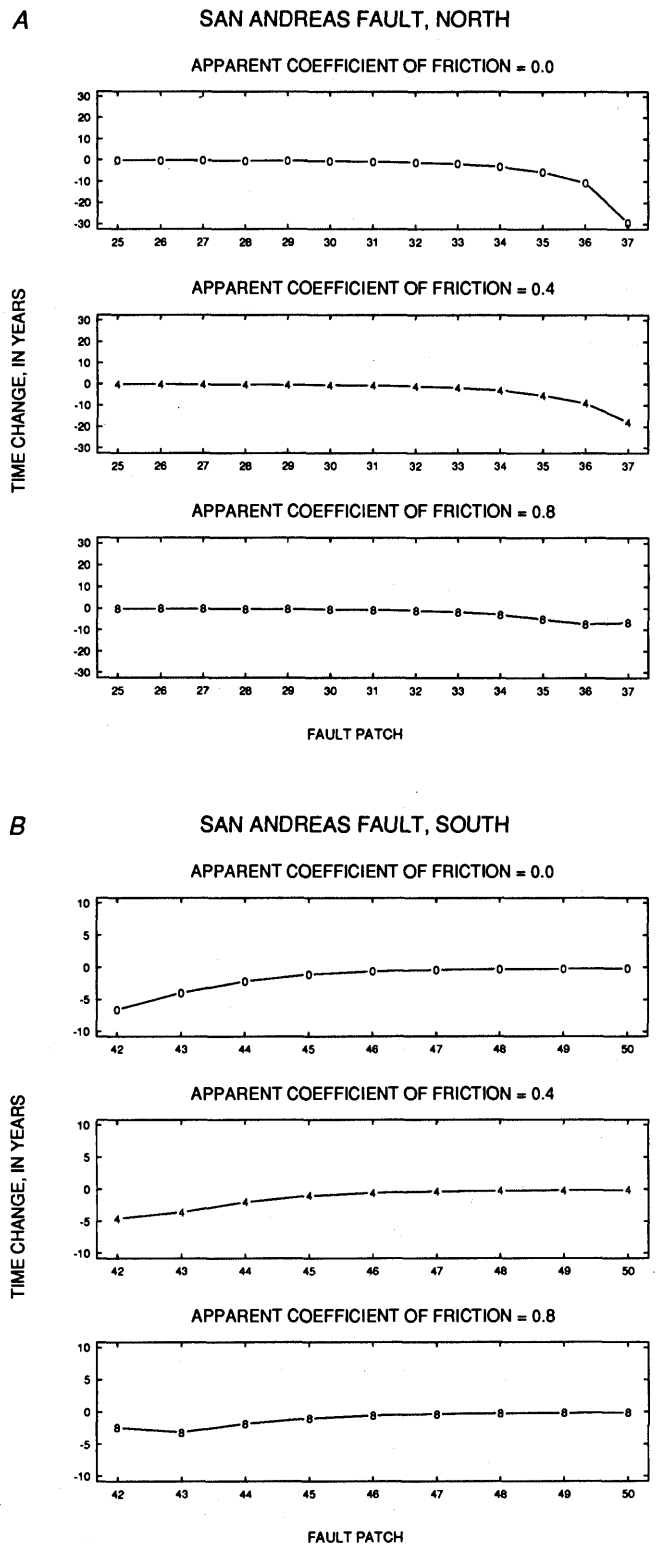

Figure 12.—Estimated delay (positive values) or advance (negative values) in time to failure introduced by 1989 Loma Prieta earthquake on patches of the San Andreas fault (*A*) north and (*B*) south of Loma Prieta rupture zone, (*C*) the Hayward fault, (*D*) the Calaveras fault, and (*E*) the San Gregorio fault, calculated by using slip distribution of Lisowski and others (1990), assuming apparent coefficients of friction μ' of 0.0 (top plot), 0.4 (middle plot), and 0.8 (bottom plot).

We note that the times of advance or delay in failure are sensitive to the assumed long-term slip rates. Large delays on the San Gregorio fault, for example (fig. 12*E*), partly reflect the low plate-loading rate resulting from an assumed deep slip rate of 4 mm/yr (table 2). Changing this rate by just 1 mm/yr would substantially affect the time changes in figure 12*E*.

The evolution of the horizontal shear stress over time on the Hayward and Calaveras faults after the Loma Prieta rupture is illustrated in figure 13. A return to light red indicates that the relaxation on a fault patch has ended and the horizontal shear stress has reached pre-1989 levels. Fault patches that were not relaxed by the earthquake continue to redden as they are loaded tectonically.

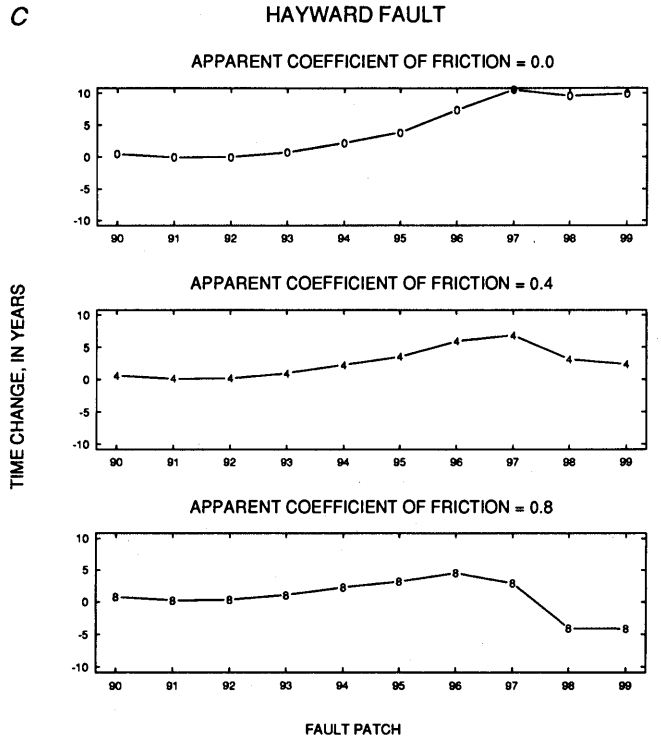

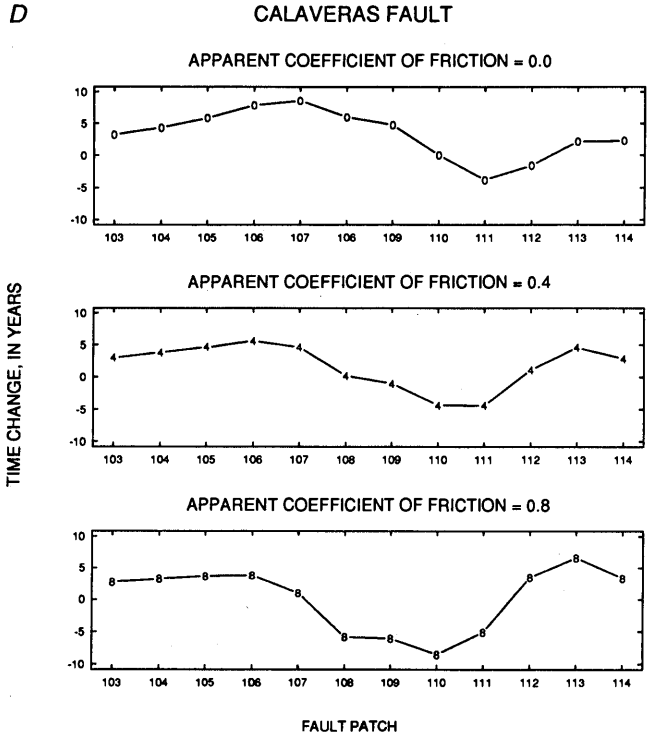

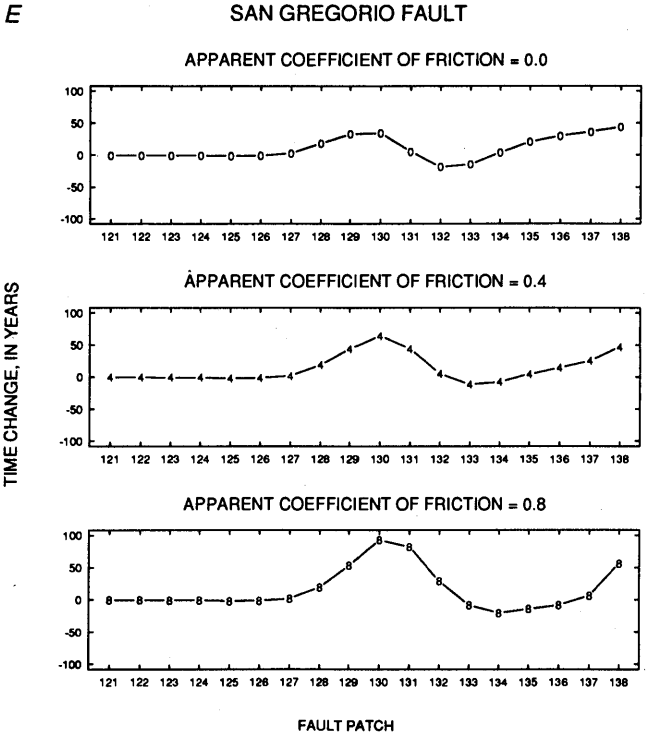

Figure 12.—Continued.

PLATE-TECTONIC LOADING AFTER THE 1906 EARTHQUAKE AND THE END TO 73 YEARS OF SEISMIC QUIESCENCE

It is of some interest to calculate the static-stress changes caused by the 1906 San Francisco (M=8+) earthquake for comparison. We used the slip distributions inferred by Thatcher (1975) and Thatcher and Lisowski (1987) from surface slip and geodetic observations to calculate these static-stress changes. The dislocation model consists of 20-km-tall by 10-km-long vertical rectangular patches representing the major faults in the San Francisco Bay region. Thatcher (1975) suggested that coseismic slip during the

1906 earthquake extended to a depth of only 10 km but that afterslip might have gone to depths as great as 30 km.

The static-stress changes in this model for bay-region faults are plotted in figure 14, and the number of years of delay or advance in failure after the 1906 rupture estimated from our dislocation model are plotted in figure 15. The creeping section of the San Andreas fault south of San Juan Bautista, Calif. (fig. 1), was more highly stressed, whereas most other bay-region faults were relaxed in their horizontal-shear component by the 1906 earthquake. We suggest that this relaxation explains the 73-yr quiescence for $M>6$ events on bay-region faults after the 1906 earthquake (except for the 1911 earthquake; Ellsworth and others, 1981; Sykes and Jaumé, 1990).

The evolution of horizontal shear stress over time on the Hayward and Calaveras faults after the 1906 earthquake is illustrated in figure 16. The effect of the 1989 earthquake can also be seen as a small perturbation at 1990 near the south end of the Hayward fault (especially fault patch 98). This perturbation helps place in perspective the relative sizes of the static-stress changes from the 1906 and 1989 earthquakes.

The locations of $M>5$ earthquakes on the Calaveras fault since 1906 (Oppenheimer and others, 1990, table 1) are shown in figure 17. The onset of $M>6$ earthquakes in the San Francisco Bay region after 73 yr of seismic quiescence began in a region near the intersection of the Hayward and Calaveras faults where the fault patches are

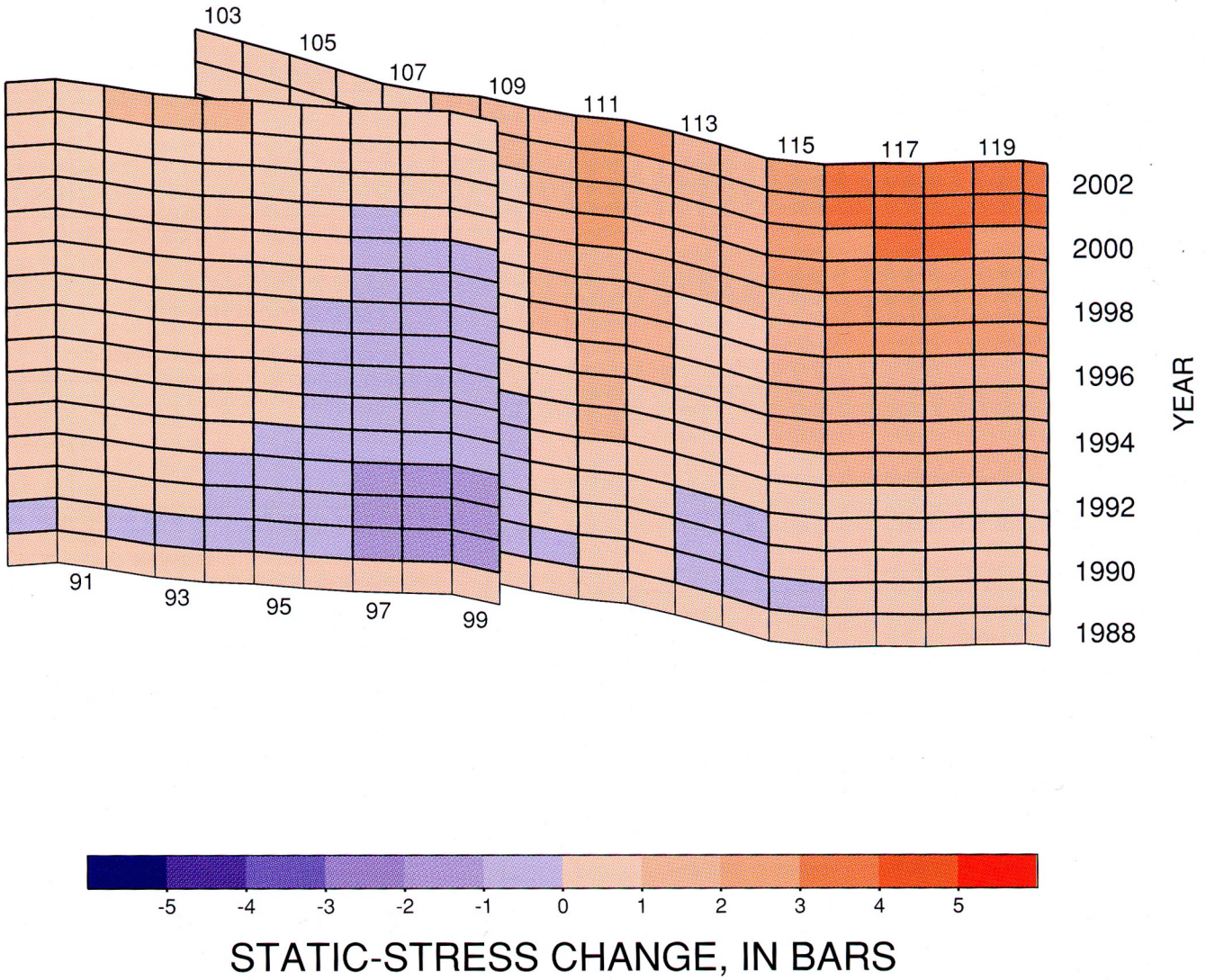

Figure 13.—Oblique view of patches on the Hayward fault (left block) and the Calaveras fault (right block), showing changes in horizontal shear from 1988 to 2002. Values for 1988 are all zero, taking that as a reference year. Large changes introduced by 1989 Loma Prieta earthquake are in some places left lateral (blue). As tectonic loading progresses (see text), additional right-lateral traction reloads sections of faults that had been relaxed. By 2000, even sections of the Hayward fault that sustained largest increments of left-lateral shear in this model are back to pre-1989 stress levels. No provision for aseismic afterslip was made in this model.

calculated to have recovered earliest from the relaxation imposed in 1906.

A note of caution needs to be applied to the results described in this subsection. Elastic-dislocation models may

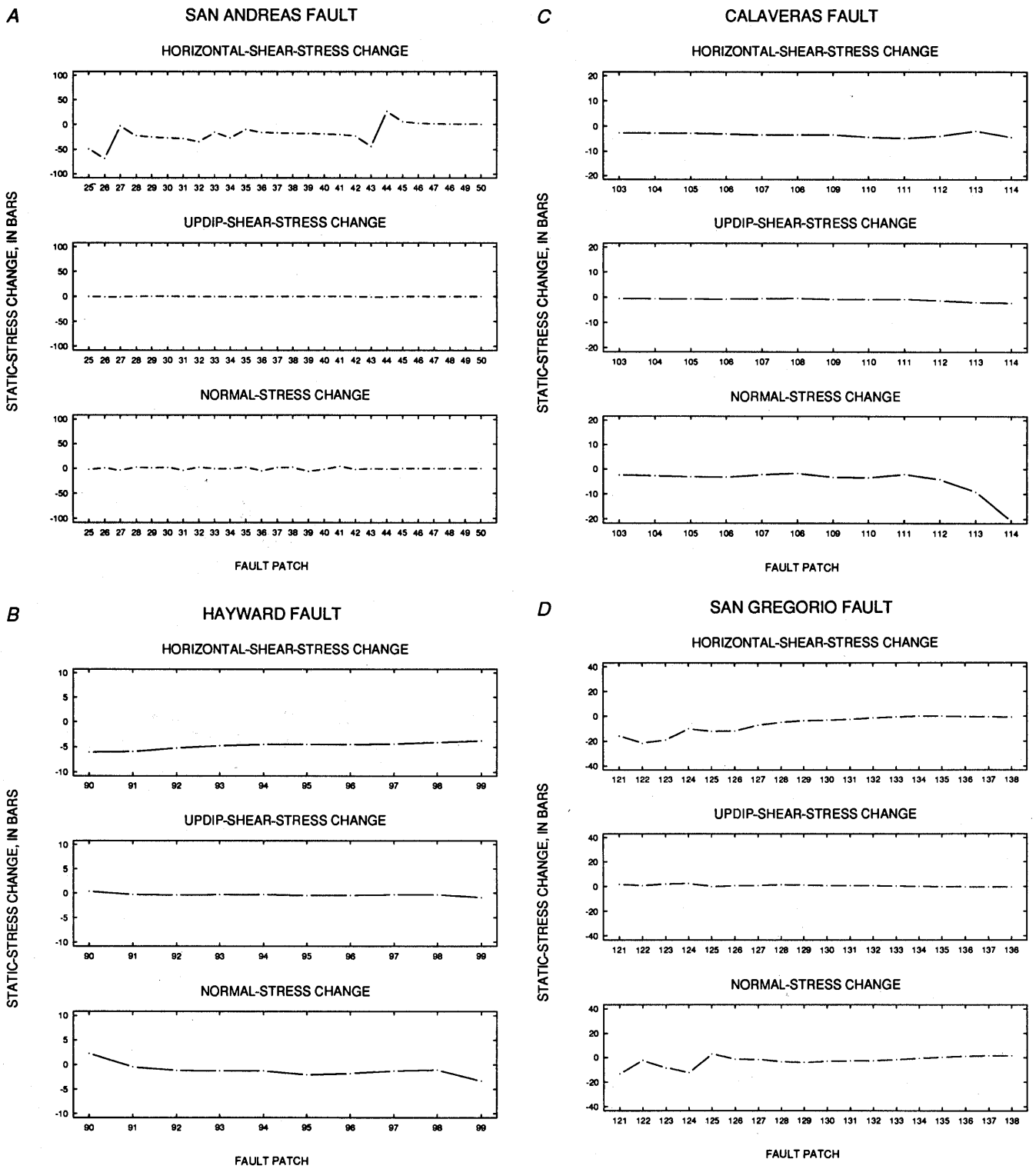

Figure 14.—Static-stress changes at 10-km depth after 1906 San Francisco earthquake on patches of (*A*) the San Andreas fault, (*B*) the Hayward fault, (*C*), the Calaveras fault, and (*D*) the San Gregorio fault, calculated by using simple model of 1906 rupture based on slip estimates of Thatcher (1975) and Thatcher and Lisowski (1987). Top plot, change in horizontal shear stress; middle plot, change in updip shear stress; bottom plot, change in normal stress. Coseismic slip was assumed to extend to 20-km depth. Excursions at fault patches 26 and 43 in upper plot in figure 14*A* arise from discontinuities in slip estimates. Same sign conventions as in figure 4.

become increasing inappropriate over time scales of tens or hundreds of years, during which nonelastic relaxation processes and off-fault nonelastic deformation could effectively change the stress distributions.

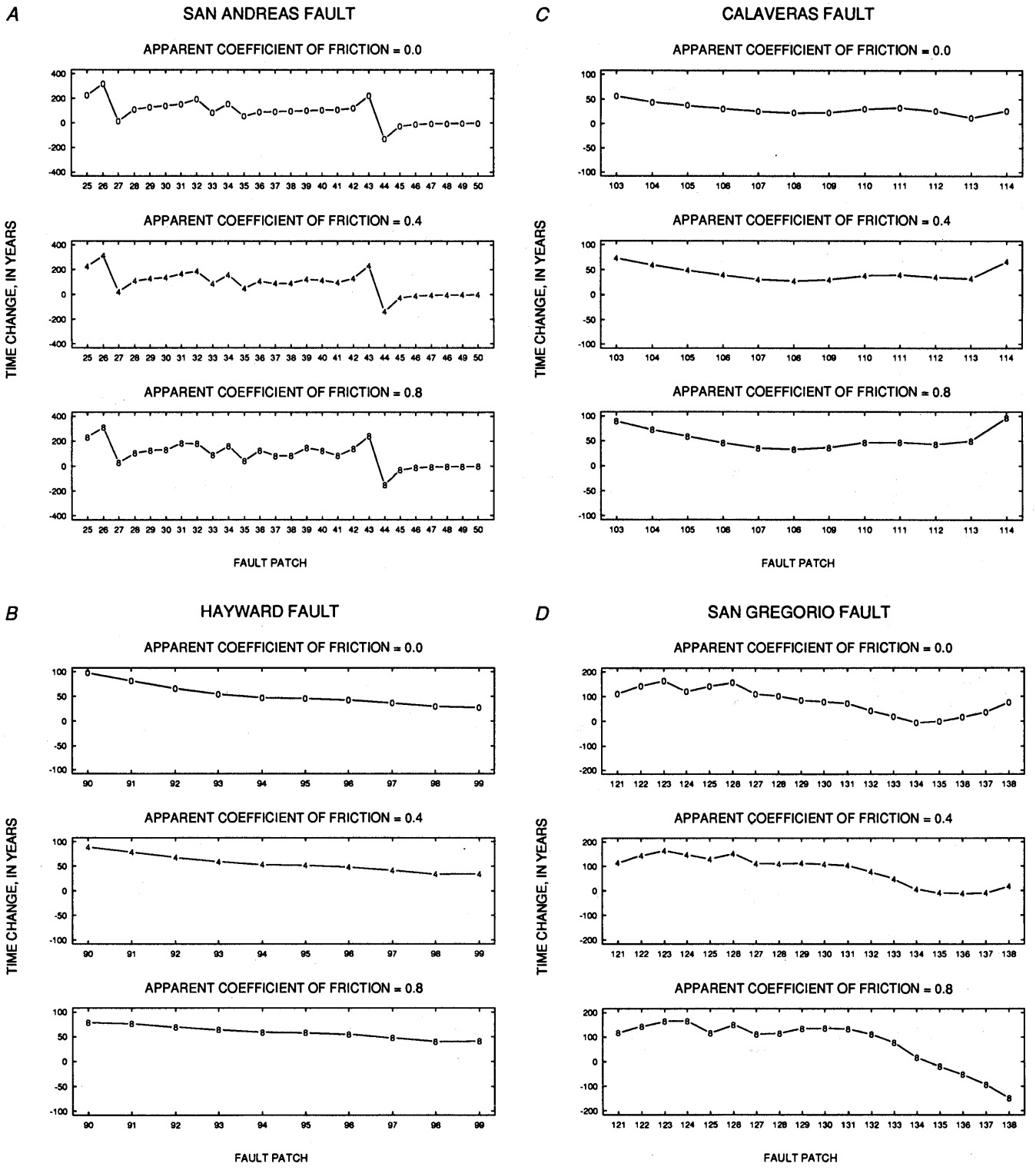

Figure 15.—Estimated delay (positive values) or advance (negative values) in time to failure introduced by 1906 San Francisco earthquake on patches of (*A*) the San Andreas fault, (*B*) the Hayward fault, (*C*) the Calaveras fault, and (*D*) the San Gregorio fault, based on static-stress changes calculated for 1906 San Francisco earthquake and on plate-tectonic-loading rates inferred from long-term slip rates listed in table 2, assuming apparent coefficients of friction μ' of 0.0 (top plot), 0.4 (middle plot), and 0.8 (bottom plot).

PAIRED EARTHQUAKES ON THE SAN ANDREAS AND HAYWARD FAULTS?

PREREQUISITES FOR INTERACTIONS

If large earthquakes on the San Andreas fault can trigger large earthquakes on the Hayward fault and vice versa, a preliminary loading stage is still required before such triggering can occur. Typical average stress drops in dislocation models of M=7 earthquakes are 20 to 40 bars, whereas the size of the stress change induced on the opposite side of San Francisco Bay by the 1989 Loma Prieta earthquake is at most a few bars. Thus, the stresses added by a M=7 earthquake across the bay are not enough by themselves to generate a large earthquake—the fault must already be substantially loaded for triggering to occur. From our models, we estimate that static-stress changes from an M=7 earthquake might, at worst, trigger a second large earthquake on the other side of the bay that would have occurred anyway within ten or several tens of years.

The occurrence of two earthquakes within a short timespan need not imply that one triggered the other at all. Reasenberg and Simpson (in press) point out that the crossbay-triggering hypothesis is not strongly supported by the existing historical record of earthquakes: The two pairings in the 1800's can be reasonably accounted for by randomly occurring, independent earthquakes. With this proviso in mind, we discuss below the geometry of the

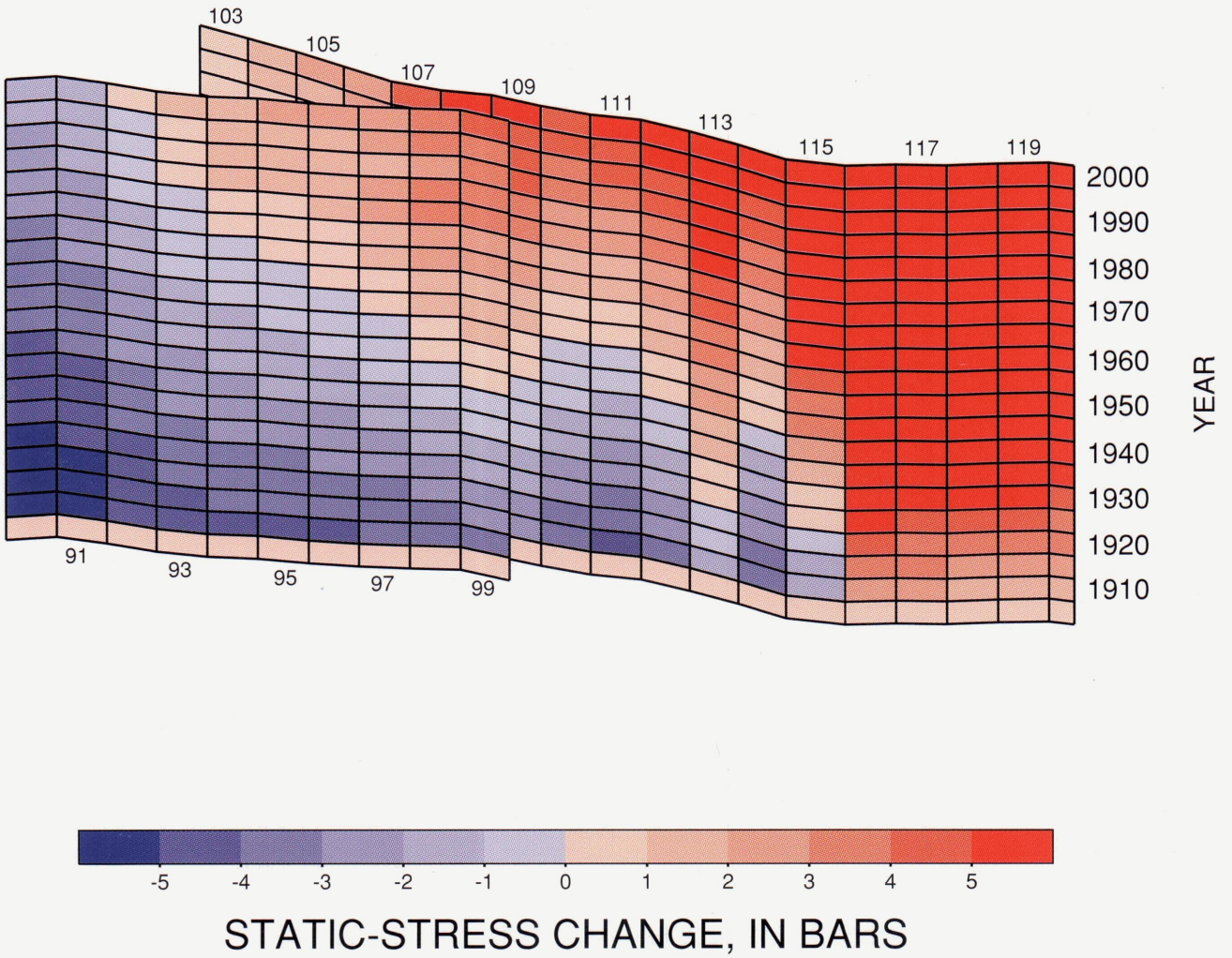

Figure 16.—Oblique view of patches on the Hayward fault (left block) and the Calaveras fault (right block), showing changes in horizontal shear stress from 1905 to 2000. Values for 1905 are all zero, taking that as a reference year. Large changes appearing in 1910 after 1906 San Francisco earthquake are left lateral (blue) for both faults except at south end of the Calaveras fault. As plate-tectonic loading progresses (see text), right-lateral traction reloads sections of faults that had been relaxed. Effect of 1989 Loma Prieta earthquake is visible at 1990 on patches 97 and 98 as slight color changes. No provision was made for aseismic afterslip in this model, including aseismic creep on central California section of the San Andreas fault, and effects of all earthquakes other than 1906 and 1989 are omitted.

two historical pairings and consider how triggering might have occurred, if caused by static-stress changes.

THE 1865/68 PAIR

In some scenarios, the 1865 earthquake would be an earlier version of the 1989 earthquake (Working Group on California Earthquake Probabilities, 1990). Here, the conclusions arrived at above regarding the triggering of an event on the southern section of the Hayward fault similar to the 1868 earthquake would still apply: The most obvious way to trigger an event on this section of the Hayward fault by static-stress changes would be through unclamping, which is most effective if coefficients of friction are high and pore-fluid pressure changes are small (or have had a chance to dissipate). This consideration suggests that the microseismicity rate along the southern section of the Hayward fault should be watched carefully for the next several years.

Tuttle and Sykes (1992) suggested that the 1865 earthquake was not a Loma Prieta-type event but occurred on some other fault to the northeast of the San Andreas fault. Although we have performed no calculations for this eventuality, we expect that the results would be similar, especially if the 1865 earthquake occurred on one of the many reverse faults between the San Andreas and Hayward faults. Unclamping on the south end of the Hayward fault would probably once again be the best mode for triggering by static-stress changes.

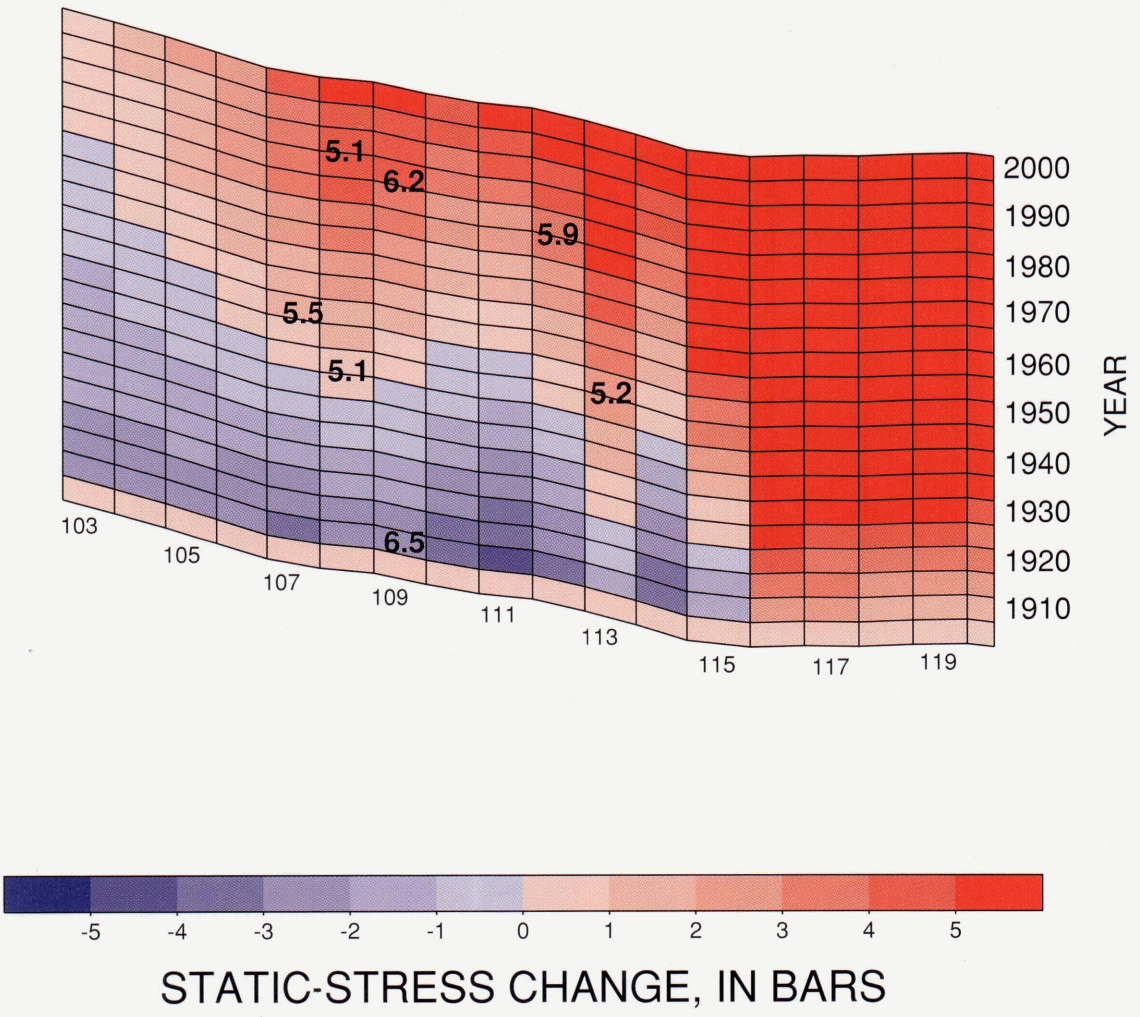

Figure 17.—Oblique view of patches on the Calaveras fault, showing changes in horizontal shear stress after 1906. Effects of individual earthquakes after 1906 are omitted; each earthquake shown (M=5.1–6.5) would cause a small local relaxation if incorporated. Stress in red area at south end of fault would be relieved to some degree by aseismic creep on central California section of the San Andreas fault, which is also omitted. Earthquake magnitudes from table 1 of Oppenheimer and others (1990), from bottom to top: M=6.5, 1911 Morgan Hill; M=5.1, 1943 Alum Rock; M=5.2, 1949 Gilroy; M=5.5, 1955 (no named location); M=5.9, 1979 Coyote Lake; M=6.2, 1984 Morgan Hill; M=5.1, 1988 Alum Rock.

THE 1836/38 PAIR

Even less is known about the locations and magnitudes of the 1836 and 1838 earthquakes (Ellsworth, 1990; Louderback, 1947; Lienkaemper and others, 1991). Most investigators suggest that the 1836 earthquake was an M=6–7 event on the northern section of the Hayward fault (for example, Lienkaemper and others, 1991). The 1838 earthquake probably was also in the range M=6–7 and ruptured at least part of the peninsular section of the San Andreas fault. The northward and southward extents of the 1838 rupture zone are quite uncertain.

The static-stress changes calculated for a hypothetical 1836-type event on the northern section of the Hayward fault are shown in figures 18 and 19. Right-lateral shear-stress increases near the north end of the San Francisco peninsula, and so nucleation might have occurred at this end, with the rupture progressing southward. The largest changes on the peninsula, however, occur in the normal component, and so unclamping might have triggered the 1838 rupture. One attractive aspect of the unclamping of normal stresses as a triggering mechanism is the built-in time delay if fluids are present. Full unclamping is attained only as the drained state is approached, a process that could take several years.

SIMULATING FAULT INTERACTIONS

Another reason for suggesting that unclamping might be more important than shear-stress changes comes from a simple interaction model based on the segmentation of bay-region faults proposed by the Working Group on California Earthquake Probabilities (1990). The model (fig. 20) consists of large dislocations representing bay-region fault segments defined by the Working Group on California Earthquake Probabilities, plus a set of dislocations at depth under these segments that are forced to slip at observed long-term slip rates. The earthquake-prone segments were given strengths commensurate with the average recurrence intervals for characteristic earthquakes on these hypothetical segments. If the model is allowed to run through thousand of years of earthquakes and only shear interactions are accounted for, then earthquakes on the San Andreas and Hayward faults tend to alternate rather than to trigger each other. The reason for this "repulsive" behavior is that if the geometry is correct, an earthquake on one of two parallel faults tends to relax the shear stress on adjacent parts of the second fault (see Rybicki and others, 1985, fig. 2), thus retarding the next earthquake on the fault—pushing it farther into the future.

Another model that includes normal-stress as well as shear-stress changes shows opposite behavior: Earthquakes on the two sides of San Francisco Bay tend to cluster in time. The reason for this clustering is that unclamping tends to advance the next earthquake, decreasing the interval between events. We note that models incorporating normal-stress changes require some assumptions about the dissipation of this component over time. Although shear stress can be set equal to zero or some appropriate lower level after an earthquake, normal stress tends to keep accumulating in the models we have used, especially at fault bends. To avoid this bind, we simply required that the normal stress on a failed segment, as well as the shear stress, be reset to zero after an earthquake. A more realistic model would account for the nonelastic deformation occurring at such fault bends.

Although these results are suggestive, the models are too simple to draw any definite conclusions. The use of long dislocations, with stress changes sampled at their centers, is also unrealistic because it can effectively insulate a model fault segment from the large stresses generated by an adjacent segment that has just slipped.

CONCLUSIONS

Static-stress changes calculated for central California faults at distances of 40 to 100 km from the Loma Prieta rupture range from less than 0.1 bar to a few bars. These stress changes are large in comparison with the stresses generated by Earth tides (typical daily variations from about 10^{-3} to 10^{-2} bar) but commensurate with annual plate-tectonic-loading rates (typically, 0.1–0.3 bar/yr for bay-region faults) and small in comparison with the average stress drops caused by M~7 earthquakes simulated in dislocation models (typically, 20–40 bars).

Calculated changes in CFF correlate with observed changes in microseismicity rates (Reasenberg and Simpson, 1992 and in press) and with measured surface creep rates (Galehouse, 1992 and in press). Low apparent coefficients of friction are favored by these correlations, suggesting that changes in normal stress are less important than

► Figure 18.—Oblique view of patches of central California faults, showing calculated static-stress changes induced by 1836 rupture of northern section of the Hayward fault (yellow patches) on other bay-region faults. Slip is 1 m on four 10-km-long by 13-km-tall patches, which approximately corresponds to an M=6.8 earthquake. Top diagram, change in horizontal shear stress, where red indicates an increase and blue a decrease in right-lateral traction; middle diagram, change in updip shear stress, where red indicates an increase and blue a decrease in west-side-up traction; bottom diagram, change in normal stress, where red indicates an increase in tension (unclamping) and blue an increase in compression (clamping).

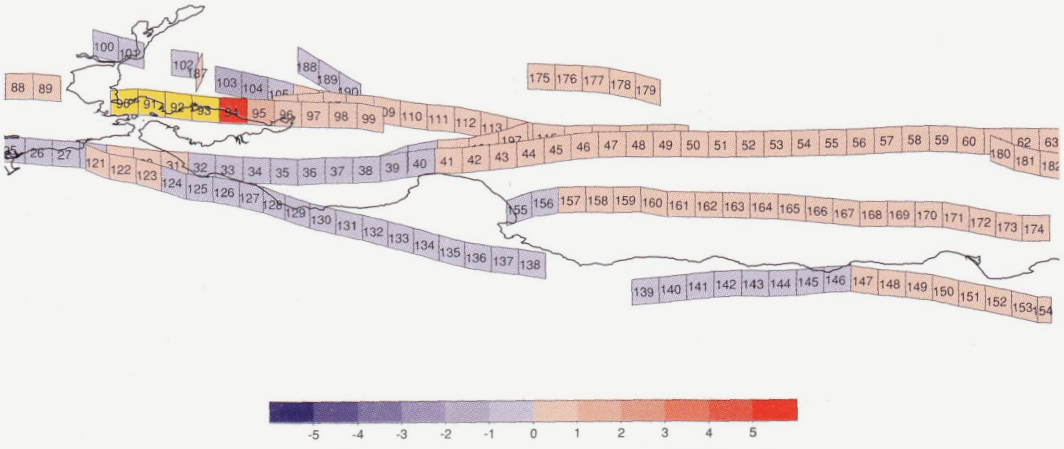

HORIZONTAL SHEAR STRESS, IN BARS - 1836

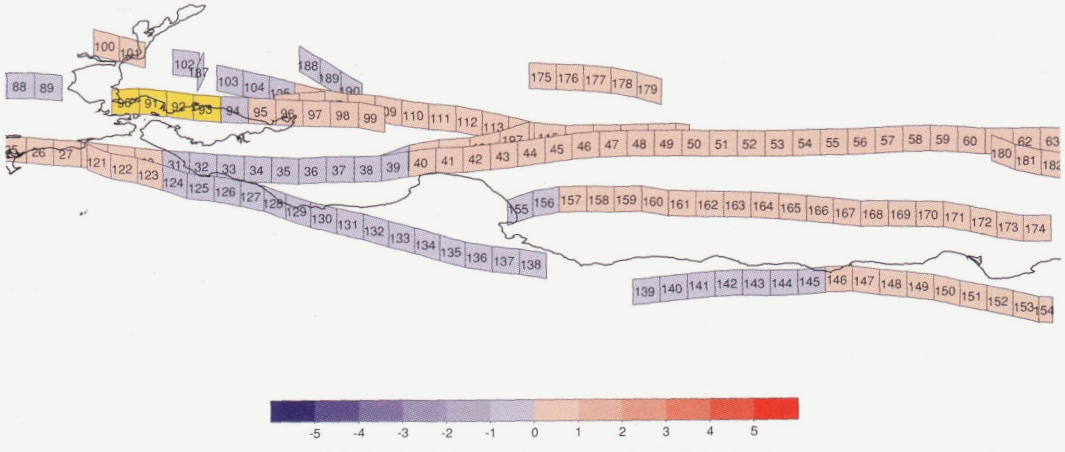

UPDIP SHEAR STRESS, IN BARS - 1836

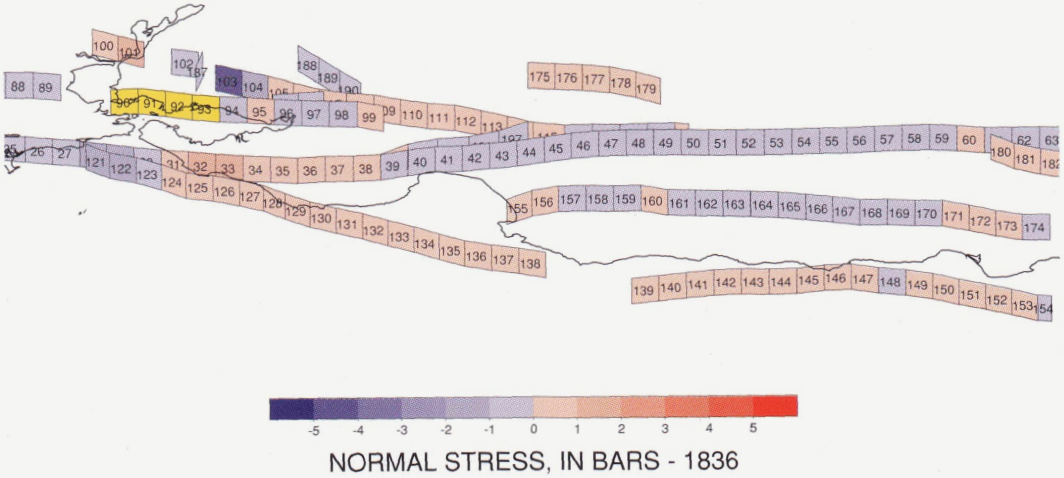

NORMAL STRESS, IN BARS - 1836

changes in shear stress for triggering microearthquakes, at least until pore fluids have had enough time to reequilibrate. The low apparent coefficients of friction could be interpreted either as low rock friction (~0.2) or as normal rock friction (~0.75) effectively decreased by pore-fluid pressure.

We have explored the effect of nonvertical dips on some bay-region faults. A range in dip, both eastward and westward, on the Hayward and Mission faults (fig. 1) had no substantial effect on the conclusions arrived at for vertical orientations. One region adjacent to the San Gregorio fault showed either a positive or negative change in CFF, depending on whether the fault was dipping or vertical. This result suggests that accurate dips on fault patches can be critical to correct CFF calculations.

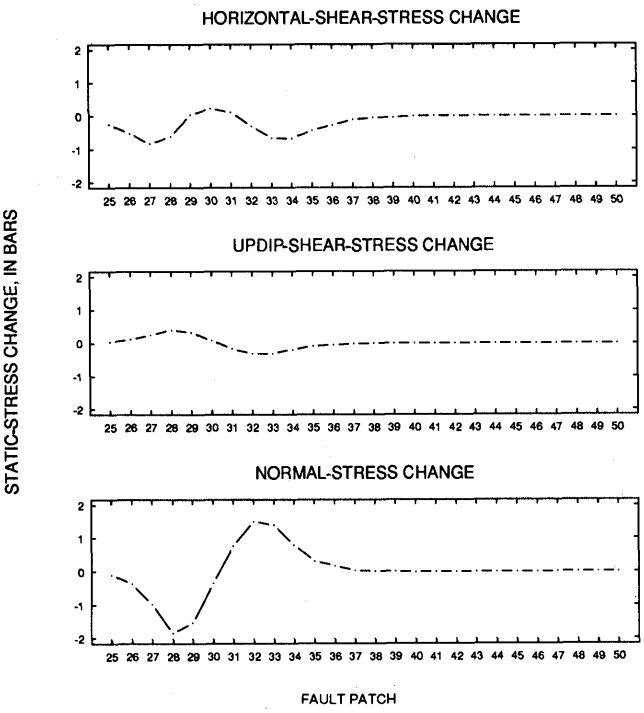

Figure 19.—Static-stress changes on the San Andreas fault corresponding to model of 1836 rupture shown in figure 18. Top plot, change in horizontal shear stress; middle plot, change in updip shear stress; bottom plot, change in normal stress.

We have qualitatively investigated the possible long-term effects of aseismic slip in response to the 1989 earthquake, first, for vertical faults at depths below the seismogenic layer and, second, on hypothetical horizontal detachment surfaces. Our models suggest that the resulting redistributions of load can alter the magnitudes of stress changes by as much as a factor of 2 in places on the bay-region faults studied but that such aseismic slip results in no important changes in the overall pattern of loading and unloading.

Using estimates of the long-term slip rate for selected faults in central California, we calculated annual plate-tectonic-loading rates by using a simple dislocation model. By comparing these calculated annual stress changes with the Loma Prieta-induced stress changes, we can estimate by how many years future earthquakes on individual fault patches may have been advanced or retarded. Fault patches that were stressed closer to failure showed advances by as much as 30 yr; various relaxed fault patches showed retardations of nearly 50 yr.

Similar calculations for the 1906 San Francisco earthquake suggest that most bay-region faults were relaxed by the static-stress changes accompanying this event. The segments of the Calaveras fault where $M>5$ earthquakes resumed in the 1940's are areas, in our models, that would recover soonest from this relaxation. Other bay-region faults may still be emerging from the 1906 relaxation shadow to the state of stress they were in just before 1906.

The close pairing in time of earthquakes in 1836/38 and 1865/68 on the San Andreas and Hayward faults raises the possibility of a major earthquake on the Hayward fault during the 1990's, although Reasenberg has demonstrated that given historical levels of seismicity, such pairings are likely to occur at random, without the aid of any physical triggering mechanism. In most of the models described

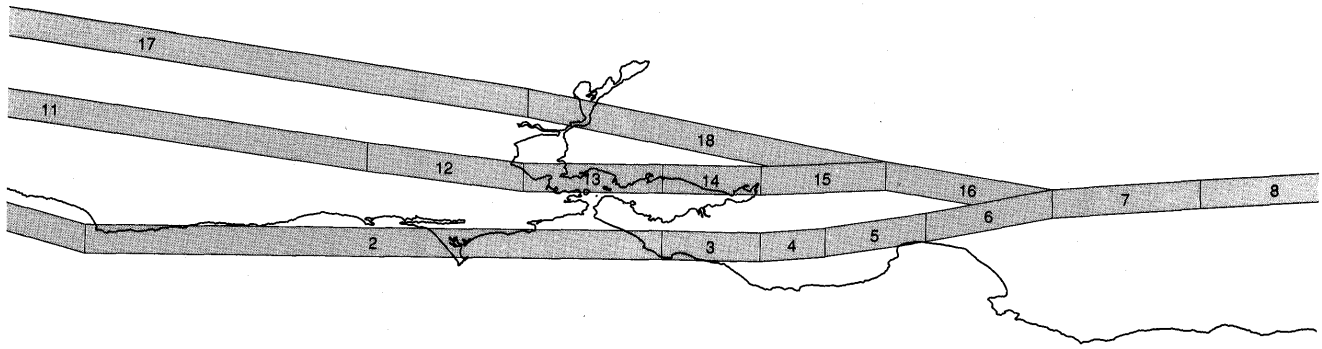

Figure 20.—Geometry for interaction model based on segmentation of bay-region faults proposed by Working Group on California Earthquake Probabilities (1990). 2, north-coastal section of the San Andreas fault; 3, peninsular section of the San Andreas fault; 4, northern Santa Cruz Mountains section of the San Andreas fault; 5, southern Santa Cruz Mountains section of the San Andreas fault; 12, Rodgers Creek fault; 13, northern section of the Hayward fault; 14, southern section of the Hayward fault.

here, the Hayward fault is relaxed by the Loma Prieta rupture, arguing against any triggering by static-stress changes, except in the high-apparent-coefficient-of-friction models for which the south end of the Hayward fault becomes unclamped, bringing it closer to failure. Although the correlations with microseismicity favor low-apparent-coefficient-of-friction models, these low apparent values could simply reflect pore-pressure effects temporarily masking a high coefficient of friction.

If pore fluids are important, then the full impact of unclamping on the south end of the Hayward fault may become apparent over time only after the pore fluids have had a chance to reequilibrate. If so, then a possible triggered event on the Hayward fault during the 1990's cannot be ruled out. Monitoring microseismicity and surface creep rates at the south end of the Hayward fault for the next few years may yield some clues as to what is happening at depth.

ACKNOWLEDGMENTS

We thank Greg Beroza, Michael Lisowski, and Grant Marshall for providing detailed information about their slip distributions before they were published, and Ruth Harris and Ross Stein for helpful reviews.

REFERENCES CITED

Allen, C.R., Wyss, Max, Brune, J.N., Grantz, Arthur, and Wallace, R.E., 1972, Displacements on the Imperial, Superstition Hills and the San Andreas faults triggered by the Borrego Mountain earthquake, *in* The Borrego Mountain earthquake of April 9, 1968: U.S. Geological Survey Professional Paper 787, p. 87–104.

Andrews, D.J., Oppenheimer, D.H., and Lienkaemper, J.J., 1993, The Mission link between the Hayward and Calaveras faults: Journal of Geophysical Research, v. 98, no. B7, p. 12083–12095.

Armbruster, J.G., and Seeber, Leonardo, 1991, A mechanically modeled seismicity precursor of the Loma Prieta, California earthquake [abs.]: Eos (American Geophysical Union Transactions), v. 72, no. 44, supp., p. 310.

Aydin, Atilla, and Page, B.M., 1984, Diverse Pliocene-Quaternary tectonics in a transform environment, San Francisco Bay region, California: Geological Society of America Bulletin, v. 95, no. 11, p. 1303–1317.

Behr, J., Bilham, Roger, Bodin, Paul, Burford, R.O., and Bürgmann, Roland, 1990, Aseismic slip on the San Andreas fault south of Loma Prieta: Geophysical Research Letters, v. 17, no. 9, p. 1445–1448.

Beroza, G.C., 1991, Near-source modeling of the Loma Prieta earthquake; evidence for heterogeneous slip and implications for earthquake hazard: Seismological Society of America Bulletin, v. 81, no. 5, p. 1603–1621.

Blanpied, M.L., Locker, D.A., and Byerlee, J.D., 1992, An earthquake mechanism based on rapid sealing of faults: Nature, v. 358, no. 6387, p. 574–576.

Brune, J.N., Henyey, T.L., and Roy, R.F., 1969, Heat flow, stress, and rate of slip along the San Andreas fault, California: Journal of Geophysical Research, v. 74, no. 15, p. 3821–3827.

Budding, K.E., Schwartz, D.P., and Oppenheimer, D.H., 1991, Slip rate, earthquake recurrence, and seismogenic potential of the Rodgers Creek fault zone, northern California; initial results: Geophysical Research Letters, v. 18, no. 3, p. 447–450.

Byerlee, J.D., 1990, Friction, overpressure and fault normal compression: Geophysical Research Letters, v. 7, no. 12, p. 2109–2112.

Chinnery, M.A., 1963, The stress changes that accompany strike-slip faulting: Seismological Society of America Bulletin, v. 53, no. 5, p. 921–932.

Clark, M.M., Harms, K.K., Lienkaemper, J.J., Harwood, D.S., Lajoie, K.R., Matti, J.C., Perkins, J.A., Rymer, M.J., Sarna-Wojcicki, A.M., Sharp, R.V., Sims, J.D., Tinsley, J.C., III, and Ziony, J.I., 1984, Preliminary slip-rate table and map of late-Quaternary faults of California: U.S. Geological Survey Open-File Report 84–106, 12 p.

Das, Shamita, and Scholz, C.H., 1981, Off-fault aftershock clusters caused by shear stress increase?: Seismological Society of America Bulletin, v. 71, no. 5, p. 1669–1675.

———1983, Why large earthquakes do not nucleate at shallow depths: Nature, v. 305, no. 5935, p. 621–623.

Eberhart-Phillips, D.M., and Stuart, W.D., 1992, Material heterogeneity simplifies the picture; Loma Prieta: Seismological Society of America Bulletin, v. 82, no. 4, p. 1964–1968.

Ellsworth, W.L., 1990, Earthquake history, 1769–1989, chap. 6 *of* Wallace, R.E., ed., The San Andreas fault system, California: U.S. Geological Survey Professional Paper 1515, p. 152–187.

Ellsworth, W.L., Lindh, A.G., Prescott, W.H., and Herd, D.G., 1981, The 1906 San Francisco earthquake and the seismic cycle, *in* Simpson, D.W., and Richards, P.G., eds., Earthquake prediction; an international review (Maurice Ewing series 4): Washington, D.C., American Geophysical Union, p. 126–140.

Erickson, Laurie, 1986, User's manual for DIS3D; a three-dimensional dislocation program with applications to faulting in the Earth: Stanford, Calif., Stanford University, M.S. thesis, 167 p.

Fuis, G.S., 1979, Displacement on the Superstition Hills fault triggered by the earthquake, *in* The Imperial Valley, California, earthquake of October 15, 1979: U.S. Geological Survey Professional Paper 1254, p. 145–154.

Galehouse, J.S., 1990, Effect of the Loma Prieta earthquake on surface slip along the Calaveras fault in the Hollister area: Geophysical Research Letters, v. 17, no. 8, p. 1219–1222.

———1992, Creep rates and creep characteristics on certain North and East Bay faults; 1979–1992; Conference on Earthquake Hazards in the Eastern San Francisco Bay Area, 2d, Hayward, Calif., Program and Abstracts, p. 24.

———in press, Effect of the earthquake on fault-creep rates in the San Francisco Bay region, California, *in* Reasenberg, P.A., ed., The Loma Prieta earthquake of October 17, 1989—postseismic effects, aftershocks, and other phenomena: U.S. Geological Survey Professional Paper 1550-D.

Griscom, Andrew, and Jachens, R.C., 1990, Crustal and lithospheric structure from gravity and magnetic studies, chap. 9 *of* Wallace, R.E., ed., The San Andreas fault system, California: U.S. Geological Survey Professional Paper 1515, p. 239–259.

Harsh, P.W., and Burford, R.O., 1982, Alinement-array measurements of fault slip in the eastern San Francisco Bay area, California, *in* Hart, E.W., Hirschfeld, S.E., and Schulz, S.S., eds., Conference on Earthquake Hazards in the Eastern San Francisco Bay Area, Hayward, Calif., 1982, Proceedings: California Division of Mines and Geology Special Publication 62, p. 251–260.

Hartzell, S.H., and Heaton, T.H., 1989, The fortnightly tide and the tidal triggering of earthquakes: Seismological Society of America Bulletin, v. 79, no. 4, p. 1282–1286.

———1990, Erratum; the fortnightly tide and the tidal triggering of earthquakes: Seismological Society of America Bulletin, v. 80, no. 2, p. 504–505.

Heaton, T.H., 1975, Tidal triggering of earthquakes: Royal Astronomical Society Geophysical Journal, v. 43, no. 2, p. 307–326.

———1982, Tidal triggering of earthquakes: Seismological Society of America Bulletin, v. 72, no. 6, p. 2181–2200.

Hudnut, K.W., Seeber, Leonardo, and Pacheco, Javier, 1989, Cross-fault triggering in the November 1987 Superstition Hills earthquake sequence, southern California: Geophysical Research Letters, v. 16, no. 2, p. 199–202.

Jachens, R.C., and Griscom, Andrew, in press, Geologic and geophysical setting of the earthquake; inferences from magnetic and gravity anomalies, *in* Wells, R.E., ed., The Loma Prieta earthquake of October 17, 1989—geologic setting and crustal structure: U.S. Geological Survey Professional Paper 1550–E.

Jachens, R.C., Griscom, Andrew, Blake, M.C., Jr., and McLaughlin, R.J., 1990, Cross-fault compression inferred from southwest dips of strike-slip faults in the south San Francisco Bay region, California [abs.]: Geological Society of America Abstracts with Programs, v. 22, no. 3, p. 31.

Jaeger, J.C., and Cook, N.G.W., 1979, Fundamentals of rock mechanics (3d ed.): London, Chapman and Hall, 593 p.

Jaumé, S.C., and Sykes, L.R., 1992, Changes in moderate seismicity in the San Francisco Bay region and stress changes due to large and great earthquakes [abs.]: Eos (American Geophysical Union Transactions), v. 73, no. 14, supp., p. 197.

Johnston, M.J.S., Linde, A.T., and Gladwin, M.T., 1990, Near-field high resolution strain measurements prior to the October 18, 1989, Loma Prieta *Ms* 7.1 earthquake: Geophysical Research Letters, v. 17, no. 10, p. 1777–1780.

Johnston, M.J.S., Linde, A.T., Gladwin, M.T., and Borcherdt, R.D., 1987, Fault failure with moderate earthquakes: Tectonophysics, v. 144, no. 1–3, p. 189–206.

Jones, D.L., Lomax, A.J.H., and McEvilly, T.V., 1991, BASIX motivation; tectonics of a transpressive plate boundary—a new paradigm for the central California Coast Ranges [abs.]: Eos (American Geophysical Union Transactions), v. 72, no. 44, supp., p. 446.

Kato, Teruyuki, Rybicki, Kacper, and Kasahara, Keichi, 1987, Mechanical interaction between neighboring active faults—and application to the Atera fault, central Japan: Tectonophysics, v. 144, no. 1–3, p. 181–188.

King, C.Y., Nason, R.D., and Burford, R.O., 1977, Coseismic steps recorded on creep meters along the San Andreas fault: Journal of Geophysical Research, v. 82, no. 11, p. 1655–1662.

Lachenbruch, A.H., and Sass, J.H., 1980, Heat flow and energetics of the San Andreas fault zone: Journal of Geophysical Research, v. 85, no. B11, p. 6185–6222.

Lachenbruch, A.H., and McGarr, A.F., 1990, Stress and heat flow, chap. 10 *of* Wallace, R.E., ed., The San Andreas fault system, California: U.S. Geological Survey Professional Paper 1515, p. 261–277.

Li, V.C., Seale, S.H., and Cao, Tianqing, 1987, Postseismic stress and pore pressure readjustment and aftershock distributions: Tectonophysics, v. 144, no. 1–3, p. 37–54.

Lienkaemper, J.J., Borchardt, Glenn, and Lisowski, Michael, 1991, Historic creep rate and potential for seismic slip along the Hayward fault, California: Journal of Geophysical Research, v. 96, no. B11, p. 18261–18283.

Linker, M.F., and Rice, J.R., 1991, The effective viscosity of the San Andreas fault beneath the seismogenic zone; constraints from the response to the 1989 Loma Prieta earthquake [abs.]: Eos (American Geophysical Union Transactions), v. 72, no. 44, supp., p. 310.

———in press, Models of postseismic stress transfer and postearthquake deformation in northern California, *in* Reasenberg, P.A., ed., The Loma Prieta, California, earthquake of October 17, 1989—postseismic effects, aftershocks, and other phenomena: U.S. Geological Survey Professional Paper 1550–D.

Lisowski, Michael, Prescott, W.H., Savage, J.C., and Johnston, M.J., 1990, Geodetic estimate of coseismic slip during the 1989 Loma Prieta, California, earthquake: Geophysical Research Letters, v. 17, no. 9, p. 1437–1440.

Louderback, G.D., 1947, Central California earthquakes of the 1830's: Seismological Society of America Bulletin, v. 37, no. 1, p. 33–74.

Marshall, G.A., Stein, R.S., and Thatcher, Wayne, 1991, Faulting geometry and slip from co-seismic elevation changes; the 18 October 1989, Loma Prieta, California, earthquake: Seismological Society of America Bulletin, v. 81, no. 5, p. 1660–1693.

Mavko, G.M., Schulz, S.S., and Brown, B.D., 1985, Effects of the 1983 Coalinga, California, earthquake on creep along the San Andreas fault: Seismological Society of America Bulletin, v. 75, no. 2, p. 475–489.

McClellan, P.H., and Hay, E.A., 1990, Triggered slip on the Calaveras fault during the magnitude 7.1 Loma Prieta, California earthquake: Geophysical Research Letters, v. 17, no. 8, p. 1227–1230.

McNutt, Marcia, and Heaton, T.H., 1981, An evaluation of the seismic-window theory for earthquake prediction: California Geology, v. 34, no. 1, p. 12–16.

Mount, V.S., and Suppe, John, 1987, State of stress near the San Andreas fault; implications for wrench tectonics: Geology, v. 15, no. 12, p. 1143–1146.

Niemi, T.M., and Hall, N.T., 1992, Late Holocene slip rate and recurrence of great earthquakes on the San Andreas fault in northern California: Geology, v. 20, no. 3, p. 195–198.

Nur, Amos, and Booker, J.R., 1972, Aftershocks caused by pore fluid flow?: Science, v. 175, no. 4024, p. 885–887.

Okada, Yoshimitsu, 1992, Internal deformation due to shear and tensile faults in a half-space: Seismological Society of America Bulletin, v. 82, no. 2, p. 1018–1040.

Olson, J.A., 1986, Seismicity of the San Andreas fault zone in the San Francisco peninsula area, California, *in* Reilly, W.I., and Hartford, B.E., eds., International Symposium on Recent Crustal Movements in the Pacific Region, Wellington, New Zealand, 1984, Proceedings: Royal Society of New Zealand Bulletin 24, p. 87–97.

Olson, J.A., and Lindh, A.G., 1985, Seismicity of the San Andreas fault from Cienega Winery to the Golden Gate, *in* Shearer, C.F., ed., Minutes of the National Earthquake Prediction Evaluation Council, July 26–27, 1985, Menlo Park, California: U.S. Geological Survey Open-File Report 85–754, p. 316–324.

Oppenheimer, D.H., Reasenberg, P.A., and Simpson, R.W., 1988, Fault-plain solutions for the 1984 Morgan Hill, California, earthquake sequence; evidence for the state of stress on the Calaveras fault: Journal of Geophysical Research, v. 93, no. B8, p. 9007–9026.

Oppenheimer, D.H., Bakun, W.H., and Lindh, A.G., 1990, Slip partitioning of the Calaveras fault, California, and prospects for future earthquakes: Journal of Geophysical Research, v. 95, no. B6, p. 8483–8498.

Prentice, C.S., 1989, Earthquake geology of the northern San Andreas fault near point Arena, California: Pasadena, California Institute of Technology, Ph.D. thesis, 252 p.

Press, Frank, 1965, Displacements, strains, and tilts at teleseismic distances: Journal of Geophysical Research, v. 70, no. 10, p. 2395–2412.

Raleigh, C.B., Healy, J.H., and Bredehoeft, J.D., 1976, An experiment in earthquake control at Rangely, Colorado: Science, v. 191, no. 4233, p. 1230–1237.

Reasenberg, P.A., and Simpson, R.W., 1992, Response of regional seismicity to the static stress change produced by the Loma Prieta earthquake: Science, v. 255, no. 5052, p. 1687–1690.

———in press, Response of regional seismicity to earthquake-induced static-stress changes, *in* Reasenberg, P.A., ed., The Loma Prieta earthquake of October 17, 1989—postseismic effects, aftershocks, and other phenomena: U.S. Geological Survey Professional Paper 1550–D.

Rice, J.R., 1992, Fault stress states, pore pressure distributions, and the weakness of the San Andreas fault, *in* Evans, Brian, and Wong, T.-F., eds., Fault mechanics and transport properties of rock; a festschrift in honor of W.F. Brace: London, Academic Press, p. 475–503.

Rice, J.R., and Cleary, M.P., 1976, Some basic stress diffusion solutions for fluid-saturated elastic porous media with compressible constituents: Reviews of Geophysics and Space Physics, v. 14, no. 2, p. 227–241.

Roeloffs, E.A., 1988, Fault stability changes induced beneath a reservoir with cyclic variations in water level: Journal of Geophysical Research, v. 93, no. B3, p. 2107–2124.

Rybicki, Kacper, Kato, Teruyuki, and Kasahara, Keichi, 1985, Mechanical interaction between neighboring active faults—static and dynamic stress field induced by faulting: University of Tokyo, Earthquake Research Institute Bulletin, v. 60, pt. 1, p. 1–21.

Rydelek, P.A., Sacks, I.S., and Scarpa, Roberto, 1992, On tidal triggering of earthquakes at Campi Flegrei, Italy: Geophysical Journal International, v. 109, no. 1, p. 125–137.

Segall, Paul, 1989, Earthquakes triggered by fluid extraction: Geology, v. 17, no. 10, p. 942–946.

Scholz, C.H., 1990, The mechanics of earthquakes and faulting: Cambridge, U.K., Cambridge University Press, 439 p.

Sharp, R.V., 1989, Pre-earthquake displacement and triggered displacement on the Imperial fault associated with the Superstition Hills earthquake of 24 November 1987: Seismological Society of America Bulletin, v. 79, no. 2, p. 466–479.

Shimada, Seiichi, Sakata, Shoji, and Noguchi, Shin'ichi, 1987, Coseismic strain steps observed by three-component borehole strainmeters: Tectonophysics, v. 144, no. 1–3, p. 207–214.

Sieh, K.E., 1982, Slip along the San Andreas fault associated with the earthquake, *in* The Imperial Valley, California, earthquake of October 15, 1979: U.S. Geological Survey Professional Paper 1254, p. 155–159.

Simpson, R.W., Schulz, S.S., Dietz, L.D., and Burford, R.O., 1988, The response of creeping parts of the San Andreas fault to earthquakes on nearby faults; two examples: Pure and Applied Geophysics, v. 126, no. 2–4, p. 665–685.

Sleep, N.H., and Blanpied, M.L., 1992, Creep, compaction and the weak rheology of major faults: Nature, v. 359, no. 6397, p. 687–692.

Smith, S.W., and Wyss, Max, 1968, Displacement on the San Andreas fault subsequent to the 1966 Parkfield earthquake: Seismological Society of America Bulletin, v. 58, no. 6, p. 1955–1973.

Stein, R.S., and Lisowski, Michael, 1983, The 1979 Homestead Valley earthquake sequence, California; control of aftershocks and postseismic deformation: Journal of Geophysical Research, v. 88, no. B8, p. 6477–6490.

Steketee, J.A., 1958, Some geophysical applications of the elasticity theory of dislocations: Canadian Journal of Physics, v. 36, no. 9, p. 1168–1198.

Sykes, L.R., and Jaumé, S.C., 1990, Seismic activity on neighboring faults as a long-term precursor to large earthquakes in the San Francisco Bay area: Nature, v. 348, no. 6302, p. 595–599.

Thatcher, Wayne, 1975, Strain accumulation and release mechanism of the 1906 San Francisco earthquake: Journal of Geophysical Research, v. 80, no. 35, p. 4862–4872.

Thatcher, Wayne, and Lisowski, Michael, 1987, Long-term seismic potential of the San Andreas fault southeast of San Francisco, California: Journal of Geophysical Research, v. 92, no. B6, p. 4771–4784.

Tuttle, M.L., and Sykes, L.R., 1992, Re-evaluation of the 1838, 1865, and 1868 earthquakes in the San Francisco Bay area [abs.]: Conference on Earthquake Hazards in the Eastern San Francisco Bay Area, 2d, Hayward, Calif., 1992, Program and Abstracts, p. 77.

Wentworth, C.M., and Zoback, M.D., 1989, The style of late Cenozoic deformation at the eastern front of the California Coastal Ranges: Tectonics, v. 8, no. 2, p. 237–246.

Williams, P.L., McGill, S.F., Sieh, K.E., Allen, C.R., and Louie, J.N., 1988, Triggered slip along the San Andreas fault after the 8 July 1986 North Palm Springs earthquake: Seismological Society of America Bulletin, v. 78, no. 3, p. 1112–1122.

Working Group on California Earthquake Probabilities, 1990, Probabilities of large earthquakes in the San Francisco Bay region, California: U.S. Geological Survey Circular 1053, 51 p.

Zoback, M.D., and Healy, J.H., 1984, Friction, faulting, and "in situ" stress: Annales Geophysicae, v. 2, no. 6, p. 689–698.

Zoback, M.D., Zoback, M.L., Mount, V.S., Suppe, John, Eaton, J.P., Healy, J.H., Oppenheimer, D.H., Reasenberg, P.A., Jones, L.M., Raleigh, C.B., Wong, I.G., Scotti, Oona, and Wentworth, C.M., 1987, New evidence on the state of stress of the San Andreas fault system: Science, v. 238, no. 4830, p. 1105–1111.

This page intentionally left blank

TECTONIC PROCESSES AND MODELS

CUMULATIVE SLIP ALONG THE PENINSULAR SECTION OF THE SAN ANDREAS FAULT, CALIFORNIA, ESTIMATED FROM TWO-DIMENSIONAL BOUNDARY-ELEMENT MODELS OF HISTORICAL RUPTURE

By Paul Bodin and Roger Bilham,
University of Colorado, Boulder

CONTENTS

ABSTRACT

We use two-dimensional boundary-element methods to investigate the variation of slip along the San Andreas fault on the San Francisco peninsula during the period 1800–1990. Faults are modeled in an elastic plate as frictionless, contiguous vertical cuts with the geometry of the mapped San Andreas system. Antisymmetric displacements are applied to edges of the elastic plate at azimuths corresponding to the relative plate motion between the North American and Pacific plates. Segments of faults corresponding to the locations of historical earthquakes since 1800 are released sequentially to estimate the cumulative distribution of slip resulting from these earthquakes. Although the model slip distribution in the 1906 San Francisco earthquake agrees with the distribution inferred from geodetic data, slip and fault-normal convergence in the 1989 Loma Prieta earthquake are underestimated by approximately 30 percent, suggesting that the failure strain may have been higher for this event. Another explanation for the underestimates may be that two-dimensional models do not adequately incorporate important three-dimensional boundary conditions, such as aseismic slip under the seismogenic layer. Our models suggest that the difference between the cumulative slip attributable to historical ruptures and the slip estimated from plate-tectonic motion in the San Francisco Bay region exceeds 1 m and in some places is as high as 3.5 m. Regions to the northwest and southeast of the Loma Prieta rupture zone currently exhibit the largest slip deficit, which may be sufficient to drive future M~6.5 earthquakes. Boundary-element models indicate that fault-normal convergence throughout the Santa Cruz Mountains reaches a maximum near the Loma Prieta rupture zone, where the amplitude of convergence may reach a third of the amplitude of dextral slip. This convergence is estimated to result in thickening of the crust at a rate of ~2 mm/yr as material is advected through the bend in the San Andreas fault where it traverses the Santa Cruz Mountains.

INTRODUCTION

Relative plate motion at the latitude of the San Francisco peninsula is partitioned among a system of faults consisting of the single continuous San Andreas fault and apparently discontinuous fault strands represented by the Hayward, Calaveras, Rodgers Creek, and other faults. Geodetic and geologic data suggest that at this latitude, approximately 50 percent of the total plate-boundary displacement is manifest on the principal trace of the San Andreas fault (Working Group on California Earthquake Probabilities, 1990). In this paper, we examine the spatial and temporal distribution of slip along the principal trace of the San Andreas fault between San Francisco and San Juan Bautista, Calif. (fig. 1). We assume a mean slip rate of 24 mm/yr on the fault north of San Francisco (Niemi and Hall, 1992) and examine the effect of the geometry of the San Andreas fault on the distribution of slip along strike to the southeast during an interval of approximately 200 yr. This interval, which represents the time period for which data on historical seismicity are available,

is equivalent in duration to the renewal time to generate 1906-size earthquakes from observed plate-boundary displacements. We assume that the strain field prevailing in 1800 was uniform, although a complex strain field probably existed, generated by unknown prehistoric earthquakes and plate motions. As time progresses, the "memory" of this initial 1800 strain field decreases in importance. Because plate-boundary slip is distributed among several fault zones in the San Francisco Bay region, mutual interactions between fault segments affect the resulting slip rates on each segment. To estimate slip, we use boundary-element methods, which account explicitly for segment interactions that depend on the geometry of the fault system (Bilham and Bodin, 1992). Therefore, to estimate slip along the San Andreas fault, our models make use of information from other faults in the region, as well as from the San Andreas fault.

Our goal in this paper is to estimate dextral-slip distributions for historical ruptures and for aseismic fault creep and to sum them to obtain the cumulative distribution of historical dextral slip along the San Andreas fault. Rupture data for earthquakes during the period 1800–1900 are not well established, and so our summations of cumulative slip and resulting slip deficits are somewhat speculative. Moreover, it is unclear whether the same failure conditions are applicable for all earthquakes on the San Francisco peninsula. We obtain some insight into this problem by constructing models that simulate the geodetically estimated slip distribution in the 1906 and 1989 earthquakes.

To account for the influence of fault geometry and fault segmentation on slip in the Santa Cruz Mountains, we use the mapped fault trace as input in our elastic models. We digitized the mapped trace of the San Andreas fault from fault-strip maps (Sarna-Wojcicki and others, 1975) and simplified the mapped trace from the Golden Gate to San Juan Bautista as a set of 17 contiguous fault segments from 3.6 to 16.2 km long (Nishenko and Williams, 1985), with an average length of about 9.5 km (fig. 1; table 1). Where the surface breadth of the fault zone is greater than 1 km, we determined a mean fault strike for all mapped strands of the fault. In subsequent analyses, we assume that historical earthquakes ruptured single segments or contiguous combinations of segments and that these ruptures terminated at bends between segments (King and Nábělek, 1985).

In the boundary-element models that follow, each fault segment is represented by a dislocation surface in a uniform elastic medium. The medium is assumed to be in a state of plane strain within which the vertical-strain components vanish. The model results simulate the response of frictionless vertical cuts in an elastic plate of uniform thickness (Bilham and King, 1989b). Seismicity suggests that the applicable elastic-plate thickness in the study area is approximately 10 km. Model results for isolated fault segments shorter than this assumed thickness would be invalid, and so the smallest isolated fault segment we used was approximately 12 km long (segment 16, fig. 1; table 1). Rupture lengths used correspond to earthquakes of M≥6. The region is subjected to an antisymmetric dextral-shear displacement at a mean azimuth appropriate to the Nuvel 1 pole of rotation for the North American and Pacific plates (N. 36° W.; DeMets and others, 1990). The effect of the change in azimuth along strike of the plate boundary due to the finite radius of the small-circle slip-vector path is negligible.

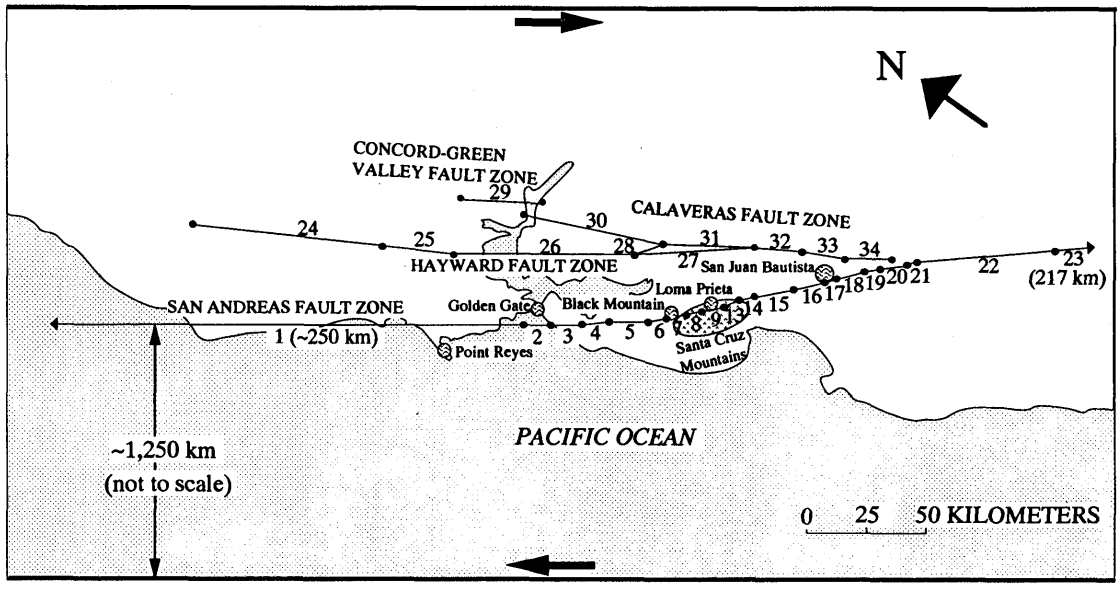

Figure 1.—San Francisco Bay region, Calif., showing locations of fault segments used in models. Segment numbers correspond to those listed in table 1. Segments 17 through 22 represent creeping section of the San Andreas fault south of San Juan Bautista. Arrows indicate direction of plate motion.

Table 1.—*Model fault segments*

[See figure 1 for locations of segments. Origin of the coordinate system is lat 36.84° N., 121.54° W.; azimuth of the negative *x*-axis is N. 36° W. All coordinates in kilometers; angle of fault segment to plate vector in degrees anticlockwise from mean slip vector]

Segment	Name	starting x-coordinate	starting y-coordinate	ending x-coordinate	ending y-coordinate	x-center	y-center	Length	Angle to plate vector
1	North Coast----------	-373.25	-9.25	-123.25	-7.75	-248.25	8.50	250.00	0.30
2	Mussel Rock----------	-123.25	-7.75	-112.00	-8.25	-117.63	8.00	11.25	-2.50
3	do----------	-112.00	-8.25	-100.25	-8.00	-106.13	8.13	11.75	1.20
4	do----------	-100.25	-8.00	-88.50	-8.50	-94.38	8.25	11.75	-2.40
5	do----------	-88.50	-8.50	-74.25	-9.25	-81.38	8.88	14.28	-3.00
6	Black Mountain----------	-74.25	-9.25	-66.25	-11.00	-70.25	10.13	8.20	-12.30
7	do----------	-66.25	-11.00	-57.25	-12.00	-61.75	11.50	9.05	-6.30
8	do----------	-57.25	-12.00	-51.50	-13.50	-54.38	12.75	5.95	-14.60
9	Loma Prieta 1----------	-51.50	-13.50	-42.50	-15.00	-47.00	14.25	9.13	-9.50
13	Loma Prieta 2----------	-42.50	-15.00	-35.50	-18.00	-39.00	16.50	7.63	-23.20
14	Loma Prieta 3----------	-35.50	-18.00	-29.75	-19.75	-32.63	18.88	6.00	-16.90
15	Loma Prieta 4----------	-29.75	-19.75	-13.75	-22.25	-21.75	21.00	16.20	-8.90
16	Pajaro----------	-13.75	-22.25	-2.00	-26.00	-7.88	24.13	12.33	-17.70
17	San Juan Bautista----------	-2.00	-26.00	3.75	-27.00	.88	26.50	5.83	-9.90
18	Creeping 1----------	3.75	-27.00	13.75	-30.50	8.75	28.75	10.60	-19.30
19	Creeping 2----------	13.75	-30.50	20.75	-32.50	17.25	31.50	7.28	-15.90
20	Creeping 3----------	20.75	-32.50	30.50	-34.25	25.63	33.38	9.90	-10.20
21	Creeping 4----------	30.50	-34.25	34.00	-35.25	32.25	34.75	3.65	-15.90
22	Creeping 5----------	34.00	-35.25	158.00	-48.75	96.00	42.00	124.73	-6.20
23	1857 rupture----------	158.00	-48.75	375.00	-62.50	266.50	55.63	217.43	-3.60
24	Maacama----------	-277.25	-53.25	-214.75	-45.75	-246.00	49.50	62.95	6.80
25	Rodgers Creek----------	-214.75	-45.75	-152.25	-38.25	-183.50	42.00	62.95	6.80
26	Hayward----------	-152.25	-38.25	-78.50	-38.50	-115.38	38.38	73.75	-.20
27	Southeastern Hayward ----------	-78.50	-38.50	-29.00	-41.50	-53.75	40.00	49.60	-3.50
28	Mission----------	-85.50	-40.25	-76.25	-42.50	-80.88	41.38	9.53	-13.70
29	Concord----------	-148.00	-61.00	-115.50	-59.50	-131.75	60.25	32.53	2.60
30	Northern Calaveras----------	-124.00	-55.00	-67.00	-43.75	-95.50	49.38	58.10	11.20
31	North Central Calaveras----------	-67.00	-43.75	-29.00	-41.50	-48.00	42.63	38.08	3.40
32	South Central Calaveras----------	-29.00	-41.50	-10.75	-40.00	-19.88	40.75	18.30	4.70
33	Southern Calaveras----------	-10.75	-40.00	6.25	-36.75	-2.25	38.38	17.30	10.80
34	Southeast Calaveras extension--	6.25	-36.75	25.50	-37.25	15.88	37.00	19.25	-1.50

Combinations of fault segments that correspond to historical earthquake ruptures or creeping segments are permitted to slip freely (without friction) in response to imposed plate-boundary displacements. The model yields the distribution of slip among those fault segments allowed to slip that minimizes the overall stress within the elastic plate. The resulting displacements, stresses, and strains within the region, including the strike-slip and fault-normal displacements along faults, are computed by using a two-dimensional boundary-element method (Crouch and Starfield, 1983; Bilham and King, 1989b). Freely slipping faults are simulated by displacement discontinuities with a zero tangential-shear-stress constraint and a zero relative-normal-slip constraint. When a fault segment with fixed slip is used as a boundary condition, it is included as a single element with a specified relative displacement. Our models are thus free of the potential numerical artifacts in the boundary-element method described by Zeller and Pollard (1992). The slip distribution that results from subjecting a single uniform-stress-drop crack to antisymmetric shear is elliptical in form (for example, Crouch and Starfield, 1983). Therefore, slip is a maximum and varies smoothly and slowly at the center of the crack but decays rapidly to zero at each end (fig. 2). In our models for ruptures of historical earthquakes, we divide each dislocation segment into three to seven subelements, each with uniform slip, so that the computed slip distributions approximate this elliptical distribution of slip.

STRAIN AT FAILURE

Three parameters are important in determining the amount of displacement that occurs during the rupture of a vertical dislocation embedded within a uniform elastic plate subjected to applied shear strain: the length of the rupture, the azimuth of the rupture relative to the shear-strain field, and the magnitude of the strain at failure. If shear strain within the medium before the rupture is nonuniform, its spatial distribution influences the resulting slip. In our models, the mean slip on a rupture of length L subjected to uniform shear strain ε is approximately εL. Observed earthquake offsets, however, reveal almost a tenfold variation

in coseismic slip versus fault length (Slemmons, 1977; Bonilla and others, 1984); and the strain at failure, fault geometry, and frictional and dynamic effects clearly vary significantly among earthquakes. In the models that follow, we assume that the strain field which drives seismic rupture and creep is generated by relative plate motion and approximates simple shear at the azimuth of the plate slip vector (Lisowski and others, 1991). If friction and dynamic effects are ignored, numerical models of a dislocation of known length and orientation within the simple-shear plate boundary permit the magnitude of the applied strain field to be estimated from the magnitude of slip accompanying a rupture. Ruptures, however, take place on fault segments that interact with other previous ruptures and creeping fault segments, both of which alter the strain field. Our boundary-element models account for those interactions and allow us to explore hypotheses about the strain field from the distribution of slip among the ruptures in the plate boundary. Alternatively, if the strength and orientation of the applied strain field are known and the seismic history constrains estimates of the location of historical rupture and creep, we can account for the interactional effects among the faults and compute the distribution of slip on any given fault segment after a rupture.

We apply this approach to the Santa Cruz mountains section of the San Andreas fault. The rupture lengths of earthquakes that are believed to have occurred in this region during the past 200 yr are plotted in figure 3. The locations and lengths of ruptures for pre-1906 events are speculative, and some may not even be on the San Andreas fault (for example, Tuttle and Sykes, 1992), but if we assume that the strain at failure is similar for all earthquakes in this region, we can estimate approximate slip distributions for these events. From these slip distributions, the cumulative slip along the fault may be summed to identify segments of the fault where slip may be overdue.

The simplest assumption that can be made about failure is that all ruptures fail at approximately the same strain level. This assumption is motivated by the observation that scatter in the relation between slip and fault length for real earthquakes is commonly reduced by restricting the events included to those from a particular tectonic or geographic region (Slemmons, 1977; Bonilla and others, 1984). To test whether a single strain value at failure prevails in the Santa Cruz Mountains, we examine the distribution of slip during the 1906 and 1989 earthquakes. In our simple plate model, antisymmetric displacements (of $\pm d$ m) are applied remotely from the fault. A shear-strain field of a given magnitude may be generated either by a large boundary displacement applied at a large distance or by a small displacement applied closer in. Displacements applied at ±1,250 km were found to generate the slip distributions for both the 1906 rupture and the creeping section of the San Andreas fault and to be consistent with known plate velocities. The magnitude of the shear-strain field ($2d$/2,500 microstrain) that best fits the observations is an estimate of the failure strain in each event.

The 1906 and 1989 ruptures differ substantially in mechanism and may have occurred partly or completely on different faults. The most important geometric difference, apart from the length of the two ruptures, is the significant component of dip-slip motion during the 1989 earthquake (Segall and Lisowski, 1990). We simulate the dip-slip component of the 1989 earthquake in our two-dimensional models by permitting simultaneous convergence and dextral slip in the boundary-element specifications for these segments of the fault. We initially assume for simplicity that the 1906 and 1989 earthquakes occurred on the same fault but that convergence did not occur in the 1906 earth-

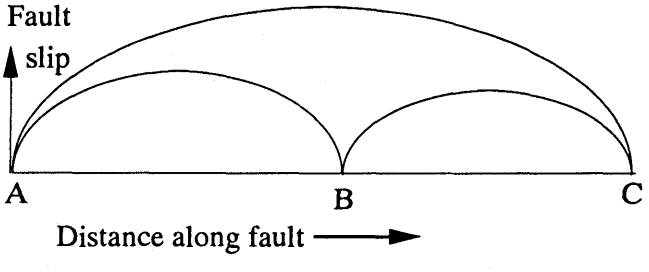

Figure 2.—Coseismic displacements along a frictionless dislocation surface vary smoothly and slowly near its center and abruptly near its ends in an elliptical slip distribution. If rupture occurs in two separate events (lines AB, BC) instead of a single event (line AC), a slip deficit occurs, especially near intersection of the two fault segments.

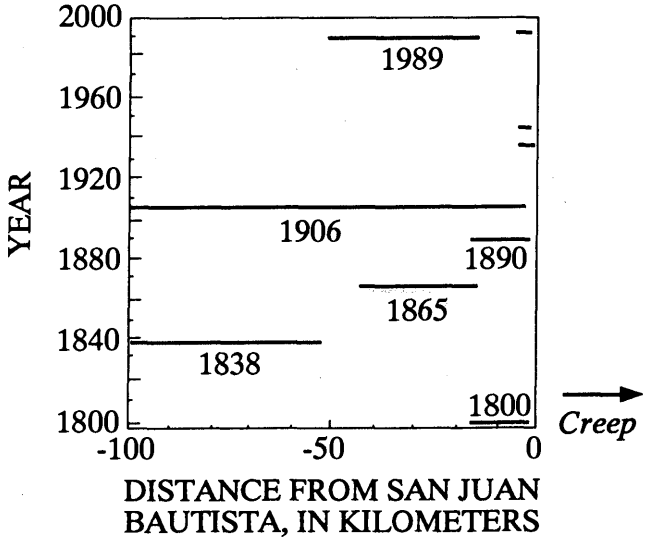

Figure 3.—Space-time plot of moderate and large earthquakes on the San Francisco peninsula; horizontal lines indicate length of rupture. Locations of these events are poorly known and some may not have been on the San Andreas fault (Lindh and others, 1982; Working Group on California Earthquake Probabilities, 1990; L.R. Sykes, oral commun., 1992). Rupture lengths are adjusted to coincide with segment boundaries shown in figure 1 and listed in table 1.

quake. The two ruptures are thus treated as isolated dislocations in an elastic plate and are both subjected to uniform shear-strain fields. In these tests, changes in the strain field caused by the earlier event are not applied to the later event. We find that to match geodetically observed displacements, the magnitude of applied strain for the 1989 earthquake must be increased by a factor of 4 relative to the strain needed to model the 1906 earthquake. In figure 4 and table 2 (case 1), we show strike-slip and fault-normal displacements on a model Loma Prieta rupture, assuming failure conditions similar to those of the 1906 rupture. Note that under these conditions, the synthetic 1989 displacements are smaller by a factor of 4 than estimates inferred from geodetic observations (case 9, table 2).

This model, however, ignores several important changes in strain that occurred on the San Andreas fault system during the 1906 earthquake and in the following 83 years. There has been some debate concerning the existence of a significant slip deficit south of Black Mountain during the 1906 earthquake (Scholz, 1985; Thatcher and Lisowski, 1987). Our models agree well with geodetic estimates of slip in 1906 in this area (Bilham and King, 1989a; Segall and Lisowski, 1990). An elliptical decay of slip toward the south end of the 1906 rupture zone results in a reduction of slip on the fault relative to areas to the north. This slip deficit influences the local strain field before the 1989 earthquake. In the 83 years between the 1906 and the 1989 ruptures, however, continued plate motion introduced additional strain. Strain was further concentrated in the Santa Cruz region because it is near the northwestward termination of steady-state creep on the San Andreas fault in central California. Moreover, strain on the San Francisco peninsula is presumably moderated by creep and seismic slip on the Calaveras and Hayward fault systems (fig. 1). We have included these effects on the strain field responsible for the modeled slip on the 1989 rupture in a succession of models (cases 2–6, table 2), which we discuss below.

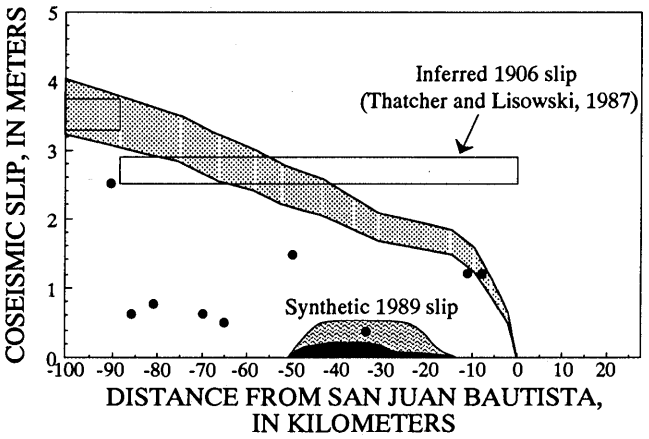

Figure 4.—Synthetic and observed slip in 1906 San Francisco earthquake and synthetic slip in 1989 Loma Prieta earthquake versus distance from San Juan Bautista, Calif. (see fig. 1), using similar plate-boundary geometry but with applied displacement increased by 83 years at a rate of 38 mm/yr inferred from geodetic data (Lisowski and others, 1991). Shaded area of curve shows range of slip predicted by 1906 models normalized to maximum slips of 4 and 5 m, respectively, on the San Andreas fault near Point Reyes (see fig. 1), about 180 km northwest of San Juan Bautista; vertical white lines are segment boundaries (bends in fault). Boxes, estimates for fault slip from geodetic observations (Thatcher and Lisowski, 1987); dots, surface observations of 1906 fault slip (Lawson, 1910). Synthetic dextral slip (patterned area) and fault-normal slip (black area) calculated for 1989 earthquake are evidently too small, suggesting that boundary conditions for 1906 and 1989 earthquakes differed, although limitations of two-dimensional modeling may also be responsible for some of the deficit.

DEVELOPMENT OF THE STRAIN FIELD, 1906–89

We first examine the development of strain during the period 1906–89. The full plate-displacement rate estimated from plate motions over the past several million years is 48 mm/yr (DeMets and others, 1990), which corresponds to plate-boundary displacements of 3.9 m during the 83 yr period since 1906. We believe, however, that more relevant estimates of the appropriate boundary displacements are provided by geodetic data obtained during the past two decades from a 100-km-wide network on the San Francisco peninsula (Lisowski and others, 1991). These observations indicate that a displacement rate of 38 mm/yr is partitioned among faults in the San Francisco Bay region. The geodetic estimates correspond to 3.2 m of plate slip in 83 yr. In the following analysis, we use a strain increment of 32 microstrain (tensor shear) in 83 yr, derived from distributing the 3.2 m of relative plate slip over the 100-km-wide zone of plate-boundary deformation observed by Lisowski and others (1991). Strain is increased in the Santa Cruz Mountains as a result of creep on the central California section of the San Andreas fault, which has its north end close to San Juan Bautista, and is influenced by creep and seismicity on the Hayward and Calaveras faults (fig. 1). To estimate the strain changes in the Santa Cruz Mountains, we assign appropriate offsets to these other faults, assuming that current creep rates have been constant for the past 83 yr.

It is less obvious how to apply the strain field generated by the southward reduction of slip in the 1906 earthquake to models of subsequent ruptures in the Santa Cruz Mountains. We adopt the following strategy: We use the 1906 slip distribution in figure 4 for each segment of the San Andreas fault, except for those near Loma Prieta, as input to an elastic model in which we include the distribution of slip in the creep process south of San Juan Bautista (fig. 1). We then apply an antisymmetric shear strain similar to that used to best model the 1906 rupture (fig. 4) but increased by 32 microstrain (tensor shear), corresponding to 83 years of plate motion. In this model, slip is fixed on all segments of the fault except the Loma Prieta segments, which are

Table 2.—*Estimated slip from the 1989 Loma Prieta earthquake driven by different boundary conditions*

[Loma Prieta fault segments are listed as segments 9 and 13 through 15 (fig. 1; table 1)]

Case	Applied boundary conditions	Dextral shear (cm)	Fault-normal convergence (cm)	Reverse slip on 60° dipping fault	Reverse slip on 70° dipping fault
1	Remote, suitable to reproduce slip of 1906 earthquake	35	19	38	55
2	Remote, suitable for 1906 earthquake plus 83 yr of plate motion	49	26	52	77
3	Remote, plus 1906 earthquake and creep on the San Andreas fault.	69	40	80	116
4	Remote, plus 1906 earthquake and creep on the San Andreas and east-bay faults	64	36	72	105
5	Remote, plus modeled slip for 1800, 1838, 1857, 1860 1890, and 1906 earthquakes, and creep on the San Andreas fault. No east-bay faults	106	42	84	123
6	Remote, plus modeled slip for 1800, 1838, 1857, 1860 1890, and 1906 earthquakes, and creep on the San Andreas fault, and east-bay faults	101	38	76	111
7	1989 on separate fault. Remote, plus modeled slip for 1800, 1838, 1857, 1860 1890, and 1906 earthquakes, and creep on the San Andreas fault. No east-bay faults	77	41	82	120
8	1989 on separate fault. Remote, plus modeled slip for 1800, 1838, 1857, 1860 1890, and 1906 earthquakes, and creep on the San Andreas fault, and east-bay faults	80	45	90	132
9	Inferred from geodetic data (Lisowski and others, 1990).	150	41	--	120

allowed to slip freely in both shear and fault-normal direction. That is, slip in the Loma Prieta region plotted in figure 4 is driven both by displacement on contiguous fault segments and by applied displacements due to relative plate motion. The resulting estimate for fault-normal and dextral slip on the Loma Prieta segments exceeds the estimates we seek for 1989 slip by the amount that this section of the fault slipped in 1906. Subtraction of the 1906 synthetic displacement plotted in figure 4 from the total synthetic displacement yields 36 and 64 cm, respectively, for synthetic fault-normal and dextral slip in 1989 (case 4, table 2). Slightly larger displacements are obtained if estimates of east-bay-fault displacements are excluded (case 3, table 2). The computed dextral slip is still less than observed, and fault-normal convergence is significantly larger than observed. If convergence occurred in 1906, it would reduce the value for 1989 convergence. Although geodetic data indicate that no convergence and, possibly, some extension may have occurred near Loma Prieta in 1906 (Segall and Lisowski, 1990), triangulation points were not densely distributed in 1906, and off-fault convergence may have occurred undetected by the historical network.

DEVELOPMENT OF THE STRAIN FIELD, 1800–1989

The calculations above assume that no slip occurred on the San Andreas fault before 1906; however, slip in the 1906 event was driven by plate-boundary strains modified by earlier ruptures on or near the fault. We thus proceed to estimate slip in these earlier events and to estimate their contribution to cumulative slip. The seismic history of the San Francisco Bay region is probably complete to M~6 since 1850 and to higher magnitudes since about 1800 (Ellsworth, 1990). In this paper, we limit our consideration to the 189-year period from 1800 to the 1989 earthquake, with reasonable confidence that no large earthquakes have been ignored. Large earthquakes occurred in the region in 1838 and 1865, and smaller earthquakes in 1800 and 1890 (Lindh and others, 1982; Working Group on California Earthquake Probabilities, 1990; Tuttle and Sykes, 1992). Locations and rupture lengths for these events are poorly constrained by observation. Using historical records of damage and felt reports to constrain the magnitudes and locations of 19th-century events, Tuttle and Sykes concluded that the 1865 and 1890 earthquakes may not have ruptured the San Andreas fault; instead, they may have originated on faults close to but northeast of the San Andreas fault. Tuttle and Sykes also concluded that the 1838 earthquake ruptured the San Andreas fault on the San Francisco peninsula northwest of and, possibly, including the Loma Prieta segment. These sparse observations, however, do not require the Loma Prieta segment to be included in the 1838 rupture. The rupture lengths and locations we use for 19th-century earthquakes differ somewhat from those presented by Tuttle and Sykes. We model the 1865 and 1890 earthquake as ruptures on the San Andreas fault because even if they were off the fault, they were near enough that the volume of crustal strain release would have included the San Andreas fault. We model the 1838 earthquake as a rupture abutting the Loma Prieta segment to the northwest. As discussed below, including the Loma Prieta segment in our models of the 1838 earthquake would nearly double its length and therefore approximately double the slip in our model of the 1838 rupture. Given these uncertainties, we model the 1800, 1838, and 1865 earthquakes as simple dislocation offsets on the mapped trace of the San Andreas fault, with locations and lengths corresponding to multiples of the segments shown in figure 1. We assume that creep in central California occurred in the 18th and 19th centuries at rates similar to those today, although we recognize that the 1857 Fort Tejon and 1906 San Francisco earthquakes may have changed or even initiated the creep process.

We augment the strain field responsible for the slip plotted in figure 4 with strain resulting from creep on the fault to the south and with strain associated with the 1857 rupture for subsequent events. Under these conditions, the maximum modeled slip in these earlier events did not exceed 12, 65, and 40 cm, corresponding to model earthquakes of M=6, 6.8, and 6.6, respectively. The slip from these earthquakes is clearly small in comparison with the inferred slip during the 1906 rupture. We note, however, that the assumptions used in modeling these early historical ruptures are similar to those that yield apparent underestimates of slip for the 1989 earthquake, and we acknowledge that our model may underestimate the slip in these early events. We added modeled slip from these earlier ruptures to the modeled slip of the 1906 earthquake to obtain a more realistic pre-1989 slip distribution, but we did not attempt to estimate the influence of the pre-1906 strain field on the 1906 rupture. Using the cumulative 1800–1906 slip distribution derived above increases the synthetic dextral slip for the 1989 earthquake to more than 1 m, with a ratio of convergence to shear of approximately 2 to 5 (cases 5, 6, table 2). These results underestimate the observed dextral displacements by about 30 percent but are close to the observed values for fault-normal convergence.

We also performed a series of experiments in which an isolated fault, parallel and 5 km SW. of the San Andreas fault, with the same location and length as those of the Loma Prieta rupture, was allowed to slip freely in shear and convergence. This fault approximates a source region off the San Andreas fault for the 1989 earthquake (for example, Segall and Lisowski, 1990). In these experiments, we imposed plate-boundary displacements equivalent to 189 years of plate motion, and assigned the cumulative synthetic displacements inferred for all pre-1989 earthquakes on the San Andreas fault since 1800. The resulting dextral slip on the new fault was less than that for an equivalent-length rupture on the San Andreas fault. Mean synthetic dextral slip was approximately half that indicated by geodetic measurements in 1989 (cases 7, 8, table 2).

SLIP DEFICIT ON THE SAN FRANCISCO PENINSULA

Our models yield estimates for dextral slip in 1989 that are approximately 30 percent smaller than that observed. Uncertainties associated with preceding earthquake slip distributions may also be partly responsible for this discrepancy. For example, increased rupture length, change in location, or different style or amount of slip on the 1838 rupture would tend to increase the synthetic slip we would calculate for a 1989 rupture, as would incomplete slip in the Loma Prieta region in 1865. Another plausible explanation is that the failure strain for reverse-slip earthquakes in the Santa Cruz Mountains (fig. 1) is greater than for pure-strike-slip earthquakes on faults of the San Andreas system. Also, the simplifications necessary in our two-dimensional approach may result in the discrepancy between synthetic and observed slip.

Despite the underestimated slip in 1989, our models clearly indicate that the 1989 earthquake occurred in a region of slip deficit and that smaller slip deficits still remain (fig. 5). In particular, small regions to the northwest and southeast of the Loma Prieta rupture zone appear overdue for additional slip. The lengths of these regions and the amplitude of the current slip deficit permit us to forecast probable magnitudes for future events. The upper surface of the black area in figure 5 represents the slip that would occur in our models on the San Andreas fault if it were to slip freely as a throughgoing fault terminating at San Juan Bautista (fig. 1). We consider this to be the potential slip developed on the fault since 1800. The slip distribution on the San Andreas fault is dictated by the geometry of the fault and the influence of slip on east-bay faults. The mean slip of more than 6 m is less than the 9.2 m of plate-boundary slip since 1800 because some slip takes place on other faults within the plate boundary, and less than the 7.3 m anticipated for the San Francisco Peninsula from current geodetic rates, presumably owing to slip on minor faults and off-fault folding. The gray areas in figure 5 show the cumulative synthetic slip associated with seismic and aseismic slip during the period 1800–1990. For the area south of San Juan Bautista we assume that the creep rate at the center of the creeping zone is 38 mm/yr, equal to the slip rate indicated by the current velocity field (Lisowski and others, 1991). The black area in figure 5 indicates the slip deficit—slip that has yet to occur on the fault.

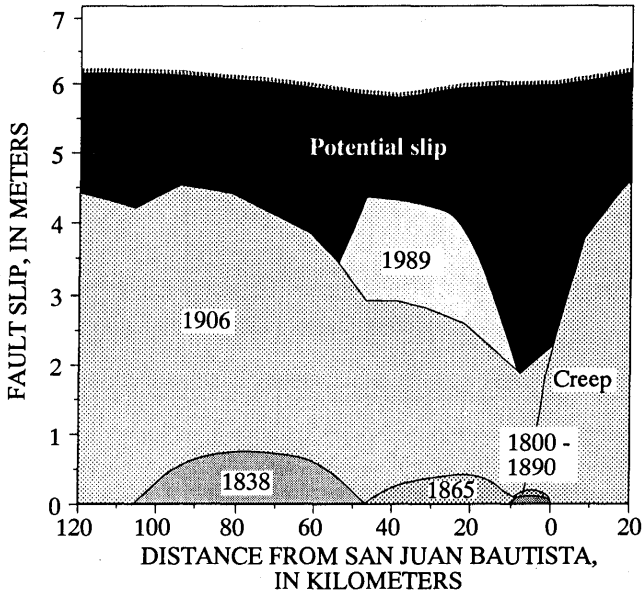

Figure 5.—Cumulative slip from earthquakes and creep in the Santa Cruz Mountains (see fig. 1) since 1800. Upper dashed line, slip on the San Andreas fault since 1800 if slip were frictionless and continuous, driven by current plate-boundary displacements; lower shaded areas, estimated dextral slip from earthquakes and creep for period 1800–1906. For 1989 earthquake, we use mean slip inferred from geodetic data (1.5 m; Lisowski and others, 1990). Black area above gray areas of cumulative slip represents current deficit of dextral slip, assuming that slip deficit in 1800 was negligible.

The mean slip deficit in figure 5 is approximately 1.5 m, but locally as much as 3.5 m of slip appears to be pending near San Juan Bautista, and as much as 2.5 m of slip may be overdue northwest of Loma Prieta (fig. 1). The upper bound of the potential slip area may be too high if we have underestimated slip on the adjoining Calaveras fault system or other faults in the region (fig. 1). The discrepancy between the mean slip on the fault and the upper bound for potential slip can be reconciled by assuming that approximately 10 mm/yr of dextral slip is absorbed outside the study area, lowering the mean slip deficit to leave small regions northwest and southeast of Loma Prieta. If these regions were to be filled now by earthquakes, their maximum rupture lengths would be 20 to 40 km, with mean slips of more than 50 cm, corresponding to earthquakes in the range M=6.3–6.7. We note, however, that cumulative plate-boundary displacements exceed 7.5 m if the recent geodetic plate-boundary slip rate of 38 mm/yr on the southern San Francisco peninsula is extrapolated for the past 200 yr. Because it is unlikely that we are missing historical M>7 earthquakes in this period, the mean slip deficit indicated in figure 5 is probably applicable.

FAULT-NORMAL SHORTENING IN THE SANTA CRUZ MOUNTAINS

Intuitively, the slip on a throughgoing transform fault must be uniform along strike. Our models, however, indicate that a fault with complex geometry will generally exhibit reduced strike slip where the strike of the fault differs from the applied plate-slip direction (Bilham and King, 1989a). The resulting slip deficit results in fault-normal displacements that are manifest in thrust faulting and uplift in such a region as the Santa Cruz Mountains, where the fault undergoes transpression, and in normal faulting and subsidence in regions of transtension (Bilham and King, 1989b). Over geologic time, the fault geometry will change to more efficiently accommodate slip on the fault.

We proceed to quantify the amplitude of fault-normal convergence that accompanies dextral slip on the peninsular section of the San Andreas fault. North of San Francisco, the fault approximately parallels the plate-slip vector (Bilham and Hurst, 1988), whereas south of San Juan Bautista (fig. 1) it is 6° oblique to it. The geometry of the San Andreas fault in the transition zone is a gentle S-curve, resulting in a reduction of strike slip accompanied by fault-normal convergence. If the fault zone were infinitely compliant, this fault-normal convergence would result in the extrusion of material from the fault zone. In practice, advection through the Santa Cruz Mountains results in uplift of a broad area (Anderson, 1990).

To determine the maximum fault-normal convergence driving uplift and reverse faulting, we model the fault as a vertical, infinitely compliant dislocation and subject it to antisymmetric plate-boundary displacements, as before. The applied strain is adjusted to cause the central part of the 1906 rupture zone north of San Francisco to slip about 5 m, which would take approximately 200 years if the fault slipped steadily (Niemi and Hall, 1992). The fault in these models is frictionless along strike and is permitted to close without friction, a process whose deformation field may be envisaged as the opposite of that resulting from dike injection. The boundary-element model yields an estimate of dextral and fault-normal slip in each fault segment (fig. 6). Dextral slip is approximately 4.6 m near the Loma Prieta segment, whereas maximum convergence is about 1.3 m, leading to a ratio of dextral slip to convergence of approximately 3 to 1. From geodetic modeling, dextral slip during the 1989 earthquake was 1.5±0.3 m, and reverse slip 1.2±0.3 m, on a 70° dipping fault plane (case 9, table 2, Lisowski and others 1990) representing a ratio of dextral slip to convergence of about 3.75, with a range of uncertainty from 2.4 to 6. Thus, the rake of the 1989 earthquake is similar to that expected if relative plate-boundary displacements within the Santa Cruz Mountains (fig. 1) were entirely accommodated by ruptures of high-angle-fault planes. Accounting for the dip of the Loma Prieta rupture, the fault-normal component of convergence during the 1989 earthquake was approximately 0.4 m. The difference between the convergence observed in the 1989 earthquake and the 1.3 m indicated in figure 6 suggests that an additional 0.9 m of convergence remains, or has already occurred in previous events since 1800. In the 1906 earthquake, however, convergence was not observed geodetically (Segall and Lisowski, 1990). We conclude that fault-normal convergence may have been accommodated by slip in earlier events or manifested as regional contraction within the southern Santa Cruz Mountains during the 1906 earthquake, but not well sampled by the distribution of geodetic control points. Off-fault folding and complex processes leading to crustal thickening must play a significant role in the morphologic development of the Santa Cruz Mountains, because reverse faulting tends to generate antisymmetric uplift and subsidence features unrepresentative of the current morphology of the range.

DISCUSSION

Our two-dimensional uniform-thickness elastic-plate model is adequate to estimate the broad features of deformation on the San Francisco peninsula because our models yield estimates for slip on faults within the body of the Santa Cruz Mountains (fig. 1), whether these faults are contiguous segments of a single throughgoing fault or isolated segments. In studies of slip in specific historical events, the boundary-element method yields reasonable estimates for slip as long as faults are assigned reasonable azimuths and lengths. Moreover, this method permits the effect of interactions of fault segments with each other and with the causative strain field to be explicitly accounted for in the regional deformation. Slip during the Loma Prieta rupture was on an inclined fault, and the earthquake had

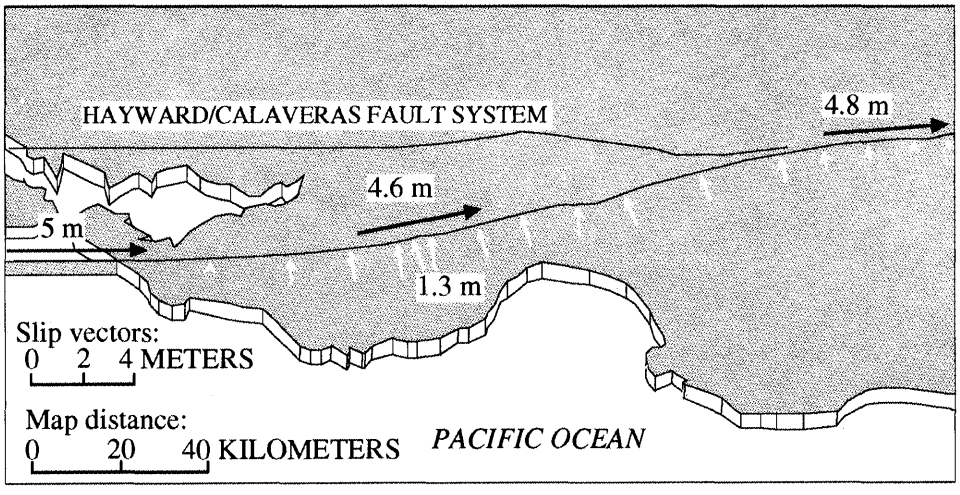

Figure 6.—Dextral and fault normal displacements on the San Andreas fault through the Santa Cruz Mountains (see fig. 1 for locations) on a transverse Mercator projection centered on North American/Pacific pole of rotation. Length of white arrows indicates mean fault-normal convergence calculated for each fault segment; black arrows indicate average dextral slip at three points along fault. The Hayward and Calaveras fault zones do not slip in this model; maximum convergence occurs near Loma Prieta and is approximately a third of dextral-slip component.

a greater hypocentral depth relative to regions to the south (U.S. Geological Survey staff, 1990), suggesting that the rupture may have taken place within a plate of relatively increased thickness. Our method, however, yields estimates for mean dextral slip and convergence that are within 30 percent of those observed.

The mean slip deficit along the peninsular section of the San Andreas fault (fig. 5) is surprisingly large; however, the size of the deficit reflects the fact that 86 yr (1906 to 1992) represents a significant fraction of the renewal time between great 1906-type earthquakes (Niemi and Hall, 1992). The cumulative slip distribution reveals regions of enhanced slip deficit to the northwest and southeast of the Loma Prieta rupture zone. The larger of these two regions of slip deficit is to the southwest, where an increase in creep rate has been reported near San Juan Bautista (fig. 1) since the 1989 earthquake (Behr and others, 1990; Sylvester and others, 1990). Creep rates would have to increase to 2 cm/yr for about 50 to 75 yr to alleviate the current deficit in this region and thus would have to more than double to accommodate this deficit and the applied slip budget. Therefore, current increased surface slip rates are inadequate to relieve the slip deficit southeast of Loma Prieta (fig. 1). If the 1838 earthquake ruptured the Loma Prieta segment (Tuttle and Sykes, 1992), our estimate of the slip deficit on the peninsular section of the San Andreas fault would be reduced by approximately 80 cm, significantly reducing the inferred slip deficit northwest of the Loma Prieta rupture zone.

The rate of convergence implied by the ratio of dextral slip to convergence in figure 6 is approximately 8 mm/yr. Uniform distribution of this convergence across a 10-km-thick, 40-km-wide region would result in a crustal-thickening rate of 2 mm/yr, approximately 4 times the rate estimated from the elevation of coastal terraces (Segall and Lisowski, 1990). We note, however, that the uplift rate is likely to be concentrated away from the coast in regions close to the fault and that isostatic adjustment will reduce this uplift rate. If we assume a mean slip rate of 24 mm/yr, the time taken for material to pass the fault bend is approximately 4 m.y. At a mean thickening rate of 2 mm/yr, this amount of slip would increase the thickness of the plate to 18 km, consistent with observed seismicity and models for advection in the region (Anderson, 1990).

CONCLUSIONS

The 1989 Loma Prieta earthquake occurred on a part of the San Francisco peninsula where a dextral-slip deficit evidently existed before the event. The summation of slip in earlier events and the 1989 earthquake suggests that smaller deficits remain to the northwest and southeast of the Loma Prieta rupture zone, which could be the locus of future $M<6.7$ earthquakes, and that a substantial slip deficit may exist along most of the peninsula. The mean slip deficit on the San Andreas fault in the San Francisco Bay region exceeds 1.5 m, and locally the deficit is inferred to exceed 3.5 m. If the 1838 rupture included the Loma Prieta segment (Tuttle and Sykes, 1992), then the slip deficit to the northwest of the Loma Prieta rupture zone would be reduced by approximately 80 cm, resulting in the slip deficit in this region being the lowest on the peninsula. Creep occurring to the southeast of the Loma Prieta rupture zone, representing extended activity on the northwest end of the creeping section of the fault, is inadequate to relieve the slip deficit southeast of Loma Prieta (fig. 1). The absence of significant surface slip suggests that the potential for future earthquakes in this region remains high.

Fault-normal convergence is a characteristic of deformation in the Loma Prieta region. The amount of convergence during the 1989 event was consistent with the component of dextral convergence expected from fault geometry. We estimate that over geologic time, this convergence results in crustal thickening at a rate of approximately 2 mm/yr, consistent with observed depths of seismicity and rates of coastal uplift.

One assumption in our models was that the pre-1800 strain field was uniform, a consequence of our current ignorance concerning prehistoric earthquakes. Some idea of the inadequacies of this assumption may be obtained from the complex slip deficit that we calculated for events since 1800 (fig. 5).

REFERENCES CITED

Anderson, R.S., 1990, Evolution of the northern Santa Cruz Mountains by advection of crust past a San Andreas fault bend: Science, v. 249, no. 4967, p. 397–401.

Behr, Jeff, Bilham, Roger, Bodin, Paul, Burford, R.O., and Bürgmann, Roland, 1990, Aseismic slip on the San Andreas fault south of Loma Prieta: Geophysical Research Letters, v. 17, no. 9, p. 1445–1448.

Bilham, Roger, and Bodin, Paul, 1992, Fault zone connectivity; slip rates on faults in the San Francisco Bay area, California: Science, v. 258, no. 5080, p. 281–284.

Bilham, Roger, and Hurst, Kenneth, 1988, Relationships between fault zone deformation and segment obliquity on the San Andreas Fault, California: China-U.S. Symposium on Crustal Deformation and Earthquakes, Beijing, 1988, Proceedings, p. 510–524.

Bilham, Roger, and King, G.C.P., 1989a, Slip distribution and oblique segments of the San Andreas Fault, California; observations and theory, *in* Schwartz, D.P., and Sibson, R.H., eds., Proceedings of Conference XLV; a workshop on fault segmentation and controls of rupture initiation and termination: U.S. Geological Survey Open-File Report 89–315, p. 80–93.

———1989b, The morphology of strike slip faults: examples from the San Andreas fault, California: Journal of Geophysical Research, v. 94, no. B8, p. 10204–10216.

Bonilla, M.G., Mark, R.K., and Lienkaemper, J.J., 1984, Statistical relations among earthquake magnitude, surface rupture length, and surface fault displacement: Seismological Society of America Bulletin, v. 74, no. 6, p. 2379–2411.

Crouch, S.L., and Starfield, A.M., 1983, Boundary element methods in solid mechanics: Winchester, Mass., Allen and Unwin, 322 p.

DeMets, Charles, Gordon, R.G., Argus, D.F., and Stein, Seth, 1990, Current plate motions: Geophysical Journal International, v. 101, no. 2, p. 425–478.

Ellsworth, W.L., 1990, Earthquake history, 1769–1989, chap. 6 *of* Wallace, R.E., ed., The San Andreas fault system, California: U.S. Geological Survey Professional Paper 1515, p. 153–187.

King, G.C.P., and Nábělek, J.L., 1985, Role of fault beds in faults in the initiation and termination of earthquake rupture: Science, v. 228, no. 4702, p. 984–987.

Lawson, A.C., 1910, chairman, The California earthquake of April 18, 1906, report of the State Earthquake Investigation Commission: Carnegie Institution of Washington Publication 87, 2 v.

Lindh, A.G., Moths, B.L., Ellsworth, W.L., and Olson, J.A., 1982, Historic seismicity of the San Juan Bautista, California region, *in* Hill, D.P., and Nishimura, Keiji, chairmen, Proceedings of the Second Joint Meeting of the U.S.-Japan Conference on Natural Resources (UJNR) Panel on Earthquake Prediction Technology, July 13–17, 1981: U.S. Geological Survey Open-File Report 82–180, p. 45–50.

Lisowski, Michael, Prescott, W.H., Savage, J.C., and Johnston, M.J.S., 1990, Geodetic estimate of coseismic slip during the 1989 Loma Prieta, California, earthquake: Geophysical Research Letters, v. 17, no. 9, p. 1437–1440.

Lisowski, Michael, Savage, J.C., and Prescott, W.H., 1991, The velocity field along the San Andreas fault in central and southern California: Journal of Geophysical Research, v. 96, no. B5, p. 8360–8389.

Nishenko, S.P., and Williams, P.L., 1985, Seismic hazard estimate for the San Jose-San Juan segment of the San Andreas fault; 1985–2005, *in* Shearer, C.F., ed., Minutes of the National Earthquake Prediction Evaluation Council, July 26–27, 1985, Menlo Park, California: U.S. Geological Survey Open-File Report 85–754, p. 351–366.

Niemi, T.M., and Hall, N.T., 1992, Late Holocene slip rate and recurrence of great earthquakes on the San Andreas fault in northern California: Geology, v. 20, no. 3, p. 195–198.

Sarna-Wojcicki, A.M., Pampeyan, E.H., and Hall, N.T., 1975, Recent active breaks along the San Andreas fault between the central Santa Cruz Mountains and the southern Gabilan Range, California: U.S. Geological Survey Miscellaneous Field Studies Map MF–650, scale 1:24,000.

Scholz, C.H., 1985, The Black Mountain asperity; seismic hazard of the southern San Francisco peninsula, California: Geophysical Research Letters, v. 12, no. 10, p. 717–719.

Segall, Paul, and Michael Lisowski, 1990, Surface displacements in the 1906 San Francisco and 1989 Loma Prieta earthquakes: Science, v. 250, no. 4985, p. 1241–1244.

Slemmons, D.B., 1977, State-of-the-art for assessing earthquake hazards in the United States; faults and earthquake magnitude: U.S. Army Corps of Engineers, Waterways Experiment Miscellaneous Paper S–3–73–1, Report 6, 166 p.

Sylvester, A.G., Burford, R.O., and Schulz, S.S., 1990, Almost no surface displacement occurred at San Juan Bautista as a result of the Loma Prieta earthquake [abs]: Eos (American Geophysical Union Transactions), v. 71, no. 8, p. 290.

Thatcher, Wayne, and Lisowski, Michael, 1987, Long-term seismic potential of the San Andreas fault southeast of San Francisco: Journal of Geophysical Research, v. 92, no. B6, p. 4771–4784.

Tuttle, M.P., and Sykes, L.R., 1992, Re-evaluation of several large historic earthquakes in the vicinity of the Loma Prieta and peninsular segments of the San Andreas fault, California: Seismological Society of America Bulletin, v. 82, no. 4, 1802–1820.

U.S. Geological Survey staff, 1990, The Loma Prieta, California, earthquake; an anticipated event: Science, v. 247, no. 4940, p. 286–293.

Working Group on California Earthquake Probabilities, 1990, Probabilities of large earthquakes in the San Francisco Bay region, California: U.S. Geological Survey Circular 1053, 51 p.

Zeller, S.C., and Pollard, D.D., 1992, Boundary conditions for rock fracture analysis using the boundary element method: Journal of Geophysical Research, v. 97, no. B2, p. 1991–1997.

This page intentionally left blank

TECTONIC PROCESSES AND MODELS

THREE-DIMENSIONAL LITHOSPHERIC KINEMATICS IN THE LOMA PRIETA REGION, CALIFORNIA: IMPLICATIONS FOR THE EARTHQUAKE CYCLE

By Kevin P. Furlong and David Verdonck,
Pennsylvania State University

CONTENTS

ABSTRACT

The earthquake has served as powerful motivation to improve our understanding of the kinematic and dynamic behavior of the boundary between the North American and Pacific plates in the San Francisco Bay region. We combine investigations of the plate-boundary evolution, the kinematics of crustal and lithospheric components of the system, and three-dimensional finite-element modeling of the deformational behavior of the region to evaluate the causality of the earthquake. Our modeling tests the implications of a proposed plate-boundary structure that includes a viscously deforming, horizontal shear zone in the lower crust connecting the Santa Cruz Mountains and peninsular sections of the San Andreas fault with east-bay (Hayward, Calaveras) faults and the plate-bounding shear zone within the lithospheric mantle. Inclusion of this plate-boundary structure is motivated by the results of studies of plate-boundary evolution, geodetic observations of crustal deformation, and modeling of fault-segment geometries. The results of our study indicate that the 1989 Loma Prieta earthquake may represent decoupling of the Santa Cruz crustal block from its underlying mantle in response to stress accumulation after such events as the 1906 San Francisco earthquake. Inclusion of a middle- to lower-crustal detachment surface in the modeling significantly changes the crustal-stress regime in comparison with purely elastic crustal models, allows more efficient transfer of stress among the fault segments in the Loma Prieta region, and provides a mechanism to increase stress on the peninsular section of the San Andreas fault consistent with the occurrence of major earthquakes on that section. Observations of transient stress and crustal deformation resulting from the 1989 earthquake during coseismic and 10- to 20-year postseismic periods can distinguish among various proposed plate-boundary models of the region. Combination of these observations with modeling studies provides a strong discriminant of the geometry and rheology of the plate boundary in the Santa Cruz Mountains and San Francisco Bay region.

INTRODUCTION

The earthquake drew immediate attention to the power and effects of plate-tectonic processes. It clearly demonstrated the inherent complexity in tectonic processes along a boundary of lithospheric plates and reminded us of the need to expand our understanding of these complexities if we hope to improve our abilities to assess future hazards from earthquakes along the San Andreas fault system. In particular, it is becoming clear, as a result of both the faulting characteristics of the earthquake and other studies, that the three-dimensional geometry of the Pacific-North American plate boundary is not nearly as simple as that typically shown for transform plate boundaries. The three-dimensional complexity of the plate boundary in the Loma Prieta region is the expected result of the thermal-mechanical evolution of this plate boundary (Furlong and others, 1989; Furlong, 1993). One key ingredient in our understanding of the causality of the earthquake is knowledge of the plate-boundary structure, its evolution, the consequences of this structure for crustal

and lithospheric kinematics, and the connections between plate kinematics and the earthquake cycle.

Most studies of the dynamics of the San Andreas fault system either have used predictions of regional relative plate motions, given in part by global models (for example, Minster and Jordan, 1978; DeMets and others, 1990), or have focused on the kinematic information contained in regional seismicity. Global models provide information on the large-scale components of relative plate motions but do not attempt to be directly applicable to investigations of the length scale appropriate for the Loma Prieta region. Kinematic studies provide detailed information on deformational behavior in the upper seismogenic crust but little information on the coupling between upper-crustal deformation and large-scale plate-tectonic processes. In this study, we focus on this link between seismogenic processes in the upper crust and the broader deformation associated with plate tectonics.

The 1989 Loma Prieta earthquake is more than a simple manifestation of plate-tectonic processes; it is also a tool that has sampled the properties of the regional lithosphere in various ways. Most direct is the information that the earthquake provided on crustal structure (both lithologic and seismic velocity). Less obvious but no less important is the sampling of the rheologic properties of the lithosphere. Some of this rheologic sampling occurred with the earthquake itself and has helped map the depth of transition from brittle to ductile modes of deformation (Furlong and Langston, 1990), the spatial extent of aseismic fault rupture, and the coseismic deformational response of the crust (for example, Marshall and others, 1991). Potentially more important in addressing questions of future earthquake hazards in the San Francisco Bay region is the information that the earthquake will allow us to gather on the transient response of the plate-boundary system to seismic events. With this information, we can better constrain the role of lithospheric rheology in the earthquake cycle. Many of these data will be gathered during the next 10 to 20 years, allowing postseismic transients driven by the seismic loading of the earthquake to constrain models of lithospheric rheology and plate-boundary structure. Although such data were not immediately available after the earthquake, such modeling studies as ours and the others described in this chapter help to identify observational strategies that can test the possible implications for the earthquake cycle.

The applicability of earthquake-hazard evaluations to the San Francisco Bay region will depend on the completeness of the earthquake-cycle models used. The degree to which seismic activity along one segment of the San Andreas fault system in the region affects the earthquake cycle on other segments is at present unclear. Historical patterns of large earthquakes in the region hint at earthquake pairing between the San Andreas and east-bay faults (Ellsworth, 1990). Although the historical record is far too short to be rigorously tested, modeling studies of the role plate-boundary structures may play in producing particular patterns of earthquake occurrence can provide needed constraints on estimating the possible consequences of the 1989 earthquake for other fault segments in the region.

In this study, we address each of the issues described above. First, we describe the plate-tectonic evolution of the Loma Prieta region and the implications of this evolution for details of the three-dimensional plate-boundary structure in the region and the rheology of the plate boundary itself. Next, we investigate the kinematics of the crust-mantle system in the region and the role Loma Prieta-type events play in this kinematic regime. Finally, using the framework provided by analyses of the plate-tectonic evolution and crust-mantle kinematics, we investigate, using finite-element modeling, the time-varying three-dimensional stress and strain regimes during simulated earthquake cycles in the region. This last issue provides important constraints on the nature of stress transfer in the region and points up characteristics of the strain field that are diagnostic of details of the proposed plate-boundary structure.

LITHOSPHERIC EVOLUTION

Most studies of the evolution and behavior of the San Andreas fault system have focused on the stress and deformation regime in the middle to upper crust, a reasonable region to investigate because it encompasses the seismogenic component of the plate boundary. We take a somewhat-different approach, focusing instead on the behavior of the lithosphere below the seismogenic layer (representation of earthquakes in our models is quite simple). The stress and deformation regime within the nonseismogenic lithosphere plays an important role in the earthquake cycle along the San Andreas fault system, and we believe that our study, in conjunction with those by Bodin and Bilham (this chapter) and Simpson and Reasenberg (this chapter), complements studies of the seismogenic layer in unraveling the processes which drive the earthquake cycle along the San Andreas fault system.

The present characteristics of the San Andreas fault system, in contrast to intraplate fault zones, can be directly linked to a series of plate-tectonic events and associated processes of lithospheric evolution. Additionally, the deformational behavior of the San Andreas fault system differs from that of intraplate fault zones because this fault system is part of a plate boundary. Because it forms only a small part of the boundary between the North American and Pacific plates, however, its rheologic characteristics play little role in the overall dynamics of either plate—that is, the San Andreas fault system does little to drive or retard plate motions but, instead, has developed in response to externally applied boundary conditions of plate motions. With the applied conditions of relative plate velocities, the evolution of the lithosphere and plate-boundary

structure can be investigated in the light of the fault system's thermal and rheologic characteristics, both of which play important parts in the linkage between the relative plate velocity and the resulting stress and strain fields in the plate-boundary region.

PLATE TECTONICS OF THE LOMA PRIETA REGION

As described by various investigators (for example, Atwater, 1970; Dickinson and Snyder, 1979; Zandt and Furlong, 1982), the formation of the San Andreas fault system resulted from the northward migration of the Mendocino triple junction. The formation of a transform boundary in place of a convergent boundary is fundamental to the rest of the fault system's evolutionary history. A three-dimensional schematic view of the plate-tectonic cause of this lithospheric evolution is shown in figure 1.

This three-dimensional view of lithospheric structure in the vicinity of the Mendocino triple junction shows a typical subduction configuration north of the triple junction, where the Gorda plate is being subducted beneath the North American plate. The specific characteristics of the relative plate motions at this fault-fault-trench triple junction require that the Gorda plate have a component of motion relative to North America comparable to the motion between the Pacific and North American plates. This requirement leads not only to the cessation of subduction with the passage of the triple junction but also to the concurrent removal of the subducted Gorda slab. These events produce a region of thin North American lithosphere, the base of which is exposed to relatively hot mantle (Lachenbruch and Sass, 1980; Zandt and Furlong, 1982; Furlong, 1984; Benz and others, 1992). This region of the upper mantle beneath the west edge of the North American plate has been variously called the slabless or asthenospheric window. The emplaced asthenospheric mantle cools over time, becoming either Pacific or North American lithosphere, and the Pacific-North American plate boundary develops within this slabless window at the center of deformation in this region of accreted lithosphere (Furlong and others, 1989; Furlong, 1993).

Schematic cross-sectional views of this lithospheric evolution are shown in figure 2, which illustrates several details of the plate-boundary structure that play important roles in the plate kinematics of the Loma Prieta region. The Pacific-North American plate boundary develops where deformation is concentrated. Because this is a plate-boundary structure, the overall relative Pacific-North American plate velocities (excluding effects of internal deformation within the North American plate, such as in the Basin and Range) must be accommodated within the plate-boundary region. Although the Pacific-North American plate boundary within the seismogenic crust is a broad deformation zone comprising several active faults, consideration of upper-mantle thermal structure and rheology indicates a fairly simple plate-boundary structure within the lithospheric mantle (Furlong and others, 1989; Furlong, 1993). The specific location of the center of deformation and the width of the high-strain region depend primarily on the temperature structure of the slabless window. The thermal regime controls the initial location of the plate boundary (Furlong and others, 1989), but mineralogic conditions (most likely

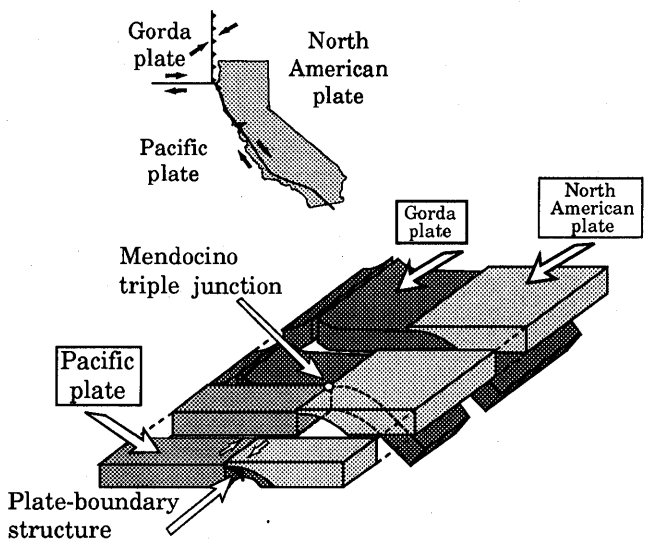

Figure 1.—Block diagram of three-dimensional lithospheric structure in vicinity of the Mendocino triple junction. Plate-boundary structure develops in region of emplaced asthenospheric mantle. Arrows indicate directions of relative plate motion. View northwestward.

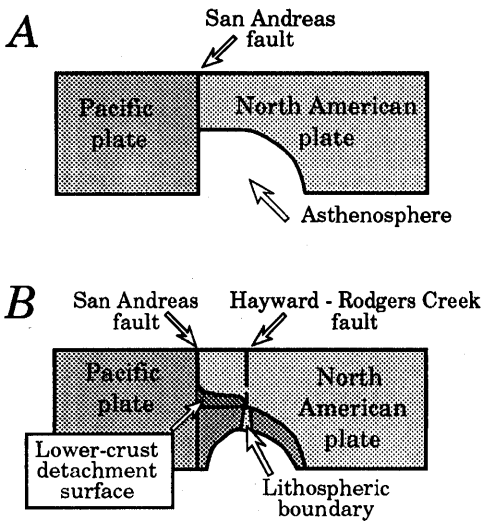

Figure 2.—Simplified cross-sectional views of proposed plate-boundary structure (A) immediately south of the Mendocino triple junction (lat 40° N.) and (B) in the San Francisco Bay region (lat 37°–38° N.). Modified from Furlong and others (1989).

regions of strain-induced reduced grain size) may serve to further localize and maintain the position of the plate boundary within the mantle lithosphere (fig. 2).

Deformation within the lithospheric mantle occurs dominantly by temperature-dependent creep processes. The nonlinear relation between strain rate and temperature for the appropriate deformation mechanisms (dislocation-creep or diffusion-creep) leads to a localization of strain to the sites of highest temperature (at any given depth). As a result, strain will localize, and the associated plate boundary will form, within the slabless window, as shown in figure 2. The exact position of this boundary depends on both the cross-sectional geometry of the slabless window and details of the kinematics of the underlying mantle. Geodetic data (for example, Lisowski and others, 1991), particularly in regions where upper-crustal faults are locked, can also be used to estimate the position of the plate boundary within the lithospheric mantle—specifically, the center of deformation of the plate-boundary deformation zone. Both thermal-mechanical modeling (Furlong and others, 1989) and geodetic data (Lisowski and others, 1991) point to a plate boundary forming within the slabless window substantially east of the west edge of the thinned North American lithosphere, in a position that approximately corresponds (on the surface) to the Hayward fault in the San Francisco Bay region.

The proposed offset between the surface trace of the San Andreas fault in northern California, which during recent geologic time has served as the primary crustal component of the plate boundary, and the deeper plate-boundary structure lies at the heart of our model for plate-boundary evolution in the Loma Prieta region. Within this model, one necessary component is a connection between the base of the San Andreas fault and the plate boundary forming within the slabless window. Rheologic considerations and the rupture behavior of the 1989 earthquake (Furlong and Langston, 1990; Langston and others, 1990) lead us tentatively to place this structure within the lower crust at approximately 18-km depth. Although we cannot tightly constrain the depth of this connecting structure, it should be contained within the lower crust, and so its maximum extent would be from approximately 18-km depth to the local Moho. We would expect strain-localization processes (as described below) to further limit this structure to less than 5 km in thickness—in our preferred model, a 2- to 3-km-thick detachment surface.

Additional aspects of plate-boundary evolution, which are important components of the kinematic and deformational model presented below, are the width and deformation regime of the plate boundary within the mantle. Within regions of significant strain, the equilibrium grain sizes of deforming minerals will be controlled by the stress regime and stress history (Karato and others, 1986; Rutter and Brodie, 1988). In addition, the mode of temperature-dependent creep that will dominate plate-boundary deformation depends strongly on the characteristic grain size within the deformation zone. We have combined laboratory-derived parameters for the stress/grain-size relations and deformation mechanism (dislocation or grain-size-dependent diffusion-creep) with the evolving thermal model of Furlong and others (1989) to investigate localization processes within the plate boundary. The results for the San Francisco Bay region are plotted in figure 3 (K.P. Furlong, unpub. data, 1992). The localized strain as a result of substantial lateral temperature variations, in combination with general cooling of the region of the original slabless window, creates a relatively narrow region (approx 10–20 km wide) of significantly reduced grain sizes and associated concentrated strain. The localization of this mineralogically preferred site for deformation, coupled with continuing lateral temperature variations, results in additional localization of strain (within a region <10 km wide). Characteristic grain sizes in this region of high strain are small, and so strain is accomplished primarily by grain-size-dependent diffusion-creep, allowing deformation at relatively low stresses. A similar process is envisioned to produce the proposed horizontal detachment surface within the lower crust.

The combination of plate-tectonic events with the thermal and rheologic evolution of the lithosphere proposed above results in a plate-boundary configuration in the Loma Prieta region similar to that shown in figure 4. In this model, the plate boundary within the crust includes both the San Andreas and east-bay (Hayward, Calaveras) faults, which connect by way of a lower-crustal structure to the plate boundary within the mantle that lies approximately below the east-bay faults. This complex, three-dimensional plate-boundary structure is ephemeral, and the faults that sit above the deeper extent of the plate boundary (for example, east-bay faults) eventually become the dominant components of the plate boundary within the crust. Such a developmental step has already occurred in central California, where the plate-boundary structure within the crust (San Andreas fault) lies above the plate boundary within the lithospheric mantle, and faults to the west of the San Andreas fault have become progressively less active. The 1989 earthquake occurred along a section of the San Andreas fault that links these two types of crustal-plate boundary and thus forms the region in which the lower-crustal detachment surface begins to play a critical part in the overall stress and strain regime. This characteristic alone makes understanding the deformational processes in the Loma Prieta region important to any analysis of earthquake hazards in the San Francisco Bay region.

KINEMATICS OF THE LITHOSPHERE

Our evolutionary model of the San Andreas fault system significantly complicates the kinematics of what is commonly considered a simple strike-slip plate boundary. The position and orientation of the plate boundary within the

lithospheric mantle reflect both the process of boundary formation (cooling of mantle material within the slabless window) and the directions of relative motion between the North American and Pacific plates. Geodetic observations and our previous modeling studies (Furlong and others, 1989) indicate that this boundary is located approximately as shown in figure 5. Plate motion at the boundary consists almost entirely of right-lateral shear, which, on the basis of rheologic modeling, we believe to be occurring in a relatively narrow deformation zone (<10–20 km wide) within the lithospheric mantle. Relative to a North American reference frame, the subcrustal Pacific lithosphere extends to this boundary. The kinematics of the crustal components of the plate boundary differs from this configuration and plays an important part in the earthquake cycle in the Loma Prieta region. The position of the plate boundary can also be inferred from results of recent seismic-tomography studies of the mantle beneath northern California (Benz and others, 1992). In those models, the east limit of the Pacific plate corresponds to the region of transition from fast to slow velocities in the depth range 30–100 km. These results indicate a similar position to that shown in figure 5 for the east edge of the Pacific plate and provide the information to link the plate boundary with the Mendocino triple junction.

Crustal kinematics leads us to consider the crust along the San Andreas fault in the Loma Prieta region in terms of the four blocks shown in figure 6. East of the lithospheric-plate boundary (east of the Hayward-Calaveras fault systems), North American crust overlies and is coupled to North American lithosphere. Similarly, offshore to the west, Pacific crust is well coupled to Pacific lithosphere. The kinematics of these crustal blocks mimics that of the underlying mantle. Between these regions of strong crust-mantle coupling lie two crustal blocks of less certain

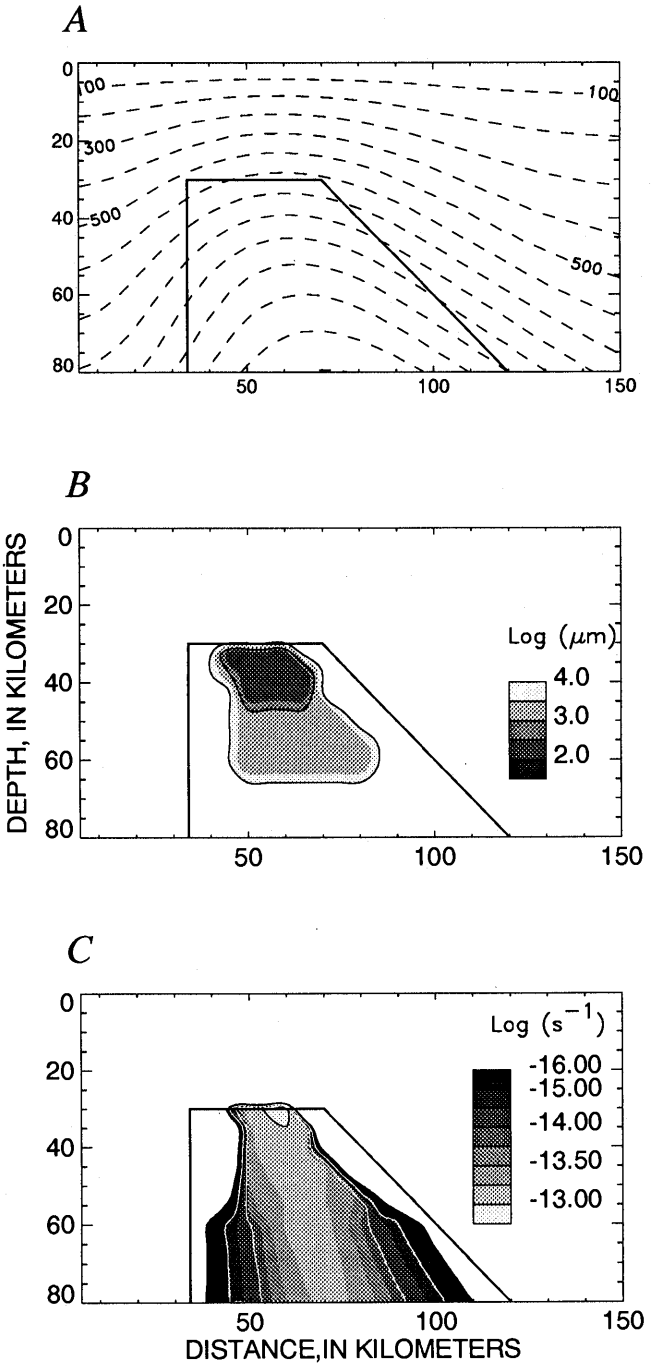

Figure 3.—Thermal-rheologic structure of plate boundary in the San Francisco Bay region. *A*, Temperature (in degrees Celsius; from Furlong and others, 1989). *B*, Grain size (from Furlong, 1990). *C*, Strain rate (from Furlong, 1990). Figures 3B and 3C localize plate boundary as a result of grain-size reduction and change in deformation mechanism to diffusion-creep. Region of highest strain rate (~10^{-13} s^{-1}) corresponds to position of plate boundary within mantle. This high-strain-rate region (<10 km wide) results from combination of lateral temperature gradients and localized regions of grain-size reduction. Trapezoidal region outlines area of slabless window after triple-junction passage.

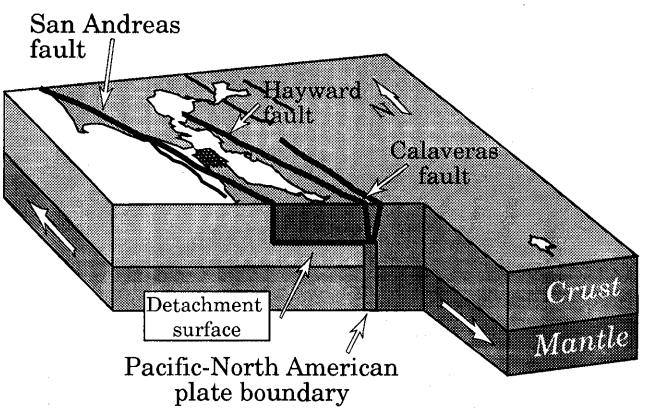

Figure 4.—Block diagram of plate-boundary structure in the San Francisco Bay region. Vertical cut is approximately at latitude of Loma Prieta. Shading indicates plate affinity of various crustal and mantle components of plate boundary. Proposed detachment surface is shown connecting base of the San Andreas fault with east-bay faults and lithospheric-plate boundary. The Pacific plate therefore extends to east-bay faults beneath this surface.

affinity. First, between the San Andreas and east-bay faults lies what we term the "Bay Area block" (similar to the Sebastopol block of Fox, 1983). In the Loma Prieta region, this block is largely uncoupled from the underlying mantle (which in our model is Pacific lithosphere; see figs. 2, 4; Furlong and Langston, 1990). The kinematics of this block is complex because the block is partly linked to North American crust to the east (when the east-bay faults are locked) and to the northeast (where the bounding faults are less well developed), and drag along its base from the motion of the underlying mantle may affect internal deformation and motion.

Second, west of the San Andreas fault lies what we term the "Santa Cruz block." The kinematics of this crustal block is similar to that of the Pacific plate, in that no obvious active fault boundary separates the block on the west from adjacent oceanic crust. However, seismicity within the block (associated with the San Gregorio fault?) and possible faulting observed in multichannel seismic profiles in the Santa Cruz region (Stephen Lewis, oral commun., 1992) indicate that the Santa Cruz block is undergoing internal deformation and possible westward displacement, particularly at the approximate latitude of Loma Prieta. The eastern margin of the block is well defined (San Andreas fault), and so its motions are prescribed by the geometry of the San Andreas fault. The kinematics of the Santa Cruz block is illustrated in figure 6. The discrepancies between the kinematics of this crustal block and the underlying mantle lead to partial coupling, possibly substantial internal strain, and likely westward partial obduction of the block over Pacific crust (structures observed in seismic data show evidence of significant east-west shortening; Stephen Lewis, oral commun., 1992).

The differences between the kinematics of the crustal and mantle components of the Pacific-North American plate boundary in the vicinity of the San Andreas fault played an important part in the generation of the 1989 earthquake. Loma Prieta is situated where the motions of the Santa Cruz block differ most from those of the Pacific plate, and in this region the proposed decoupling of the block from the underlying mantle must occur (Furlong and Langston, 1990). Thus, the generation of the earthquake reflects two types of processes: (1) decoupling of the Santa Cruz block from the underlying mantle and (2) interactions between the largely uncoupled Bay Area block and the Santa Cruz block. Both of these processes are ultimately driven by Pacific-North American plate motions, but because of the complexity of the Loma Prieta region, we must consider both crustal and mantle kinematics in our investigation of the earthquake.

A schematic cross section (fig. 7) of the plate interactions near Loma Prieta (along the strike of relative Pacific-North American plate motions) indicates the correlation of the

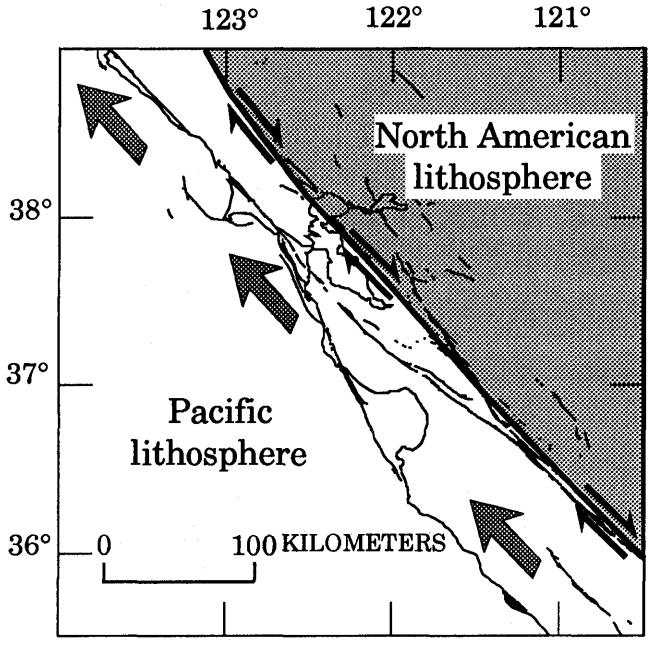

Figure 5.—San Francisco Bay region, showing location and kinematics of Pacific-North American plate boundary within lithospheric mantle. Double arrows indicate directions of fault movement; large arrows indicate direction of Pacific-plate motion. Plate boundary is constrained to lie approximately below east-bay fault system by analysis of regional geodetic results (Lisowski and others, 1991), thermal-rheologic modeling (Furlong and others, 1989), and seismic tomography (Benz and others, 1992).

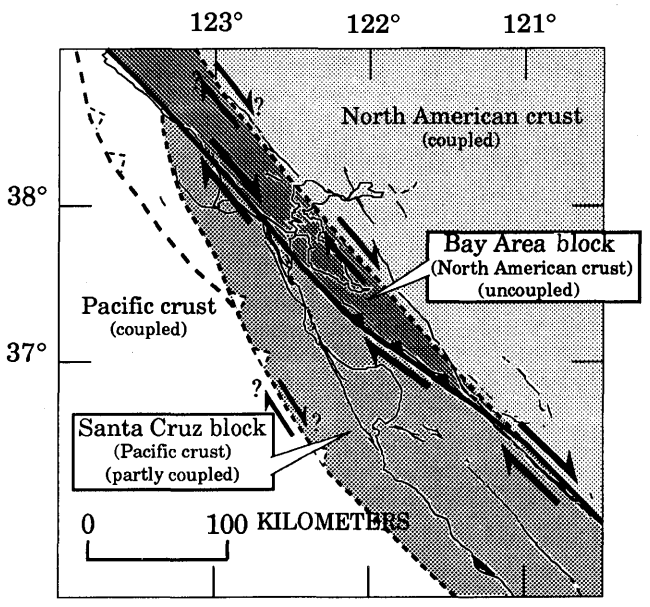

Figure 6.—San Francisco Bay region, showing location and kinematics of crustal blocks in plate-boundary region. Dashed lines, inferred boundaries of crustal blocks, with sawteeth on upper plate. Double arrows indicate directions of fault movement (queried where uncertain). Bay Area block is proposed to be effectively decoupled (along detachment surface shown in fig. 4) from underlying mantle, whereas Santa Cruz Block (which includes both Salinian and San Simeon [Franciscan] terranes) appears to be partly coupled to underlying mantle but undergoes some internal deformation.

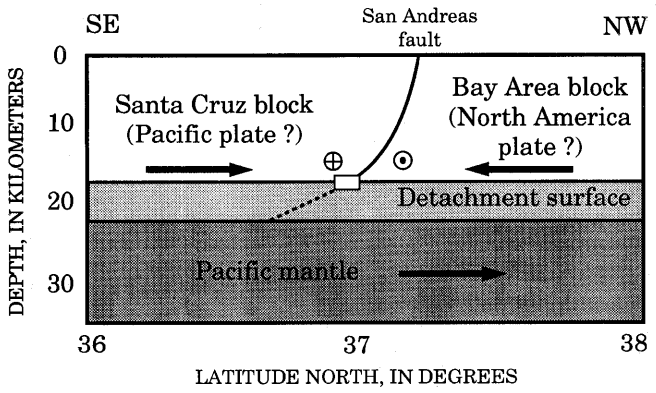

Figure 7.—Schematic cross section of Loma Prieta region, Calif., illustrating kinematics of crustal and mantle components of plate-boundary system (modified from Furlong and Langston, 1990). Arrows indicate directions of relative plate motion given by lithospheric system: bull's-eye, toward viewer; crosshairs, away from viewer. Rectangle, focus of 1989 Loma Prieta earthquake.

Loma Prieta rupture with the location of initial decoupling of the Santa Cruz block from the underlying mantle. We recall that the crustal kinematics of the region includes significant motion/deformation out of the plane of the cross section as the Santa Cruz block is translated westward.

The conceptual aspects of deformation processes shown schematically in figure 7 are supported by the results of fully three dimensional modeling of the dynamics of the plate boundary. The details of this modeling are presented in the next section, and three cross sections applicable to the Loma Prieta region in figure 8. This series of cross sections parallel the relative Pacific-North American plate motion and show the velocity in the plane of the cross section for the 10-year period before the earthquake: Figure 8*A* is located entirely within the Pacific plate west of the plate-boundary-deformation zone; figure 8*B*, which is equivalent to the schematic cross section in figure 7, slices through the plate-boundary-deformation zone; and figure 8*C* is east of the plate boundary entirely, within the North American plate. Figures 8*A* and 8*C* show the displacement fields expected for a well-coupled

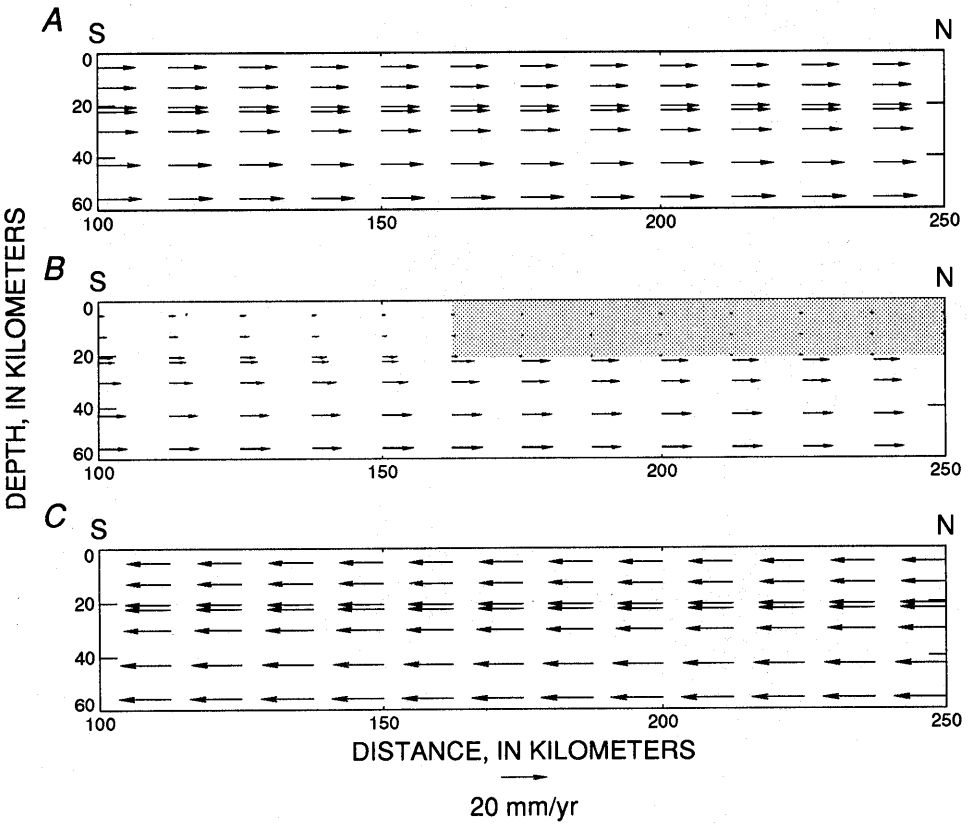

Figure 8.—Velocity field in plane parallel to relative Pacific-North American plate motion. *A*, Cross section entirely within Pacific plate (west of the San Andreas fault), with well-coupled Pacific crust. *B*, Cross section through Santa Cruz and Bay Area blocks, showing partial coupling of Santa Cruz block to underlying mantle. Uncoupling of Bay Area block (shaded area) is shown by velocity differences and large gradient across crustal detachment surface (dashed horizontal line). 1989 Loma Prieta earthquake occurred at transition from Santa Cruz block (unshaded area) to Bay Area block (shaded area). Cross section approximately corresponds to cross section in figure 7. *C*, Cross section entirely within North American plate (east of the San Andreas and east-bay faults), with well-coupled North American crust.

crust-mantle system away from the plate boundary, and figure 8*B* indicates the complex pattern of displacement within the plate-boundary-deformation zone, the transitional behavior of the Bay Area block relative to both Pacific and North American plate displacements, and the abrupt change in crustal motions near Loma Prieta.

The kinematics of the Bay Area and Santa Cruz blocks relative to the larger scale motions of the North American and Pacific plates leads to significant spatial variation in the lithospheric stress regime. In particular, the crust-mantle decoupling (Santa Cruz block from underlying mantle) and the internal strain in the Santa Cruz block near Loma Prieta produced by displacements along the San Andreas fault (for example, in the 1906 San Francisco earthquake) lead to a stress increase in the source region of the 1989 Loma Prieta earthquake. The details of the assumptions and constraints of this modeling are discussed in the next section, and the cross sections in figure 9 show the large spatial variation in shear stress (acting in the horizontal plane—the decoupling shear stress) and the evolution of shear stress in our model from before the 1906 earthquake until just before the 1989 earthquake. The stress that increases with the 1906 earthquake is relaxed in areas where the horizontal detachment surface exists but persists southwest of the San Andreas fault in the Loma Prieta region. The kinematics of the two crustal blocks and the associated crust-mantle decoupling play crucial roles in the generation of the 1989 earthquake, a seismic event that thus reflects both the local effects of plate-boundary geometry and the regional effects of plate motions.

The kinematic model described above provides a framework within which to evaluate, through finite-element modeling, the events that led up to the 1989 Loma Prieta earthquake and the postearthquake effects on the crustal and lithospheric stress regime throughout the San Francisco Bay region. The response of the regional stress field to the earthquake is not static but varies in time and space. In the finite-element model described below, we investigate the first-order effects of the earthquake on patterns of deformation and stress in the San Francisco Bay region. Our results provide additional insight into the possible effects of the earthquake on the seismic potential of other faults in the San Andreas system, as well as a means to relate observations of crustal deformation to the underlying plate-tectonic framework of the region.

MODELING PLATE-BOUNDARY DEFORMATION DURING THE EARTHQUAKE CYCLE

We tested several models of plate-boundary structure and rheology in evaluating the plate-boundary deformation leading up to the earthquake and the subsequent effects on the stress regime along adjacent segments of the San Andreas fault system. In each model, we placed the primary plate boundary through the mantle lithosphere, as shown in figure 5, and focused on the effects of different types of coupling between the crust and underlying mantle. Although the models described here are fully three dimensional, it is easiest to visualize the differences among our three types of models by considering schematic cross sections of each model. The three model geometries (fig. 10) include our preferred (detachment) model, in which a mid-crustal shear zone connects the base of the San Andreas fault through its Santa Cruz Mountains and peninsular sections to east-bay faults and the plate boundary in the lower crust and upper mantle (lithospheric shear zone). This first model contrasts with the second, elastic-crust model, in which all stress transfer between the San Andreas and east-bay faults is simply through the elastic crust (see Simpson and Reasenberg, this chapter, for a similar elastic-crust model under different boundary conditions). Although we do not believe that this model is compatible with the observations of large displacements on the San Andreas fault and the post-1906 transient-deformation pattern, the elastic-crust model is appropriate for the crustal-deformation regime in the San Francisco Bay region. Our third model, here termed the weak-crust model, incorporates a weak (low viscosity) lower crust throughout, where the crust-mantle coupling is reduced but similar everywhere in the region. In the detachment model, we assume that because of strain localization, the shear zones in both the lower crust (horizontal) and lithospheric mantle (vertical) deform by diffusion-creep. In the weak-crust model, the lithospheric shear zone deforms by diffusion-creep, whereas the lower crust (with distributed deformation) undergoes dislocation-creep. In the elastic model, only the lithospheric shear zone deforms by ductile mechanisms (diffusion-creep). Specific parameters for these models are listed in table 1. The values chosen for effective viscosity (and, equivalently, relaxation time) in all the models are appropriate for the inferred thermal conditions and assumed deformation mechanism in the lower crust and upper mantle (for example, Rutter and Brodie, 1988). No data were available for diffusion-creep in lower-crustal rocks, and so we use the same viscosity in the lower-crustal detachment surface as in our mantle shear zone. We believe that this estimate is reasonable for the properties of such a lower-crustal shear zone because the expected increase in viscosity with the lower temperatures at shallower depths will be offset by a decrease in viscosity with the change in composition from mantle to crustal rocks.

FINITE-ELEMENT MODEL

The finite-element program TECTON (Melosh and Raefsky, 1980, 1981) was used in our modeling. This program

allows the use of various rheologies (for example, elastic, viscous, viscoelastic, and so on) and the inclusion of faults of finite dimension that are held locked except during "earthquakes." Earthquakes are simulated in a simple manner: Specified displacements (in three-dimensional space) are applied to the faults (which are unlocked over a specified depth) during the time step of an earthquake. The faults within the seismogenic crust are represented by the split-node technique of Melosh and Raefsky (1981) in the finite-element formulation, allowing us to specify displacements of arbitrary orientation (relative to the orientation of the initial element boundary) during earthquakes. Thus, we can incorporate the strike, dip, and rake for each earthquake simulated. This approach is essentially equivalent to that used by both Bodin

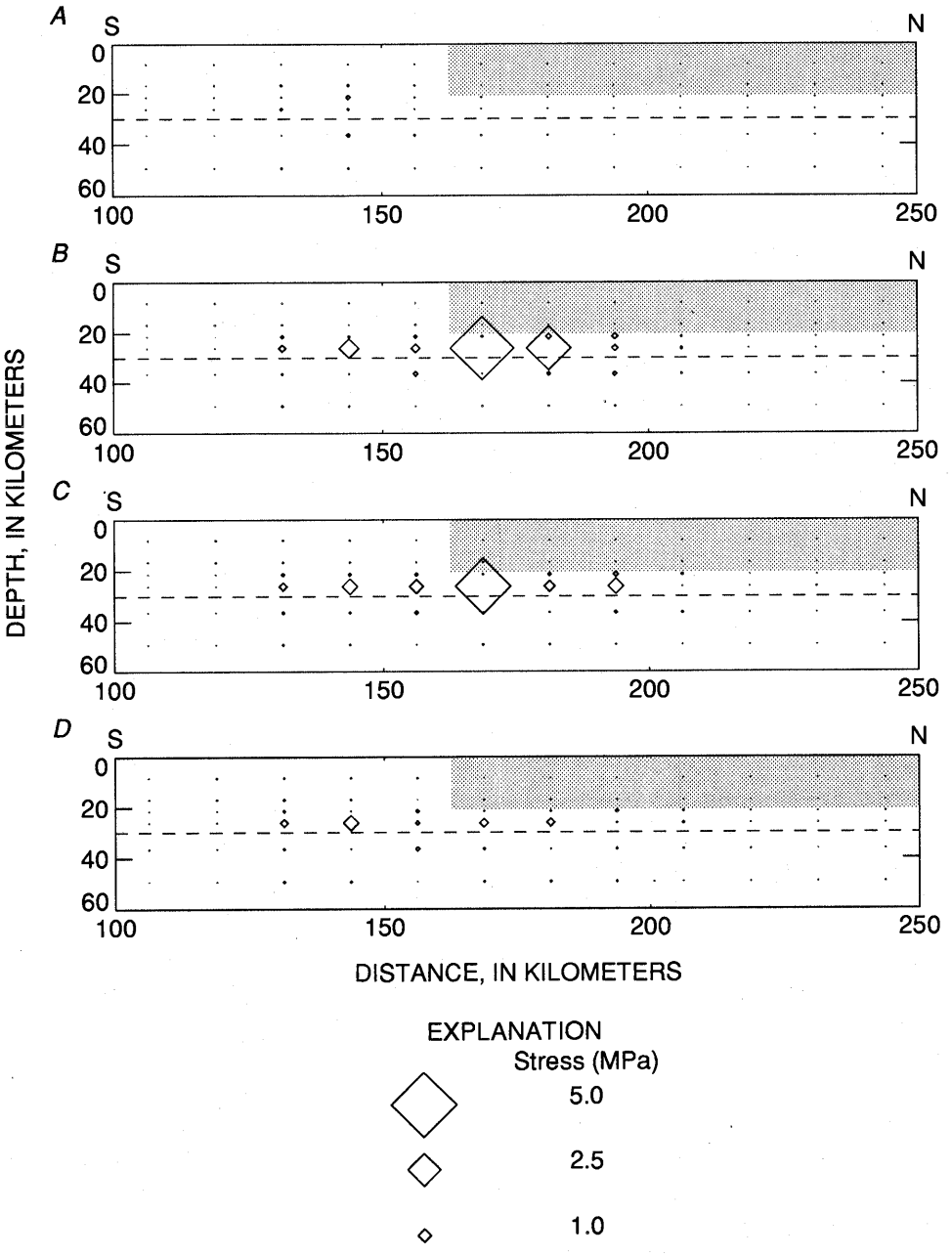

Figure 9.—Horizontal shear stress in detachment model (*A*) before 1906 San Francisco earthquake, (*B*) 10 yr after 1906 earthquake, (*C*) 20 yr after 1906 earthquake, and (*D*) before 1989 Loma Prieta earthquake. Cross sections correspond to those in figures 7 and 8*B*. Shaded area, extent of Bay Area block. Large stresses produced by 1906 earthquake decay rapidly within and below Bay Area block but do not decrease significantly within Santa Cruz block. Accumulation of this shear stress through occurrence of several 1906-type events may lead to less frequent but periodic Loma Prieta-type events.

and Bilham (this chapter) and Simpson and Reasenberg (this chapter).

The 1906 San Francisco earthquake was simulated by 4 m of slip on the entire model length of the San Andreas fault, similar to estimates of average slip over the simulated region (Thatcher, 1975). In this earthquake, fault nodes were unlocked from the surface to a depth of 18 km. This coseismic displacement represents both brittle deformation (0–12-km depth) and rapid postseismic relaxation in the middle crust (for example, Thatcher, 1975). The 1989 Loma Prieta earthquake was simulated by 2.25 m of strike slip and 2 m of dip slip (strike, N. 150° E.; dip, 60°; rake, 138°; total displacement, 3 m), compatible with the range determined by geodetic and seismic studies (Marshall and others, 1991) on a 60-km-long section of the Santa Cruz Mountains section of the San Andreas fault. The slip at Loma Prieta extended to a depth of 18 km but did not include the surface node in the finite-element model, to be consistent with observations of little or no rupture at shallow levels (for example, Langston and others, 1990; Wald and others, 1991). Although the finite-element model shown in figure 11 has a vertical boundary along the Loma Prieta rupture, the split nodes allow us to account to first order for the strike, dip, and rake of the rupture. The result is a representation of the rupture (essentially composed of two "shingled" fault segments) that does not exactly simulate the near-field effects but for all practical purposes adequately simulates the overall displacement patterns observed after the earthquake—both the reverse dip slip on the fault and the vertical and horizontal deformation in the Loma Prieta region. This simple simulation of earthquakes is intended not to provide information on the instantaneous response of the stress regime during and in the immediate vicinity of the earthquake but to evaluate the deformational behavior on the time scale of crust and mantle relaxation.

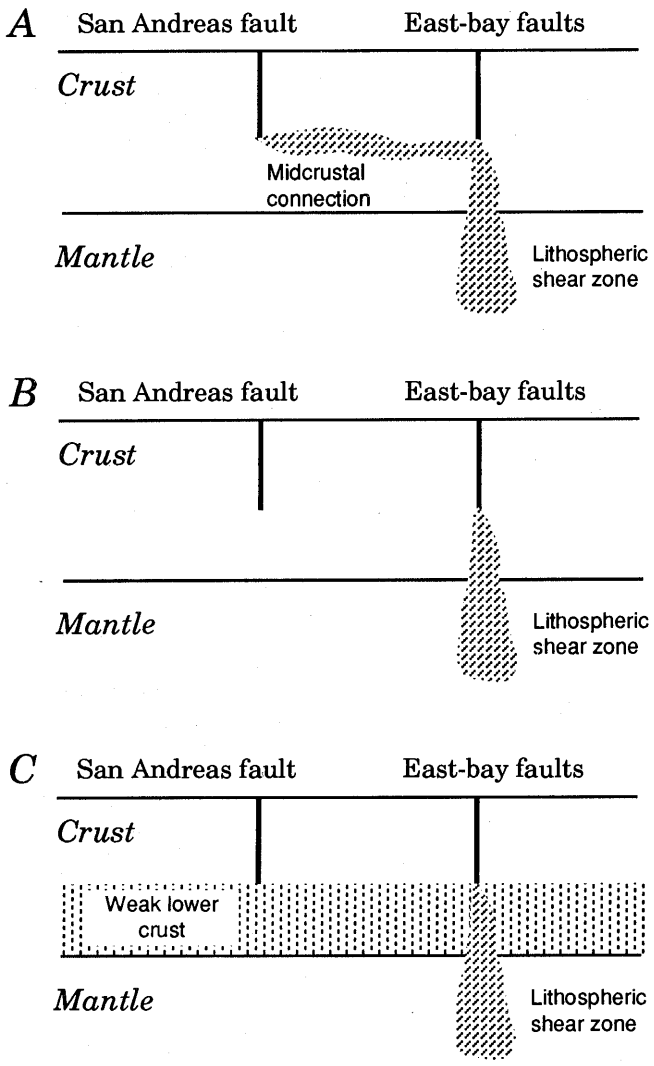

Figure 10.—Schematic cross sections (at approximately latitude of San Francisco) showing three models of plate-boundary structure investigated with finite-element method: (*A*) detachment model, (*B*) elastic-crust model, and (*C*) weak-crust model. Rheologic characteristics of components of each model are listed in table 1. In each figure, location of principal plate-bounding shear zone is beneath east-bay (Hayward, Calaveras) faults. Models in figures 10*B* and 10*C* test rheologies similar to those used by Simpson and Reasenberg (this chapter), although boundary conditions differ somewhat.

The three-dimensional finite-element mesh is composed of 3,080 nodes and 3,192 elements. The global-stiffness matrix contains 8,734,797 terms, with a mean bandwidth of 1,070. A plan view of the mesh is shown in figure 11, with this same horizontal mesh throughout the vertical extent of the model. The shaded area shows the model domain on which we focus our analysis. This region is sufficiently removed from side boundaries to be relatively insensitive to artifacts produced by assumed conditions along the boundaries.

A vertical view of the finite-element mesh and the implementation of the three types of models is shown in figure 12. We have modeled the entire depth of the lithosphere (assumed thickness of the mechanical lithosphere, ~60 km), allowing us to apply what we consider the most realistic boundary conditions for the plate velocities along the sides and bottom of the model. A relative Pacific-North American plate velocity of 40 mm/yr (NUVEL–1 velocity of DeMets and others, 1990, modified by Sierra Nevada-North American motions of Argus and Gordon, 1991) was used for this boundary condition. We believe that the principal deformation associated with the San Andreas fault is driven by far-field plate motions. Such an assumption is easily converted to appropriate side and end boundary conditions. It is less clear, however, how to implement this condition along the base of the model. If basal drag serves to help or hinder plate motion in the Loma Prieta region, the appropriate condition is a specified displacement rate along the base of the model. If basal drag is insignificant near the plate boundary, however, then a free-slip boundary condition should be applied to the base. In our modeling, we tried

Table 1.—*Rheologic parameters for finite-element model*

[E, Young's modulus; η_e, approximate effective viscosity for a strain rate of 10^{-13} s^{-1}. Do., ditto]

Region of model	Material	E (GPa)	Deformation mechanism	η_e (Pa-s)	Relaxation time (yr)
Crust	Granite	70	Elastic		
Crustal shear zone	do	70	Diffusion	5.0×10^{18}	23
Lower crust (weak-crust model).	do	70	Dislocation	5.0×10^{20}	2,300
Mantle	Olivine	100	do	1.0×10^{26}	30×10^{6}
Mantle shear zone	do	100	Diffusion	5.0×10^{18}	23

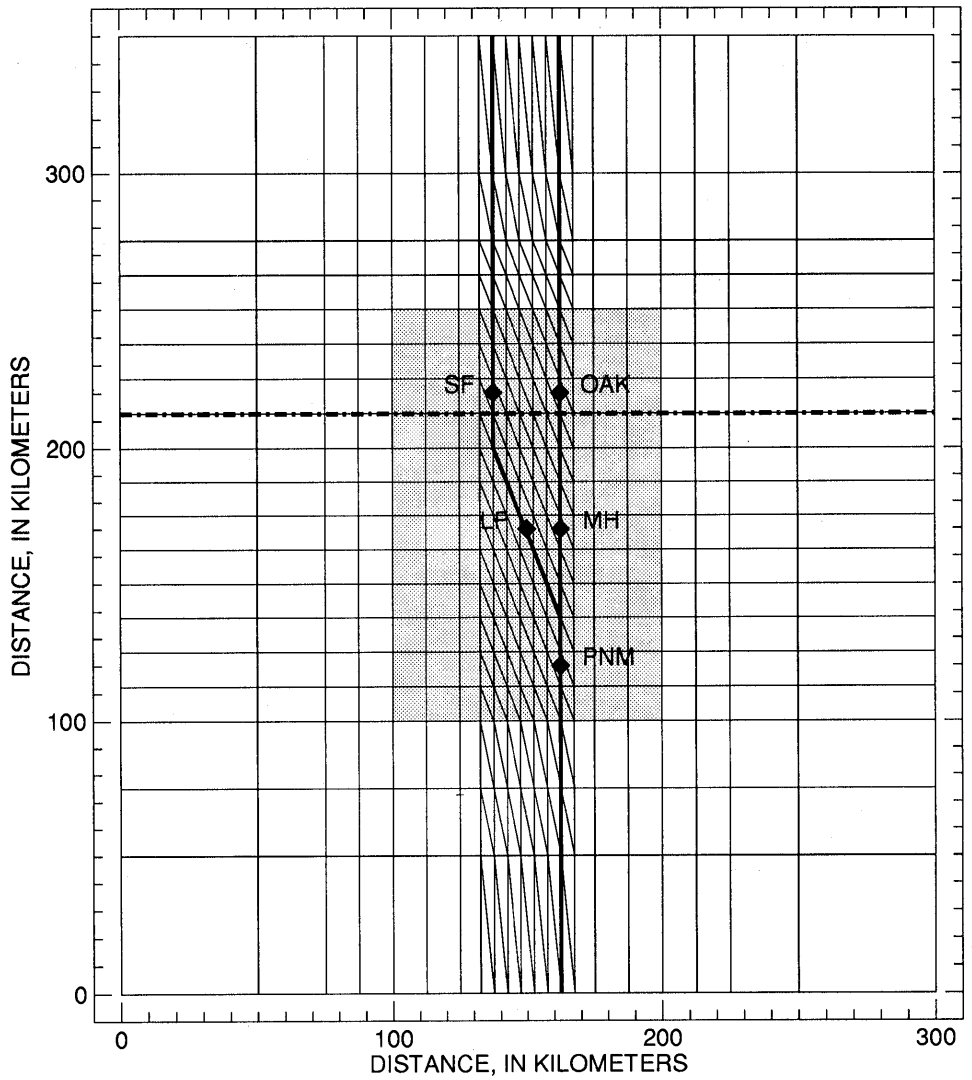

Figure 11.—Plan view of finite-element mesh used in modeling. Shaded area, region of interest in this study. Heavy lines, locations of faults (split nodes) in model, sections of which are displaced during simulated earthquakes; faults extend to depth of 18 km. Diamonds, locations of stresses plotted in figure 14, corresponding approximately to geographic locations of San Francisco (SF), Oakland (OAK), Loma Prieta (LP), Morgan Hill (MH), and Pinnacles National Monument (PNM). Dot-dashed line, location of vertical cross sections shown in figure 12.

various conditions and found that the results for the region of interest (crust and uppermost mantle) are relatively insensitive to the width of the zone at the base of the model under free-slip conditions. In the results shown here, basal conditions of free slip were applied over the distance range 100–200 km in the model coordinates of figures 11 and 12; elsewhere, plate velocities of ±20 mm/yr were applied.

The results of our modeling are shown here in several forms. In these three-dimensional time-dependent models, complete descriptions of both the stress and strain fields are available at all points for all time steps. Interpreting such results is a daunting task, and so we have tried to distill these results into a suite of figures that contain the fundamental aspects and implications of our modeling. The results are shown in two forms, stress and velocity, for each of the three models in figures 13 through 19. The stress field is presented in two ways. Along the faults, the fault-parallel shear stress is shown at specific times throughout the earthquake cycle (pre-1906 to post-1989), providing some insight into the interaction of the stress field among fault segments and the spatial variation of the stress regime. We emphasize that the faults are not necessarily the sites of maximum shear stress but are reasonable places to consider in each model because they represent regions that have failed repeatedly in earthquakes (see Linker and Rice, in press; Bodin and Bilham, this chapter; Simpson and Reasenberg, this chapter). In addition, the stress histories at the sites indicated in figure 11 are shown throughout the model history. Such stress histories provide a means to investigate both the relaxation phase of crustal deformation and the coseismic and postseismic interaction of the various fault segments.

The results for the deformation field are shown in terms of velocities throughout the earthquake cycle. In most of

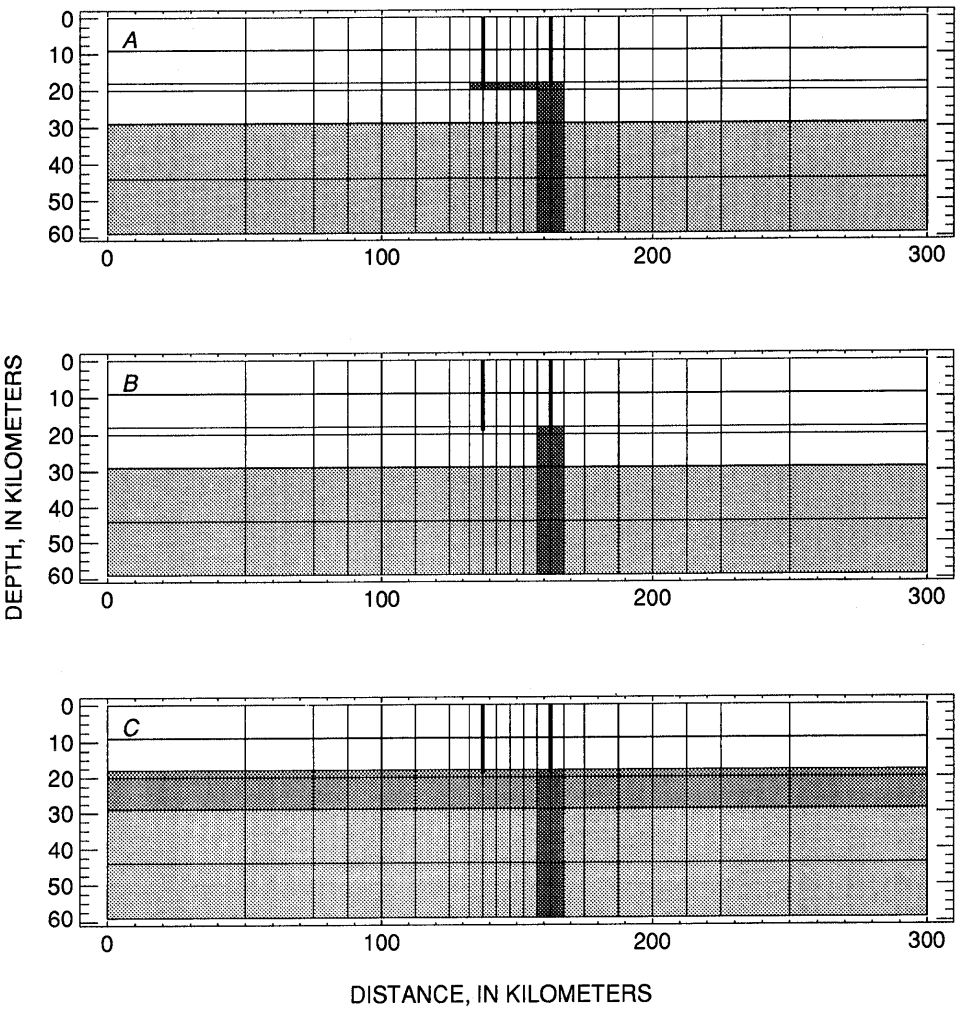

Figure 12.—Cross-sectional views of finite-element mesh (fig. 11), showing implementation of three models shown in figure 10: (*A*) detachment model, (*B*) elastic-crust model, and (*C*) weak-crust model. Heavy lines, faults; dark-shaded area, shear zones; medium-shaded area (fig. 12*C*), lower crust; light-shaded area, viscoelastic mantle. Rheologic parameters assigned to various elements are listed in table 1.

the figures, the difference between the upper-crustal and lithospheric-mantle velocity fields is shown. We followed this approach because the velocity difference highlights locations where crustal displacement/deformation differs from that of the underlying mantle: Regions of the crust well coupled to the underlying mantle appear as regions of minimum velocity difference, and regions with large velocity-difference vectors are sites of significant stress accumulation in the lower/middle crust and (or) decoupling between the crust and underlying mantle. To allow for the application of these results to observations of crustal displacement/deformation, we also show some results for surface velocity. This presentation helps delineate target areas where the deformation response allows discrimination among the assumptions of the various models.

STRESS HISTORY

The results shown here encompass the effects of both the 1906 San Francisco and 1989 Loma Prieta earthquakes. Results are shown in each model for the time period beginning about 10 yr before the 1906 earthquake until about 20 yr after the 1989 earthquake. Note that the model "runs" for approximately 500 yr before the 1906 earthquake in an attempt to prestress the regime, so that the coseismic and postseismic strain relaxation occur in conjunction with a simulation of the inherited stress field, as is necessary for consideration of viscous relaxation because strain rates are proportional to stress levels. Our prestress conditions should be seen simply as an attempt to incorporate first-order effects. We have omitted all events during the 1800's, partly because of the large uncertainties in their location, rupture characteristics, and extent. As shown in the figures, the effects of the 1906 earthquake are still significant at the time of the 1989 earthquake; however, any effects of smaller events before 1906 were probably overwhelmed by 1906 displacements. Because the continuously deforming lithospheric shear zone is located beneath the east-bay faults, that region accumulates the largest stresses which are not significantly relieved by 1906 displacements. During the prestress period, all the faults are locked, and stress accumulates everywhere in conjunction with strain on the lithospheric shear-zone plate boundary (and on the lower-crustal detachment surface and (or) weak lower crust, where present). In the simplified geometry of our models, surface faults generally parallel the plate boundary, except for the Santa Cruz Mountains section of the San Andreas fault. As a result, we monitor shear stress in the plane oriented along the fault, although the shear stress on any plane can be calculated from our results (full stress tensor computed). Thus, the effects of such situations as fault-normal compression can be evaluated, if desired, by resolving the stress tensor onto the appropriate planes.

The results for fault-parallel shear stress at both the base of the seismogenic layer (that is, base of the locked fault) and in the lower crust (that is, above the crust-mantle boundary) in the three models are illustrated in figure 13, and the corresponding stress histories at the sites identified in figure 11 are plotted in figure 14. With the inclusion of a detachment surface within the lower/middle crust connecting the peninsular and east-bay fault segments, the stress on the peninsular section of the San Andreas fault in the detachment model is increased relative to that in both the elastic- and weak-crust models. In all the models, shear stresses on the peninsular section of the San Andreas fault are lower than on the east-bay faults. A first-order result of this and previous modeling (Verdonck and Furlong, 1992) is that the apparent role played by the peninsular section of the San Andreas fault as the major plate-bounding fault in the San Francisco Bay region implies that this fault section must somehow be weaker than the east-bay faults because it appears to fail at lower fault-parallel shear stresses.

Comparing the results shown in figures 13 and 14, we see that the detachment model produces a stress field which differs from those in the other two models in several important ways. First, as mentioned above, the detachment model produces the highest stresses on the base of the locked Santa Cruz Mountains and peninsular sections of the San Andreas fault. Second, the detachment model allows the stress (on the peninsula section) that is transferred to the lower crust during the 1906 earthquake to be relaxed postseismically, whereas such stress cannot be relaxed in the elastic- or weak-crust model. Clearly, the elastic-crust model contains no deformation mechanism to relax the stress.

The minimal stress relaxation in the weak-crust model results from the characteristics of the crust in the Loma Prieta region, which, though weak relative to the upper crust and underlying upper mantle, still has a characteristic viscous-relaxation time of thousands of years (consistent with lower-crustal temperatures in the range 300–400°C and a dislocation-creep deformation mechanism). Although a lower viscosity for the entire lower crust would allow stress relaxation over interseismic time intervals, such a low viscosity would imply unreasonable temperatures in the lower crust. We cannot solve this problem by assuming that diffusion-creep acts throughout the entire lower crust as a "weaker" deformation mechanism. Diffusion-creep, which is grain-size dependent, requires regions of highly reduced grain size (such as localized shear zones) to operate. We do not believe that such wholesale lower-crustal grain-size reduction is likely for the crust in the San Francisco Bay region. The existence of a weak shear zone within the lower crust in the plate-boundary region (deforming by diffusion-creep), however, does allow plate motions without substantial stress accumulation and is consistent with the temperature regime and deformation history.

The stress histories during the earthquake cycle shown in figure 14 provide insight into the effects of the 1906 San Francisco earthquake on the other fault segments and the possible stress loading caused by the 1989 Loma Prieta earthquake. In all three models, the 1906 earthquake causes a decrease in shear stress (acting in the vertical plane along the fault strike) at all sites. This stress drop is greatest along the fault segments that ruptured in 1906 but is also evident at the east-bay sites (MH, OAK, fig. 11). In the elastic- and weak-crust models, the stress drop associated with the 1906 earthquake places the peninsular section of the San Andreas fault into a left-lateral stress regime (that is, the stress drop is larger than the preevent stress). This result appears to be incompatible with contin-

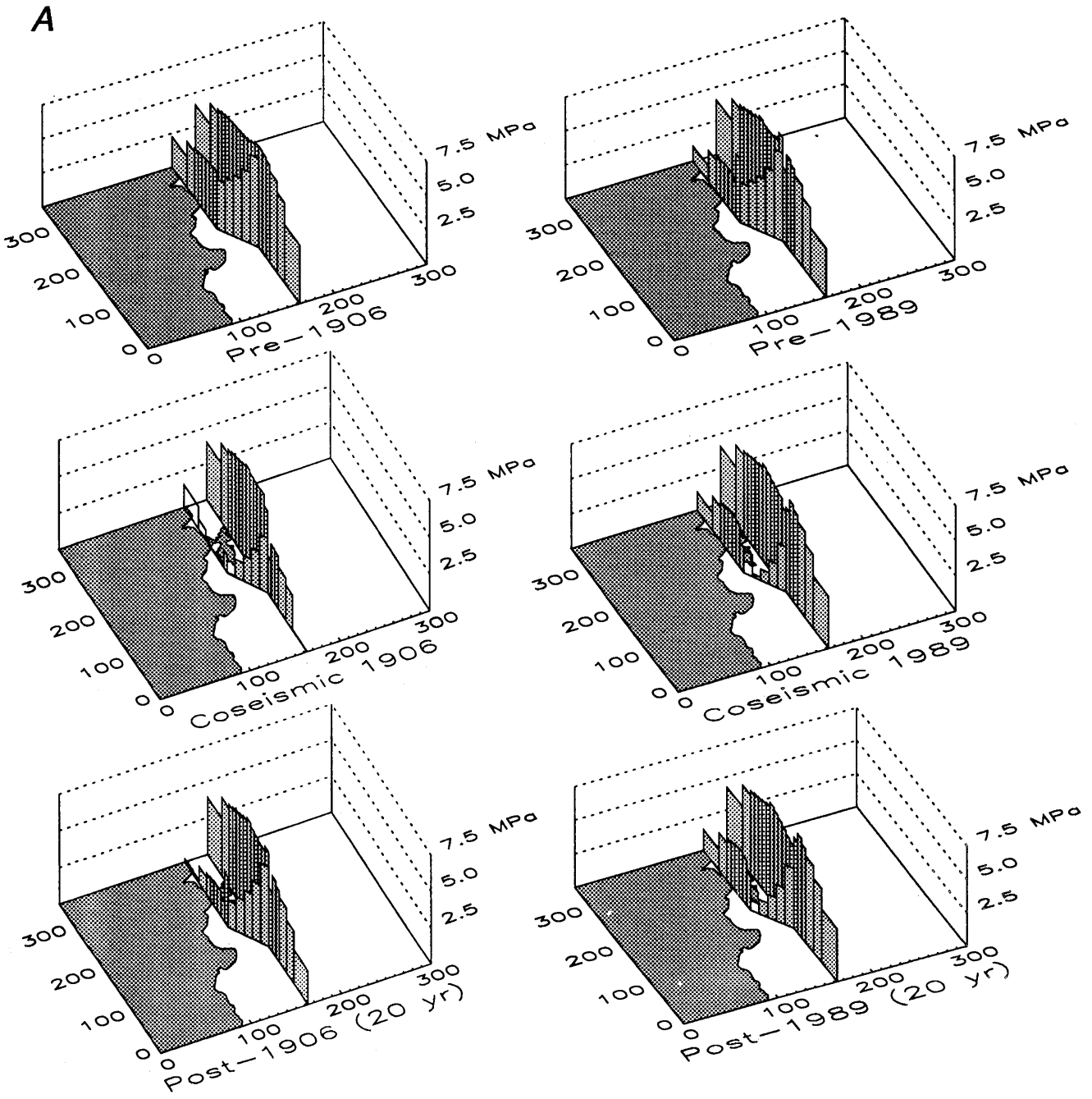

Figure 13.—Stress regimes at specific times in earthquake cycle in (*A*) detachment model, (*B*) elastic-crust model, and (*C*) weak-crust model, showing fault-parallel (horizontal) shear stress along segments of major faults in the San Francisco Bay region at base of seismogenic layer (18 km deep) but above detachment surface (left half) and in lower crust above crust-mantle boundary (right half). Shaded rectangles, segments with right-lateral stress; unshaded rectangles, segments with left-lateral stress. All distances in kilometers from arbitrary origin.

ued right-lateral postseismic stress relaxation (Thatcher, 1975) but may reflect an underestimation of the pre-1906 stress regime. Such a result is not obtained in the detachment model, because pre-1906 stresses (boosted over the stresses in both the elastic- and weak-crust models by strain transfer across the detachment surface) are comparable to the 1906 stress drop along the peninsular section of the San Andreas fault. In both the elastic- and weak-crust models, the stress increase in the Loma Prieta region after the 1906 earthquake is minimal, and relative stresses at the time of the 1989 earthquake are quite low. The detachment model shows a somewhat greater stress increase and higher stresses in the Loma Prieta region (see fig. 9 for depth/time patterns of stress in the horizontal plane in the Loma Prieta region), reinforcing the concept that the 1989 earthquake is more likely representative of a release of horizontal decoupling stresses rather than a typical San Andreas-type strike-slip event.

The 1989 Loma Prieta earthquake was significantly smaller than the 1906 San Francisco earthquake, and so

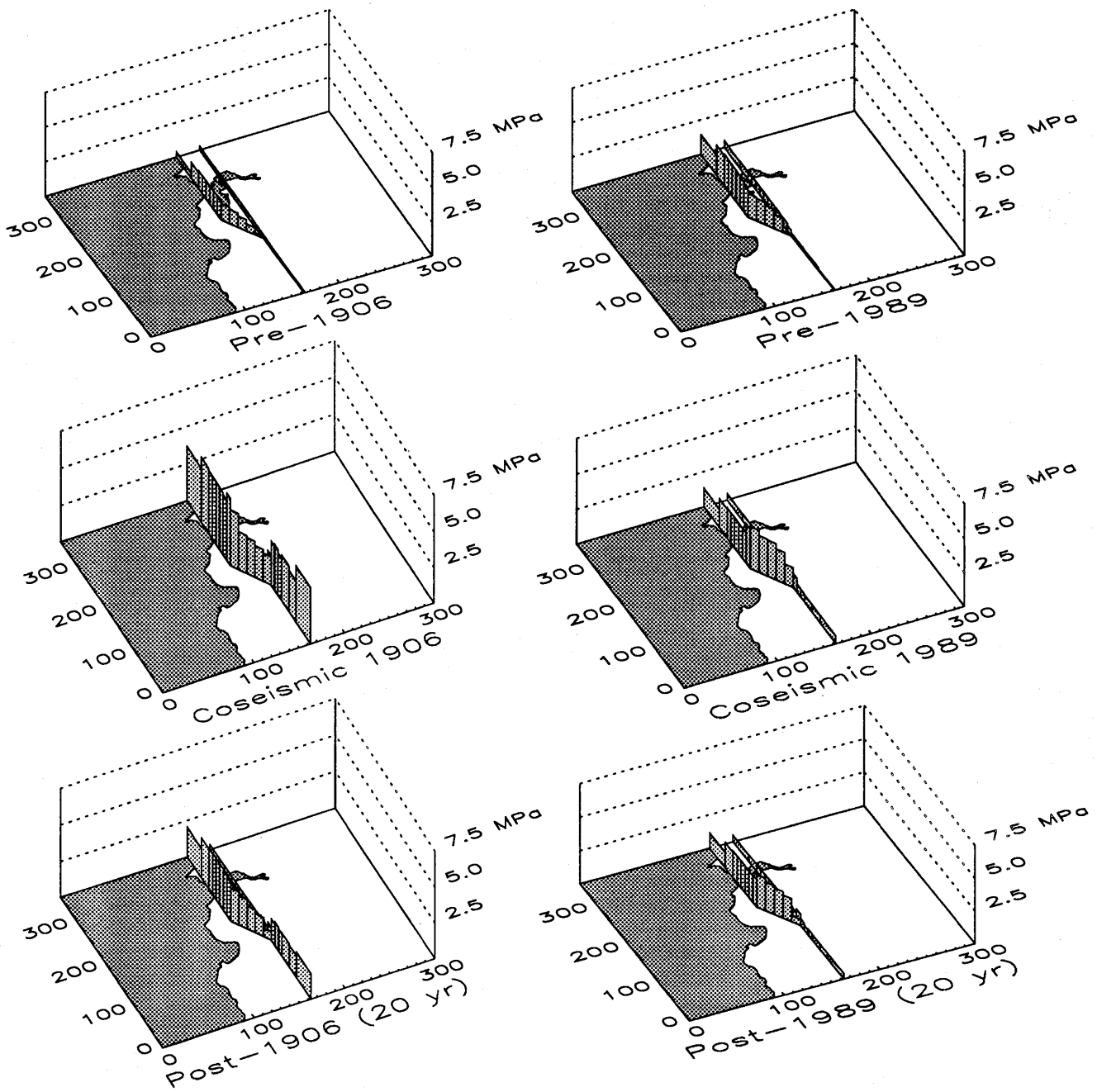

Figure 13.—Continued.

the effects of the 1989 earthquake on the regional stress field are reduced over those in 1906. However, as a result of the more complex rupture geometry (dipping fault, no surface rupture), the pattern of stress response in 1989 is more complex than in 1906. The 1989 earthquake produces a stress drop at Morgan Hill (MH, fig. 11) but no effect or a stress increase at the other sites. The effect on the peninsular section of the San Andreas fault is relatively minor but shows a slight increase in the detachment model. The stress changes from the 1989 earthquake are small (≤1 MPa), and so it is hard to imagine that they alone can trigger paired earthquakes. What may be more important than the actual decrease or increase in stress associated with the 1989 earthquake (because the changes are small) is the change in stress patterns. Although this change is quite small and must be validated by more complete modeling studies, the 1989 earthquake changed the relative stress levels along both the east-bay faults and the

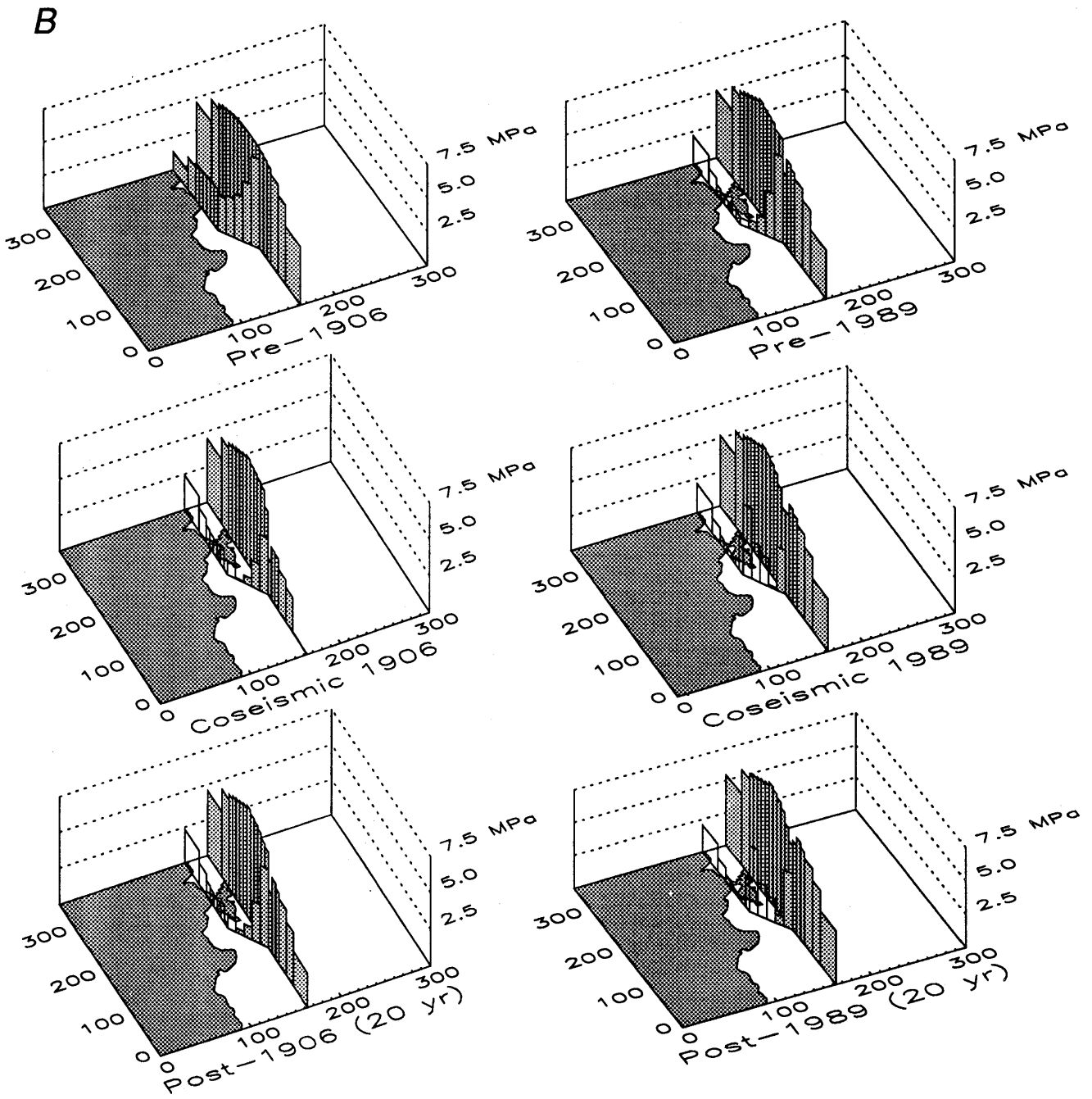

Figure 13.—Continued.

Santa Cruz Mountains and peninsular sections of the San Andreas fault. Just before the earthquake, Oakland (OAK, fig. 11) shows a minimum stress, and Morgan Hill (MH) and Pinnacles National Monument (PNM) slightly higher stresses. After the 1989 earthquake, however, Morgan Hill shows a minimum stress, Oakland effectively no change, and Pinnacles National Monument a higher stress. How this result may relate to future earthquakes is not entirely clear, because earthquakes are not simply a consequence of crustal stresses, although it is tempting to speculate that changes in stress patterns may play an important part in the earthquake cycle along the San Andreas fault in the San Francisco Bay region.

As briefly discussed earlier, the initiation of the Loma Prieta rupture and the style of faulting may be largely controlled by decoupling of the Santa Cruz block from the underlying mantle (which continues to move in the direction of relative plate motion). The shear stress in the horizontal plane along a profile parallel to plate motion through the Santa Cruz Mountains (approximately the

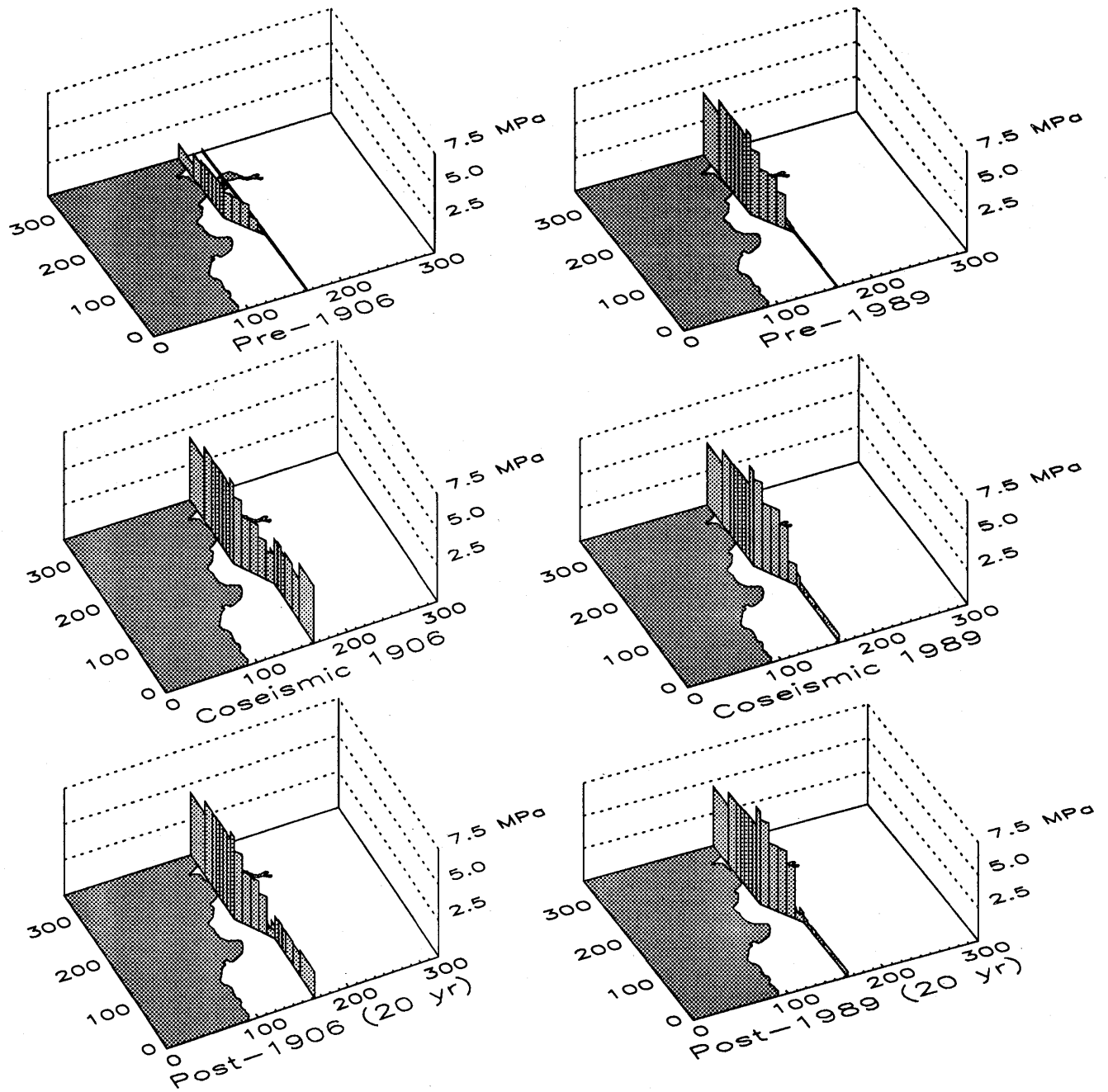

Figure 13.—Continued.

stress component that would produce an initial decoupling event) is shown in figure 9. This stress is largest in the vicinity of the focus (or slightly south) of the 1989 earthquake, and so it may reflect the stress regime that initiated the Loma Prieta rupture. In the sequence shown in figure 9, this stress results from the displacements associated with the 1906 earthquake, but is not substantially relaxed during the interseismic period. A series of 1906-type events can thus lead to a significant increase in this stress component, generating less frequent (but still quasi-periodic) Loma Prieta-type events.

VELOCITY FIELD

The various models produce different results for the evolution of the stress regime. Although the results may be most directly applicable to understanding the earthquake

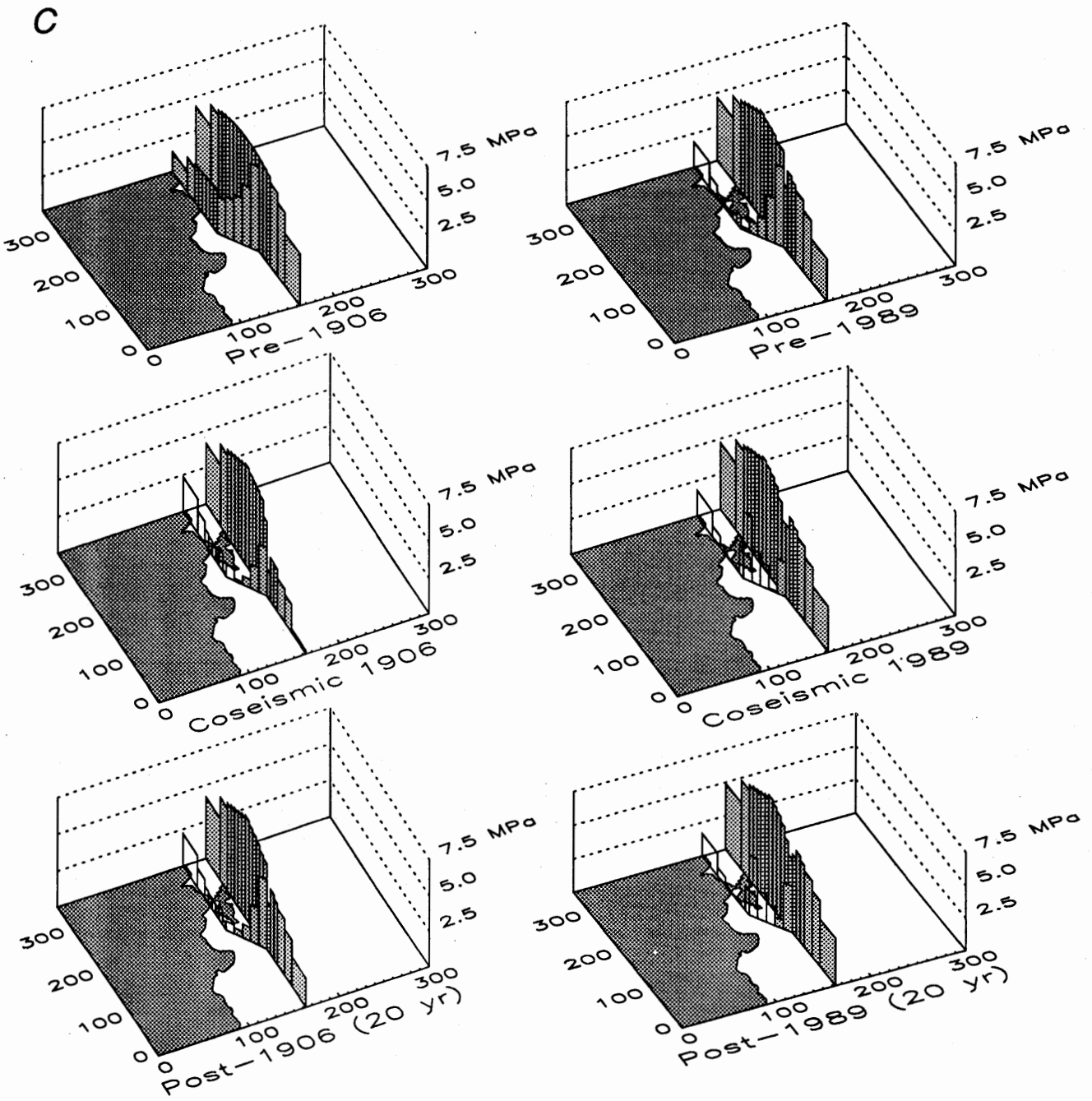

Figure 13.—Continued.

process in the San Francisco Bay region, stress observations (particularly magnitude) are difficult, and so these results cannot easily be compared directly with observations. We can, however, directly observe the displacement field. Excellent data describing the behavior of the crust in the San Francisco Bay region have been collected since 1900 (see Lisowski and others, 1991 for a recent synthesis) and can provide constraints on and, possibly, distinguish among the various models. Time-dependent finite-element modeling provides results on the displacement history of all nodes in the mesh. To focus on the component of crustal displacement that differs from the overall plate-boundary behavior (as given by the displacement history of the lithospheric mantle), we present our results in the form of the velocity difference between the upper crust and the mantle. We use velocity rather than strain simply for ease in relating the results to plate-boundary processes. The velocity fields in the various models for the interval from just before the 1906 earthquake until approximately 20 years after the 1989 earthquake are plotted in figure 15.

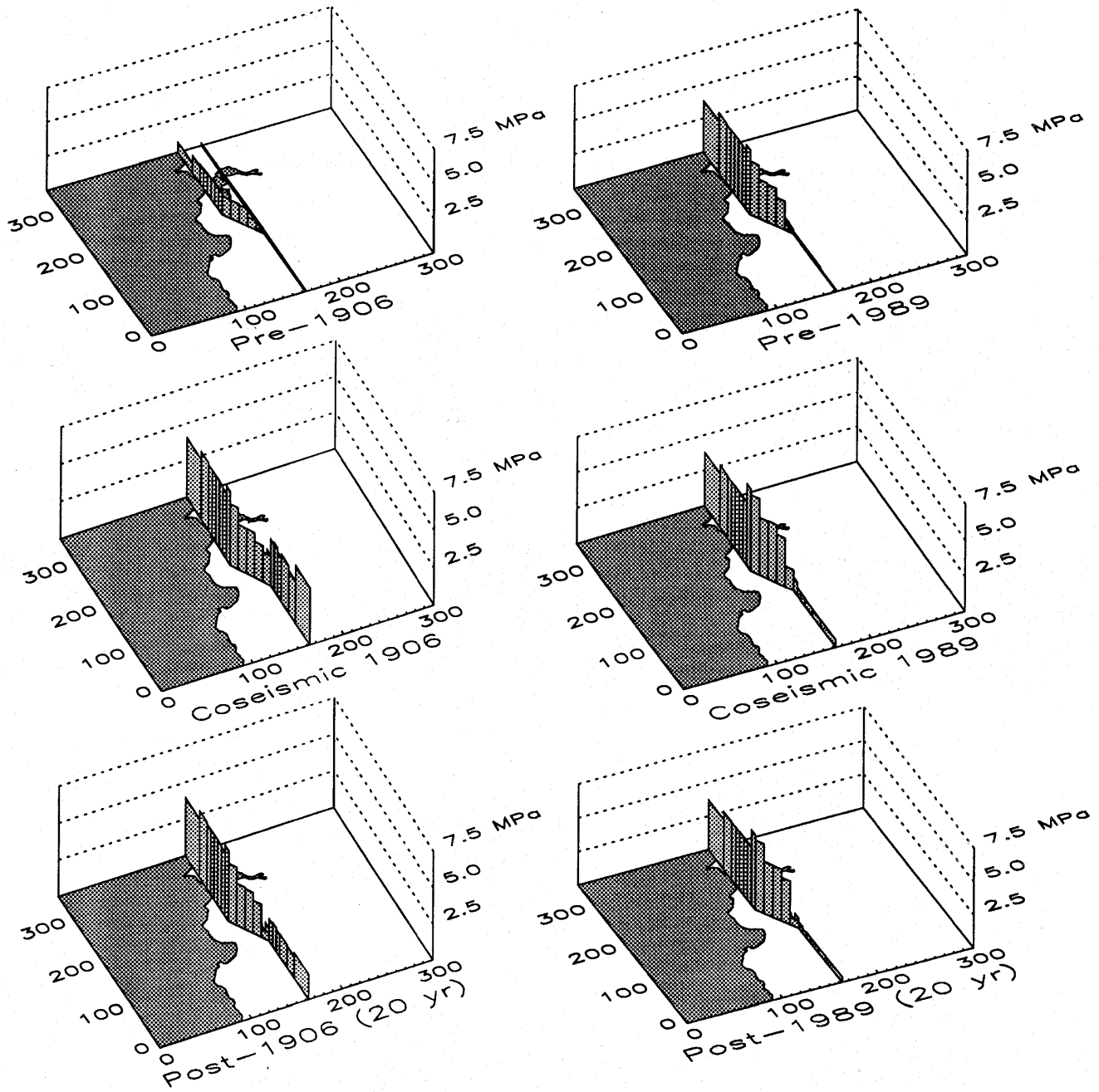

Figure 13.—Continued.

The behavior of the velocity field changes drastically throughout the earthquake cycles studied here. Under the assumptions of the detachment model, the velocity of the Bay Area block (see fig. 6) differs substantially from that of the underlying mantle. Thus, a substantial gradient in velocity difference exists across the San Andreas fault between the Bay Area and Santa Cruz blocks during interseismic periods (after loading by the 1906 earthquake). The detachment model also produces a Bay Area block that undergoes relatively little internal deformation (that is, velocity-difference gradients across the block are small) relative to the other models. This result is consistent with

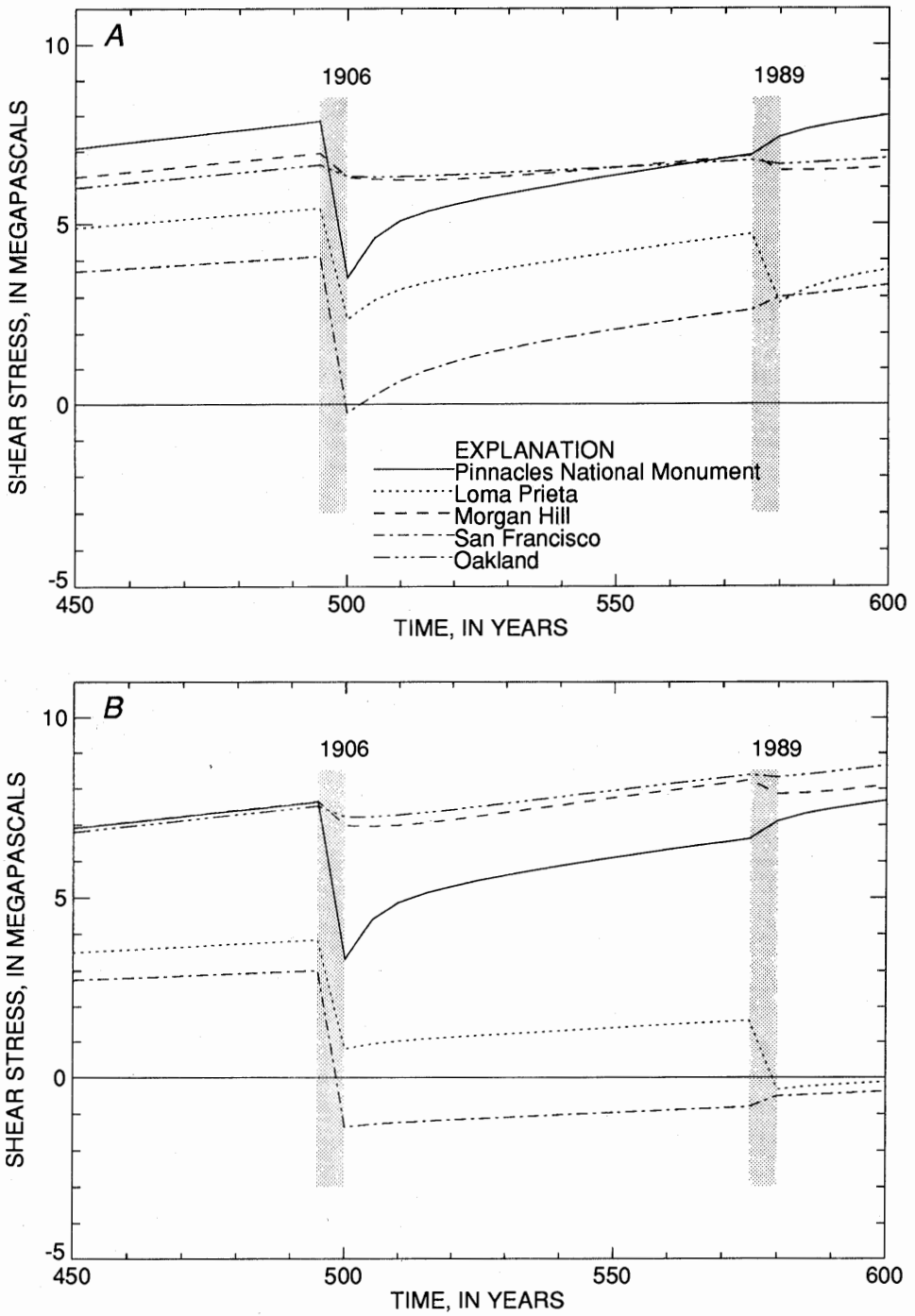

Figure 14.—Stress histories at base of seismogenic layer in (*A*) detachment model, (*B*) elastic-crust model, and (*C*) weak-crust model. Curves correspond to sites identified in figure 11. Shaded bars, intervals of "earthquake" slip. Time scale begins 500 yr before 1906 San Francisco earthquake; time step, 5 yr.

the observation by Fox (1983) of the absence of deformation of his Sebastopol block relative to the adjacent North American crust in the region north of San Francisco Bay. In general, as might be expected, the detachment model produces a deformation field in which the Bay Area block behaves differently from the adjacent Santa Cruz block or the North American plate, whereas the other models show the Bay Area block behaving similarly (except during coseismic periods) to the adjacent Santa Cruz block.

Of particular interest in these results are the differences in the models for the coseismic and postseismic responses to the 1989 earthquake. The first 5- to 10-yr period after the 1989 earthquake will provide the opportunity to differentiate among the possible plate-boundary scenarios. To clarify these effects, surface velocity (rather than velocity difference) for the Loma Prieta region during the post-1989 period is plotted in figure 16. Velocity profiles (perpendicular to the plate boundary) of the south bay and Loma Prieta region for the pre-1906, pre-1989, and post-1989 periods are plotted in figures 17, 18, and 19, respectively. Such results can be used in conjunction with geodetic observations to constrain the model parameters and assumptions. Both the elastic- and weak-crust models rapidly return to interseismic deformation patterns (see figs. 15*B*, 15*C*), whereas with the inclusion of a detachment surface, deformation in the south bay and Loma Prieta region is significantly altered by the 1906 earthquake, and the post-1906 transients in conjunction with the Loma Prieta stress relaxation produce strain patterns quite different from those in the elastic- and weak-crust models.

The critical period for distinguishing the effects of the 1989 earthquake is the first 5 to 10 yr after the event. In the elastic- and weak-crust models, the deformation pattern is essentially equivalent for all three periods shown (figs. 17–19). The detachment model, however, shows three quite distinct deformation patterns. For the pre-1906 period (equivalent to very late in the earthquake cycle), the effects of a detachment surface are minimal, and the patterns are nearly identical to those in the other two models (fig. 17). The effects of the 1906 earthquake are substantial in the detachment model and continue to affect the deformation pattern up to the time of the 1989 earthquake (fig. 18). A signal of the 1989 earthquake included in the overall response that is visible in the 5-yr post-1989 model (figs. 16, 19) can distinguish it both from the deformation patterns in the other models and from the post-1906 effects. Variations in the displacement rate of about 2 to 3 mm/yr that are also visible, primarily near Loma Prieta (southern part of the Bay Area block and vicinity of east-bay faults), will require detailed observations in that area over the critical period. Although the results plotted in figure 19 indicate patterns for a single profile, the spatial variation in the displacement field visible in figure 16 should help to delineate the earthquake response.

DISCUSSION

Combining our understanding of the three-dimensional plate-boundary structure and kinematics with numerical

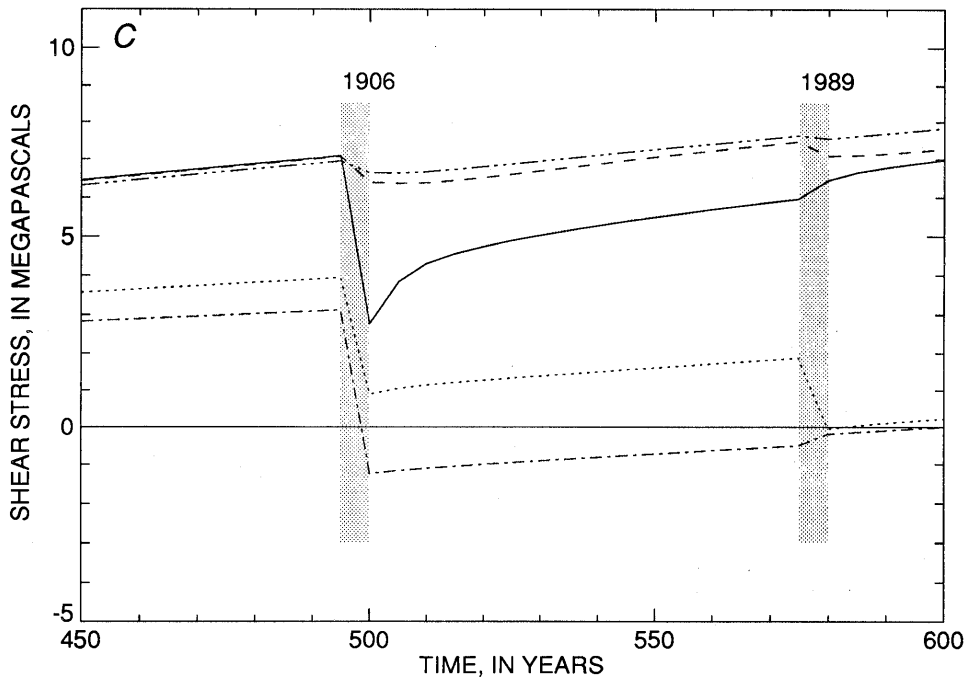

Figure 14.—Continued.

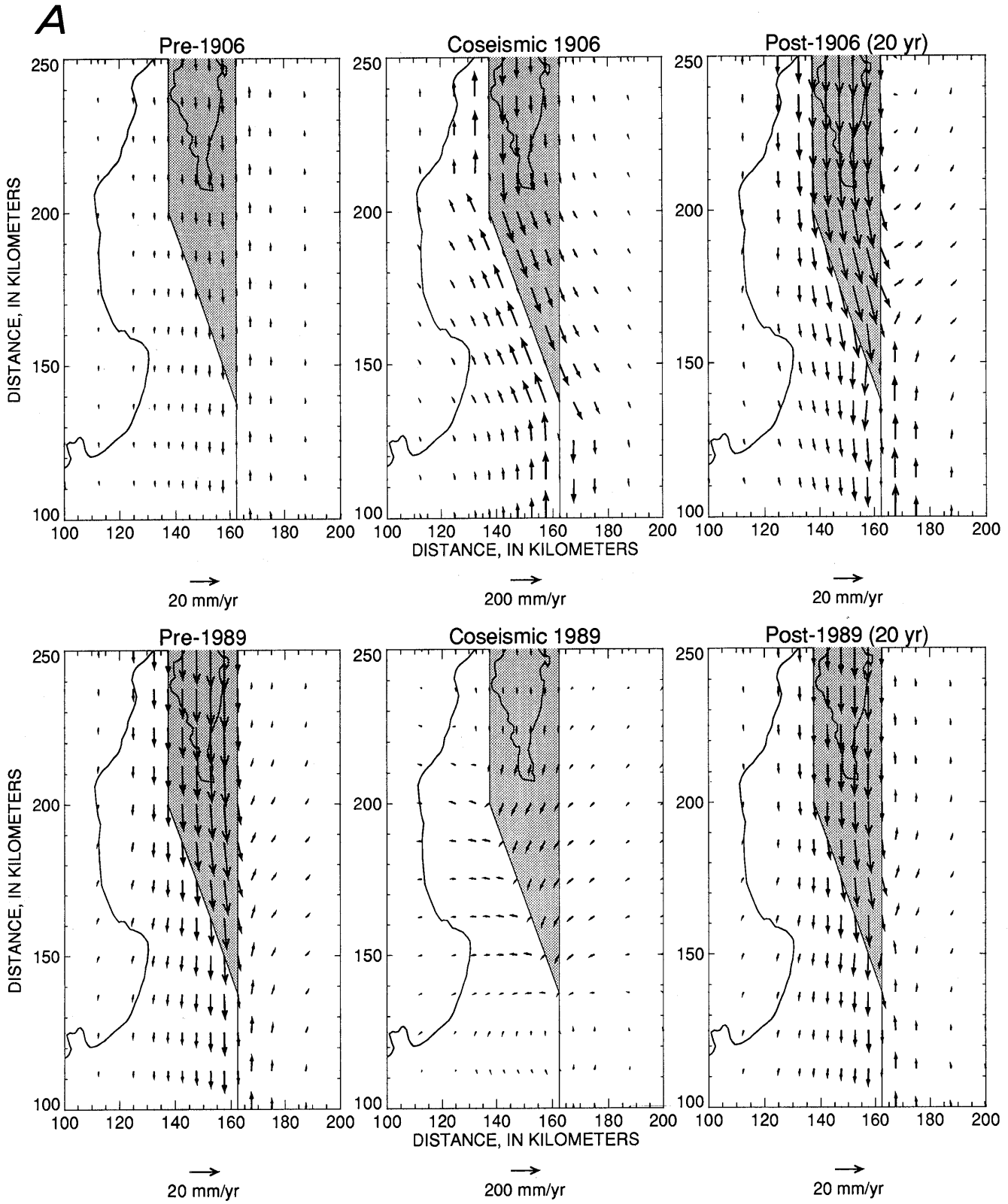

Figure 15.—Velocity-difference fields during earthquake cycle in (*A*) detachment model, (*B*) elastic-crust model, and (*C*) weak-crust model. Shaded area, Bay Area block. Velocity vectors are plotted as difference between upper-crustal and upper-mantle velocities (V_{crust}–V_{mantle}). Vectors shown for coseismic periods are scaled by a factor of 10 to those shown for interseismic periods.

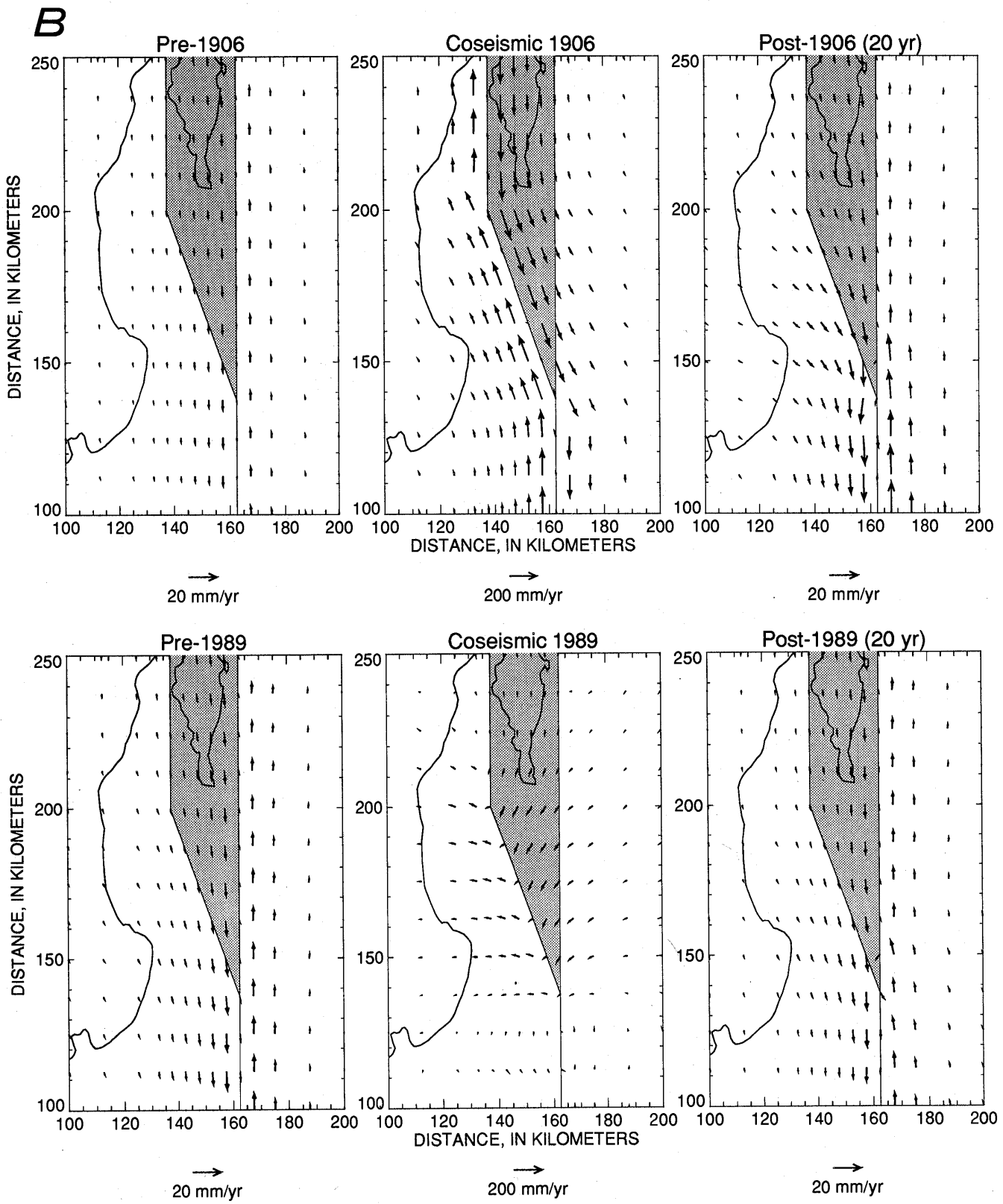

Figure 15.—Continued.

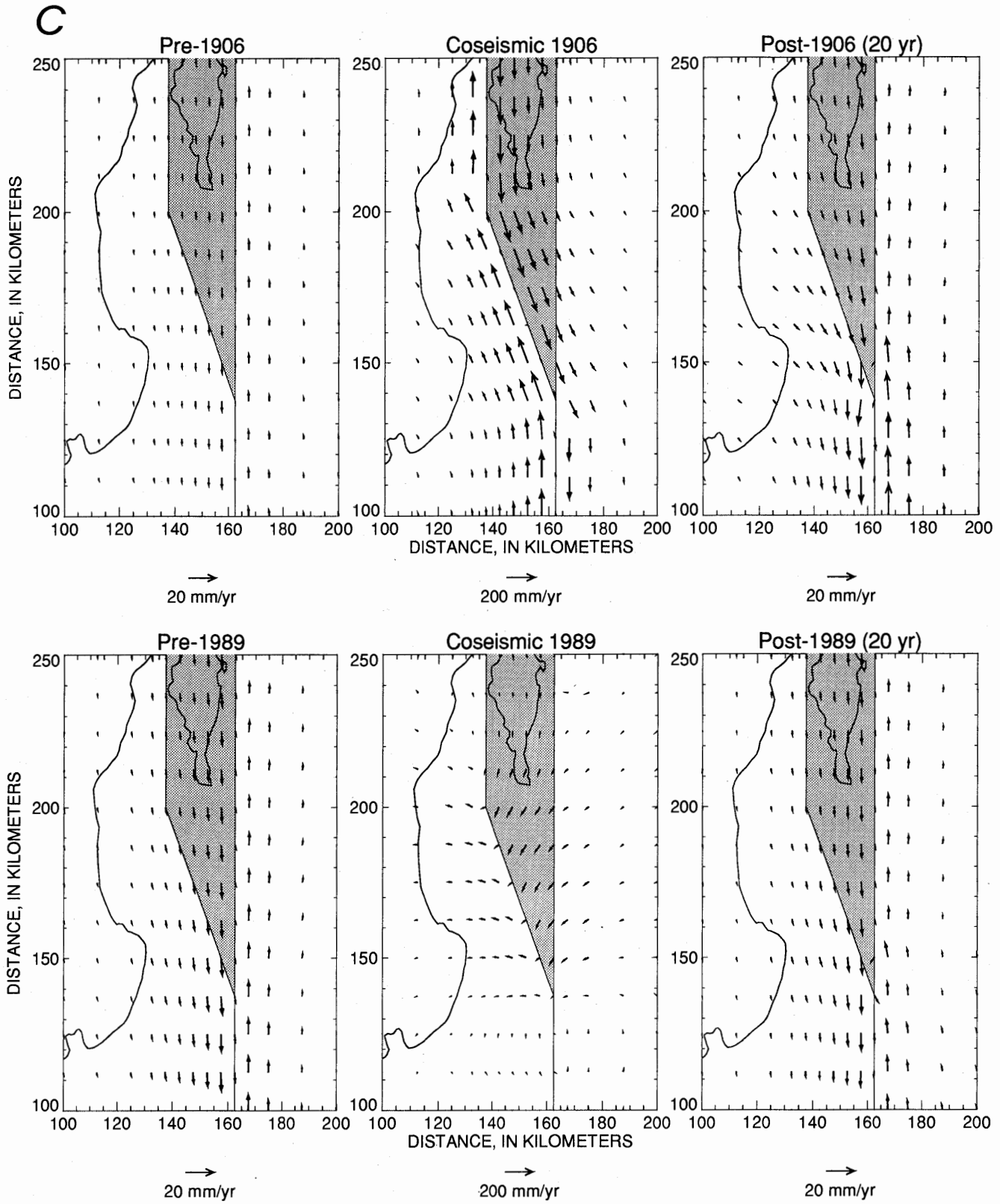

Figure 15.—Continued.

modeling of the stress and deformational response of the lithosphere to earthquakes along the San Andreas fault system provides insight into the causality of the 1989 Loma Prieta earthquake. First, viewed from the perspective of our model of three-dimensional plate kinematics and stress loading after the 1906 San Francisco earthquake, the occurrence of the 1989 earthquake can be considered to be associated with decoupling of the Santa Cruz block from the underlying mantle, rather than simply as a smaller version of the 1906 earthquake. Such events as the 1906 earthquake lead to stress accumulation within the crust in the Santa Cruz Mountains section of the San Andreas fault. These stresses produce crustal deformation (growth of the Santa Cruz Mountains) and in the detachment model are largely relieved by postseismic creep at the base of the Bay Area block (for the region north and east of the San Andreas fault), resulting in a large stress accumulation in the middle crust south and west of the San Andreas fault and a substantial stress gradient across the San Andreas fault in the Santa Cruz Mountains. Second, particularly when incorporating the transient response to an earthquake, it is important to evaluate the deformational effects of the 1989 earthquake in concert with the deformation associated with the 1906 earthquake and with larger scale plate motions, as seen in lithospheric deformation. Models of viscous deformation after an isolated Loma Prieta-type event (without a strain history) will not include the effects of continuing post-1906 relaxation. Third, during the first 5- to 10-yr period after the 1989 earthquake, observations of crustal deformation can provide important constraints on the details of the three-dimensional structure and rheology of the plate boundary in the San Francisco Bay region. In particular, the behavior of the Bay Area block relative to both the North American plate and the Santa Cruz block during this period differs considerably in each of the models tested here. Detailed observation can help to test and calibrate the assumptions in the various models, allowing the results to be more confidently applied to tectonic models of the earthquake cycle in the Loma Prieta region.

The occurrence of the 1989 Loma Prieta earthquake along a segment of the San Andreas fault system that also

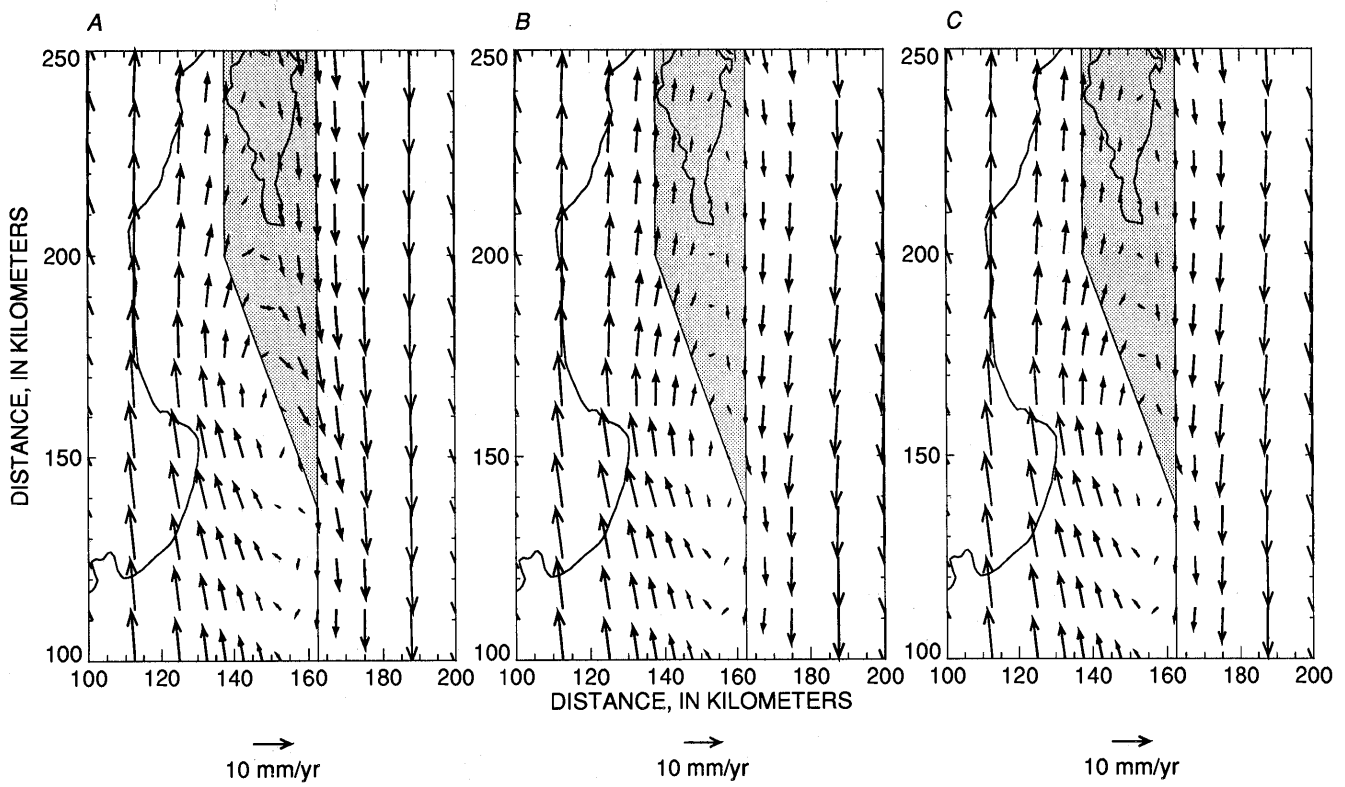

Figure 16.—Surface-velocity fields for 5-yr period after 1989 Loma Prieta earthquake in (*A*) detachment model and (*B*) elastic-crust model, and for 20-yr period after 1989 earthquake in weak-crust model (*C*). Shaded area, Bay Area block. Far-field velocities are at ±½ rate of relative Pacific-North American plate motion. Results plotted in figure 16*A* (particularly in vicinity of Bay Area block) indicate potential to discriminate detachment model from other two models by using post-1989 geodetic observations. Results plotted in figure 16*C* do not differ significantly from those for shorter periods after earthquake.

ruptured in 1906 makes it natural to relate processes associated with the 1989 earthquake to those associated with the 1906 earthquake. The initiation of rupture on the Santa Cruz Mountains section of the San Andreas fault at the base of the seismogenic layer is compatible, we believe, with considering the 1989 earthquake to be associated with decoupling of the crust from the underlying mantle (which continues along the path shown in fig. 5). The increase in stress (shear stress in the horizontal plane) in the vicinity of the Loma Prieta rupture during the interval 1906–89 (fig. 9) provides the mechanism for such a style of rupture. This horizontal shear stress (and one-sided relaxation) increases with each 1906-type event and thus can lead to less frequent (but quasi-periodic) Loma Prieta-type events. The longer recurrence interval for Loma Prieta-type events (events with a significant vertical component) relative to 1906-type events (Anderson, 1990; Valensise and Ward, 1991) may reflect the need for several strike-slip events to increase this decoupling stress to the point of generating an earthquake. The existence of an easily deforming detachment surface on the "North American" side of the fault through the Santa Cruz Mountains and San Francisco Bay allows the dissipation of any similar horizontal stresses in that region (fig. 9).

Consideration of the series of events that led to the 1989 Loma Prieta earthquake is important in evaluating the effects of this earthquake. Although much of the postseismic relaxation after the 1906 San Francisco earthquake had already occurred, the stress regime in the San Francisco Bay region before the 1989 earthquake evolved in response to both the 1906 relaxation and post-1906 plate motions. This preloading of the system plays an important part in post-1989 events. Although much of the coseismic deformation and even some of the long-term deformation field can be adequately simulated by elastic-dislocation models, we believe that explicit incorporation of viscous rheologies more closely represents the deformational behavior of the crust, lithospheric mantle, and plate-boundary zone

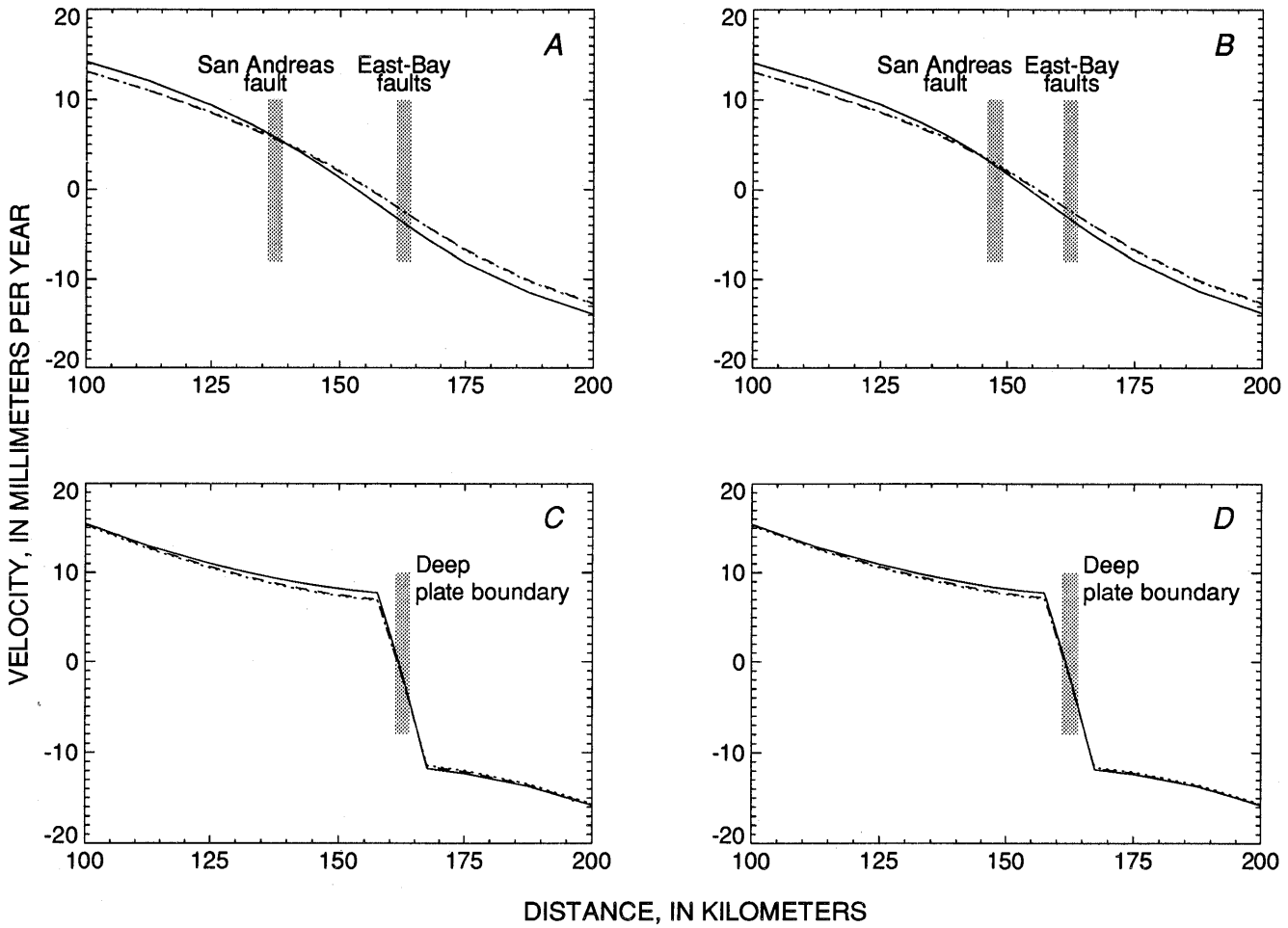

Figure 17.—Pre-1906 surface velocity (*A*, *B*) and lithospheric-mantle velocity (*C*, *D*) in profiles (perpendicular to plate boundary) in south-bay region (*A*, *C*; at ~220 km, fig. 16) and Loma Prieta region (*B*, *D*; at ~170 km, fig. 16) in detachment model (solid curve), elastic-crust model (dotted curve), and weak-crust model (dashed curve). Before 1906 San Francisco earthquake (that is, late in earthquake cycle), all models produce similar displacements.

than do simple elastic models. The evaluation of crustal deformation on the time scale of the earthquake cycle in the San Francisco Bay region, which for large events is about 100 to 200 yr, requires the incorporation of viscous rheologies and the inclusion of the series of events (at least the largest) that precede the earthquake of interest.

Although the 1989 Loma Prieta earthquake does not rank with the great earthquakes that have occurred along the San Andreas fault system in northern California, it does provide an important tool for improving our understanding of lithospheric behavior. Throughout our modeling, we have tested several scenarios for lithospheric structure and plate-boundary rheology. Our preferred model, which incorporates deformable structures in the lower crust, produces deformational behavior that can be tested by observations during the first 5- to 10-yr period after the earthquake. The preearthquake deformation regime, though well documented in the San Francisco Bay region, cannot conclusively distinguish among the various models, which have quite different implications for the overall stress regime in the bay region, and so the resulting seismic potential of the various fault segments differs from model to model. The early stages of postearthquake lower-crustal and plate-boundary relaxation may provide the key to unlocking intermodel differences.

We emphasize that three-dimensional modeling of the deformation field associated with a complex plate boundary is still in its infancy. Our models serve as important extensions of other models of the coseismic response of the San Francisco Bay region and regional deformation. We have found that combining this modeling with improved kinematic models of plate-boundary behavior allows us to focus on those details of plate-boundary deformation which are important in the earthquake cycle.

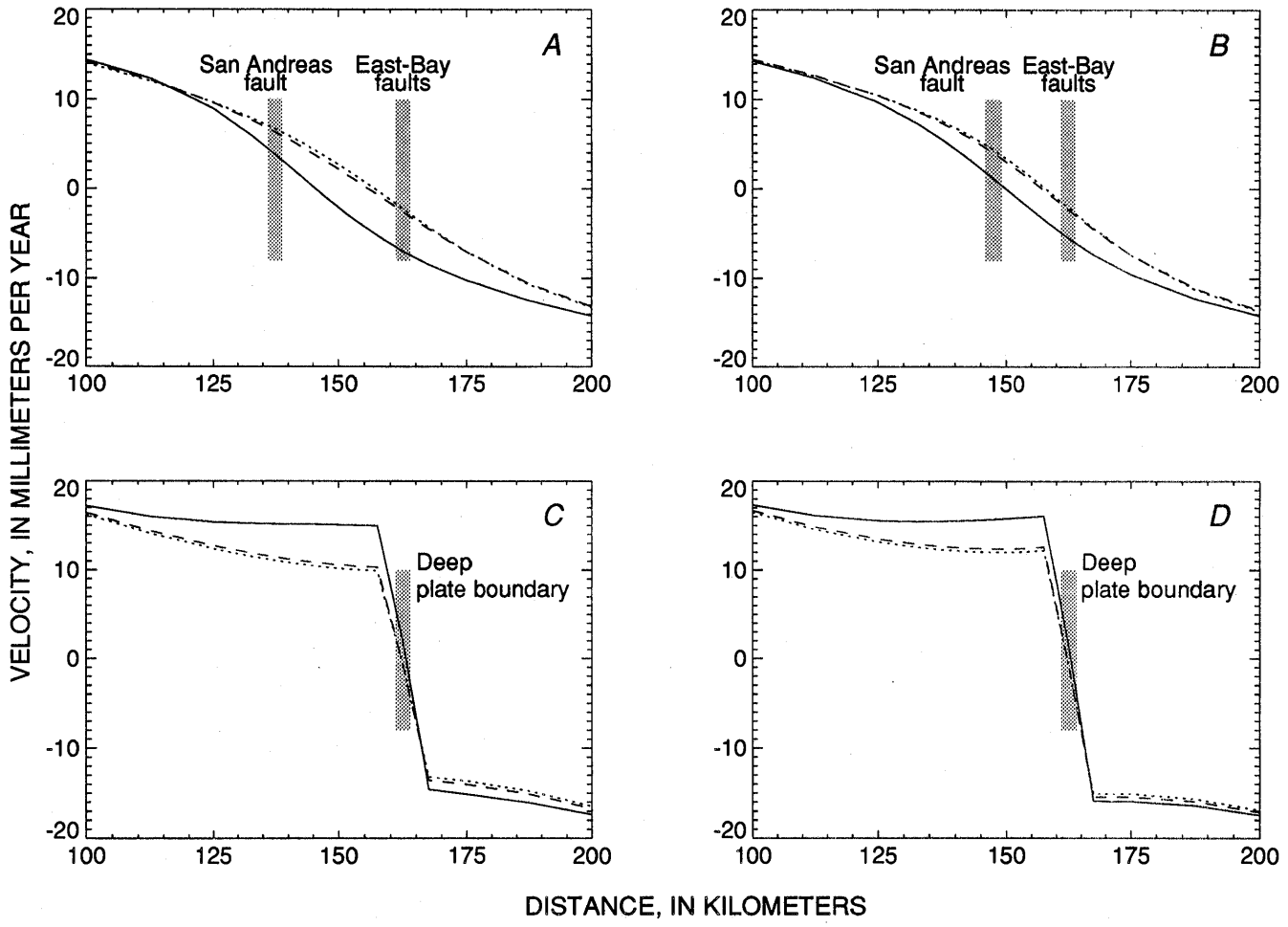

Figure 18.—Pre-1989 surface velocity (*A*, *B*) and lithospheric-mantle velocity (*C*, *D*) in profiles (perpendicular to plate boundary) in south-bay region (*A*, *C*; at ~220 km, fig. 16) and Loma Prieta region (*B*, *D*; at ~170 km, fig. 16) in detachment model (solid curve), elastic-crust model (dotted curve), and weak-crust model (dashed curve). Before 1989 Loma Prieta earthquake, both elastic- and weak-crust models produce similar displacements, essentially no different from pre-1906 patterns, whereas detachment model still shows effects of 1906 San Francisco earthquake—that is, velocity curve is shifted toward the San Andreas fault and away from deep plate boundary.

However, use of these results to directly answer questions of earthquake potential on specific fault segments is still premature. Although it is tempting to cite the results shown in figure 14*A* as providing the information needed to evaluate the concept of paired earthquakes, we do not believe that our results, at present, argue conclusively for or against such a concept. We do, however, believe that the style of modeling we have undertaken can improve our understanding of the spatial and temporal variations in stress and deformation associated with the earthquake cycle. This improved understanding of the underlying dynamics of plate-boundary deformation in the San Francisco Bay region is a key to an improved assessment of earthquake risk and potential in the region. The 1989 earthquake has focused attention on these processes and has served as an important tool that will allow improved observations of the postseismic response of the plate boundary.

ACKNOWLEDGMENTS

This research was supported by U.S. National Science Foundation grants EAR–8816966 and EAR–9104185 and U.S. Geological Survey grant NEHRP 1434–92–G–2213. We thank Jay Melosh for the use of his finite-element program TECTON. Discussions with numerous individuals throughout this research have been invaluable to us in crystallizing our thoughts; in particular, we thank George Zandt, Charles Langston, Charles Ammon, Harley Benz, Thorne Lay, and Michael Lisowski. Computations were performed in part on a Cray YMP–2E computer, courtesy

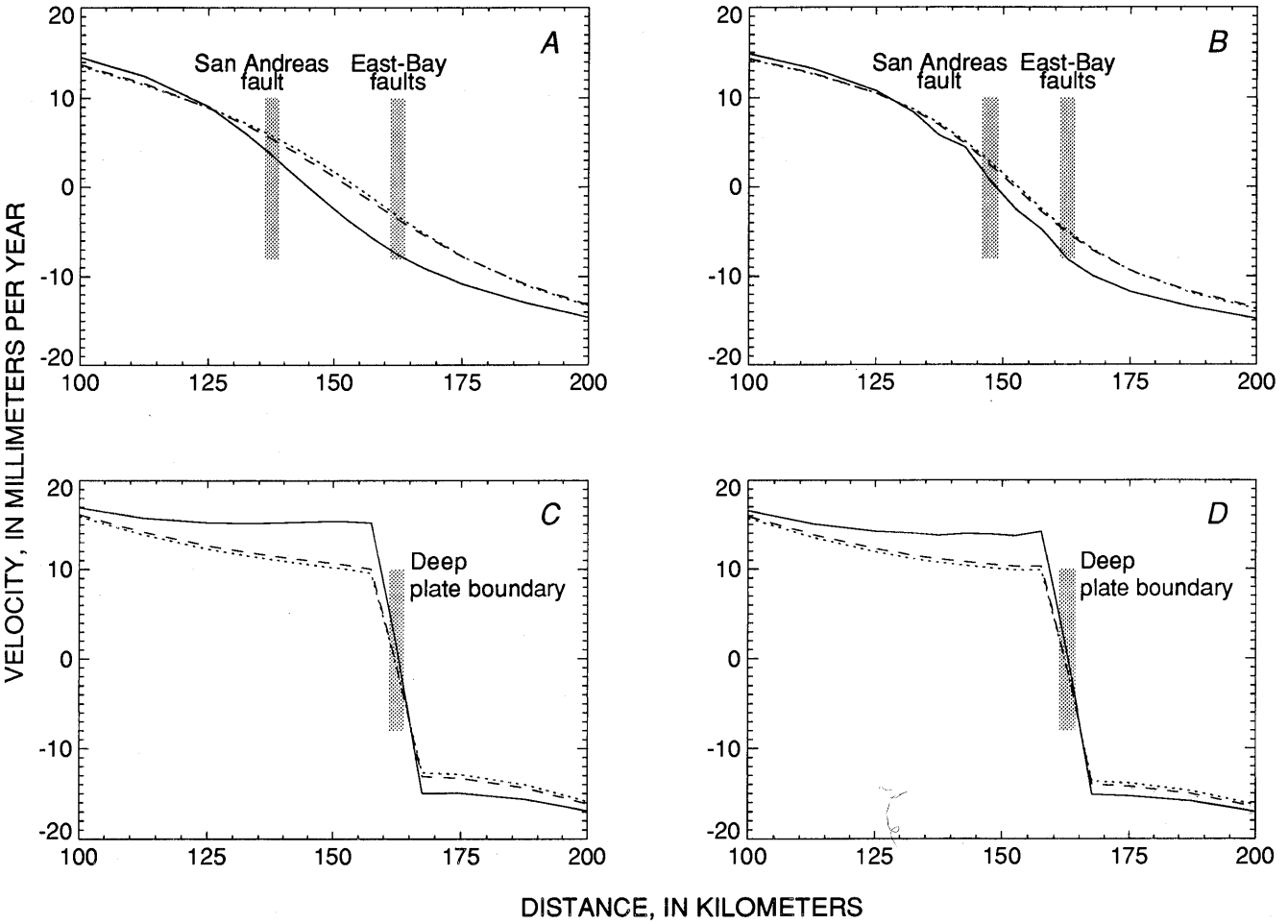

Figure 19.—Surface velocity (*A*, *B*) and lithospheric-mantle velocity (*C*, D) during 5-yr period after 1989 Loma Prieta earthquake in profiles (perpendicular to plate boundary) in south bay (*A*, *C*; at ~220 km, fig. 16) and Loma Prieta region (*B*, *D*; at ~170 km, fig. 16) in detachment model (solid curve), elastic-crust model (dotted curve), and weak-crust model (dashed curve). Shortly after 1989 earthquake, both elastic- and weak-crust models produce similar displacements, essentially no different from pre-1906 or pre-1989 pattern, whereas detachment model still shows effects of 1906 San Francisco earthquake, although these effects are overprinted by transient effects of 1989 earthquake. That is, velocity curve for detachment model is shifted even closer to San Andreas fault, away from deep plate boundary, and region of concentrated deformation is narrower. If 1989 earthquake had ruptured to surface, its effects would be more noticeable in these plots.

of the Earth System Science Center at the Pennsylvania State University, and on equipment graciously donated by the Hewlett-Packard Co. Reviews of the manuscript by Gene Humphreys, Joseph Andrews, and Robert Simpson are greatly appreciated.

REFERENCES CITED

Anderson, R.S., 1990, Evolution of the northern Santa Cruz Mountains by advection of crust past a San Andreas fault bend: Science, v. 249, no. 4967, p. 397–401.

Argus, D.F., and Gordon, R.G., 1991, Current Sierra Nevada-North America motion from very long baseline interferometry; implications for the kinematics of the western United States: Geology, v. 19, no. 11, p. 1085–1088.

Atwater, Tanya, 1970, Implications of plate tectonics for the Cenozoic tectonic evolution of western North America: Geological Society of America Bulletin, v. 81, no. 12, p. 3513–3535.

Benz, H.M., Zandt, George, and Oppenheimer, D.H., 1992, Lithospheric structure of northern California from teleseismic images of the upper mantle: Journal of Geophysical Research, v. 97, no. B4, p. 4791–4807.

DeMets, Charles, Gordon, R.G., Argus, D.F., and Stein, Seth, 1990, Current plate motions: Geophysical Journal International, v. 101, no. 2, p. 425–478.

Dickinson, W.R., and Snyder, W.S., 1979, Geometry of subducted slabs related to the San Andreas transform: Journal of Geology, v. 87, no. 6, p. 609–627.

Ellsworth, W.L., 1990, Earthquake history, 1769–1989, chap. 6 *of* Wallace, R.E., ed., The San Andreas fault system, California: U.S. Geological Survey Professional Paper 1515, p. 153–187.

Fox, K.F., Jr., 1983, Tectonic setting of Late Miocene, Pliocene, and Pleistocene rocks in part of the Coast Ranges north of San Francisco, California: U.S. Geological Survey Professional Paper 1239, 33 p.

Furlong, K.P., 1984, Lithospheric behavior with triple junction migration; an example based on the Mendocino triple junction: Physics of the Earth and Planetary Interiors, v. 36, no. 3–4, p. 213–223.

———1990, Localization of lithospheric deformation along transform plate boundaries; modeling the San Andreas [abs.]: Eos (American Geophysical Union Transactions), v. 71, no. 17, p. 643.

———1993, Thermal-rheologic evolution of the upper mantle and the development of the San Andreas fault system: Tectonophysics, v. 223, no. 1/2, p. 149–164.

Furlong, K.P., Hugo, W.D., and Zandt, George, 1989, Geometry and evolution of the San Andreas fault zone in northern California: Journal of Geophysical Research, v. 94, no. B3, p. 3100–3110.

Furlong, K.P., and Langston, C.A., 1990, Geodynamic aspects of the Loma Prieta earthquake: Geophysical Research Letters, v. 17, no. 9, p. 1457–1460.

Karato, S.-I., Paterson, M.S., and Fitzgerald, J.D., 1986, Rheology of synthetic olivine aggregates; influence of grain size and water: Journal of Geophysical Research, v. 91, no. 8, p. 8151–8176.

Lachenbruch, A.H., and Sass, J.H., 1980, Heat flow and energetics of the San Andreas fault zone: Journal of Geophysical Research, v. 85, no. B11, p. 6185–6222.

Langston, C.A., Furlong, K.P., Vogfjord, K.S., Clouser, R.H., and Ammon, C.J., 1990, Analysis of teleseismic body waves radiated from the Loma Prieta earthquake: Geophysical Research Letters, v. 17, no. 9, p. 1405–1408.

Linker, Mark, and Rice, J.R., in press, Models of postseismic stress transfer and postearthquake deformation in northern California, *in* Reasenberg, P.A., ed., The Loma Prieta, California, earthquake of October 17, 1989—postseismic effects, aftershocks, and other phenomena: U.S. Geological Survey Professional Paper 1550–D.

Lisowski, Michael, Savage, J.C., and Prescott, W.H., 1991, The velocity field along the San Andreas fault in central and southern California: Journal of Geophysical Research, v. 96, no. B5, p. 8369–8389.

Marshall, G.A., Stein, R.S., and Thatcher, Wayne, 1991, Faulting geometry and slip from co-seismic elevation changes; the 18 October 1989, Loma Prieta, California, earthquake: Seismological Society of America Bulletin, v. 81, no. 5, p. 1660–1693.

Melosh, H.J., and Raefsky, Arthur, 1980, The dynamical origin of subduction zone topography: Royal Astronomical Society Geophysical Journal, v. 60, no. 3, p. 333–354.

———1981, A simple and efficient method for introducing faults into finite element computations: Seismological Society of America Bulletin, v. 71, no. 5, p. 1391–1400.

Minster, J.B., and Jordan, T.H., 1978, Present-day plate motions: Journal of Geophysical Research, v. 83, no. B11, p. 5331–5354.

Rutter, E.H., and Brodie, K.H., 1988, The role of tectonic grain size reduction in the rheological stratification of the lithosphere: Geologische Rundschau, v. 77, no. 1, p. 295–308.

Thatcher, Wayne, 1975, Strain accumulation and release mechanism of the 1906 San Francisco earthquake: Journal of Geophysical Research, v. 80, no. 35, p. 4862–4872.

Valensise, Gianluca, and Ward, S.N., 1991, Long-term uplift of the Santa Cruz coastline in response to repeated earthquakes along the San Andreas fault: Seismological Society of America Bulletin, v. 81, no. 5, p. 1694–1704.

Verdonck, David, and Furlong, K.P., 1992, Stress accumulation and release at complex transform plate boundaries: Geophysical Research Letters, v. 19, no. 19, p. 1967–1970.

Wald, D.J., Helmberger, D.V., and Heaton, T.H., 1991, Rupture model of the 1989 Loma Prieta earthquake from the inversion of strong-motion and broadband teleseismic data: Seismological Society of America Bulletin, v. 81, no. 5, p. 1540–1572.

Zandt, George, and Furlong, K.P., 1982, Evolution and thickness of the lithosphere beneath coastal California: Geology, v. 10, no. 7, p. 376–381.